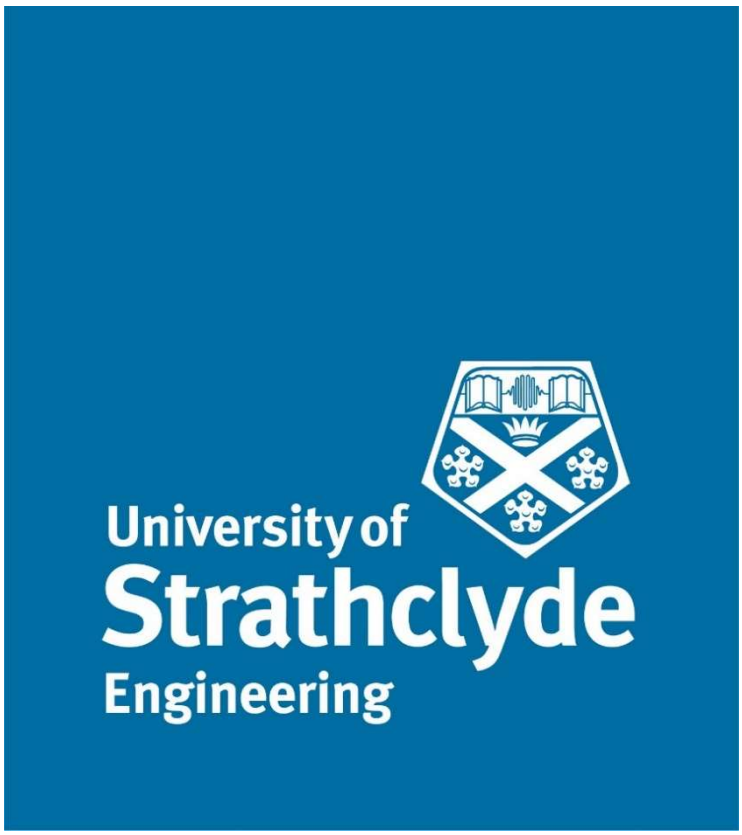

Investigation of a micromechanical methodology for assessing the influence of processing variables and fibre sizing on composite interphase

A thesis in fulfilment of the requirements for the degree of
Doctor of Philosophy

By

David Bryce

Department of Mechanical and Aerospace Engineering
University of Strathclyde
Glasgow, Scotland
UK
2021

DECLARATION OF AUTHENTICITY AND AUTHOR'S RIGHTS

This thesis is the result of the author's original research. It has been composed by the author and has not been previously submitted for examination which has led to the award of a degree.

Signed: 

Date: 9/5/21

ACKNOWLEDGMENTS

I would firstly like to extend sincere gratitude to my supervisor Professor James Thomason. His guidance, patience, encouragement, and support were invaluable during the course of my studies, and without which this thesis would not have been possible. I appreciate being given the opportunity to develop personally and professionally as a researcher within a field that interests me a great deal. I would also like to thank my second supervisor Dr Liu Yang, whose time, experience, and expertise were always given generously. In addition, my thanks go to all past and present members of the Advanced Composites Group. Their advice, support, and friendship over the last few years has been greatly appreciated. It was a pleasure to work with you all. Gratitude is also extended to undergraduate students Iain Lowther and Rosalyn Brown for their contributions to MATLAB script development and experimental data. I appreciate the time and expertise given by Dr Pik Leung Tang in assisting with the interpretation of Fourier-transform infrared spectroscopy data and experimental method recommendations. I gratefully acknowledge the financial support of Suzlon Energy Ltd. and the University of Strathclyde. Finally, I am incredibly grateful to my parents and Jaye for their love, support, and encouragement during the entirety of my studies.

Thank you. I am indebted to you all.

PUBLICATIONS

A number of findings in this thesis have been published over the course of the PhD project in the form of journal articles and conference contributions:

Bryce D, Thomason J, Yang L. Micromechanical and spectroscopic characterisation of the curing performance of epoxy resins in the microbond test. IOP Conference Series: Materials Science and Engineering 2020;942.

Jenkins PG, Bryce D, Xypolias G, Thomason JL. Micro-mechanical investigation of glass fibre/resin interface failure in mode I and mode II. IOP Conference Series: Materials Science and Engineering 2020;942.

Thomason JL, Nagel U, Yang L, Bryce D. A study of the thermal degradation of glass fibre sizings at composite processing temperatures. Composites Part A: Applied Science and Manufacturing 2019;121:56–63.

Bryce D, Thomason JL, Yang L. An Investigation of Fibre Sizing on the Interfacial Strength of Glass-Fibre Epoxy Composites. Proceedings of the 18th European Conference on Composite Materials (ECCM18) 2018:24–8.

ABSTRACT

The fibre surface coating (or sizing) is one of the most crucial components involved in the manufacture of glass fibres and their composites. It plays a key role in determining the profitability, processability, and both the short- and long-term performance of a composite product. Given the importance of fibre sizing to the optimisation of the interface, there is a critical need to improve understanding of how this region is affected by fibre sizing composition. The objective of this thesis was to develop methodologies and micromechanical techniques to provide definition of the role of current and developmental glass fibre sizings in the interphase performance of glass fibre reinforced composites for wind turbine blade applications.

A round-robin study of the adhesion enhancing capabilities of a wide range of glass fibre sizing components and full sizing packages has been investigated. It was found that glass fibre/epoxy adhesion was increased by application of a glycidoxypropylmethyldiethoxysilane (GPMES) coupling agent compared to amino-, methacryl-, and other epoxysilanes. The adhesion enhancing capabilities of a GPMES coupling agent may also have been responsible for comparable interfacial shear strength (IFSS) values for a series of epoxy-compatible full sizing formulations. However, the use of a matrix-incompatible full sizing resulted in adhesion properties lower than that of unsized fibres despite the presence of an undisclosed coupling agent. An apparent adhesion-inhibiting effect of the thermoplastic film former appeared to counteract any improvement due to the silane.

Acetone extraction of fully sized fibres showed that IFSS was improved compared to the as-received fibres in all cases. Increased IFSS compared to the as-received fibres may have been related to removal of residual surface impurities, improved coupling agent homogeneity, or removal of sizing additives and processing agents whose contribution to the properties of the composite are not well defined. Interfacial adhesion values approximating and exceeding those attainable by use of a number of silane coupling agents and full sizing packages were achieved by treating glass fibres with an unreacted epoxy/acetone solution. The coating served as both a model polymeric film former and a post-sizing treatment. Increased IFSS as a result of the epoxy coating application may have been attributable to interdiffusion of the epoxy coating with the epoxy matrix material and enhanced cross-linking at the interface between unreacted DGEBA in the sizing and an amine curing agent.

Thermal analysis, spectroscopic, and micromechanical testing methods were used to investigate the thermal degradation of a number of experimental and commercial glass fibre sizings. TGA of three fully sized epoxy-compatible glass fibres (SE1500, SE2020, W2020) indicated that the majority of the mass loss occurred in the 200–400°C range and was attributable to the decomposition of the polymeric film former component of the sizing. An initial 70–80 nm sizing layer was reduced by approximately 50% following 300°C heat treatment and was removed almost entirely following treatment at 500°C. Fourier-transform infrared spectra (FTIR) of thermally degraded fully sized glass fibre bundles indicated that the intensity of spectral bands attributable to an epoxy resin film former decreased linearly with increasing treatment temperature and were removed completely at temperatures of 300–350°C. Spectra showed excellent correlation with TGA data that indicated that sizing mass loss in in the 200–400°C range was attributable to degradation of an epoxy film former. The accumulation of carbonyl groups may have been due to oxidation of the epoxy film former component in the sizing.

Interfacial adhesion measurements indicated that IFSS had an inverse relationship with fibre treatment temperature and was concurrent with decomposition of the glass fibre sizing measured by TGA. Reduced IFSS appeared to onset at 300–350°C and at treatment temperatures of 400°C and above interfacial adhesion was comparable to that of unsized fibres, suggesting that the majority of the sizing components which influence IFSS had been removed. Spectra of fibres treated at 500°C indicated that some residues of degraded silane coupling agent material were present at the glass fibre surface, though the silane coupling agent may have been degraded to the extent that the adhesion-enhancing capabilities were lost. Interfacial adhesion may also have been inhibited after higher treatment temperatures by the accumulation of weakly bound oxidised film former/sizing material on the glass fibre surface.

Further investigation of fibre sizing parameters was initially attempted using two epoxy resin matrices used in the production of wind turbine blades. It was discovered that the degree to which these resins formed cured droplets suitable for microbond testing was dependent on a modification to the recommended macroscale cure schedule. Microbond samples showed exceedingly low IFSS values when exposed to immediate heating, failed to cure, and deformed plastically under loading. Poor microdroplet curing and low apparent droplet glass transition temperature was attributable to a stoichiometric imbalance caused by evaporation of components essential to the polymerisation reaction. Off-stoichiometric droplet behaviour was further evidenced by a number of modifications to the curing schedule and sample preparation methodology. The inclusion of a room temperature pre-curing stage for a minimum of 2 h

resulted in a profound increase in the apparent IFSS after which further standing times showed no significant improvement.

Finally, a novel FTIR method was developed to address a fundamental need for a method to directly characterise the cure state of microbond droplets and investigate poor microscale curing performance in the industrial resin systems. Glass fibres were substituted by 50 μm diameter steel wire filaments in the preparation of microbond samples to improve signal clarity due to the combination of controllable and consistent increased microdroplet size and a favourable reflectance effect. Off-stoichiometric matrix compositions were used as models of the varying extents of curing agent evaporation that might exist in microbond droplets. DSC and FTIR were used to determine the relationship between degree of epoxy conversion and glass transition temperature. Droplet degree of cure was determined by FTIR and droplet glass transition temperature was estimated by comparison to off-stoichiometric data. FTIR spectra of microbond samples cured immediately at elevated temperature showed the presence of unreacted epoxy groups, reduced hydroxyl and secondary amine group accumulation, and a weaker etherification peak, commensurate with spectra indicating a non-stoichiometric epoxy-amine network. Quantitative analysis of unreacted epoxy groups and determination of cure state indicated that samples cured immediately at high temperature had degrees of epoxy conversion in the region of 0.55, indicating a loss of up to 60% of the initial curing agent and a sub-ambient glass transition temperature. Conversely, samples that were allowed to pre-cure at room temperature for a minimum of 2 h before heating showed increased degree of cure (0.85–0.93) and droplet T_g some 80°C greater than that of immediately hot-cured samples. Good correlation was shown between micromechanical and spectroscopic methods, in that an increase in IFSS was commensurate with spectra indicating droplets were closer to the stoichiometric ratio and had higher degrees of cure, thus demonstrating a clear relationship between apparent interfacial adhesion and droplet cure state.

.

TABLE OF CONTENTS

NOMENCLATURE

Abbreviations

AFM	Atomic Force Microscopy
AAPS	Aminoethyl Aminopropyltrimethoxysilane
APS	Aminopropyltriethoxysilane
ASLX	Poly(aminopropyl)siloxane
ATR	Attenuated Total Reflectance
BGE	Butyl Glycidyl Ether
DAP	Diaminopropane
DCH	Diaminocyclohexane
DEA	Diethanolamine
DETA	Diethylenetriamine
DGEBA	Bisphenol-A Diglycidyl Ether
DMF	Dimethyl Formamide
DRIFT	Diffuse Reflectance Infrared Fourier-Transform
DSC	Differential Scanning Calorimetry
FTIR	Fourier-Transform Infrared Spectroscopy
GFRP	Glass Fibre Reinforced Polymer
GPMES	Glycidoxypropylmethyldiethoxysilane
GPMMS	Glycidoxypropylmethyldimethoxysilane
GPTMS	Glycidyloxypropyltrimethoxysilane
GSLX	Poly(glycidyloxypropyl)siloxane
IFSS	Interfacial Shear Strength
IPD	Isophorondiamine

LOI	Loss On Ignition
ILSS	Interlaminar Shear Strength
J403	Jeffamine 403
J700	Jeffamine 700
MAPP	Maleic Anhydride Grafted Polypropylene
MDA	Methylene Dianiline
MDEA	4,40 Methylenebis2,6-diethyleneaniline
mIR	Middle Infrared
m-PDA	Meta-Phenylene Diamine
MPTMS	Methacryloxypropyltrimethoxysilane
MSLX	Poly(methacryloxypropyl)siloxane
MTHPA	Anhydride cis 4-methyl 1,2,3,6-tetrahydrophtallic
nIR	Near Infrared
NMA	Nadic Methyl Anhydride
NMR	Nuclear Magnetic Resonance
PEG	Polyethylene Glycol
PEO	Polyethylene Oxide
PP	Polypropylene
PPD	Polyoxypropylenediamine
PTMO	Propryltrimethoxysilane
PVA	Polyvinyl Acetate
Py-GC-MS	Pyrolysis-Gas Chromatography-Mass Spectrometry
PVOH	Polyvinyl Alcohol
SEM	Scanning Electron Microscopy
SFM	Scanning Force Microscopy

TEOS	Tetraethoxysilane
TEPA	Tetraethylenepentamine
TETA	Triethylenetetramine
T_g	Glass Transition Temperature
TGA	Thermogravimetric Analysis
TGA-MS	Thermogravimetric Analysis-Mass Spectrometry
TGDDM	Tetraglycidyldiaminodiphenyl Methane
TMA	Thermomechanical Analysis
TMAFM	Tapping Mode Atomic Force Microscopy
UD	Unidirectional
UHMW-PE	Ultra-High-Molecular-Weight Polyethylene
VSLX	Poly(vinyl)siloxane
VTMO	Vinyltrimethoxysilane
XPS	X-ray Photoelectron Spectroscopy

LIST OF FIGURES

LIST OF TABLES

CHAPTER 1: INTRODUCTION

1.1 PROJECT BACKGROUND

The rapidly growing use of glass fibre reinforced polymers (GFRP) in a wide range of industries, from automotive to wind turbine applications, means that the demand for the development of new and improved composite materials has never been higher. The fibre/matrix interface region is critical to the mechanical performance of a composite, thus optimisation of the stress-transfer capability of this region is extremely important. The fibre sizing is a key factor in controlling the stress-transfer capabilities of the interface and also plays a critical role in defining a number of the parameters which influence long-term composite performance. Given the importance of the fibre sizing to the optimisation of the interface, there is a critical need to improve understanding of how this region is affected by sizing composition.

Wind turbine blade manufacturers are continually challenged by the need to develop longer, better performing blades. Furthermore, the exposure of blades to high static and dynamic loads over a broad temperature range requires high performance composite materials which will perform reliably over the lifetime of the structure. Optimisation of the fibre/matrix interface region is critical to achieving the required performance levels in these advanced composite materials. It is clear that the fibre surface and any coating on the fibre must play an important role in the formation and properties of the composite interface. Since all reinforcement fibres are surface-treated to increase their interaction with polymer matrices, the ability to efficiently characterise the influence of these surface treatments on the interphase stress-transfer capability is critical to the development of the next generation of high performance advanced composites.

It is essential to be able to characterise the interface and associated level of adhesion through a robust methodology in order to fully understand composite performance. The basic procedure for the microbond test involves a single filament being pulled from a restrained droplet of cured matrix while measuring the force required to detach the filament While the use of micromechanical techniques, such as the microbond test, to characterise the adhesion between various fibre and polymer systems has been widely reported in the literature, only a very few authors have commented on an apparent disparity in matrix material properties at the microscale and the implications this holds for the validity of test results. If the microbond test is to be presented as an efficient and robust methodology for effectively characterising the fibre/matrix interface it is essential for this phenomenon to be understood in greater detail.

Accordingly, a significant portion of the research work concerns analysis of the microbond testing method and a detailed investigation of the discrepancy between macro- and microscale thermomechanical properties and characterisation of microdroplet cure state.

1.2 AIMS AND OBJECTIVES

In order to produce advanced composite materials with improved mechanical performance it is essential to improve our understanding of the mechanisms involved in interfacial adhesion, how these are affected by the application of sizing, and in turn, how these sizings are affected by factors such as elevated temperature exposure. Outlined broadly, the goal of the thesis can be divided into three main objectives:

1. Micromechanical characterisation of the interphase strength generated by both current and developmental glass fibre sizings, including definition of any performance changes attributable to the degradation of the sizing.
2. Development of a robust sample preparation methodology which allows direct relationships to be established with the industrial processing parameters used in manufacturing wind turbine blades. This will allow for a method wherein a number of industry supplied sized fibres and resin systems can be assessed in terms of interfacial performance.
3. An investigation of robust micromechanical measurement methodologies to characterise the interphase of glass fibre-epoxy systems

1.3 OUTLINE OF THESIS

Chapter 1 covers a brief introduction to the project background and objectives and outlines the structure of the thesis. Specific reviews of the literature relevant to each chapter are found within the main body of the text rather than being presented as a stand-alone review chapter.

Chapter 2 presents a round-robin investigation of the effect of a number of commercial and experimental sizings on glass fibre/epoxy interfacial shear strength. The microbond test was used to investigate the adhesion-enhancing properties of a range of silane coupling agents and full commercial sizings of varying matrix compatibility. A model glass fibre sizing consisting of an unreacted epoxy/acetone solution was used to investigate the adhesion properties of an epoxy film former component that constituted the majority of epoxy-compatible sizings by weight. The epoxy/acetone solution was also used to post-treat fibres that were already sized

with a silane coupling agent or a full epoxy-compatible formulation. Some of the experimental work that comprises Chapter 2 was first presented as *"An Investigation of Fibre Sizing on the Interfacial Strength of Glass-Fibre Epoxy Composites"* at the 18th European Conference on Composite Materials and is published under the same title in the accompanying conference proceedings.

Chapter 3 reports on the thermal analysis, spectroscopic, and micromechanical testing methods used to characterise the thermal degradation of a range of glass fibre sizings and the effect of sizing degradation on interfacial adhesion after treatment at 200–500°C. TGA was used to quantify sizing mass loss and characterise the depletion of the sizing layer as treatment temperature was increased. Fourier-transform infrared spectroscopy was used to characterise glass fibre sizings and the ensuing changes in composition following exposure to elevated temperature treatment. The relationship between interfacial adhesion and glass fibre sizing degradation was investigated using the microbond test. The micromechanical and thermogravimetric work contained in Chapter 3 has contributed to the development of a journal article published under the title of "*A study of the thermal degradation of glass fibre sizings at composite processing temperatures*".

In Chapter 4, the microscale curing performance of a number of amine-cured epoxy resins was investigated. It was discovered that the degree to which certain resin and curing agent combinations formed cured droplets suitable for microbond testing was dependent on a modification to the recommended macroscale schedule. An extensive literature review of this rarely reported behaviour was conducted. Modification to the recommended macroscale curing schedule by the introduction of a room temperature pre-curing stage, high temperature post-curing, the addition of excess curing agent, and varying curing atmosphere was investigated using the microbond test. A differential scanning calorimetry method was initially used to investigate droplet glass transition temperature and hot-stage microscopy was used to observe droplet curing in-situ. Some of the work in Chapter 4 was first presented at the 5th International Conference on Mechanics of Composites under the title of "*Microscale Curing Performance of Epoxy Resin in the Microbond Test.*

Chapter 5 details the development and implementation of a novel FTIR method to characterise the degree of cure of microbond samples and investigate poor curing droplet performance. Glass fibres were substituted by 50 μm diameter steel wire in the preparation of microbond samples to improve signal clarity due to the combination of controllable and consistent increased microdroplet size and a favourable reflectance effect. Droplet degree of cure was determined by FTIR and droplet glass transition temperature was estimated by

intersection with off-stoichiometric matrix degree of cure versus T_g curves. Much of the experimental work that comprises Chapter 5 was first presented at the 41st Risø International Symposium on Materials Science under the title of "*Micromechanical and Spectroscopic Characterisation of the Curing Performance of Epoxy Resins in the Microbond Test*" and is published under the same title in the accompanying IOP conference proceedings.

Chapter 6 summarises the conclusions of the thesis and outlines recommendations for future work.

CHAPTER 2: MICROMECHANICAL CHARACTERISATION OF SIZED GLASS FIBRE INTERFACIAL SHEAR STRENGTH

2.1 INTRODUCTION

Glass fibres account for the majority of the fibre reinforcement used in the fibre reinforced polymer composites industry due to their attractive cost/performance ratio compared to more conventionally well-regarded "high tech" reinforcement such as carbon fibres [1]. Sizings are applied to bare glass fibres in order to improve their adhesion properties, in addition to protecting the fibres from damage, and are well recognised as a key component in determining the success or failure of the reinforcement. Sizings typically consist of primarily aqueous solutions containing 0.05–10% solids [1]. The solid portion is comprised of a film former (to bind the filaments in a strand and to protect the fibre during processing), a coupling agent (typically silane) to promote adhesion (among other properties such as interphase strength and hydrothermal resistance), and other additives such as anti-static agents, emulsifiers, and wetting agents [2]. The beneficial effects of sizing on composite performance are widely recognised, though there exists a need to better understand the nature of this improvement in order to work towards new, higher-performing sizings [2–4].

In addition to functioning as an essential processing aid during fibre and composite manufacturing, sizings are a critical component in the formation and properties of the fibre/matrix interface as a result of their location on the fibre surface. Accordingly, any investigation of the interphase must involve examination of the contribution of sizing. Optimisation of the stress-transfer capabilities of the interface is well recognised as being essential in achieving required levels of short- and long-term performance in composite materials.

In order to meet the developing needs of modern advanced composite materials, a fundamental understanding of the fibre/matrix interface and its effect on material structure-property relationships is required. Accordingly, the work in Chapter 2 involves a round-robin investigation of the effect of a number of current and developmental glass fibre sizings on glass fibre/epoxy interfacial shear strength. The microbond test is used to characterise the interfacial adhesion of unsized glass fibres, fibres coated with various silane coupling agents, combinations of silane coupling agent and polymeric film former, full commercial sizing packages, and model sizings consisting solely of an epoxy film former component.

2.2 LITERATURE REVIEW

2.2.1 Glass Fibre Reinforced Composites

Composites can be broadly defined as complex, multi-phase materials of two or more components with different properties and forms. By combining various matrix and reinforcement materials, composite material parameters and characteristics can be effectively tailored for use in a range of industrial applications and environments. The internal structure of a composite material consists of three physical phases:

1. The polymer matrix phase which remains continuous throughout the materials
2. The reinforcement phase which is distributed within and surrounded by the matrix phase
3. The composite interphase that exists between the reinforcement and matrix phases

Composite materials are formed from two dissimilar components, the matrix and the reinforcement, with the interphase forming as a result of the interaction between the components. In simple terms, the interphase can be interpreted as an interfacial boundary region that separates the bulk polymer matrix phase from the bulk reinforcement phase. Each of these phases interact with one another, with the interface acting as the bridge between matrix and reinforcement phases and allowing loads to be shared and transferred between the two. The nature and structure of each phase and their interaction with one another can all affect the performance of the composite.

Composite material performance is dictated not only by individual fibre and matrix properties, but also on the strength of the interfacial bond where constituent parts interact both chemically and mechanically. As a result, load-transfer at the interface is largely governed by the extent of chemical and mechanical bonding. Composite properties may be further defined by structural defects such as voids, impurities, and microcracks, all of which tend to be found in the interface region. More comprehensive mechanical models consider an interphase region with its own characteristics, defined as the region extending from the point near the fibre where local properties begin to deviate from bulk fibre properties, through the interface, and into the point in the matrix where local properties are the same as those of the bulk matrix material [5–8]. The depth of this region can range from a few nanometres to a few thousand nanometres depending on the material system. Interphase properties are controlled by a number of parameters related to the properties of the constituent materials and the fabrication process of the composite part. Accordingly, the interphase that is formed has both a complex chemical structure and mechanical behaviour.

In more complex terms, the interphase can be examined as a number of sub-regions [9]:

1. A fibre surface layer: A thin layer located below the fibre free surface. Defects may be present at the outermost surface layer due to exposure to reactive environments during fibre processing. Atomic and molecular composition of the fibre surface may also be notably different from that of the bulk fibre [5].
2. An interface layer where fibre and matrix chemically and mechanically bond: Interfacial bond strength is largely dictated by the fibre sizing applied. The interface layer is typically the most complex component of the interphase and is highly stressed as a result of the disparity between fibre and matrix.
3. An interlayer typically consisting of a thin coating of fibre sizing: Studies by Drzal [5] and others [10] have proposed that the interlayer in epoxy composites has a gradient where amine concentration decreases from that of the surrounding bulk matrix, with lowest amine concentrations located nearest the fibre surface. Deviations from the stoichiometric ratio results in an interlayer that is often stiffer than the bulk matrix, among other potential property changes. Matrix material within 250 nm of the fibre may be significantly softer than the bulk matrix while the matrix adjacent to the fibre may possess a higher modulus due to the constraining effects of the fibre. Interlayer properties are thus dictated by both chemical interactions and fibre constraints.
4. A constrained matrix layer located between the interlayer and bulk matrix consisting of pure matrix material and influenced by the fibre. Matrix stiffness will typically be higher than that of the bulk matrix due to reduced polymer chain mobility and differences in macromolecule packing density as a result of fibre constraints and fibre/matrix interactions [11].

A schematic diagram of the composite interphase region is shown in *Figure 2:1* [9].

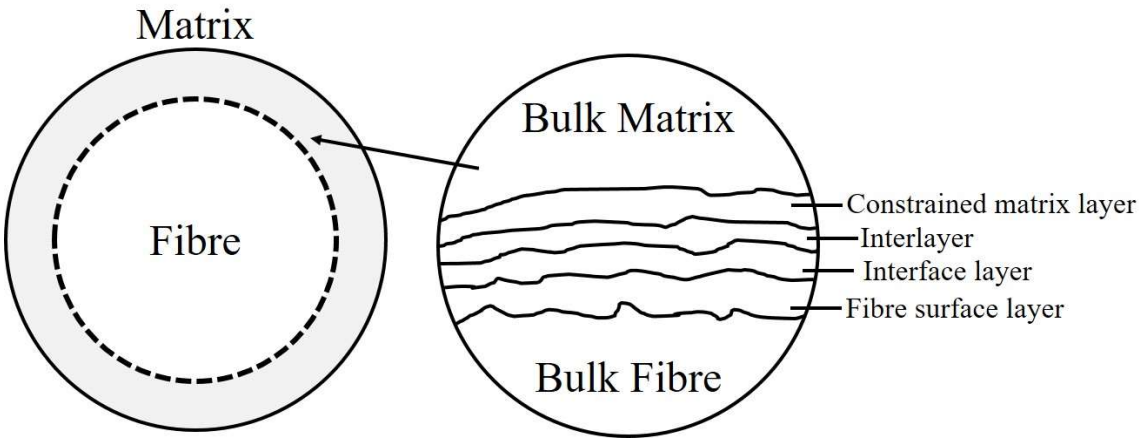

Figure 2:1: Schematic diagram of the composite interphase

The interphase region should not be modelled as a simple surface where fibre and matrix meet, but as an inhomogeneous interaction zone with defects and stress concentrations. The interphase region possesses a different structure, chemical composition, and mechanical properties compared to those of the bulk fibre and matrix. As a result, the mechanical properties of the interphase and the practical composite are directly related to the physical characteristics and quality of the interfacial bond strength in this region.

Interfacial stresses in composites occur as a result of resin shrinkage and difference in elasticity modulus between the polymer matrix and fibre reinforcement [12]. Effective stress transfer at the interface thus requires efficient coupling between fibre and matrix and optimised interfacial bonding is necessary to produce composites with excellent mechanical properties.

2.2.2 Glass Fibres

Glass fibres are the most commonly used reinforcing element found in composite materials. Their inherent properties of high strength, durability, flexibility, and low weight, coupled with resistance to heat and moisture, makes glass fibre an essential component in reinforced polymer composites.

The majority of glass fibres are based on silica, with oxides of aluminium, boron, calcium, iron, and sodium added. The glasses formed are typically non-crystalline solids and fall into three categories that are popular for use in composite materials: E-glass (electrical), C-glass (corrosion) and S-glass (strength). E-glass is noted for its strength and stiffness in addition to electrical and weathering properties. C-glass has better resistance to corrosion than E-glass, albeit at the cost of lower strength. S-glass has higher strength, Young's modulus, and temperature resistance than E-glass, though this comes with an economic trade-off as S-glass is more expensive [13]. Further application-specific glass fibre formulations include M-glass (modulus), A-glass (alkali), and D-glass (dielectric) [14].

Glass fibres are produced by heating the glass components in a reservoir until molten before feeding into a series of platinum bushings. Each of these bushings has several thousand fine holes in its base. The molten glass is drawn downwards as the glass extrudes from the holes before being wound onto a drum at speeds of up to several thousand metres per minute. The fibre diameter can be adjusted through a number of factors including: the viscosity of the glass, the winding speed of the drum, and the diameter of the bushing holes. The strength of a glass fibre can be seriously undermined should it sustain surface damage from rubbing against other fibres during processing Accordingly, the sizing is applied early in the manufacturing process.

The diameter of commercial E-glass fibres typically ranges between 8 and 24 μm, though glass fibres are available in many different diameters subject to requirement.

Glass fibre reinforced polymer (GFRP) composites are widely used in the construction and transportation sectors, though the demand for renewable energy in the form of wind turbines and light-weight, fuel-efficient vehicles and aircraft are equally important sectors. More recently, there has been a growing demand for GFRP piping, industrial tanks, and other corrosion resistant equipment and apparatus [15,16]. Using glass fibre composites instead of metals offers numerous structural advantages as GFRP materials are lighter, more flexible, and are capable of producing products with higher resistance to temperature, humidity, and corrosion with relative ease. Further attractive properties include non-conductive and non-magnetic characteristics.

2.2.3 Glass Fibre Sizing

One of the most critical components involved in the manufacture of glass fibres and composites thereof is the fibre sizing. Sizing is a thin surface coating applied to almost all varieties of man-made fibres during their manufacture. The sizing can largely be considered like a "jacket" for glass fibres [13]. Much in the same way that there are different jackets for different weather conditions, glass fibres have different sizings to suit different applications [17]. Sizing is a key component of glass fibres, largely dictating the success or failure of most reinforcement products. This is primarily due to its role in the price, processability, and performance of the final composite product. As the sizing is physically located on the surface of the fibre, characterisation of the properties of the fibre/matrix interphase and optimisation of the stress-transfer capabilities of this region are key in determining both the short- and long-term performance of composite materials.

Sizing is applied to the fibres directly as a water-based emulsion containing around 2–10 wt.% solids with final solid content on the fibre ranging from 0.3–1.5% by weight depending on the final application of the product. A glass fibre sizing typically contains [2]:

1. 5–15%: Organofunctional silane coupling agent(s) to provide adhesion between the surfaces of the glass and the resin matrix.
2. 50–70%: Film former(s) to provide protection and strand integrity to the roving in addition to aiding compatibility with matrix resins such as epoxy, polyester, and vinyl ester. While the range of film formers reflects the range of matrix materials available, commonly used film formers include polyvinyl acetates, polyurethanes, polyolefins,

polyesters, epoxies, and modified epoxies. Typically, these are low molecular weight compounds either identical to or highly compatible with the matrix resin.

3. 10–30%: Lubricant(s) to provide lubrication and protection of the filaments during processing.
4. 0–5%: Other additives such as anti-static agents, emulsifiers, anti-foaming agents, and bactericide.

The sizing application process is an extremely complex operation [17]. The fibre bundle is pulled at speeds as high as 60 m/s with collection of sizing occurring in less than 0.5 ms. The sizing must then fully impregnate the bundle prior to arriving at the first winding sheave less than 0.2 s afterwards. High purity water is also important in glass fibre manufacturing and sizing processes. It is used to cool fibres and acts as a sizing carrier and diluent. Distribution of the sizing on the glass surface is aided by the high wettability of the glass and to some degree, water also serves as a lubricant during manufacture. Following coating, continuous fibres are wound onto bobbins (or chopped to form mats), dried, and cured in an oven. In all cases, the optimisation of the sizing involves balancing cost, processing, and performance.

While the primary role of a glass fibre sizing is to act as a processing aid during manufacturing, it is also critical in the formation of a strong interface, thus ensuring that there is good transfer of the load applied to the composite from the polymer matrix material to the reinforcement fibres. To this end, a silane coupling agent is typically a key component of the sizing and plays a crucial role in ensuring the formation a strong interface [18].

Silanes typically take the structure [$X\text{-}Si(OR)_3$], where X is a reactive group and R is a methyl or ethyl group. Silane used in the treatment of glass fibre in an aqueous sizing is first hydrolysed to a silanol before being condensed onto the surface of the fibre through elimination of water molecules and formation of a siloxane network. Most silanes commonly used in glass fibre sizing applications have an X group containing either amino, epoxide, methacryl, or vinyl functionality [19]. The glass fibre sizing used is typically specific to the choice of polymer matrix material used and the application of the final composite. A variety of silane coupling agents may be used depending on the choice of matrix. For example: γ-aminopropyltriethoxysilane (APS) and γ-glycidoxypropyltrimethoxysilane (GPTMS) are typically used for epoxy resin applications, while γ-methacryloxypropyltrimethoxysilane (MPTMS) is typically used in vinyl ester and unsaturated polyester applications. The reactive groups present in the silane react with resin or hardener reactive groups. Beyond fibre/matrix linkage, silanes are well regarded as being essential in promoting interfacial adhesion and providing hydrothermal resistance at the interphase [20].

2.2.4 Micromechanical Testing Methods

It is well recognised that the nature of the fibre/matrix interface exerts a major influence on the mechanical properties of composite materials. Accordingly, a great deal of research has been focused on analysis of the interaction between glass fibres and polymer matrices. Testing methods designed to study the stress-transfer capabilities of composites typically fall into two categories, depending on the nature of the sample involved and the scale of the testing employed. Macromechanical testing methods concern bulk composite specimens and the measurement of inter-/intralaminar shear strength or transverse tensile strength, from which the interfacial properties are then inferred [21]. Conversely, micromechanical testing methods typically involve single fibre microcomposite samples [22].

Macromechanical testing methods may include interlaminar and short beam shear tests (promotes interfacial failure in shear mode) and 0°/90° tensile tests (relates interfacial shear strength to transverse cracking in the central 90° plies). In such tests there is little control of microscopic loading conditions or failure modes. While testing of composite specimens provides valuable information on the macroscopic properties of the material, the need to better understand the role of the fibre/matrix interface has led to the development and application of micromechanical techniques designed to specifically measure interfacial shear strength (IFSS). Macroscale testing of the composite material can only infer the IFSS, as this property is not directly measured, while the use of micromechanical tests introduces a greater sensitivity to changes in interfacial properties [23]. Methods of micromechanical testing include the pull-out test, the microbond test, the fragmentation test, the indentation test, and the push-out test. All testing methods are fundamentally concerned with probing behaviour at the individual fibre level.

Furthermore, single fibre methods require the use of less materials and are consequently cheaper than testing large-scale composite samples. This makes them well suited to the economical and time-efficient development of fibre sizings and assessment of composite processing parameters by enabling screening and optimisation without the need to scale-up to fabric production, laminate processing, and macromechanical testing [24,25]. Accordingly, the use of single fibre testing methodologies remains desirable in both research and industrial environments.

The Single Fibre Pull-Out Test

The single fibre pull-out test is one of the earliest of the interfacial testing methodologies developed [26]. A single fibre is embedded in a pool of liquid resin with the fibre axis perpendicular to the surface before curing [27]. A tensile tester or similar apparatus is then used to pull the fibre out of the cured matrix. An assumption is made that the force measured is equal to the shearing force applied to the entire interface and is uniformly distributed. *Figure 2:2* illustrates a schematic diagram of the single fibre pull-out test.

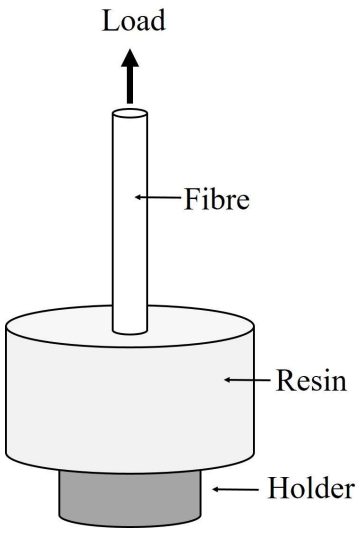

Figure 2:2: Schematic diagram of the pull-out test

A serious limitation of the method becomes apparent when fine fibres are used, as is often the case with typical composite reinforcement fibres such as carbon, glass, or aramid. If the force required to pull the fibre from the matrix exceeds the breaking strength of the fibre then the fibre will rupture before debonding is able to take place, invalidating any measurement of interfacial tenacity. Given the small diameters of reinforcement fibres, this requires an embedded length of less than 0.1 mm. One of the fundamental problems that limits the effectiveness of the single fibre pull-out test is that any method that involves partial immersion of the fibre results in the formation of an elevated meniscus. Unless the matrix material is extremely dense, the height of the meniscus can be up to 1 mm, making it difficult to ensure embedded lengths are below this value. Furthermore, successful use of small diameter fibres with the pull-out test requires an extremely thin matrix film (of the order of 0.05 mm) in order to allow the fibre to be successfully debonded from the matrix material without the fibre fracturing prematurely.

In terms of beneficial applications, Piggott and Xiong reported that, under appropriate conditions, single fibre pull-out testing could give results on interfacial yielding stress and

interface work of fracture without requiring corrections to account for friction [28]. The microbond test has, however, largely superseded the single fibre pull-out test due to more lenient sample preparation requirements.

The Microbond Test

The microbond test was developed by Miller *et al.* as an improvement to the single fibre pull-out test and addresses some of the issues t with the test [29]. In comparison to the resin blocks produced for the pull-out test, it is a great deal easier to create microdroplets (of diameter approximately 40 to 100 μm) for testing. The test typically involves a single microdroplet of matrix material cured in place on an individual fibre. The microdroplet is then restrained by opposing shearing blades and tensile force applied to the fibre until the fibre debonds from the matrix material. As with the single fibre pull-out test it is important to ensure that a successful debond has taken place, instead of fibre fracture. *Figure 2:3* shows a schematic diagram of a typical microbond test experiment configuration.

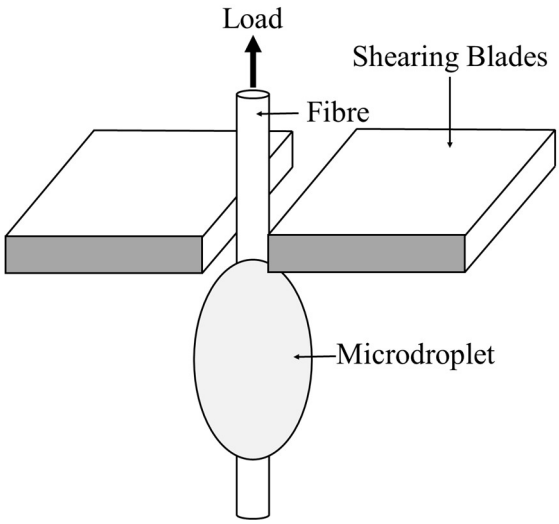

Figure 2:3: Schematic diagram of the microbond test

IFSS is calculated by dividing the force required to debond the droplet by the droplet embedded area. Successful and unsuccessful tests (due to premature fracture or otherwise) can be discriminated by examination of load versus displacement plots. The primary benefit of the microbond test is that the force at the moment of debonding can be accurately measured. In addition, the technique allows for almost any combination of fibre and matrix to be used.

Inherent limitations to the microbond test are often related to the meniscus formed on the fibre resulting in inaccuracies in measuring the embedded length. The presence of this meniscus may also have a sizeable effect on the variation of interfacial stresses along the length

of the embedded fibre and induce premature failure of the microdroplet [30]. The small size of the microdroplet can also make the failure process difficult to observe clearly (though this can be mitigated to some extent by a suitable microscope and camera set-up). The state of stress in the droplet may vary with both the size of the droplet and the points of contact with the blades. Large scatter in the data is common and has been attributed to testing parameters such as blade positioning [22] and droplet gripping [31]. Furthermore, the nature of the fibre (chemical, physical, and morphological) may vary along its length and influence IFSS measurements which consider only a small section of fibre [32].

Variations on the microbond testing technique have been developed by a number of researchers in order to expand the scope and capability of the test. Some of these include fixed [33] or movable [34] shearing blades, circular loading configurations [35], or alterations to the apparatus in order to test for IFSS dependence on other factors such as temperature [36] and humidity [37]. The microbond test has been used extensively in the literature in order to characterise the tenacity of the interface between a number of different types of fibre (glass [38], carbon [39], aramid [40], polyethylene [41], silk [42], cellulose [43], polyamide [44]) and various polymer matrices (epoxy [45], polyester [46], polypropylene [47], vinyl ester [48]) encompassing a wide range of both thermosetting and thermoplastic materials.

The Fragmentation Test

The single fibre fragmentation test involves tensile loading of an embedded single fibre within a cured matrix dogbone. The specimen is typically cast in an open-faced silicone mould or compression moulded depending on the selection of liquid thermoset [49,50] or thermoplastic matrix materials [51,52]. It is essential that the matrix is ductile enough to absorb the energy released when the fibre breaks without fracturing when subjected to a tensile load. Loading is continued and additional fibre breaks occur until the specimen fractures. Fibre breakages and interfacial debonding of transparent matrices can be observed using polarised light microscopy. Opaque matrix materials can be removed by post-test heat treatment and fibre fragmented lengths may be measured retroactively. The test operates on the principle that fibres continue to fragment into shorter lengths until they are unable to develop tensile stresses through shear transfer from the matrix sufficient to break the fibre further. The critical fibre length is defined as the shortest fragment length capable of breaking on stress application and can be used in combination with the fibre tensile strength to calculate the IFSS [53]. *Figure 2:4* shows a schematic diagram of a typical fragmentation test.

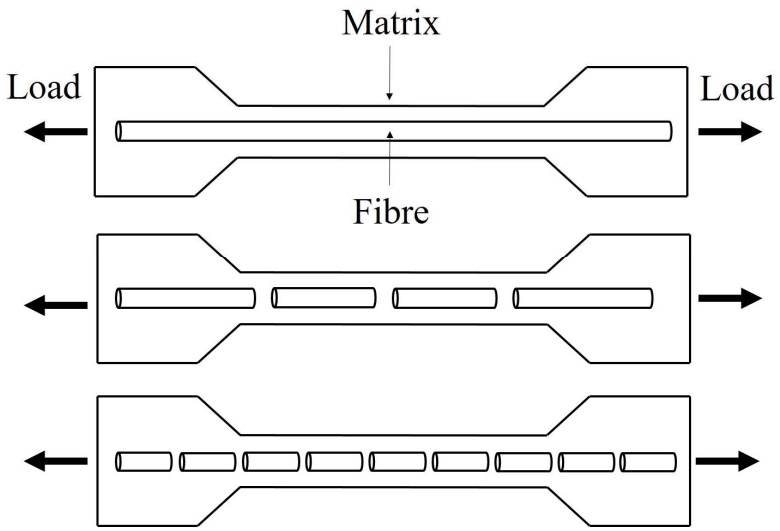

Figure 2:4: Schematic diagram of the fragmentation test

The primary benefits of the fragmentation test are that the technique yields a fairly large amount of information for statistical sampling, allows observation of the failure process under polarised light (for transparent matrices), and more closely replicates in-situ composite behaviour. The fragmentation test is limited by the fact that the matrix strain limit must be at least three times greater than that of the fibre and must be sufficiently tough to prevent failure via induced fibre fracture [54]. Furthermore, calculation of fibre strength at the critical length relies on Weibull analysis methods that have been criticised [55]. Additional shortcomings of the method include higher transfer normal stresses induced by Poisson's effect leading to higher IFSS values, stress state at the interface being complicated by the presence of cracks that affect values of IFSS, and reliance on an oversimplified representation of stress state at the interphase.

In their analysis of stress transfer in the fragmentation test, Nairn *et al.* reported that the assumption that IFSS was constant was simply unrealistic for many interfaces. The use of one-dimensional methods revealed no information about radial stresses and did little to account for thermal stresses and frictional effects [56]. Furthermore, only qualitative measurements of interfacial parameters could be garnered from such assumptions, which are ultimately of little practical use in predicting the role of interface in composite laminates. Criticism was also levelled at the body of work that employed the fragmentation test and reported only on the critical length and corresponding IFSS. The authors suggested that due to the dependence of critical length on a damage zone, it was possible that critical length measurements were not entirely relevant when scaled up to real laminates.

A number of authors have criticised the fragmentation test due to assumptions made in deriving interfacial strength from critical fibre length measurements. A study by Dai and Piggott concluded that reliance on an extrapolation of fibre strength (from around 20 mm down to 0.3 mm) was totally invalid, and was potentially responsible for a number of discrepancies observed when the fragmentation, and other, testing methods were used to measure interfacial properties of the same system [55]. The application of Weibull statistics to carbon fibres was considered very misleading, with little in the way of a suitable alternative to measure fibre strength at fragmentation lengths. Further criticisms involved the use of hypothetical flaw distributions and statistical variations due to variance in fibre diameter. Measurement of strength at approximately four-thirds of the mean fragmentation length, or observation using polarised light, were suggested methods for improving the feasibility of the test. However, the former is difficult to perform and contains unknown variations along the fibre length, while the latter loses the simplicity of the original testing method. Further studies by Galiotis [57], Piggott [58], and Figueroa *et al.* [59], have invalidated the assumption that interfacial stress is constant along the fibre surface. Work by Feillard *et al.* indicates that one-dimensional models are too simplistic, micro- and macroscopic parameters are not comparable, and that fragmentation test analysis is often not rigorous [60].

Tripathi and Jones note that the use of the method is limited by the absence of a data reduction methodology for an interfacial parameter which can be correlated to changes in the fibre surface chemistry [53]. The presence of sizing on most fibres further complicates the method as sizing may affect matrix resin properties in the stress-transfer region. The authors also conclude that, as a result of these limiting factors, the fragmentation test cannot be used with confidence for the selection of suitable surface treatments for glass, carbon, or aramid fibres. Furthermore, though sophisticated statistical techniques are used to characterise the fibre fragment length distribution, the IFSS is calculated using an oversimplified representation of the stress occurring at the interface.

The Indentation Test

The indentation test is one of the newer methods of measuring IFSS. Despite being a single fibre method, the test utilises a practical composite specimen [61–63]. Sample preparation involves sectioning and polishing a unidirectional composite normal to the direction of the fibre. An optical microscope is used to accurately centre a microprobe on an individual fibre and a compressive load is applied until the fibre debonds from the matrix material at the

surface. Analysis can be performed to calculate the stresses at the interface during failure. *Figure 2:5* shows a schematic diagram of a typical indentation test experimental configuration.

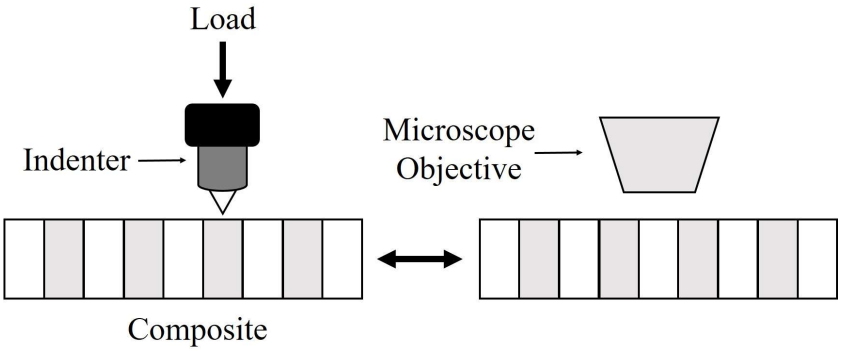

Figure 2:5: Schematic diagram of the indentation test

The primary benefits of the indentation test are that it allows for in-situ measurements on debonding force and assessment of the interface in "real" composite samples. Data collection is both fast and automatable (making the process attractive to industry) and multiple data points are yielded. In comparison with single fibre micromechanical tests, more realistic simulations of thermal stresses, polymer morphology, and the influence of the neighbouring fibres are accounted for. The indentation test is limited by the fact that failure modes or locus of failure cannot be observed, the introduction of artefacts and damage to the interface during the surface polishing process, potentially invalid assumptions being used to calculate IFSS, and fibre crushing limiting the types of fibres that can be effectively used with the test. The presence of surrounding fibres also complicates the calculation of the stress state around the fibre and makes choosing an appropriate failure criterion more difficult.

The single fibre push-out test is a variation on the indentation test that uses is a thin polished section of unidirectional composite material [64,65]. The other primary difference between the two tests is that the push-out test results in the fibre being fully removed from the matrix as opposed to being indented. A microprobe is used to push individual fibres out from the matrix. Apparatus typically used include probes with tip diameters in the region of 5 μm and samples of composite sheet in the region of 20–40 μm thickness. IFSS can be calculated by dividing the force required to push out a single fibre by the area of the interfacial bond. Compared to single fibre methods, push-out tests allow direct assessment of interfacial parameters from practical composites and have the benefit of allowing the determination of fatigue and environmental effects on laboratory samples and in-service components [66]. The calculation of the stress state around the fibre is, however, complicated by neighbouring fibres. Furthermore, the method is both difficult to perform and requires complex sample preparation methods. The interface may also sustain damage during cutting and polishing [22,67].

2.2.5 Comparison of Micromechanical Testing Methods

A number of single fibre tests have been developed over the years in order to characterise fibre/matrix interfacial adhesion. Common to all methods is the measurement of fibre/matrix IFSS. However, methods typically differ in regards to both specimen geometry and how the data is interpreted. Accordingly, there is a growing number of sometimes conflicting data, depending not only on the testing method selected but also on the choice of materials and the assumptions that are made in order to calculate interfacial shear strength. Single fibre tests allow generation of comparative values between fibres with various sizings in combination with a wide range of matrix formulations, essentially providing an effective materials screening process. Doubts remain, however, as to what extent quantitative data from such methods can be effectively scaled up for macroscale design purposes. Furthermore, the relationship between interfacial shear strength values obtained from microscale testing methods and interlaminar shear strength in practical composites is not fully understood.

Stress-transfer conditions at the fibre/matrix interface are critical in optimising the properties of composite materials. While this parameter is often reduced to a discussion of "adhesion", it is important to consider that essential contributions to fibre efficiency, toughness, and stress-redistribution are closely tied to stress-transfer conditions. Scaled to the level of fibre production, it is highly desirable to have a method of material screening to either improve or reject various surface treatments, coatings, and/or sizings without considerable time and resources having to be invested in the manufacturing of a practical composite part as a control specimen. In theory, the ultimate goal of micromechanical testing techniques should involve the understanding of micromechanics being scaled to practical composite materials. Difficulties arise in the form of microstructural features being dependent on fibre volume fraction and the tenacity of the interphase in a real composite being highly sensitive to fabrication conditions. Nevertheless, micromechanical techniques offer a cost-effective method for assessing fundamental aspects of composite performance through characterisation of the load-transfer behaviour of the interface.

Galiotis observed in 1991 that "it is clear that the quest for the development of a standard technique for measuring the shear strength of the fibre/matrix interface, both in isolation and in real composites, is as pressing today as it was thirty years ago" [57]. Some thirty years further on it would appear that this statement holds equally true today. There remains little, if any, standardisation of micromechanical testing methods, with researchers and laboratories typically developing their own apparatus and specific methodologies.

Comparison of push-out and fragmentation tests results conducted by Mandell *et al.* showed disagreement between testing methods [66]. In a graphite/epoxy system, IFSS measured by fragmentation test was 67 MPa compared to 44 MPa measured by push-out test, both of which were lower than the short beam shear strength. IFSS of glass fibre/epoxy and glass fibre/polyester measured by fragmentation test were 79 MPa and 28 MPa, while push-out results were again significantly lower at 57 MPa and 23 MPa, respectively. Discrepancies were attributed to a difference in how bond strength was interpreted between the methods, though the authors proposed that the push-out test results, while consistently lower, provided absolute bond strengths of the same relative order as the fragmentation test.

Jacques and Favre reported that fragmentation and pull-out test results showed no correlation despite the same carbon fibre/epoxy system being studied [68]. IFSS of DGEBA epoxy and unsized untreated carbon fibre samples measured by pull-out test was more than double that of fragmentation test measurements. Further divergence was observed following the application of a surface treatment. Fragmentation tests were not successful when a tetraglycidyldiaminodiphenyl methane (TGDDM) resin matrix was used (due to high crack sensitivity and strong adhesion), while pull-out test results were high. Significant disparity was also observed when using a second smaller diameter carbon fibre. The authors concluded that the fragmentation test was suitable for examination of the effects of surface treatments on carbon and glass fibres, though its use was restricted to compliant and tough matrices.

Cranmer *et al.* proposed that no one method of micromechanical testing was suitable for all materials, and that no individual test provided measurement of all of the necessary information [69]. The combination of small fibre diameters, high processing temperatures, and handling required for each specimen made the use single fibre pull-out tests impractical for materials such as SiC_4, while indentation tests tended to crush fibres and caused inaccurate measurements. Pull-out tests were confirmed as the most direct method of determining interfacial strength, but relied on sufficiently large fibre diameters. Indentation tests used minimal material volumes but measurements were dependent on indenter geometry. Push-out tests required a more complex sample preparation procedure than indentation tests but analysis was both simpler and more reproducible. Contrary to other method comparisons, the authors reported that interfacial and debonding strength determined by a number of different methods showed good agreement. It was concluded that the push-out test appeared to be the most desirable testing method.

Galiotis reported that different methods of measuring IFSS of the same Kevlar 49/epoxy system resulted in significant differences in the range of values obtained [57]. IFSS determined by fragmentation tests ranged between 17 and 23 MPa, while pull-out test results ranged between 27 and 33 MPa. For a second epoxy matrix, closer correlation was found by comparison of microbond and pull-out tests, with values of 38 MPa and 41 MPa, respectively. Fragmentation test measurements were considered approximations of the shear stress between fibre and matrix, bearing little genuine comparison to the "actual" IFSS of the system under study. Measurement of true critical fibre length was also difficult to estimate due to fibre debonding occurring at strains as low as 1%, which accounted for the lower IFSS values reported. Conventional single fibre pull-out tests relied on the assumption that the applied force was equal to a uniformly-distributed shearing force along the interface which lowered values of IFSS. In the microbond test, the reduction of average IFSS proportional to lower embedded length was attributed to a non-uniform application of load to the droplet. However, it was noted that the higher value of 55 MPa obtained at embedded lengths of 50–100 μm was generally comparable to the values obtained using a Raman spectroscopy method.

In a discussion of comparison of interfacial micromechanical testing methods Piggott reported that data obtained from both pull-out and fragmentation tests was contaminated by friction. The same was true, albeit to a lesser extent, for the microbond test, which had its own complications due to the non-cylindrical bead shape [58]. It was concluded that these methodologies could be used to generate comparative data, though care must be taken when results from different methodologies were considered.

Piggott also proposed that discrepancies been results from different testing methods could be, in part, due to different force balances between friction and debonding stresses, those being dependent on differences in fibre and polymer Poisson shrinkages [58]. In fragmentation tests, the tendency towards lower values implied stronger frictional effects, and that fibre fragments were almost fully debonded. The fact that push-out tests generated IFSS values even lower than fragmentation tests implied that the method was influenced by friction to an even greater extent.

Herrera-Franco and Drzal compared microbond, fragmentation, and indentation tests to three macroscale composite laminate testing techniques (tensile, Iosipescu, and short beam shear) [22]. In agreement with the findings of Jacques and Favre [68], significant discrepancies were observed between carbon/m-PDA IFSS values generated by different micromechanical testing techniques. Contrary to the findings of [68], however, microbond tests always yielded lower results than fragmentation tests. The difference was attributed to the material properties

of the epoxy microdroplets being lower than those of the bulk matrix surrounding the embedded single fibre in fragmentation tests due to loss of curing agent related to a large surface-to-volume ratio. Indentation tests yielded the highest IFSS values, though the authors conceded that refinement of the technique was required in order to account for the effects of debonding criteria, free surface, residual stresses, effects of neighbouring fibres, and surface damage during specimen polishing.

An important consideration is that the effect of the same surface treatment was reflected differently in the IFSS data. Fragmentation and microbond tests indicated that the interfacial strength was almost doubled, while indentation data indicated an improvement of only 17%. Such results are a strong indication that micromechanical techniques react differently to conditions at the interphase. Good agreement was cited between fragmentation test results and ILSS measured by short beam shear test as both methods measured the same shear stress component. Closer correlation was shown between fragmentation and 45° off-axis tensile tests, however. The authors concluded that, despite the fact that micromechanical methods produced IFSS results comparable to those measured on practical composite specimens, reliance on single fibre techniques should be avoided until composite properties can be more reliably predicted. Single fibre methods yielded different sensitivities to interfacial strength, and no one technique offered an unambiguous method for measuring IFSS.

Comparison of microbond and fragmentation data for a Kevlar/epoxy system by Wagner *et al.* showed that IFSS measured by fragmentation test tended to be around 50% higher [35]. The authors disputed Herrera-Franco and Drzal's [22] proposal that diffusion of curing agent in microbond droplets lead to generally lower mechanical properties than the matrix surrounding fragmentation test samples. The discrepancy in IFSS values was instead attributed to the hypothesis that fragmentation tests tended to *over*estimate IFSS (as fragmentation phenomenon is not observed unless a minimum interfacial bond strength is reached), while the microbond test tended to *under*estimate the value (only samples where the interfacial bond strength is not high enough to cause fibre fracture are accepted). As a result, samples with larger embedded lengths and stronger interfaces were not sampled using the microbond test. Accordingly, "true" values of IFSS were predicted to fall somewhere between the values measured by the two methods.

Pitkethly *et al.* conducted an extensive round-robin programme to assess the compatibility of interfacial testing methods [70]. Twelve laboratories were invited to participate in an evaluation of the single fibre pull-out, microbond, fragmentation, and indentation tests. Each was supplied with the same untreated and surface treated carbon fibres, in addition to epoxy

resin, hardener, and catalyst from the same batch. All samples were cured according to an identical curing cycle. Pull-out tests adhered to the same general trend between laboratories, in that surface treated fibres always had higher IFSS than untreated fibres, though IFSS values for the same systems differed. Embedded length measurements varied by as much as an order of magnitude between laboratories. Depending on which laboratory conducted the test, IFSS was increased by 7.3 to 38.7 MPa following the application of the surface treatment. Microbond test results showed a similar behaviour. IFSS values for untreated carbon fibres ranged between 31.6 MPa and 63.2 MPa, while the IFSS of treated fibres was increased by a factor of 1.2 to 2. Contrary to the findings of Herrera-Franco and Drzal [22], and in agreement with Jacques and Favre [68], fragmentation test results were consistently lower than those generated using other testing methods. Indentation tests reflected a smaller increase in IFSS by a factor of approximately 1.1 for surface treated fibres, though data scatter in indentation test results was sufficient to render the effect of surface treatment marginal. A number of laboratories reported that IFSS depended on embedded length, while another found that, for untreated fibres, IFSS was entirely independent of embedded length. Despite high data scatter in both the results of individual test methods and between different test methods, scatter within individual laboratories was sufficient for confidence in the results. Variations in the experimental set-up and data scatter, however, complicated comparisons between laboratories.

Pitkethly *et al.* concluded their round-robin with the intimation that there was "great potential for achieving standard procedures and reducing the inter-laboratory scatter", though to date, experimental procedures are still typically developed and utilised on a lab-to-lab basis. It seems clear that, despite the relative simplicity of many micromechanical testing methods, discrepancies arise between the results determined by: I) different testing methods using the same fibre/matrix combination, and II) the results of different laboratories using the same testing method to investigate identical systems.

2.2.6 The Microbond Test: Experimental Parameters and Considerations

The microbond test was selected as the micromechanical method used for the duration of the investigation. The fragmentation test was deemed unsuitable for an experimental investigation involving current and experimental glass fibres sizings and multiple matrix materials due to the absence of a data reduction methodology for an interfacial parameter which can be correlated to changes in the fibre surface chemistry [53], a lack of confidence in Weibull analysis methods [55], unrealistic assumptions used in the determination of IFSS [56], and exacting fibre/matrix compatibility requirements [54]. Micromechanical tests involving

practical composite parts such as the indentation and pull-out were not considered due to expensive and time-consuming procedures required to produce the initial macroscale composite parts and concerns related to the sample preparation and polishing processes required. While the review of the literature would suggest that no micromechanical test is free of drawbacks, the compatibility of the microbond test with a range of fibres and matrices makes it the best-suited methodology for use in the investigation. Further consideration is thus given to assessment of experimental parameters pertaining exclusively to the successful use of the microbond testing method.

Microdroplet Dimensions and Geometry

Miller *et al.* reported glass fibre/epoxy IFSS was relatively insensitive to droplet size in the 80–200 μm range [29]. Distribution of IFSS appeared to become narrower as embedded length increased, possibly indicating a lower average interfacial strength. However, the authors noted that both observations may have been an artefact of fibre fracture prior to debonding which reduced the data pool. Around 5% of glass fibre/epoxy samples with embedded length of 60–99 μm fractured prior to debonding while the fracture rate of samples in the 140–179 μm range was more than 60%. The authors concluded that as droplet embedded length increased, the probability of premature fibre fracture increased. As a consequence, when fibre tensile and interfacial strengths overlapped, a bias in favour of lower IFSS values became evident as embedded length increased.

Gaur and Miller later reported that the shearing force applied during microbond testing was not uniformly distributed over the embedded area and was instead concentrated on the upper part of the microdroplet [71]. Despite this, varying embedded length and ensuing contact area resulted in relatively insignificant changes in glass fibre/epoxy IFSS due to embedded area values covering only a narrow range. The authors proposed that embedded area would have to increase by several factors for a significant reduction in IFSS values to be observed.

Straub *et al.* similarly reported no bead size effects on IFSS within a predetermined testing range [72]. Adusumalli *et al.* observed epoxy considerably smaller “sub-droplets” adjacent to the primary droplet applied to aramid fibres [73]. IFSS measurements, however, remained constant between primary and sub-droplets, despite higher maximum debonding forces with larger droplets.

In their critical evaluation of the microbond test Haaksma and Cehelnik reported that the range of droplet sizes suitable for testing with small diameter fibres (such as aramid, carbon

and glass) was bounded by a lower limit of approximately 40 μm as a result of the ratio of a critical bead volume to the fibre diameter for successful formation of droplets [74]. The upper limit of the size of the droplet was dependent on the fibre tensile strength and was reached when fracture of the fibres occurred prior to successful debonding from the matrix. Furthermore, apparent IFSS was found to increase with embedded length/droplet size for certain fibre/matrix combinations.

Li *et al.* investigated the effect of droplet dimensions on glass and carbon fibre/epoxy interfacial shear strength [75]. Microdroplet embedded lengths ranged between 80-600 μm and 50-200 μm for glass and carbon fibre samples, respectively. Both experimental and simulation results showed that maximum load and IFSS increased as embedded length was increased.

Further specific recommendations for microbond droplet size include a recommendation by Gao *et al.* that droplet diameters should not exceed 180 μm in order to ensure that debonding occurs before fibre tensile failure based on a calculated IFSS upper bound of 50 MPa for epoxy-based matrices [76]. Herrera-Franco and Drzal have suggested that maximum embedded length in the microbond test ranges between 0.05–1.0 mm when using fibres of diameter 5–50 μm [22]. Pandey *et al.* proposed that droplet embedded length must be sufficiently small that shear failure occurs at the matrix and sufficiently large that droplets do not slip between the microvice blade [77]. Excessively large droplets may result in interfacial stress transfer exceeding fibre tensile strength, causing premature fibre fracture and introducing a bias in favour of lower IFSS values. More recently, Laurikainen *et al.* have advocated for the use of microdroplets encompassing a wide range of embedded lengths in order to mitigate data scatter [78].

A number of authors have also reported on experimental variations to the standard ellipsoidal microbond droplet shape to improve test compatibility with specific matrices. Liu *et al.* reported on the use of a modified microbond test method for the measurement of IFSS in an aqueous-based adhesive and a polyamide fibre [44]. As a result of the low viscosity of water-based polyurethane it was not possible to form droplets suitable for testing using conventional microbond sample preparation techniques. Disc-shaped microbond samples were prepared by aligning a vertical fibre through a 0.8 mm diameter pinhole punched in a mounting card. A needle was used to deposit the matrix onto the fibre, filling the hole, before the samples were cured and removed from the mounting card. The modified microbond test was successfully used to measure the influence of silane (APS) and plasma surface treatment on polyamide fibre/aqueous polyurethane IFSS. The authors reported that the distribution of

interfacial shear strength of the disc-shaped samples was in good agreement with that of a conventional ellipsoidal droplet model.

Morlin and Czigany reported on the development of a microbond testing method using cylindrical test specimens [79]. The authors reported that a cylindrical sample geometry resulted in significant reduction in the standard deviation of the measured data and that failure was observed exclusively at the fibre/matrix interface. Furthermore, apparent IFSS increased with sample embedded length.

Microvice Blade Angle and Gap Width

Analysis of the microbond test design by Haaksma and Cehelnik indicated that the method of load application had a significant influence on experimental results. Criticism was levelled at methods employing point loading (droplets in contact with shearing blade/vice edges) and it was found that ideal loading was achieved using a circular area of contact [74]. Similarly, Herrera-Franco and Drzal reported that as little as a 4 μm variation in the point of contact of the microdroplet with the support could cause notable differences in both the magnitude and location of shear stresses, a variable that the authors concluded was responsible for the high scatter in carbon fibre/epoxy microbond data [22]. Variations in relative point of contact were induced as microvice blades required adjustment between specimens to allow the fibre to pass through.

Chou *et al.* reported that the vice angle (as a function of microvice gap width) had a degree of influence at lower angles but little influence once higher values were reached [80]. The authors concluded that apparent IFSS tended to increase as gap width was widened. Analysis of the stress distribution and force balances, however, indicated that the apparent increase in IFSS represented an overestimation. Accordingly, it was recommended that the gap width of the microvice be kept as small (and as close to the fibre) as is practicable.

Heilhecker *et al.* investigated the effect of the vice angle in the microbond test [81]. Finite element analysis showed a non-uniform distribution of IFSS as a function of distance along the fibre/matrix interface. Specifically, that the position of maximum shear stress moved from the initial point of fibre/matrix contact towards the centre point of the fibre/matrix interface as the vice angle increased. The result was indicative that the vice angle played a significant role in the measurement of IFSS. Experimentally measured glass fibre/polyester average IFSS appeared to increase linearly with increasing vice angle, while maximum IFSS decreased linearly. The authors concluded, however, that large error bars in the experimental data

effectively masked any observable effects and that the sensitivity of their test apparatus was insufficient to observe any discernible differences in average IFSS.

Pandey *et al.* investigated the effect of testing parameters on microbond data scatter, examining both blade sharpness and separation [77]. Scatter was attributed to the large number of experimental parameters involved in a single measurement, such as vice angle, blade separation, and blade sharpness. The authors concluded that, as microbond tests are conducted on an extremely small scale, even slight variations in experimental test parameters may influence the results to a significant degree.

Conversely, Work by Wagner *et al.* indicated that IFSS measured by the microbond test was altogether insensitive to varying microbond loading configuration (parallel plate, parallel conical plate, circular loading) [35]. Results were practically identical between all three methods. The strong effect of microvice geometry previously reported by Haaksma and Cehelnik [74] was instead attributed to differences between the epoxy matrices and curing conditions used leading to compliant matrix microbond samples that were significantly more sensitive to loading conditions

Day and Rodrigez also reported that microvise gap width (between 20–80 μm) had no significant effect on experimentally measured Kevlar/epoxy IFSS [31]. On the other hand, and contrary to the findings of Chou *et al.* [80], a finite element model appeared to indicate that microvise edges placed close to the fibre caused stress, strain distribution, and maximum IFSS to be dependent on the gripping position. Placing knife edges further apart rendered stress distributions insensitive to blade position.

Crosshead Speed

Järvelä *et al.* investigated the effect of pull-out speeds between 0.05 and 1.0 mm/min using a three-fibre method [82]. The authors reported that at higher testing speeds the “bond does not have time to find its correct position” and often fractured before debonding, while conversely, lower pull-out speeds may affect the fracture mechanism of a viscoelastic system. Low pull-out speeds generally led to high scatter in the data due to small defects in the bond and the relatively long time between incremental pulls allowing fracture propagation to occur. The authors concluded that, while maximum IFSS was largely independent of crosshead speed, smaller scatter in the data was reported at speeds of 0.5 mm/min and increased on either side as a result of the phenomena discussed.

Gaur and Miller investigated the loading rate of epoxy microbond samples cured on Kevlar, glass, and carbon fibres by varying crosshead speed [71]. Loading rates within normal ranges (1–3 g/s), corresponding to a crosshead speed of 1 mm/min had no effect on IFSS in any of the fibre/matrix systems. Loading rate was varied by over two orders of magnitude (0.1–100 g/s) in the Kevlar/epoxy system, resulting in an IFSS increase of approximately 10%. The authors concluded that, provided extension rate was kept constant, there was no significant effect on apparent IFSS measured due to relatively small variations in loading rate caused by droplet distance from the load cell.

Straub *et al.* investigated the effects of time and temperature on the interfacial shear strength of aramid/epoxy composites using the microbond test [72]. Microbond tests were conducted with testing speeds ranging across three orders of magnitude (0.1–100 mm/min) and a temperature range of 21–130°C. It was observed that IFSS appeared to decrease with increased testing rate. At room temperature conditions, however, IFSS varied by less than 3 MPa when testing speed was raised from 0.1 to 10 mm/min. A significant reduction in IFSS, (around 50%) only became apparent when the testing speed was raised to 100 mm/min. Average IFSS values decreased with increased testing temperature.

Conversely, Zinck *et al.* have reported that crosshead speed had a significant influence on glass fibre/epoxy IFSS and interfacial toughness as measured by the microbond test [83]. Average IFSS was increased by 34 MPa when crosshead speed was increased from 0.05 mm/min to 0.5 mm/min and by only 6 MPa when crosshead speed was increased from 0.05 mm/min to 5 mm/min. The fracture behaviour of glassy polymers with low shear yield stresses may have changed with loading rate, evidenced by ductile failure of the interface at low pull-out speeds (0.05 mm/min). Interfacial failure transitioned to brittle as crosshead speed was increased. Visco-elastic and plastic contributions to matrix deformation were also dependent on the loading rate

Similarly, Morlin and Czigany investigated the testing speed of cylindrical microbond samples and found that IFSS was reduced in the 0.05–0.2 mm/min range, then increased up to speeds of 10 mm/min, after which IFSS remained constant [79]. The authors recommended cylindrical sample microbond tests be conducted at testing speeds of 10–100 mm/min.

Liu *et al.* have reported on the effect of testing speed during the microbond test using a carbon fibre/polyphenylene sulphide system [84]. Apparent IFSS increased with increasing embedded length at testing speeds below 0.02 mm/s and greater than 0.04 mm/s. IFSS remained constant at testing speeds in the range between the two values. This behaviour was attributed to a competitive equilibrium being reached between the effects of microdefects and

stress concentration in the fibre/matrix interface. The authors concluded that a testing speed in the range of 0.02–0.04 mm/s was effective for the evaluation of IFSS of a carbon fibre/polyphenylene sulphide composite.

More recently, testing speeds in the m/s range have been investigated by Tamrakar *et al.* [85]. A finite element model was used to determine optimum specimen geometry and a displacement rate wherein the sample remained in dynamic equilibrium at loading rates of up to of 10 m/s. The combination of a 2 mm gauge length and a 200 µm droplet had the greatest potential for high loading rates. The authors reported that glass fibre/epoxy IFSS was improved by a factor of 1.7 when testing speed was increased from 1 µm/s to 1m/s.

It can be concluded from study of the literature that glass fibre/epoxy IFSS is generally insensitive to crosshead speed within the 0.1–1 mm/min range. A strong effect of crosshead loading speed appeared to become apparent when non-ideal droplet curing behaviour was observed. Excessively high crosshead speeds (10 mm/min) may result in lower apparent IFSS and increased frequency of premature fibre fracture. Testing speeds in the m/s range may also result in significantly higher values of apparent IFSS. Higher testing speeds may be preferable, however, when the sample geometry is changed from an ellipsoidal microdroplet to a cylindrical specimen.

The effect of crosshead speed on IFSS is summarised in *Table 2-1*.

Material	Testing Speed	Conclusion	Ref.
Glass/urea-formaldehyde [TS]	0.05–1.0 mm/min	IFSS independent of crosshead speed. Lowest scatter at 0.5 mm/min. Increased fibre fracture at higher speeds.	[82]
Kevlar/glass/carbon /epoxy [TS]	0.1–100 g/s	No effect on IFSS within normal range. 10% increase when loading rate was increased by two orders of magnitude.	[71]
Aramid/epoxy [TS]	0.1–100 mm/min	Small decrease in IFSS in 0.1–100 mm/min range. Significant decrease at 100 mm/min.	[72]
Glass/epoxy [TS]	0.05–10 mm/min	Large IFSS increase when speed increased from 0.05 to 0.5 mm/min. Smaller increase wat 5 mm/min.	[83]
Glass/polyester [TS]	0.01–200 mm/min	0.1–0.2 mm/min IFSS decrease. 0.2–10 mm/min IFSS increase. 10–200 mm/min no effect.	[79]
Carbon/polyphenylene sulphide [TP]	0.001–0.15 mm/s	IFSS constant at 0.02–0.04 mm/s. Increased with embedded outside this range	[84]
Glass/epoxy [TS]	1 μm/s – 10 m/s	IFSS increase by a factor of 1.7 when tested at 10 m/s.	[85]

Table 2-1: Summary of effect of crosshead speed

[TS] = thermoset, [TP] = thermoplastic

Experimental Data Scatter

Significant scatter in the data is an issue found in all methods of micromechanical testing and is often a limiting factor in the efficacy of these testing methods. Scatter is particularly prevalent in microbond data, and can complicate comparisons of material systems or fibre surface treatments. Sources of error and experimental data scatter in the microbond test are identified and mitigation strategies proposed in the literature are reviewed.

Variation in microvice point of contact causing significant differences in the magnitude and location of shear stress has been cited by Herrera-Franco and Drzal as the primary cause of experimental data scatter in the microbond test [22]. As only the maximum debonding force is recorded in the microbond test, it is possible that due to variations in position of blade

contact, interfacial failure strengths can be reached at different values of applied force for droplets of the same dimensions, consequently affecting the values of IFSS calculated. Pitkethly *et al.* similarly note that an apparent lack of reliability in micromechanical testing methods can be ascribed to a combination of experimental procedures and the data reduction methodologies used to derive values of interfacial shear strength [70].

Conversely, Wagner *et al.* reported that data scatter was equally high for experimental set-ups where: I) the microvice gap width was adjusted between each sample, II) the microvice blade gap was identical for each sample, and III) when the loading geometry was changed [35]. Such results would imply that data scatter is a function of some other parameter unrelated to loading configuration. Furthermore, average IFSS was unaffected by loading conditions. The authors concluded that the only explanation for data scatter was the non-uniformity of fibre surfaces reported by Penn and Lee [32] and Miller *et al.* [86]. Typically, only a small number of fibres are selected from commercial fibre rovings that contain thousands of individual fibres.

Laurikainen *et al.* have recently investigated error sources in the microbond test and addressed the issue of high scatter in microbond test results [78]. Approximately 30–50 microdroplets of epoxy resin were deposited onto 50 individual W2020 filaments (1527 droplets in total) in order to study the effect of variation in sized glass fibre surfaces. Microbond tests were performed using an automated high-throughput testing device (FIBRObond). Filaments were 15 cm long and were removed in batches of ten, approximately 150 mm apart, from the larger roving, covering a total length of approximately 1.3 m. The authors reported that droplets deposited in close proximity to one another on the same filaments exhibited similar interfacial properties and that more significant data scatter emerged when different filaments were compared. Average IFSS of a W2020 glass fibre/epoxy system was reduced from around 53 MPa to 20–25 MPa in small sections of the roving. The findings proposed that much of the commonly observed scatter in microbond data originated from variation between filaments and that, contrary to the conventional wisdom in the literature, error from experimentation was quite small comparatively. Scatter could be mitigated by measurement of multiple droplets on a single filament encompassing a wide range of droplet sizes. The effect of microvice blade gap could also be largely removed by ensuring that the blades were touching, but not compressing, the fibre. As a result of the variations in IFSS values due to fibre surface changes, it was recommended that a suitably large number of individual filaments should be utilised in order to reliably characterise the interfacial properties of a given fibre/matrix combination.

Scatter in micromechanical experimental data has previously been attributed to the effects of different operators using the same apparatus to study the same material systems [69,87]. These concerns, however, have largely been addressed by a number of experimental investigations in the literature. Wagner *et al.* concluded that different operators did not contribute to data scatter, provided that operators were well-trained, conducted the test properly, and followed identical instructions detailing the experimental procedure [35]. Järvelä *et al.* have similarly reported that maximum IFSS values and data scatter was approximately the same for three different operators testing three different resins [82]. Laurikainen *et al.* reported that data scatter in the microbond test was due to variations in fibre surface, and that there was little significant error based on measurements from five different operators [78]. Determination of error in the measurement of embedded lengths by computer vision algorithm and human operator using a number of optical microscopy techniques indicated that the accuracy of each method was generally similar, and that variations between operators was small. Finally, test results of the round robin study conducted by Pitkethly *et al.* showed scatter within different individual laboratories was reasonably low but that scatter between laboratories was high due to differences in the experimental techniques and data reduction schemes employed [70].

Droplet Deposition Process

The process involved in the deposition of matrix droplets onto fibres is not widely reported in the literature though a number of different institutions and laboratories have employed various methods of application. Methods included collecting a small bead of resin on fine glass applicators [31], short lengths of steel wire [36], the tip of a syringe [41], tapered glass needles [42], steel needles [44], carbon fibre filaments [72], glass fibre filaments [88], wooden needles [89], and copper thread [90], which were then touched briefly to the fibre. Droplets form concentrically around the fibre due to surface tension and retain an ellipsoidal geometry after curing [29]. More recently, an automated FIBRObond apparatus that deposits multiple droplets by automated vertical movement of a single fibre through a resin well has been developed [91]. Thermoplastic matrix droplets are typically not applied to the fibre directly. Instead thermoplastic filaments [47] or films [43] may be attached to the fibre and heated to produce droplets. Burn *et al.* have, however, reported a similar application procedure using a B-staged epoxy matrix [92].

2.2.7 Glass Fibre Sizing and Interfacial Adhesion

A measure of the performance of a composite can be determined by the characteristics of the interphase region resulting from the interaction of a polymeric matrix with a reinforcing fibre. In order to facilitate efficient load-transfer through the interphase region it is essential to effectively utilise the strength and stiffness of reinforcement materials. A basic understanding of the chemistry, microstructure, and mechanics of the composite interphase region is of great value in optimising the design of new composite materials for a range of applications. The ability to transfer load is often discussed in terms of adhesion, that being a simple catch-all term that describes a combination of complex phenomena with no exact definition. As sizing is a critical component in the formation of the fibre/matrix interface, any investigation of interface similarly necessitates a degree of understanding relating to the science of sizing and the ability of sizing formulations to influence interfacial adhesion parameters.

Silane Coupling Agent

Silane coupling agents are generally well regarded as promoters of chemical interaction between fibre and matrix through covalent bonding and their ability to enhance interfacial adhesion is widely reported in the literature. Hydrolysis and condensation reactions promote the formation of a siloxane network with silanol groups available to react on the glass fibre surface. According to Tanoglu *et al.,* on contact with the matrix resin, the sizing and matrix begin to interdiffuse, resulting in the matrix dissolving the majority of the film former and emulsifiers and leaving only an interpenetrating network of cross-linked polysiloxane and resin interphase [93]. Accordingly, silane coupling agents are widely considered as a critical component responsible for good fibre/thermoset matrix adhesion by chemical bonding [94].

Miller *et al.* treated unsized glass fibres with 0.1–1% concentration solutions of APS [29]. The authors reported that glass fibre/epoxy IFSS was increased from 33 MPa to approximately 50 MPa following treatment with a 0.1% silane solution. Treatment with 0.5% and 1% solutions resulted in no appreciable increase in apparent IFSS. The inability of higher concentration solutions to effectively contribute to interfacial adhesion was attributed to cohesive failure within the thicker silane coatings.

A similar lack of effectiveness as a result of silane overtreatment has also been observed by Koenig and Emadipour using the pull-out test [20]. Contrary to the findings of *Miller et al.*, however, IFSS glass fibre/epoxy was unaffected following treatment with a 0.1% N-2-aminoethyl-3-aminopropyl trimethoxysilane (AAPS) solution and was optimised by treatment with a 0.5% solution. At treatment solutions greater than 0.5% IFSS decreased linearly and

was 14% and 27% lower than that of the unsized fibres when treated with 5% and 10% silane solutions, respectively.

Feresenbet *et al.* investigated the influence of blended silane sizings on both fibre surface morphology and glass fibre/epoxy IFSS [95]. Unsized E-glass fibres were coated with solutions containing a mixture of hydrolysed propryltrimethoxysilane (PTMO) and APS. Tapping mode atomic force microscopy (TMAFM) and elipsometry were used to characterise the morphology and thickness of coupling agent mixtures deposited on silicon wafers. Diffuse reflectance infrared Fourier-transform (DRIFT) analysis showed that E-glass fibres were only partially coated at coupling agent concentrations below 0.01%. Contact angle measurements showed an increase in polarity corresponding to increased APS content in the mixture. Apparent IFSS, determined by fragmentation test, increased with increasing APS concentration in the silane mixture, though there was no significant difference between IFSS values for 100% PTMO and 25% APS solutions or between 50% and 100% APS solutions. The authors concluded that both the coupling agent and the composition of the coupling agent mixture contributed to adhesion between the glass fibres and the epoxy matrix.

Gao *et al.* investigated the effect of fibre surface texture created from silane blends on the strength of the glass fibre/epoxy interface [76]. GPTMS and tetraethoxysilane (TEOS) were applied to glass fibres in various concentrations and blends. Atomic force microscopy (AFM) was used to characterise the fibre surface and interfacial adhesion was determined by the microbond test. The authors reported that IFSS was increased by approximately 40% compared to unsized fibres following the application of GPTMS. The increase was attributable to the silane acting as a bridge and facilitating chemical reaction with both the glass fibre and the epoxy/amine matrix. The use of a blended GPTMS/TEOS silane increased IFSS by approximately 70% at low TEOS concentration. Increasing TEOS concentration, however, resulted in a linear reduction in IFSS. Reduced adhesion in such cases was attributed to either a lack of significant change to fibre surface roughness related to TEOS content, or the large molar fraction of TEOS forming weak and brittle aggregates that sheared relatively easily.

Film Former

Given that “full” sizings constitute a combination of a number of components, consideration must also be given to the role of components such as film formers in the optimisation of the fibre/matrix interface. In their review of recent advances in fibre/matrix interphase engineering Karger-Kocsis *et al.* reported that “the effect of film former on the fibre/matrix adhesion cannot be neglected” given the complex polysiloxane network formed by the hydrolysis and

polycondensation of organosilanes in the presence of other additives present in the sizing formulation [96]. During the polycondensation process glass fibre surface hydroxyl groups can react with the hydrolysed organosilanes. Film formers, however, are typically linear polymers (as opposed to surface bonded cross-linked polysiloxane) and should be able to interdiffuse into the matrix. Accordingly, the film former component of a sizing should be highly compatible with the selected matrix material and silane coupling agent in the sizing.

Drown *et al.* reported on glass fibre sizings and their role in fibre/matrix adhesion [3]. Analysis was performed on model interphases consisting of epoxy resin mixed with a commercial glass fibre sizing (containing film former, silane coupling agent, anti-static agent, and lubricant) and unidirectional composite laminates. The authors reported that DMA measurements showed that glass transition temperature (T_g) reduced with increasing sizing content due to reduced crosslink density caused by the presence of silanes and other sizing components. Tensile modulus, storage moduli, and tensile strength were, however, improved with increased sizing content due to an anti-plasticisation effect. Characterisation of fibre/matrix adhesion by indentation test showed that the use of an epoxy-compatible sizing in conjunction with an epoxy matrix resulted in a 35% increase in IFSS compared to bare glass fibres and resulted in a change in failure mode. Improvements to IFSS were also consistent with increased composite mechanical properties such as ILSS, flexural strength, and failure stress. The increase in ILSS for epoxy-compatible fibres over bare fibres was 12%, significantly less than that of the increase in IFSS observed. The difference was attributed to a change in failure mode. It is also possible that the unsized interphase may have been affected to a greater extent by specimen polishing issues related to the indentation test process [22,67].

Mäder reported on the use of different sizing treatments for controlling the interphase properties of glass fibre/epoxy composites [97]. Glass fibres were sized with polyvinyl alcohol (PVOH) or mixed PVOH/PVA film formers only, APS coupling agent alone, or full sizings containing APS and either a polyurethane or epoxy film former. Dynamic wetting measurements were used to characterise fibre surface energy and the pull-out test was used to characterise adhesion between fibre and matrix. The authors reported that fibres sized with film former only exhibited IFSS values some 6–12 MPa below that of unsized fibres, while APS coupling agent alone produced the strongest interfacial adhesion. APS and PU film former increased IFSS, albeit less so than coupling agent alone, while APS and epoxy film former IFSS was statistically similar to unsized glass fibres. High IFSS values showed good correlation with high Wilhelmy forces and lower contact angles, and were indicative that phase interaction had occurred during wetting. Pure APS sizing did not appear to show shear stresses

during wetting, while shear stresses due to swelling of the film former were observed in APS/polyurethane samples. Strongest interfacial adhesion in the APS only samples was attributed to a combination of strong interaction between amino groups in the APS and the epoxy matrix and swelling/dissolution of film former not occurring due to its absence. Furthermore, the relatively strong adhesion properties of bare glass fibres (despite poor mechanical properties) were due to good wetting, hydrogen bond performance, and high surface free energy. The authors also reported that wetting tests could be used to study fibre/matrix interaction but that micromechanical and macromechanical testing is necessary to draw conclusions about the interphase. IFSS and transverse tensile strength were generally commensurate, while interlaminar and compressive shear strength did not reflect the expected adhesion and interphase properties.

Berg and Jones investigated the role of sizing film formers, coupling agents, and blends thereof on the formation of the interphase in glass fibre/epoxy composites [98]. Unsized E-glass fibres were dip-coated with sizings based on APS coupling agent and epoxy resin emulsions of low, medium, and high molecular weights. A commercial epoxy-compatible fibre was included as a control. The thickness and uniformity of the sizing layer was investigated using a combination of X-ray photoelectron spectroscopy (XPS) and SEM and IFSS was characterised using the fragmentation test. The possible properties of a silane-rich interphase were simulated by blending two of the film formers and the matrix resin. It was shown that the addition of film formers resulted in significant changes to the modulus, strength, and glass transition temperature of the matrix in certain cases. The authors reported that all the sized fibres exhibited lower IFSS than unsized fibres. Increasing silane concentration appeared to have little effect on apparent IFSS. Fibres containing epoxy film former alone generally had marginally greater IFSS values than when coupling agent was also present, due to modifications to the interphasial region. The degree of scatter in the results, however, rendered no real significant differences between the results of different fibres sizings and no evidence of fibre/matrix debonding was observed.

Zhao and Takeda sized glass fibres with GPTMS and MPTMS silane coupling agents only, a full sizing (consisting of APS, urethane film former, and paraffin lubricant), and urethane film former only [99]. Unsized glass fibres were included as baseline. Fragmentation tests showed that glass fibre/epoxy IFSS was increased by 10 and 20 MPa following the application of MPTMS and GPTMS, respectively. IFSS was significantly lower than unsized fibres (53 MPa) when a film former only (34 MPa) was applied, and further reductions occurred following application of the full sizing (20 MPa). Maximum IFSS observed in the GPTMS

fibres was attributed to possible chemical interaction between the silane and the epoxy matrix in addition to higher fibre tensile strength. Critical length measurements were, however, extremely similar between the two silanes. The adhesion-enhancing capability of an MPTMS coupling agent was attributed to improved fibre wettability and surface hydroxyl groups. Micro-damage modes were also strongly influenced by the choice of sizing. Fibres sized with GPTMS failed due to matrix cracking, while those sized with MPTMS exhibited a combination of interfacial debonding and matrix cracking. Low IFSS samples containing film former showed a two-stage interfacial damage region consisting of a smooth interfacial debonding region near the end of the fragmented fibre and a discontinuous spot-like debonding region similar to stick-slip some distance from the fracture. Finally, maximum composite tensile strength was not commensurate with maximum IFSS (MPTMS resulted in strongest composite parameters) due to differences in micro-damage modes. The authors concluded that interfacial adhesion must be optimised, and not necessarily maximised to improve UD composite properties. While higher IFSS enabled effective stress transfer, matrix microdamage was not appropriate for improving composite strength or tensile behaviour.

Pisanova and Mäder investigated the effect of silane coupling agent and a number of film former combinations on glass fibre/epoxy IFSS using the pull-out test [100]. Unsized glass fibres were compared to those coated with APS silane only, PVA film former only, or an APS/PU film former dispersion. Application of an APS coupling agent increased IFSS by a factor of more than 2 compared to the unsized glass fibres, while fibres sized with PVA film former only showed a marginal decrease in IFSS. The sizing containing APS coupling agent and PU film former increased IFSS by approximately 40% but was significantly lower compared to silane coupling agent alone. Covalent bonding formation was cited as the dominant contributor in determining adhesion and was promoted by the addition of silane. Amino groups present in the APS, which react with epoxy groups at the interface, may have acted as additional hardener for the epoxy. Furthermore, small contributions from chemical bonding between epoxy groups and the glass fibre surface may have significantly increased interfacial bond strength [101]. Reduced IFSS with the PVA film former was due to prevention of both covalent and acid-base bonds between the fibre surface and epoxy matrix and lack of reactive groups. Interdiffusion of PVA and epoxy chains may have also altered matrix properties around the fibre. Composite tensile strength showed good correlation with interfacial adhesion results and a linear relationship with IFSS.

Zinck *et al.* demonstrated that the structure of interphases resulting from different silane only (APS) and silane/film former combinations possessed significantly different properties [102]. Both epoxide- and polyester-compatible film formers were investigated. Silane coated fibres produced higher IFSS values than glass fibres sized with a commercial formulation containing the same APS coupling agent and a film former for two different epoxy/amine matrices. Adhesion when a film former was present was, however, improved over water sized fibres containing an anti-static agent only. For both matrices, adhesion performance when film former was present was further reduced by 12–15 MPa when tex and fibre diameter were increased. Micromechanical tensile testing results indicated that the average tensile strength of the fibres correlated with some of the adhesion measurements [103]. Silane only fibres were strongest, while those containing film former were weaker than water sized fibres.

Tanoglu *et al.* investigated the properties of the fibre/matrix interphase formed due to glass fibre sizings [93]. Epoxy/amine-compatible sized fibres were custom made for the investigation and contained an epoxy film former, surfactant, and GPTMS coupling agent. Acetone extraction indicated that only 17% of the total sizing was bound to the fibre and nuclear magnetic resonance (NMR) analysis of the extracted sizing showed that it consisted entirely of film former and surfactant, while the bound portion consisted of silane and surfactant. Furthermore, preparation and examination of model interphases showed that mechanical properties were significantly lower than those of the surrounding bulk matrix. Glass transition temperature of the interphase was determined to be –5°C, some 160°C below that of the bulk matrix, due to plasticisation by low molecular weight components in the fibre sizing. The authors concluded that mixtures of silane monomers, epoxy film former, and surfactant formed a single homogeneous interphasial phase that separated due to the condensation reaction of the silane component of the sizing and caused significant changes to the material thermomechanical properties.

Film former may also play a major role in the durability of interface. Work by Plonka *et al.* has shown that multiple-component fibre sizings underwent a considerable reduction in adhesion parameters (local IFSS, critical energy release rate) following hydrothermal treatment, while those containing only APS silane coupling agent were largely unaffected [104]. Local IFSS of the APS coated fibre was increased following hydrothermal treatment due to water removing excess physically bonded APS and reducing flaw severity. Highest initial IFSS values were obtained when an epoxy film former was used in combination with the silane, which correlated to the sizing with the highest surface polarity. IFSS was less than that of silane coated fibres when a PU film former was included in the sizing formulation,

while the inclusion of a polyester film former resulted in IFSS values approximately the same as silane coated fibres. The authors concluded that interfacial strength was highly dependent on the chemical nature of the fibre surface (controlled primarily through sizing formulation) and surface roughness.

The findings presented by Plonka *et al.* regarding the interfacial durability of silane coated fibres would, however, appear to contradict the proposal of Zinck *et al.* that "film former plays a major role in the durability of interfaces, since the sized fibre displays a much stronger resistance to hydrothermal treatment than the silane treated one" [105].

Mäder *et al.* sized E-glass fibres with formulations containing APS coupling agent alone, or APS and either polyurethane or epoxy resin film formers [106]. Unsized glass fibres were included as a comparative baseline and fibres were also sized with a matrix-incompatible polyvinylacetate film former (without coupling agent) in order to simulate weak interfacial adhesion. Pull-out test results showed that the application of a compatible fibre sizing increased apparent IFSS in all cases. The inclusion of APS alone increased IFSS by a factor of more than 100% compared to the unsized fibres, while APS/film former formulations also showed improved adhesion properties, albeit to a lesser extent than APS alone. IFSS was around 10 MPa higher with epoxy film former compared to fibres containing polyurethane film former. Samples containing the matrix-incompatible polyvinylacetate film former showed adhesion properties that were generally the same as unsized fibres. Strong interfacial strength in APS and APS/epoxy samples was attributed to tough ductile sizings promoting fibre/matrix adhesion and matrix interdiffusion. The moderate increase in IFSS observed in APS/polyurethane samples was possibly attributable to interdiffusion and development of an interpenetrating network, though improvements to adhesion strength by such methods alone is limited. Unsized and polyvinylacetate film former samples showed particularly low adhesion due to sudden debonding at smaller forces without prior stable crack propagation. Interfacial properties were commensurate with improved composite mechanical properties in that samples with high adhesion (APS, APS/epoxy) showed non-liner elastic behaviour and increased strain to failure, while those with low adhesion (APS/polyurethane, polyvinylacetate) failed at low strains.

Work by Jensen and McKnight showed that the addition of an epoxy-incompatible silane (PTMO) to a commercial sizing formulation containing an epoxy-compatible reactive silane (GPTMS) and a common epoxy dispersion film former had no significant effect on the measured IFSS [107]. The authors concluded, however, that the chemistry of the fibre/matrix

interphase was the main parameter in determining optimal composite structural and impact properties.

Gao *et al.* reported on the contribution of different sizing components to measured IFSS [108]. Microbond testing and AFM were performed on two model sizings and four commercial sizings. Model sizings contained either GPTMS silane only or a colloidal silica surface roughening agent only. Model glass fibres were sized using a dip-coating procedure that eliminated the influence of processing aids and surfactants present in the commercial sizing formulations. Commercial full sizings shared a common DGEBA epoxy dispersion film former and a silane coupling agent that was either compatible (GPTMS), mixed (GPTMS + PTMO), or incompatible (PTMO) with the epoxy matrix. A hybrid sizing containing, GPTMS, PTMO, and a silica roughening agent was also investigated. PTMO was selected based on its incompatibility with an epoxy matrix, while the compatibility of GPTMS was thought to improve chemical covalent bonding between fibre and matrix. GPTMS silane only specimens showed a moderate improvement of approximately 10 MPa (36 MPa) compared to unsized glass fibres (26 MPa), while colloidal silica treatment alone did not significantly improve IFSS within confidence limits (29 MPa), despite a large increase in surface roughness measured by AFM. The sizing containing an epoxy film former and matrix-compatible GPTMS increased IFSS to 41 MPa, while the matrix-incompatible coupling agent (28 MPa) was comparable to unsized fibres. The mixed silane/epoxy film former formulation (39 MPa) was comparable to the compatible sizing despite reduced chemical bonding potential due to the presence of PTMO. Direct comparison of the GPTMS only model sizing and the compatible sizing containing GPTMS indicated that the commercial sizing showed improved interfacial performance. This behaviour was potentially attributable to sizing additives such as film former, surfactants, and anti-static agents not present in the silane only samples and an interphase toughening effect. Maximum IFSS with the hybrid sizing (51 MPa) was commensurate with the highest value of surface roughness and was achieved by a combination of chemical bonding and surface texturing that promoted a progressive debonding mode while absorbing more energy via sliding compared to the compatible sizing.

The authors later correlated modifications to interfacial adhesion to macromechanical quasi-static punch shear testing results using the same sizing formulations [109]. Composite panel punch shear strength and energy absorption capabilities were increased by the hybrid sizing compared to the incompatible sizing due to the absence of reactive functional groups and mechanical interlocking, indicating a linear correlation with the IFSS data. The results confirmed the contribution of chemical bonding between fibre and resin to practical composite

strength following the inclusion of a matrix-compatible coupling agent. Surface texturing also contributed to increased composite strength. The authors concluded that clear linear correlation between micromechanical and macromechanical tests proved that the methodology was a good predictor of composite strength and energy absorption properties based on single fibre measurements.

Dey *et al.* reported on the influence of sizing formulation on glass/epoxy interphase properties [24]. The interfacial properties of five different S-glass sizing compositions with varying degrees of chemical reactivity were assessed using the microbond test. Glass fibres were sized with formulations containing the same film former (DGEBA epoxy) and different silane coupling agents (GPTMS, GPTMS/PTMO blend) or the same silane coupling agent (APS) and different film formers (polyazamide, polyurethane). Fibres were also sized with a silane coupling agent that contained a mixture of GPTMS, APS, and PTMO and a film former that was a blend of both DGEBA epoxy resin and polyurethane. Microbond testing results showed that the sizing containing reactive aminosilane and polyazamide film former clearly exhibited the highest IFSS value and strongest interfacial adhesion. Conversely, the sample with lowest IFSS contained an identical APS silane coupling agent in combination with a PU film former, some 90% less than that of APS/polyazamide. Highest IFSS was attributed to the reactivity of both the silane and film former with the epoxy matrix and a reaction between the silane and film former components themselves. Both the nature of and the quantity of the silanes remained constant, proving the substantial influence of film former reactivity. Sizings containing GPTMS and epoxy film former fibres showed moderate IFSS values. An increase of approximately 10 MPa was observed in GPTMS samples compared to GPTMS/PTMO samples due to the incompatibility of the mixed silane blend. The use of a mixed silane and mixed film former improved adhesion properties to a greater extent than GPTMS/epoxy combinations, attributable to silane and film former reactivity. The authors concluded that sizing chemistry and film former wettability played a key role in fibre/matrix adhesion. The inclusion of a matrix-compatible film former was shown to have a far greater effect than the use of a compatible silane.

Contrary to the findings of Gao *et al.* [108], optimised adhesion was not commensurate with maximum surface roughness. APS/polyazamide and mixed silane/mixed film former samples had the lowest surface roughness and highest IFSS, while highest surface roughness in APS/PU samples corresponded to the lowest IFSS values.

Epoxy Resin

Epoxy resin film former is a key component in many glass fibre sizings, indicated both by analysis of patent literature [110] and spectroscopic characterisation of sized glass fibres and sizing extracts [111]. However, to the best of the author's knowledge, no studies in the literature examine the influence of this sizing component on glass fibre/thermoset adhesion in any significant detail. The literature review was thus extended to studies of carbon fibre/thermoset adhesion.

Peters and Springer coated unsized graphite fibres with DER 332 DGEBA epoxy resin at a concentration of 1–2% of the fibre bundle weight [112]. Increased coating concentration, and corresponding epoxy sizing layer thickness, resulted in higher fracture strains. The application of the sizing influenced the fracture strain measurement by: I) affecting the fibre/matrix bond strength at the interface and II) affecting the fibre density within the bundle. It was proposed that the detrimental effect of increased fibre density was compensated by an increase in interfacial bond strength.

Drzal *et al.* investigated the role of chemical bonding and surface topography on adhesion between carbon fibre and epoxy matrices [101]. Carbon fibres were treated with varying amounts (20–600%) of DGEBA epoxy and m-PDA identical to the matrix materials used. Monofunctional butyl glycidyl ether (BGE) epoxy was also examined. XPS was used to perform fibre surface analysis and interfacial adhesion was characterised by fragmentation test. The authors reported that IFSS of as-received and acetone washed fibres was generally similar. Treatment with BGE alone had a detrimental effect on adhesion and reduced IFSS by 8–18 MPa depending on the amount of surface treatment. Poor adhesion in such samples was a direct result of chemical blocking of the fibre reactive sites by the BGE and prevention of a reaction with the epoxy/amine matrix. The samples were considered to be generally representative of the level of adhesion that could be attained without any chemical bonding between fibre and matrix. Fibres treated with m-PDA were statistically similar to both as-received and acetone washed fibres despite chemical bonding being detected. IFSS was highest in samples that were treated with DGEBA epoxy due to either improved chemical interaction with the bulk epoxy matrix, longer molecular chain length, or improved chemical bonding. In all cases, IFSS was increased with increasing level of fibre surface treatment. The results are indicative that a non-reactive epoxy film former was detrimental to interfacial adhesion in a carbon/fibre epoxy system, while a reactive DGEBA epoxy film former improved IFSS by some 34%.

Xu and Drzal reported on the improvement of carbon fibre/vinyl ester interfacial adhesion by use of a reactive epoxy coating [113]. An Epon 828 DGEBA and trimethylpropane amine (Jeffamine T403) mixture was allowed to begin curing at room temperature for 1.5 h before being added to acetone to form a 5 wt.% sizing solution. Unsized surface treated PAN-based AS4 carbon fibres (ø ≈ 8 μm) were sized using a pre-impregnation machine to simulate the sizing application and pre-pregging of carbon fibre/vinyl ester pre-preg in an industrial process. Dynamic mechanical thermal analysis and physical testing of composite specimens were used to evaluate the mechanical properties of matrix formulations and interfacial adhesion was characterised using the indentation test. Sizing uniformity was investigated with SEM, TGA was used to measure sizing layer thickness, and nanoindentaiton was used to determine the gradient of the sizing and the interphase between the applied DGEBA epoxy and the vinyl ester matrix. The authors reported that the application of a lightly cross-linked amine-cured epoxy polymer (DGEBA/T403) increased apparent IFSS compared to as-received fibres. Highest IFSS was attributed to diffusion of styrene monomers into the epoxy sizing creating a substantial change to fibre/matrix interphase, or possibly the formation of a gradient interphase. SEM analysis of fibres coated in 1–10% wt.% epoxy coatings indicated that, while sizing material distribution was uneven, a 5 wt.% sizing solution resulted in the most uniform coating. At higher concentrations visible "sizing bridges" appeared between fibres. Sizing layer thickness was also shown to play a role in adhesion, with a thickness of 90 nm giving the highest value of IFSS. It was proposed that an excessive amount of the softer sizing material at higher solution concentrations reduced IFSS.

In a later publication expanding on the work, Vautard and Drzal showed that improved interfacial adhesion following application of an epoxy coating correlated to macroscale composite mechanical properties [114]. Interface sensitive 90° transverse flexural properties showed good correlation with indentation test results. Flexural strength was increased by some 73% over uncoated fibres following the application of an epoxy coating. Optimal properties were obtained at a layer thickness (70 nm) below that of the [113], though good agreement was shown with a finite element model [115]. Furthermore, FTIR was used to characterise the degree of conversion of the epoxy used in the coating after a range of room temperature standing times (0–30 h) in addition to post-curing at 75°C and 125°C. The authors reported that flexural strength was optimised at a degree of conversion of 0.5. Higher conversions resulted in poor mechanical properties due to prevention of interpenetration between epoxy and vinyl ester molecules. A fully cured epoxy coating ($\alpha = 1$) produced values similar to that of uncoated fibres, a result that was also reflected in ILSS data. The 0° flexural strength was optimised at a coating thickness of 60 nm and was attributed to protection of the fibre integrity

during processing. Furthermore, the application of an epoxy coating appeared to retard some of the detrimental effects of cure shrinkage [115]. Diffusion of styrene into the epoxy coating was thought to result in coating expansion and annealing of residual stresses generated by volumetric cure shrinkage.

Zhang thermally desized carbon fibres (T700GC) at 700°C before recoating with DGEBA epoxy/polyetheramine dissolved in acetone to form 0.5 to 4 wt.% solutions [116]. Surface characterisation using SEM indicated good coating uniformity when epoxy coating concentration was below 4 wt.%, after which non-uniformity and sizing bridges between fibres became apparent. Fragmentation test results showed that desized carbon fibre/epoxy IFSS (34.2 MPa) increased by a factor of around 2 following the application of a 0.5 wt.% epoxy coating (66.4 MPa) to a value comparable to that of the baseline as-received sized fibres (65.4 MPa). IFSS increased with epoxy solution concentration and was maximised at 2 wt.% (87.9 MPa), after which IFSS improvement was reduced (57.4 MPa). IFSS of 2 wt.% epoxy coated fibres was improved over desized fibres by 54 MPa and induced a change in interfacial failure mode. Improved adhesion was attributed to a combination of increased surface roughness and enhanced chemical compatibility with the matrix. Furthermore, maximum IFSS corresponded to the most uniform coating. Epoxy/amine stoichiometry may have influenced the network structure and composition of the fibre sizing and excess amine may have reacted with the epoxy matrix. Poorer adhesion performance in the excessively coated 4 wt.% solution samples was attributed to reduced sizing uniformity and observed sizing "peel off" on the fibre surface. An epoxy coating did not improve IFSS of a second PAN-based epoxy-compatible sized carbon fibre (HTS40). IFSS was lower than the baseline as-received and desized fibres in all cases, due to potential differences in surface chemical composition. Furthermore, fibre tensile strength measurements were generally insensitive to the application of an epoxy coating.

Zhang *et al.* reported that the application of a carbon fibre sizing containing DER 331 epoxy resin, polyethylene glycol (PEG 4000), and triphenylphosphine catalyst showed significantly improved fibre tensile strength and ILSS [117]. Increased tensile strength was attributed to uniform distribution of the sizing agent preventing excessive stress spreading from flaws and sized fibres had less flaws than their unsized counterparts. Increased interfacial adhesion was attributed to enhanced chemical interaction due to increased oxygen content on the carbon fibre surface. SEM analysis of fracture surfaces showed clean pull-out profiles and confirmed weak adhesion on unsized samples. Work by Zhang *et al.* has also indicated that the molecular weight of the epoxy component in sizings may play a role in the determination of interfacial adhesion [118]. The authors reported that the ILSS of carbon fibre/epoxy composites

containing three model sizings containing epoxy resins of varying equivalent weight was decreased when both high and low molecular weight sizing agents were used. Conversely, the use of a moderate molecular weight epoxy resin in the sizing resulted in increased interfacial adhesion and resistance to hygrothermal ageing.

He *et al.* sized carbon fibres with 2–11 wt.% novolac resin/acetone solutions corresponding to 1.6–15.6% LOI [119]. Short beam shear test results indicated optimised adhesion properties following a 5% sizing treatment after which ILSS decreased sharply to a level below that of the untreated fibres. Improved adhesion in 5 wt.% samples was confirmed by fracture surface analysis. Furthermore, SEM observation of "hooklike protuberances" was indicative of strong interfacial bonding and a change in fracture mechanism from adhesive to cohesive failure. Decreased adhesion following 8–11 wt.% treatments was attributed to smooth fibre surfaces inducing weak bonding between the carbon fibres and epoxy matrix.

Conversely, Liao and Tung reported that interfacial adhesion was, in all cases, reduced following the application of an unreacted epoxy/acetone solution [120]. Microbond testing results showed that carbon fibre/epoxy IFSS was highest with baseline desized fibres and decreased linearly with increasing epoxy content (6.25–100 wt.%) in the coatings. The authors reported that decreased IFSS was attributable to reduced interlayer modulus. Furthermore, reduced IFSS with increasing epoxy/acetone solution concentration was reproducible across a number of epoxy matrix and curing agent combinations.

2.2.8 Conclusions of Literature Review

The findings of the literature review indicated that there is little, if any, agreement as to mechanism behind fibre sizing and improved interfacial adhesion. A number authors would appear to report markedly different, and often contradictory, results regarding which sizing components are responsible for contributions to increased or diminished adhesion properties. It would appear to remain unclear whether silane coupling agents alone, or full sizings containing both silane and a polymeric film former, are responsible for optimised IFSS. Furthermore, the contribution of the film formers and processing agents (such as surfactants and lubricants) are generally not well understood.

A number of investigations have reported that glass fibre/epoxy IFSS was significantly increased by the application of a silane coupling agent alone [29], and that coupling agent performance depended on silane solution concentration [20,29] and composition [76,95]. Furthermore, silanes have been shown to offer improved adhesion properties in the absence of

a film former [97,99,106]. Conversely, IFSS has previously been maximised when an epoxy film former was used in combination with an APS silane compared to silane alone [104]. Interaction between silane and film formers is also an important consideration [24].

Improvement of carbon fibre interfacial adhesion with vinyl ester [112–115] and epoxy matrices [101,116] by the use of a reactive epoxy coating has been reported by a number of authors. An epoxy coating significantly improved interfacial adhesion at the microscale and enhanced composite properties. Adhesion was optimised by controlling epoxy reactivity [101], thickness of the sizing layer [113], and the degree of conversion of the epoxy resin [115]. Improved adhesion was attributed to improved chemical bonding [101], diffusion of styrene monomers into the sizing affecting fibre/matrix interphase [113], and chemical interaction with the matrix [117]. Excessive solution concentrations and layer thicknesses, however, resulted in poor adhesion due to the formation of visible "sizing bridges" and reduced sizing uniformity. Improvement to interfacial adhesion by the application of an epoxy coating in carbon/epoxy systems and the lack of previous investigation of the adhesion-enhancing properties of the epoxy film former component in glass fibre sizings suggests excellent scope for investigation of sizings consisting of an epoxy film former alone.

The effect of sizing composition (silane coupling agent, polymeric film former, and other additives) on glass fibre/epoxy interfacial adhesion is summarised in *Table 2-2.*

Test	Coupling Agent	Film Former	Other	IFSS (MPa)	Ref.
Microbond		Unsized		33.1	[29]
	APS (0.1%)	-	-	47.7[1]/49.6[2]	
	APS (0.5%)	-	-	35.4[1]/29.1[2]	
	APS (1.0%)	-	-	35.5[1]/32.1[2]	
Pull-out		Unsized		18.5	[20]
	AAPS (0.1%)	-	-	17.2	
	AAPS (0.5%)	-	-	32.6	
	AAPS (1.0%)	-	-	27.2	
	AAPS (1.5%)	-	-	24.1	
	AAPS (2.0%)	-	-	21.1	
	AAPS (5.0%)	-	-	15.9	
	AAPS (10.0%)	-	-	13.5	
Fragmentation	APS	-	-	*97.0	[95]
	APS/PTMO (50/50)	-	-	*99.0	
	APS/PTMO (25/75)	-	-	*68.0	
	PTMO	-	-	*71.0	
Microbond		Unsized		*25.5	[76]
	GPTMS	-	-	*36.5	
	GPTMS/TEOS (75/25)	-	-	*43.0	
	GPTMS/TEOS (50/50)	-	-	*38.0	
	GPTMS/TEOS (25/75)	-	-	*28.0	
Indentation		Unsized		44.6	[3]
	Undisclosed epoxy-compatible full sizing			60.1	
Pull-out		Unsized		49.9	[97]
	-	PVA	-	44.0	
	-	PVA/PVOH	-	38.0	
	APS	-	-	71.4	
	APS	PU	-	62.5	
	APS	Epoxy	-	51.2	
Fragmentation		Unsized		49.0[A]/48.0[B]	[98]
	APS (0.1%)	-	-	*41.0[A]/37.0[B]	
	APS (1%)	-	-	*38.0[A]/37.0[B]	
	-	Low M_w epoxy	-	*40.5[A]/39.0[B]	
	-	Med. M_w epoxy	-	*41.0[A]/36.5[B]	
	-	High M_w epoxy	-	*39.0[A]/35.0[B]	
	APS (0.1%)	Low M_w epoxy	-	*40.0[A]/-	
	APS (0.1%)	Med. M_w epoxy	-	*38.5[A]/-	
	APS (0.1%)	High M_w epoxy	-	*34.0[A]/-	
	Epoxy-based commercial sizing			*39.5[A]/34.0[B]	
Fragmentation		Unsized		53.0	[99]
	GPTMS	-	-	72.0	
	MPTMS	-	-	62.0	
	-	Urethane	-	34.0	
	APS	Urethane	Paraffin lubricant	20.0	

Pull-out		Unsized		$45.9^{mean}/59.7^{ult}$	[100]
	APS	-	-	$101.1^{mean}/160.7^{ult}$	
	APS	PU		$65.6^{mean}/84.3^{ult}$	
	-	PVA	-	$48.8^{mean}/51.0^{ult}$	
Microbond	-	-	Anti-static agent	$56.0^{A}/71.0^{B}$	[102]
	APS	-	-	$89.0^{A}/84.0^{B}$	
	APS	Epoxy/polyester-compatible	Lubricant	$80.0^{A}/77.0^{B}$	
	APS	Epoxy/polyester-compatible	Lubricant, increased tex and diameter	$65.0^{A}/65.0^{B}$	
Pull-out	APS (0.3%)	-	Surfactant, lubricant	56.1	[104]
	APS (0.3%)	PU		48.8	
	APS (0.3%)	Epoxy		69.2	
	APS (0.3%)	Polyester		56.4	
	Undisclosed commercial sizing			60.2	
Pull-out		Unsized		$46.7^{app}/59.4^{ult}$	[106]
	APS	-	-	$99.2^{app}/104.4^{ult}$	
	APS	PU	-	$70.0^{app}/77.9^{ult}$	
	APS	Epoxy	-	$88.6^{app}/96.1^{ult}$	
	-	PVA	-	$49.7^{app}/58.6^{ult}$	
Short beam shear	GPTMS	Epoxy	-	39.8	[107]
	GPTMS/PTMO	Epoxy	Colloidal silica	41.7	
Microbond		Unsized		26.0	[108]
	-	-	Colloidal silica	29.0	
	GPTMS (0.5%)	-	-	36.0	
	GPTMS (0.5%)	Epoxy	-	41.0	
	PTMO (0.5%)	Epoxy	-	28.0	
	GPTMS/PTMO	Epoxy	-	39.0	
	GPTMS/PTMO	Epoxy	Colloidal silica	53.0	
Microbond	GPTMS	Epoxy	-	*72.0	[24]
	GPTMS/PTMO	Epoxy	-	*63.0	
	APS	Polyazamide	-	*114.0	
	APS	PU	-	*60.0	
	GPTMS/APS/PTMO	Epoxy/PU	-	*92.0	

Table 2-2: Summary of the effect of sizing composition on glass fibre/epoxy IFSS

$^{+}$ = present in all sizings, * = estimated from graph, ^{1} = data set 1, ^{2} = data set 2, ^{A} = epoxy 1, ^{B} = epoxy 2, ^{app} = apparent IFSS, ^{ult} = ultimate IFSS

2.3 EXPERIMENTAL

2.3.1 Materials

Glass Fibres

Bare (water-sized) and silane coated E-glass fibres were taken from larger rovings supplied by Owens Corning. Fibres were produced on a pilot-scale bushing and wound as 20 kg continuous rovings of nominal tex 1200 g/km with an average fibre diameter of 17.5 μm. Bare fibres were sprayed only with water during the cooling phase of production. Silanes were applied immediately following the cooling phase with a rotating cylinder (kiss roller) applicator. Following the coating procedure all fibre packages were dried at 105°C for 24 h. Despite the relatively large range of different silane molecules, the sizing products used by the majority of the glass fibre industry are typically based on four silane chemistries containing, in order of prevalence in the literature, either amino, epoxide, methacryl, or vinyl functionality [19]. Accordingly, the silane coupling agents investigated were:

1. γ-aminopropyltriethoxysilane (APS)
2. γ-glycidyloxypropyltrimethoxysilane (GPTMS)
3. γ-methacryloxypropyltrimethoxysilane (MPTMS)

Due to their significantly lower prevalence in the literature and industry, vinyl silanes were not investigated [1]. A number of silanes were applied in-house to encompass a wider range of silane chemistries and investigate any differences attributable to the method of silane application (kiss-rolled, dip-coated). Bare (water-sized) fibres were sized with the same epoxy-functional GPTMS coupling agent and two additional epoxysilanes described in glass fibre sizing formulation patent literature [110]. Silanes were purchased from Sigma Aldrich and Fluorochem.

1. γ-glycidyloxypropyltrimethoxysilane (GPTMS)
2. γ-glycidoxypropylmethyldimethoxysilane (GPMMS)
3. γ-glycidoxypropylmethyldiethoxysilane (GPMES)

For all in-house silane coatings, a pH meter was first calibrated using buffer solutions of pH 4,7 and 10. A dilute acetic acid solution was used to adjust the pH of deionised water to between pH 5 and 5.5 in order to promote hydrolysis of the silane in water. A 1 vol.% silane solution was prepared and hydrolysed for 24 h in a sealed volumetric flask. Three unsized glass fibre bundles were completely immersed in the silane solution for 15 min, removed, and dried for 12 h at 110°C [121,122].

Fully sized epoxy-compatible commercial fibres (Advantex SE1500 and SE2020) were taken from larger rovings supplied by 3B and HiPer-Tex W2020 was supplied by Suzlon Energy Ltd. For all fibres provided in the form of a roving bobbin, only fibres from the inside of the roving were used due to concerns related to damage during packing, storage, and transportation. Flat edges of the roving were avoided due to potentially increased sizing concentrations. Additional fully-sized commercial fibres, two epoxy-compatible (Si-E1, Si-E2) and one polypropylene-compatible (Si-PP) were taken from larger rovings supplied by Şişecam. Sizing formulations were not disclosed.

An acetone extraction procedure was performed to remove the majority of the sizing from commercially sized fibres [123]. SE1500, SE2020, and W2020 glass fibre bundles were completely immersed in a sealed container of acetone for 24 h, rinsed with clean acetone, then dried for 24 h at room temperature.

Bare, silane coated, and fully sized glass fibres were coated with an unreacted epoxy resin/acetone film former solution. The thickness of the epoxy sizing layer was controlled by using different concentrations (0.1 to 10 wt.%) of epoxy/acetone solution, following a procedure similar to those reported by Xu and Drzal [113], Thomason [124], and others [125]. Acetone and unreacted DER 332 epoxy resin were combined in a glass beaker before being mixed at 1200 rpm for 1 min using a magnetic stirrer to ensure the resin was fully dissolved. The solution was then poured into a plastic container and the fibre bundles were immersed for 15 min. Once removed, the coated fibres were dried for 12 h at 60°C.

The fibres used during the round-robin investigation of glass fibre sizing components and their designations are summarised in *Table 2-3*. LOI values were determined by thermogravimetric analysis performed at 25–700°C with a heating rate of 10°C/min using a TA Instruments Q50 TGA.

Designation	Coupling Agent	Film Former	Other	Supplier	D_f (µm)	LOI (%)
BF	-	-	Water	OC	17	< 0.1
APS	APS	-	-	OC	17	< 0.1
GPTMS	GPTMS	-	-	OC	17	< 0.1
MPTMS	MPTMS	-	-	OC	17	< 0.1
BF-GPTMS	GPTMS	-	-	In-house	17	< 0.1
BF-GPMMS	GPMMS	-	-	In-house	17	< 0.1
BF-GPMES	GPMES	-	-	In-house	17	< 0.1
SE1500	Epoxy-compatible full sizing			3B	18	0.8
SE2020	Epoxy-compatible full sizing			3B	18	0.6
W2020	Epoxy-compatible full sizing			3B	18	0.6
Si-E1	Epoxy-compatible full sizing			Şişecam	18	0.6
Si-E2	Modified epoxy-compatible full sizing			Şişecam	18	0.5
Si-PP	Polypropylene-compatible full sizing			Şişecam	18	0.5
SE1500 AW	SE1500		Acetone	In-house	18	< 0.2
SE2020 AW	SE2020		Acetone	In-house	18	< 0.2
W2020 AW	W2020		Acetone	In-house	18	< 0.2
Epoxy 0.1–10 wt.%	-	Epoxy resin	-	In-house	17	0.4–7.4
GPTMS-E10	GPTMS	Epoxy resin	-	In-house	17	5.2
SE2020-E10	SE2020	Epoxy resin	-	In-house	18	3.0

Table 2-3: Glass fibre sizings and designations

D_f = fibre diameter, OC = Owens Corning

Epoxy Resin

The matrix material used in the investigation was DER 332 bisphenol-A diglycidyl ether (DGEBA) epoxy resin cured with a stoichiometric (14.3 phr) amount of triethylenetetramine (TETA) tetrafunctional amine curing agent, technical grade 60%. Epoxy resin and curing agent were purchased from Sigma Aldrich/Merck. Calculation of epoxy/amine stoichiometric ratio is detailed in Appendix A.

2.3.2 Micromechanical Testing: Microbond.

Sample Preparation

Glass fibre bundles of approximate length 20 cm were removed from the larger rovings. Individual fibres were removed from the bundle and aligned along the vertical axis of a card mounting template. Fibres were mounted using double-sided tape and secured with Loctite gel super glue. The glue was allowed to set for 24 h before droplet application. Epoxy resin and curing agent were mixed at the stoichiometric ratio. Approximately 2 g of resin was added to a small plastic container using a 1 mL syringe and curing agent was added using a pipette while masses were recorded using a microbalance. The mixture was stirred thoroughly and degassed under vacuum for 10 min to remove trapped air and improve mixture homogeneity. Droplets were applied to the fibres using a small length of 125 µm diameter steel wire. A small bead of resin was collected on the end of the wire and briefly touched to the fibre on either side of droplet alignment markers 5 mm from the edge of the card tab. A single resin droplet was used to prepare six specimens before a new droplet was collected. Samples were cured at 60°C for 1 h followed by 120°C for 2 h with a 2°C/min temperature ramp used throughout and were allowed to cool overnight in the oven before being removed. A schematic illustration of the sample preparation procedure is shown in *Figure 2:6*.

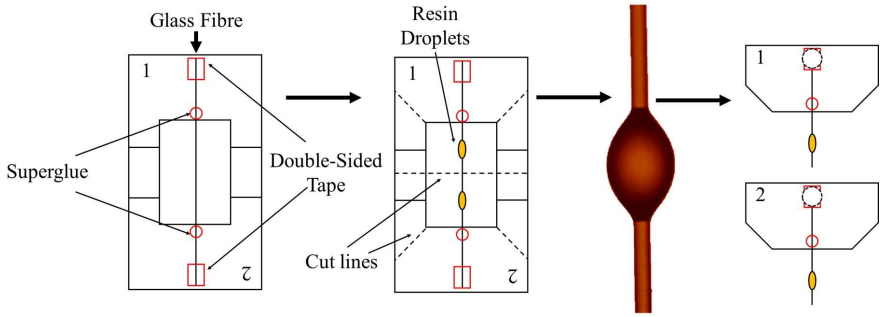

Figure 2:6: Schematic diagram of microbond sample preparation procedure

Micrographs of cured droplets were collected using a Leitz Ergolux optical microscope at 200x magnification. Droplets that were excessively large, small, or non-axisymmetric were not tested due to concerns regarding premature fibre fracture, slippage between shearing blades, and uneven load distribution, respectively. Fibre diameter, droplet embedded length, and droplet diameter were measured using ImageJ software following pixel/µm calibration with a glass precision slide. Prior to testing, samples were cut across the horizontal axis and inverted to produce two samples from each template. Sample tabs were hole-punched to hang from the load cell hook and excess card trimmed to avoid contact with the shearing blades. Each sample set consisted of approximately thirty microbond specimens to ensure generation of sufficient data for a good statistical basis [70].

Test Procedure

The basic procedure for the microbond test involves a single filament being pulled from a restrained droplet of cured matrix while measuring the force required to detach the filament. The microbond testing apparatus was designed around an Instron 3342 universal tensile testing machine equipped with a 10 N load cell and a microvice with adjustable shearing blades. Shearing blade horizontal movement was controlled at a resolution of 1 µm by a pair of adjustable parallel micrometers mounted on either side of the microvice. The development of the specific apparatus used in this work has been described in previous literature [34].

The card mounting tab was affixed to the hanging hook of the load cell and the droplet positioned below the shearing blades. The shearing blades were then brought into close proximity to the hanging fibre. The left-hand blade was brought into contact with the fibre briefly, then moved backwards slightly to account for a blade dipping effect. The right-hand blade was then brought into contact with the fibre until visible pinching was observed, then opened slightly to allow vertical movement of the fibre while the droplet was constrained. During testing the droplet was pulled upwards and subjected to a vertical shearing force. When the shearing force exceeded interfacial strength, the fibre was debonded from the matrix droplet. Fibres fractured prematurely if the shearing force exceeded filament tensile strength and were excluded. Tests were performed at a crosshead speed of 0.1 mm/min. Instron Bluehill software was used to record crosshead displacement and applied load. Successful debonding or premature fibre fracture was confirmed by in-situ observation of droplet loading using 45x magnification stereo microscopy and a live camera feed. The microbond testing experimental set-up is shown in *Figure 2:7*.

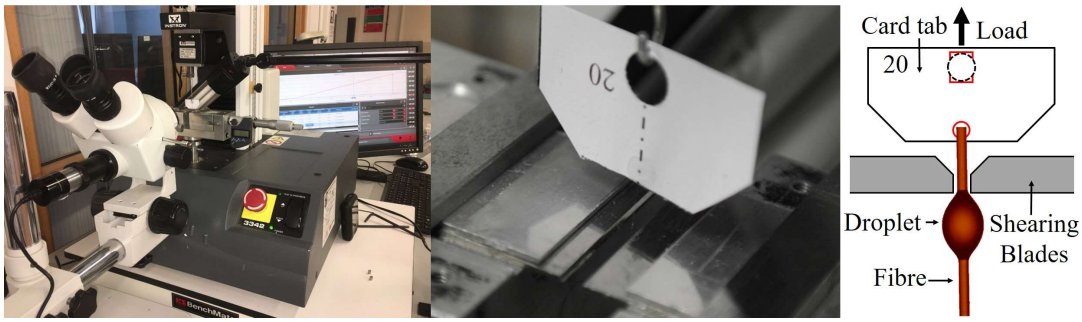

Figure 2:7: Microbond test experimental jig

Interfacial shear strength (IFSS) was calculated by *Eq. 2-1* [29].

$$IFSS = \frac{F_{max}}{A_e} = \frac{F_{max}}{\pi L_e D_f} \quad \text{(Eq. 2-1)}$$

Where: IFSS is interfacial shear strength, F_{max} is the maximum applied load, A_e is embedded area, L_e is droplet embedded length, and D_f is fibre diameter measured for each sample.

Successful fibre/matrix debonding and premature fibre fracture were confirmed by in-situ observation of droplet loading and load versus displacement plots. Debonding was verified by observation that the post-test fibre remained intact and was further evidenced by the development of frictional component in the plot attributable to the debonded droplet continuing to slide along the length of the glass fibre. Load versus displacement plots showing successful debonding and premature fibre fracture are shown in *Figure 2:8*.

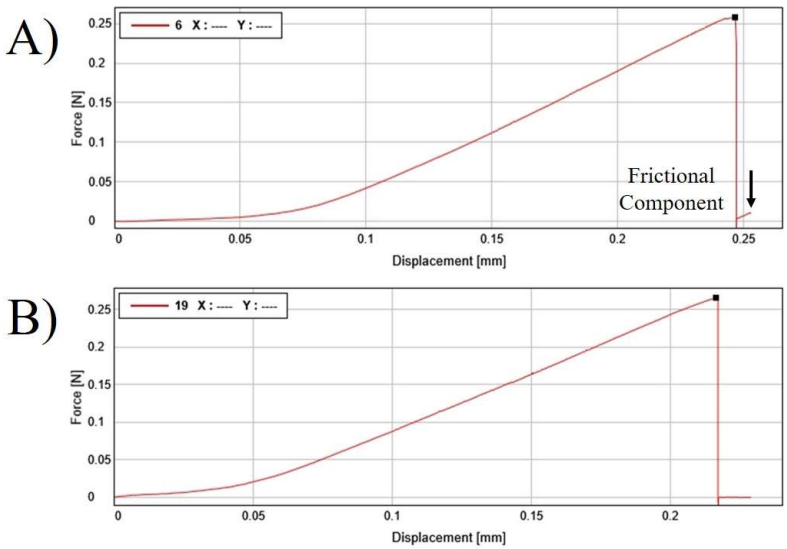

Figure 2:8: Microbond load versus displacement plot showing: A) successful debonding and B) premature fibre fracture

2.3.3 Single Fibre Tensile Test

Single fibre tensile tests were performed according to ASTM standard C1557-20 *Standard Test Method for Tensile Strength and Young's Modulus of Fibres*. Specimen preparation was identical to that of microbond samples except that a matrix droplet was not applied to the fibre. Fibre micrographs were collected using a Leitz Ergolux optical microscope at 500x magnification and fibre diameters were measured with ImageJ software. Tests were performed at a rate of 0.3 mm/min using a Testometric M250-2.5CT tensile tester equipped with a 5 N load cell.

2.3.4 Scanning Electron Microscopy

Scanning electron microscopy (SEM) was used to examine sized glass fibre bundles, fibre surfaces, and the microdroplet debond region. For fibre bundle samples, copper tape was applied to lengths of glass fibre roving to isolate approximately 10 mm bundles and maintain bundle integrity during sample preparation and SEM. Carbon tape was applied to SEM specimen stubs and three bundles were mounted on each stub. For single fibre samples, carbon tape was applied to SEM specimen stubs before mounting approximately twelve post-test microbond samples. Fibre and droplet assemblies were mounted with the card tab attached to enable accurate placement before cutting excess fibre and the tab off with a scalpel. Once mounted, specimen stubs were sputter gold coated using an Agar sputter coater. Sputter coating was performed under argon atmosphere with an operating pressure of 0.08 mbar, 30 mA current, and a 40 s coating time. Analysis was performed using a Hitachi SU 6600 scanning electron microscope with an accelerating voltage of 15.0 kV and a 10 mm working distance. The scanning electron microscope, mounted fibre bundle samples, and mounted microbond droplet samples are shown in *Figure 2:9*.

Figure 2:9: Scanning electron microscope, fibre bundle, and mounted/coated microbond droplet SEM specimens.

2.4 RESULTS AND DISCUSSION

A round-robin investigation of the effect of a number of current and developmental glass fibre sizings on glass fibre/epoxy interfacial shear strength was performed. Interfacial adhesion of an epoxy matrix to unsized glass fibre was characterised to provide a comparative baseline for subsequent sizing treatments. The microbond test was used to characterise interfacial adhesion of fibres coated with various silane coupling agents, combinations of silane coupling agent and polymeric film former, full commercial sizing packages, and model sizings consisting solely of an epoxy film former. The matrix material used in the investigation was DER 332 bisphenol-A diglycidyl ether (DGEBA) epoxy resin cured with a stoichiometric (14.3 phr) amount of triethylenetetramine (TETA) tetrafunctional amine curing agent.

2.4.1 Interfacial Adhesion: Silane Coupling Agent

IFSS of unsized and silane coated glass fibres is shown in *Figure 2:10*.

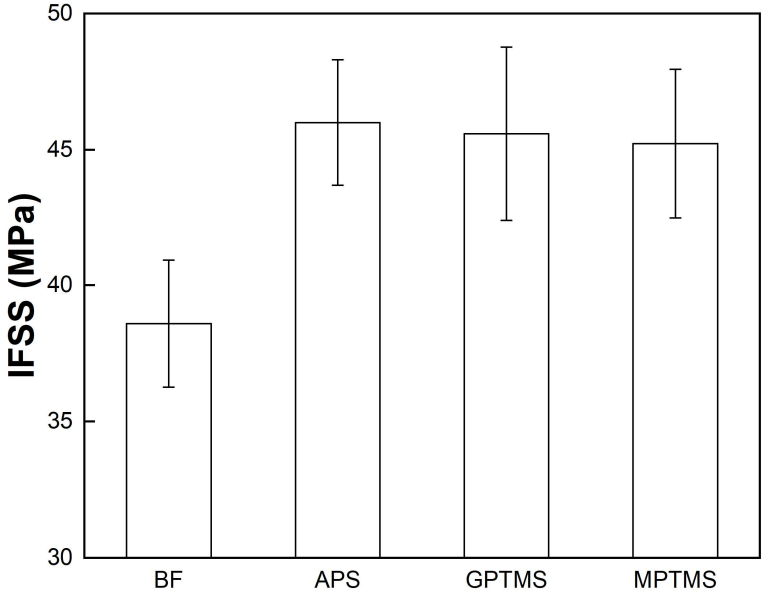

Figure 2:10: IFSS of silane coated glass fibres

A baseline IFSS value of around 39 MPa with unsized glass fibres was measured. Reasonably high baseline adhesion can be attributed to a combination of polar interaction between the epoxy matrix and hydroxyl ions on the glass fibre surface, physical contributions from compressive stresses generated by droplet cure shrinkage, and static friction [126]. Adhesion may have also been promoted by the formation of hydrogen bonds due to high surface free energy [97]. Dwight *et al.* have similarly reported that unsized glass fibres were able to bond well to an epoxy matrix due to Lewis acid-base interaction between the acidic epoxy matrix and basic bare glass surface [127]. Furthermore, these interactions were thought to be enhanced by the presence of a silane coupling agent. In a comparative study of a number fibre sizings, Larson and Drzal predicted that unsized glass fibres would have shown strongest interfacial adhesion based on thermodynamic arguments. The fact that the predicted behaviour was not attainable in practice was attributed to an artefact of indentation test sample preparation related to lack of protection by a silane coupling agent and water exposure during polishing [67]. In this work, higher IFSS values were generally not attainable with the unsized fibres due to an apparent threshold defined by filament tensile strength and premature fibre fracture prior to droplet debonding.

The application of a silane coupling agent increased glass fibre/epoxy apparent IFSS by approximately 17–20%. Within confidence limits, however, there was little significant difference between the silane coatings. This result may be indicative that, despite some

measure of universal increase to adhesion properties, specific chemical interactions between the glass fibre and epoxy matrix were not changed much by the silane used. On the other hand, the lack of a protective coating and subsequent tensile failure of the unsized fibres may have resulted in a premature estimation of baseline adhesion as higher individual IFSS values within the data set could not be measured.

As the three most commonly used silanes in the glass fibre sizing industry, determination of optimised thermoset adhesion properties with these coupling agents is of great interest. Mäder reported optimised adhesion with an APS coupling agent alone due to strong interaction between amino groups in the silane and epoxy groups in the matrix [97]. Fragmentation test data by Zhao and Takeda has suggested that GPTMS adhesion was increased by a factor of around 2 compared to MPTMS using a similar matrix and curing agent combination [99]. Increased adhesion properties were attributed to stronger interaction between GPTMS and an epoxy matrix, increased fibre tensile strength, and improved wetting. Conversely, the interfacial adhesion results in this work would appear to show that increased adhesion with a TETA-cured DGEBA matrix was generally independent of the silane coupling agent used. Similar IFSS values were achieved by the use of an MPTMS coupling agent typically optimised for vinyl ester matrices [128].

Investigation of the adhesion enhancing properties of silane coupling agents was extended to a range of epoxysilane chemistries and is shown in *Figure 2:11*. Furthermore, application of an identical GPTMS coupling agent by an industrial glass fibre sizing process and an in-house fibre bundle coating process was compared.

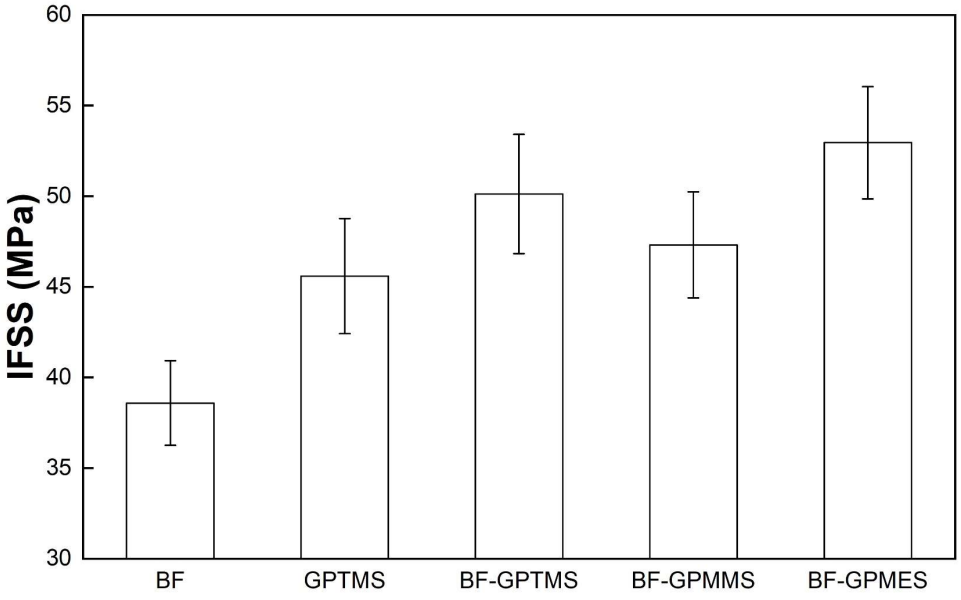

Figure 2:11: IFSS of epoxysilane coated glass fibres

Interfacial adhesion appeared to be generally independent of the mode of GPTMS silane application within confidence limits. IFSS values were slightly higher for the in-house coated fibre bundles, possibly due to increased regional silane concentration due to the immersion coating method used. The results were indicative that laboratory scale fibre sizing procedures were appropriate for characterisation of the effect of sizing formulations using simple sizing solutions. Deviation from industrial sizing procedures may become more apparent if expanded to multiple-component sizing formulations where factors such as roller speed and order of component application become important considerations [21]. Maximum adhesion was achieved with unsized glass fibres coated with GPMES coupling agent. Lenhart *et al.* have proposed that epoxy functional groups in the GPS molecule may participate in the cross-linking reaction with an amine curing agent [129]. It is possible that this is a contributing factor in the increased IFSS observed. However, it is not immediately clear why GPMES adhesion was increased compared to the other epoxysilanes. In any case, the adhesion enhancing capabilities of this coupling agent may be inferred from its utilisation in W/SE2020 series commercial sizing packages according to analysis of glass fibre sizing patent literature [110]. Appropriate selection of epoxysilane coupling agents for use in thermoset epoxy composites should, however, be carefully considered. Thomason reported that interfacial strength (ILSS) was lowest with a sizing containing, among other components, GPTMS and that the coupling agent may have had poor compatibility with certain amine-cured epoxy matrices [11]. However, it was noted that without definitive knowledge of the chemical nature of other sizing components, hard conclusions could not be drawn.

2.4.2 Interfacial Adhesion: Full Glass Fibre Sizing

The interfacial adhesion of a number of fully sized glass fibres to an epoxy matrix was investigated. SE1500, SE2020, and W2020 are epoxy-compatible sizing packages produced by 3B. The prefixes “SE” and “W” differentiate between boron-free Advantex glass and borosilicate HiPer-tex glass, respectively. Fibres with the “2020” suffix shared a common sizing package and differed only in the glass fibre material. Further epoxy-compatible (Si-E1), modified epoxy-compatible (Si-E2) and polypropylene-compatible (Si-PP) sized fibres were produced by Şişecam. Sizing compositions were not disclosed. IFSS of the fully sized commercial glass fibres are shown in *Figure 2:12*.

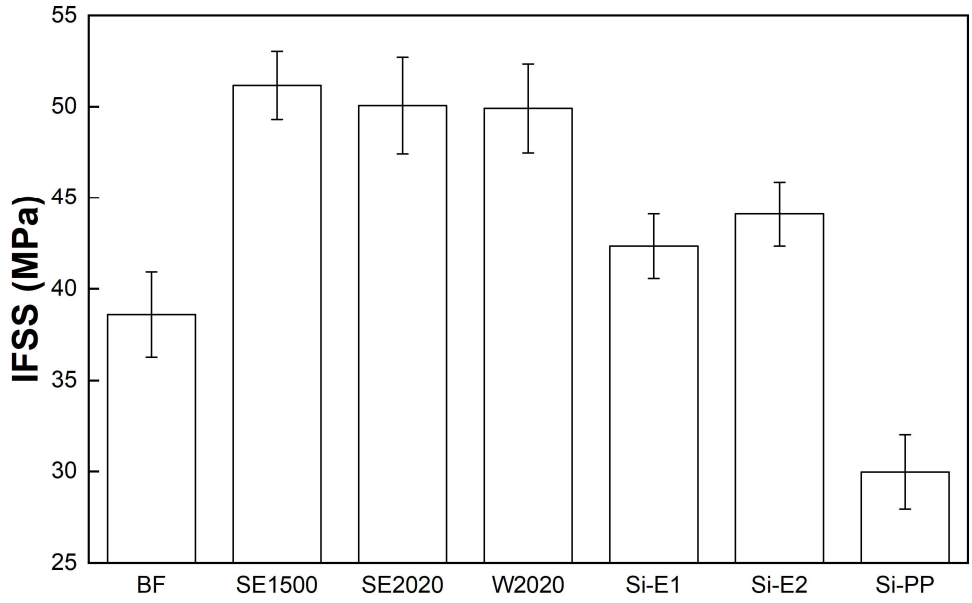

Figure 2:12: IFSS of fully sized glass fibres

IFSS of SE1500, SE200, and W2020 fibres sized with epoxy-compatible full sizing packages was increased by around 30% compared to the unsized fibres. Little significant difference in the adhesion properties of these three sizings was observed and adhesion appeared to be independent of the glass formulation (Advantex/HiPer-tex). While IFSS was increased to an extent greater than APS, GPTMS, or MPTMS silane coupling agents alone (*Figure 2:10*), values approximated those achieved with a GPMES modified epoxysilane sizing. Increased IFSS compared to the silane only fibre series may be indicative of some adhesion contribution from the presence of a compatible film former component. Dey *et al*. have similarly reported that film former compatibility with the matrix contributed more to IFSS than silane chemistry [24]. On the other hand, data presented in *Figure 2:11* has shown that IFSS values in this region were attainable by selection of an epoxy-functional silane coupling agent that may have been present in the full sizing [110].

Gao *et al*. reported that IFSS with a full sizing containing GPTMS coupling agent and an epoxy film former was enhanced to a greater extent than a model sizing containing GPTMS only [108]. The authors proposed that increased adhesion to an epoxy matrix may have been attributable to additives such as film former, surfactants, and anti-static agents not present in the silane only sizing contributing to an interphase-toughening effect. Zhang *et al.* have reported that increasing sizing emulsifier content in the sizing improved interfacial properties of carbon fibre/epoxy composites [130]. Similarly, work by Liu *et al.* found that application of polyethylene glycol (PEG), commonly found as a lubricant in full sizings [110], improved glass fibre/PP IFSS [131]. Zeng *et al.* also reported increased glass fibre/bismaleimide–triazine

thermoset IFSS when PEG was introduced due to the effect of a "flexible bridge" at the interface [132]. The contributions of these sizing components to glass fibre/epoxy IFSS are apparently not well understood or rarely reported.

IFSS of Si-E1 and Si-E2 fibres approximated that of the silane only fibre series in *Figure 2:10*, and modification of the sizing formulation did not produce any significant variation in adhesion properties. The exact nature of the sizing modification was, however, undisclosed. Variability of IFSS between the 3B and Şişecam fibres may be attributable to differences in sizing compositions. Adhesion performance with various epoxy matrices would appear to vary from sizing to sizing despite a common label of "epoxy-compatible" sizing formulation [11].

Matrix-incompatible Si-PP fibres (containing a polypropylene film former) exhibited adhesion properties lower than that of the unsized fibres despite the presence of an undisclosed coupling agent. The result is particularly interesting, in that an apparent adhesion-inhibiting effect of the thermoplastic film former appeared to counteract any improvement due to the silane. As sizing formulations are undisclosed, consideration should also be given to the fact that the Si-PP fibre may have contained a coupling agent poorly suited for optimised adhesion with an epoxy matrix, though PP-compatible sizings often contain an APS or GPTMS silane [133,134]. Reduced adhesion is thus more likely to be attributable to the incompatible of the film former component of the sizing.

2.4.3 Interfacial Adhesion: Effect of Acetone Treatment

SE1500, SE2020, and W2020 fully sized epoxy-compatible fibre rovings were immersed in a sealed container of acetone for 24 h, rinsed with clean acetone, then dried for a further 24 h to remove the soluble portion of the fibre sizing. Solvent extractable sizing content determined according to ASTM standard D4963 following 24 h acetone treatment was around 0.3% and can be attributed to removal of a significant portion of the polymeric film former and sizing additives such as surfactants and anti-static agents [11,93]. IFSS of the fully sized commercial fibres following an acetone treatment is shown in *Figure 2:13*.

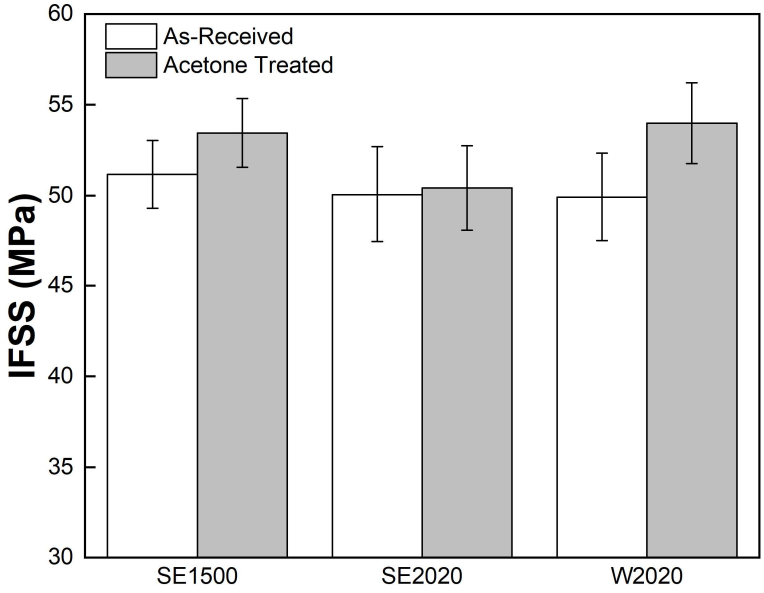

Figure 2:13: IFSS of epoxy-compatible fully sized fibres after acetone treatment

While IFSS values following acetone treatment were not significantly different within confidence limits, IFSS was improved compared to the as-received fully sized fibres in all cases. NMR analysis of the acetone extracted soluble portion of glass fibre sizings by Thomason indicated that it consisted of around 70% epoxy resin film former and 30% polyethylene oxide (PEO) surfactant [11]. Silane was not detected in the sizing extracts. XPS analysis of glass fibre surfaces, however, indicated that some portion of the epoxy film former remained following acetone extraction and was possibly bound to the silane coupling agent. Subsequent NMR analysis of an extracted sizing consisting of GPTMS, epoxy film former, and surfactant by Tanoglu *et al.* indicated that almost all of the silane remained at the glass surface [93]. Silane monomers were condensed into a network that remained bound to the glass fibre surface and constituted 87% of the bound sizing. In this work, the retention of a high apparent IFSS following acetone extraction may be attributable to the bound portion of the sizing remaining on the fibre surface. This bound portion may consist primarily of a silane coupling agent, but the possibility of interaction with residual epoxy film former bound to the silane cannot be discounted.

Increased IFSS compared to the as-received fibres may be related to removal of residual surface impurities [135] or improved coupling agent homogeneity by removal of excessively bound silane aggregates [104]. Alternatively, this behaviour may be related to the removal of sizing additives whose contribution to the properties of the composite are not well defined [11]. Contrary to proposals by Gao *et al*. [108] and others [130–132], increased IFSS following the removal of sizing additives (surfactants, lubricants, anti-static agents) by a solvent

treatment may indicate that these components, while essential for processing, do not contribute much to interfacial adhesion. The application of film former typically requires a large fraction of both surfactants and lubricants in the sizing, as much as 40% of the sizing for some epoxy-compatible formulations [110]. It may be possible that processing agents have some adhesion-inhibiting parameter that mask any improvements to IFSS related to the film former component of the sizing. Removal of these processing agents by the acetone extraction procedure, while leaving some portion of the film former bound to the fibre surface, may be the cause of the increased IFSS observed in this work.

2.4.4 Interfacial Adhesion: Model Epoxy Film Former

Epoxy Solution Treatment of Unsized Fibres

Epoxy film former is a key processing component in many glass fibre sizings and high IFSS of acetone-extracted fully sized fibres may have been due to a bound sizing portion where silane coupling agent and epoxy film former interacted. Furthermore, the adhesion properties of an epoxy film former component in isolation are not well understood and rarely reported outside of carbon fibre sizing applications. Unsized glass fibres were coated with an epoxy resin/acetone solution to produce a model sizing consisting solely of an unreacted epoxy film former. The thickness of the epoxy sizing layer was controlled by using 0.1–10 wt.% solution concentrations to produce a range of layer thicknesses [114]. IFSS of the epoxy sized glass fibres and the relationship between solution concentration and epoxy layer thickness are shown in *Figure 2:14*.

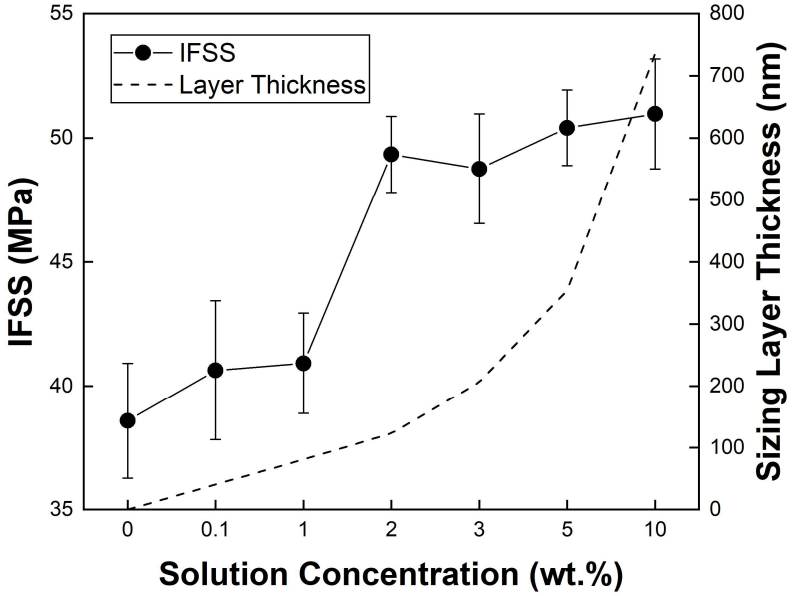

Figure 2:14: IFSS of epoxy coated fibres and layer thicknesses

It was shown that the application of 0.1–1 wt.% epoxy/acetone solution with corresponding sizing layer thickness of 40–80 nm did not have any significant effect on IFSS within confidence limits. At solution concentrations of 2 wt.% and sizing layer thickness of around 120 nm or more, a significant increase in interfacial adhesion was observed. Within confidence limits, IFSS appeared to plateau after 2 wt.%, after which increasing the coating concentration to 10 wt.% had little effect on adhesion. IFSS was increased to an extent greater than that of APS, GPTMS, or MPTMS silane coupling agents alone, and approximated that of the interfacial adhesion achieved with a GPMES coupling agent and full epoxy-compatible sizing formulations (SE1500, SE2020, W2020). However, increased adhesion in the epoxy coated fibres did not become apparent until the sizing layer thickness exceeded that typically found in a commercial full sizing (≈ 80 nm) by around 50% [128].

Single fibre tensile tests of epoxy coated fibres were performed to verify that increased apparent adhesion properties were not simply a result of improvement to initially poor unsized fibre mechanical properties and are shown in *Figure 2:15*. It was found that fibre tensile strength was not affected to any significant degree by the application of an epoxy coating and results between unsized fibres, 0.1 wt.%, and 10 wt.% coatings were generally comparable. It would seem possible to conclude that while increased adhesion is achievable with these sizings, glass fibre tensile behaviour shows a similar trend to epoxy coated carbon fibres in this regard and is not improved [116,136].

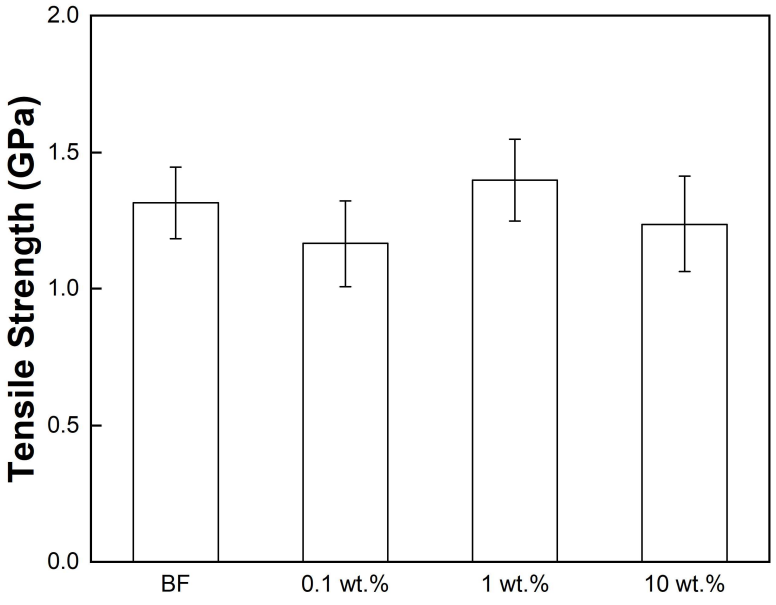

Figure 2:15: Tensile strength of epoxy coated glass fibres

While there is little precedent in the existing literature for a similar glass fibre sizing procedure, some indication of the adhesion enhancing properties may be inferred from previous carbon fibre investigations. Increased IFSS by a partially cross-linked epoxy sizing has been attributed to interdiffusion of matrix monomers into the sizing [113], increased surface roughness, and chemical compatibility with the matrix [116]. The fact that an apparent step change occurred between the 1 wt.% and 2 wt.% glass fibre coatings may be suggestive that chemical bonding theories, where a linear relationship between IFSS and sizing layer thickness would be expected, are not sufficient to explain the improvement observed in this work. Increased IFSS as a result of an epoxy coating in this work may be attributable to interdiffusion of the epoxy sizing with the epoxy matrix material and enhanced cross-linking at the interface between unreacted DGEBA in the sizing and the amine curing agent.

It would appear that the interfacial behaviour of glass fibre sized with an unreacted epoxy sizing is markedly different from that of carbon fibres sized with similar formulations reported in previous literature [113–116]. The interfacial adhesion of glass fibres sized with an epoxy solution was not affected much by 0.1 wt.% or 1 wt.% solutions, was significantly increased at a solution concentration of 2 wt.%, and remained high with increased solution concentrations of up to 10 wt.%. Conversely, it is relatively well reported that similarly treated carbon fibres show a linear relationship between adhesion and epoxy concentration until a critical sizing layer thickness is achieved by solution concentrations of around 4–5 wt.% [113,116,119]. According to Vautard and Drzal, epoxy coating concentrations below 1 wt.% were unable to evenly coat fibres [114]. A concentration of 3 wt.% was sufficient to ensure uniform coating and concentrations of 4 wt.% (sizing layer thickness > 100 nm) resulted in visible “bridges” between fibres that hindered processing and reduced IFSS. Reduced adhesion at excessively high epoxy concentrations and sizing layer thicknesses due to development of “sizing bridges” has also been reported by Xu and Drzal [113] and Zhang [116]. Alternatively, He *et al.* have proposed that smooth fibre surfaces following 8–11% LOI treatments decreased adhesion by inducing weak fibre/matrix bonding [119]. In any case, reduced IFSS at high coating concentrations was not observed with epoxy coated glass fibres. This behaviour may be related to larger glass fibre diameter and resulting differences in epoxy layer distribution.

SEM was used to characterise epoxy sized fibre bundles and individual sized fibre uniformity. SEM micrographs of epoxy sized glass fibre bundles and individual sized fibres following treatment with 0.1–10 wt.% epoxy/acetone solutions are shown in *Figure 2:16* and *Figure 2:17*, respectively. *Figure 2:16* shows that "sizing" bridges were apparent at solution concentrations as low as 1 wt.%, and clearly visible at 5 wt.% and 10 wt.%. It is possible that poor adhesion related to the formation of sizing bridges reported by others is related exclusively to the use of partially cross-linked epoxy coatings [113,116]. Accumulation of poorly distributed epoxy was visible on the 1 wt.% fibres and node-like structures were visible on the fibre surface following a 3 wt.% coating. These fibre surface phenomena did not appear to influence the adhesion enhancing capabilities of the sizing, however. Furthermore, distribution of surface phenomena such as nodes and sizing aggregates was inconsistent throughout the bundles.

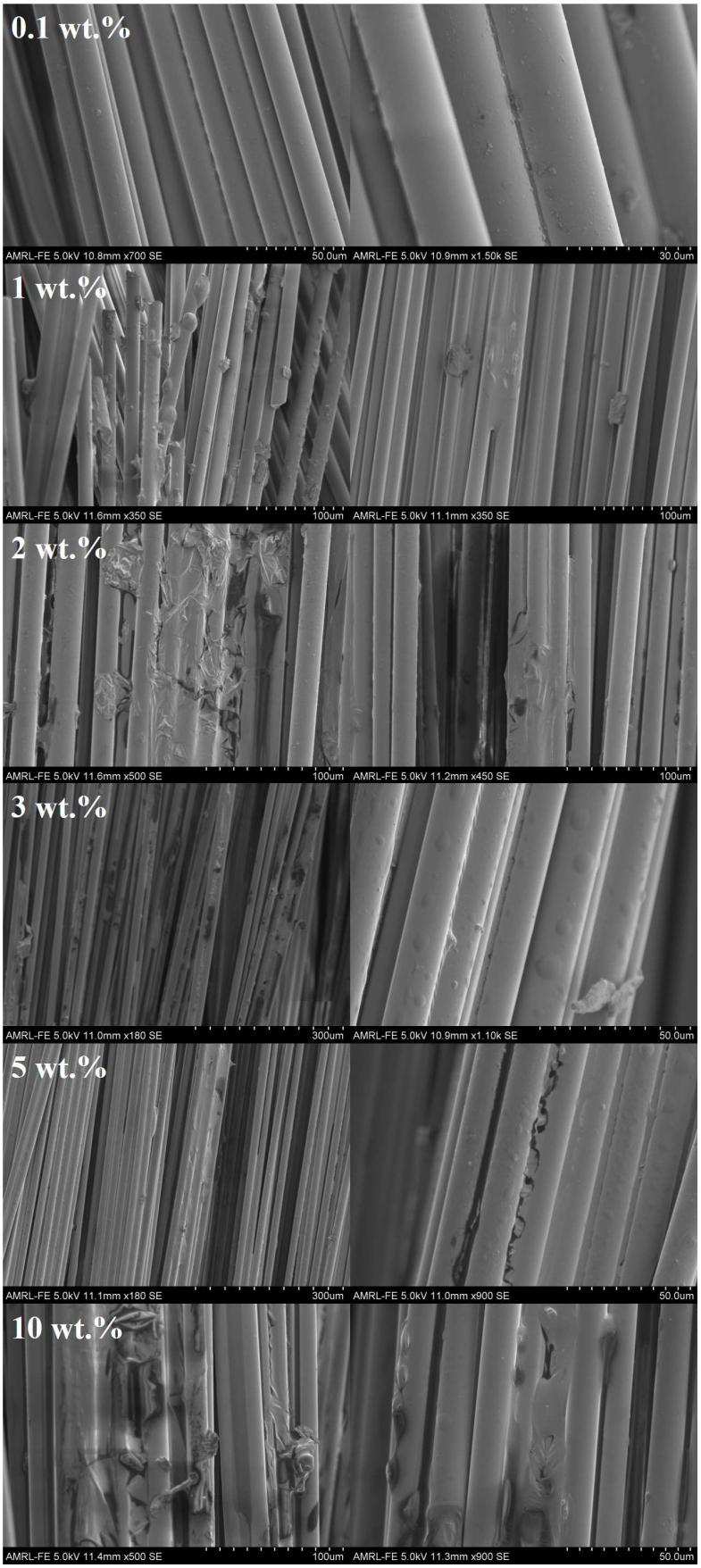

Figure 2:16: SEM micrographs of epoxy coated glass fibre bundles

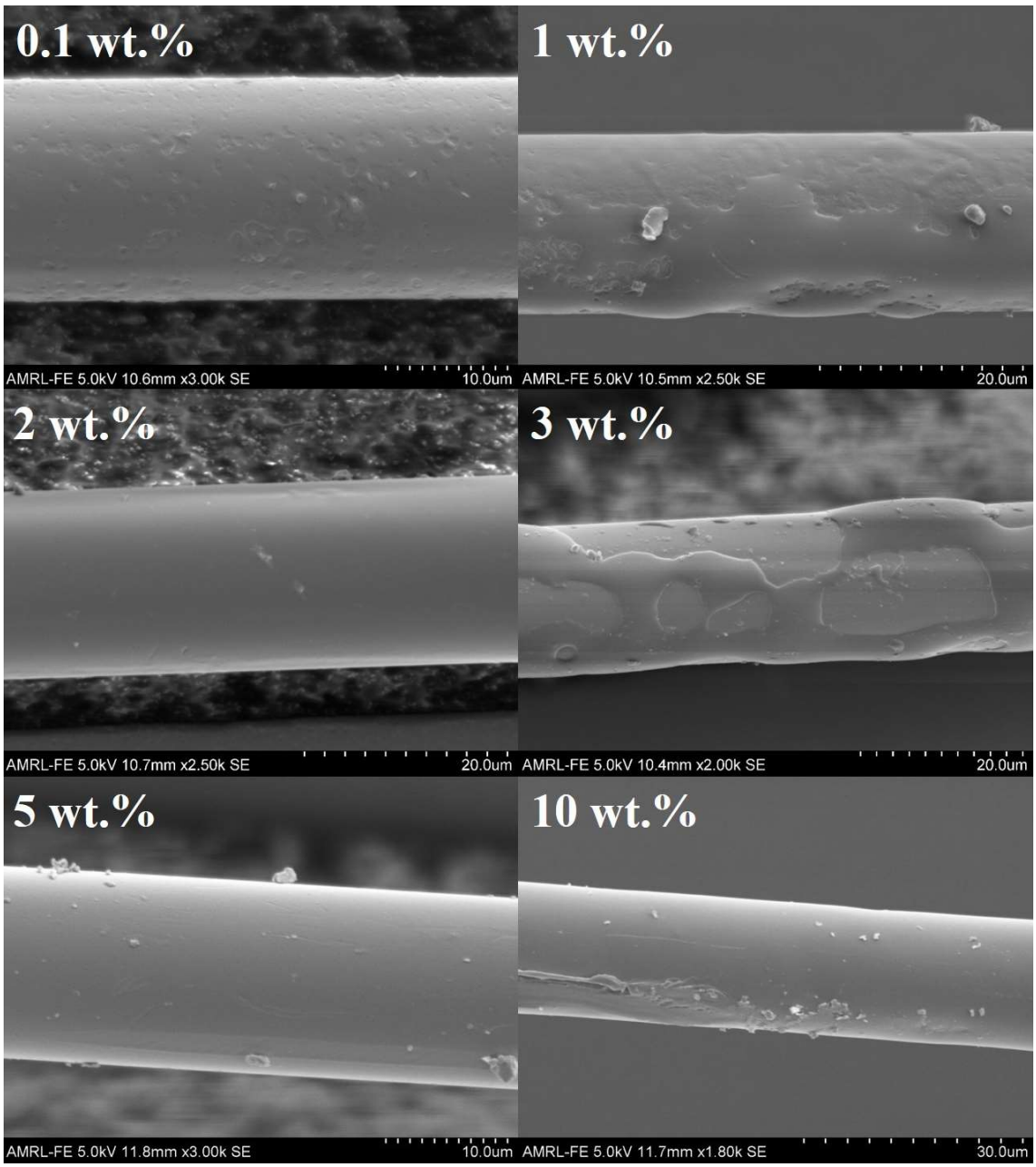

Figure 2:17: SEM micrographs of epoxy sized glass fibres

Figure 2:17 appears to show that epoxy coating distribution was poor following treatment with 0.1 wt.% and 1 wt.% solutions. Potential damage to the sizing during removal from the bundle and sample mounting should also be considered. Sizing distribution was similarly poor in the 3 wt.% single fibres and the node-like structures observed in the fibre bundle were not apparent. Sizing distribution appeared uniform at 5 wt.% and 10 wt.%, though some peeling of excess unreacted matrix is visible in the 10 wt.% sample [116].

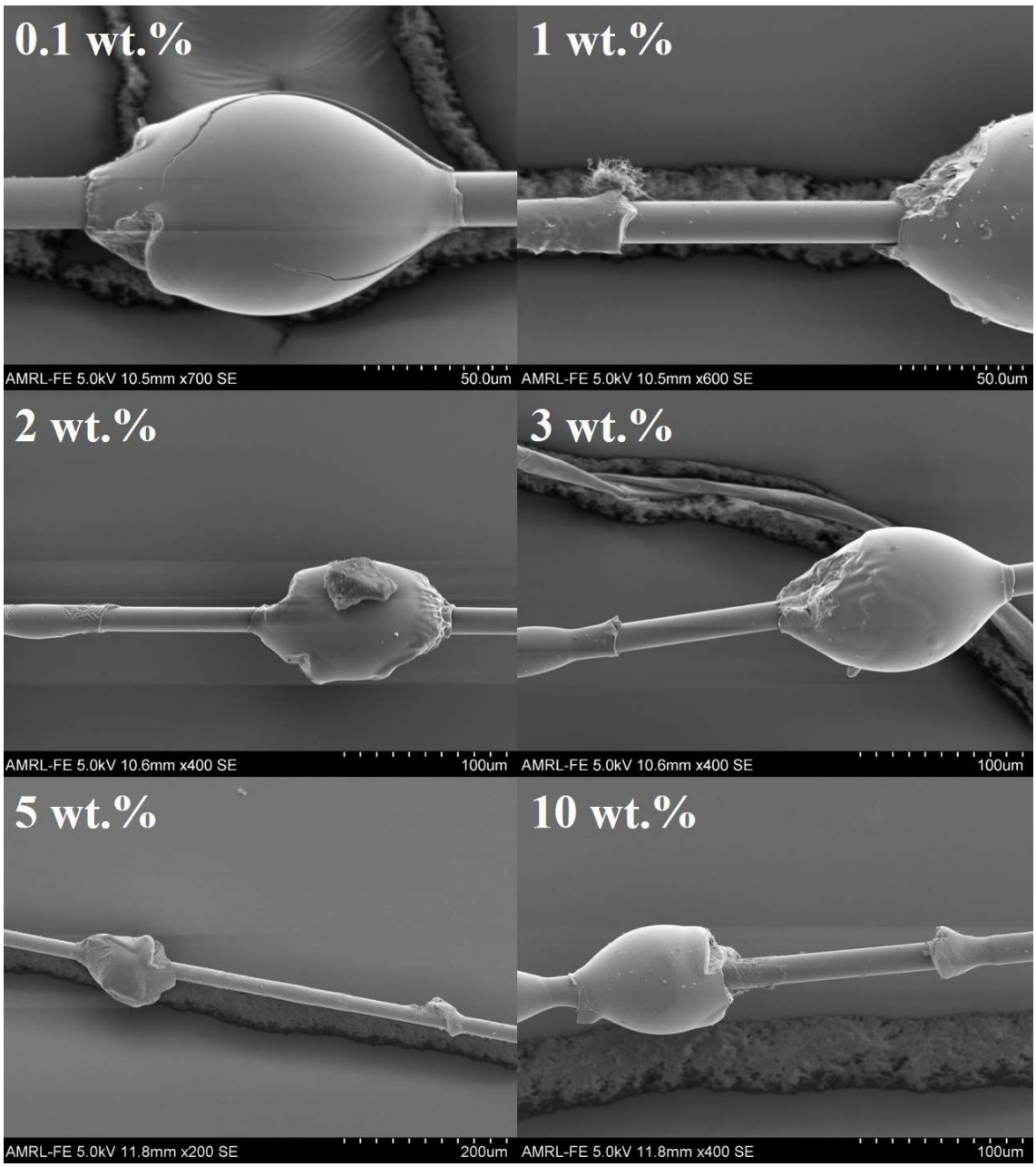

Figure 2:18: SEM micrographs of droplet debond region of epoxy sized glass fibres

Droplet debonded areas were also investigated with SEM as shown in *Figure 2:18*. In all cases, micrographs confirmed fibre/droplet debonding and was evidenced by a residual meniscus. The 0.1 wt.% sample showed some surface damage attributable to the shearing blades of the microvice and was pushed some distance down the fibre from the meniscus after debonding. No clear conclusions regarding differences in the adhesion strength could be determined from the micrographs, however.

Another interesting observation particular to the epoxy/acetone solution sizings was an apparent change to droplet debonding behaviour. Load versus displacement plots generated during the test showed a distinctive sawtooth phenomenon that implies some manner of alteration to interface or droplet properties not achieved with the sizings investigated previously. While the plots generated are reminiscent of classical stick-slip behaviour, in-situ observation of droplets during the test indicated no visible sliding. Conversely, plots generated during testing of the silane coupling agents and full fibre sizings were uniformly linear. Load versus displacement plots with increasing severity of apparent stick-slip behaviour and corresponding SEM micrographs of the post-test debonded droplet are shown in *Figure 2:19*.

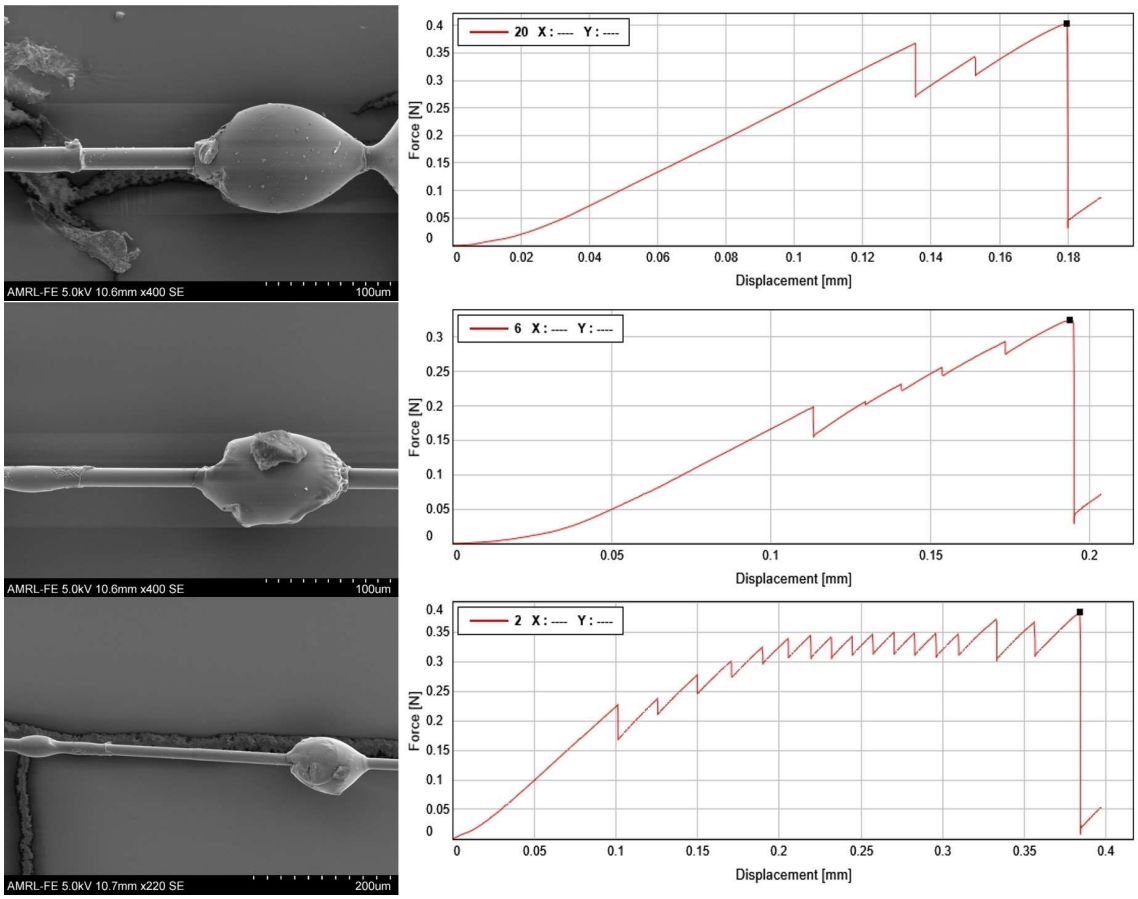

Figure 2:19: Comparison of SEM micrographs of droplet debond region and load versus displacement plots

To the best of the author's knowledge, this phenomenon has not been reported in previous microbond literature. Investigation of the mechanics of the single fibre pull-out test by Tsai and Kim has, however, shown a stick-slip stage prior to the debonding of 125–200 µm optical fibres from an epoxy matrix [137]. The fact that this sawtooth behaviour was not apparent with other sizings would suggest some fundamental modification to either interphase or droplet properties that may be related to a plasticising effect [138].

Consideration should also be given to the possibility of modification of the local properties of the epoxy droplet by the unreacted epoxy in the sizing. Vautard and Drzal have suggested that the application of an epoxy fibre coating appeared to play a role in matrix cure shrinkage behaviour [115]. Diffusion of matrix styrene into the epoxy coating was thought to result in expansion of the latter and had annealing effect on residual stresses generated by volumetric cure shrinkage. In this work, it is not immediately clear to what extent, if any, the epoxy coating influenced local droplet properties. However, Minty *et al.* reported that glass fibre/DGEBA-TETA IFSS was maximised below the stoichiometric ratio for GPTMS coated fibres, while IFSS was maximised at the stoichiometric ratio for APS coated fibres [36]. It is possible that excess epoxy in the coating may have resulted in a somewhat epoxy-rich droplet.

Sawtooth behaviour was investigated by manually stopping the test prior to droplet debonding following the appearance of one to five sawtooth stages in the plot. Samples were removed from the microbond test jig and mounted on SEM specimen stubs before collection of micrographs. SEM micrographs and corresponding load versus displacement plots are shown in *Figure 2:20*. Micrographs confirmed that "full" droplet debonding did not occur during the sawtooth stage of loading. The steep force reduction and residual frictional component typical of debonding was not visible in load versus displacement plots. Furthermore, SEM micrographs confirmed that debonding did not occur during sawtooth stages as a residual meniscus (shown *in Figure 2:18*, *Figure 2:19*) was not observed.

Droplets unloaded after increasing sawtooth stages appeared to show accumulation of surface damage around the region where the droplet was in contact with the shearing blades. The sample stopped after four sawtooth stages appeared to be partially sheared from the fibre. It is possible that crack propagation of damaged matrix regions occurred during removal of the droplet from the testing jig or SEM specimen mounting. Sawtooth phenomena may have been related to small portions of droplet matrix material chipping off during the test and subsequent sliding of the droplet between the shearing blades before contact is quickly re-established. This behaviour would appear to suggest a brittle, or amine-rich, droplet rather than a droplet with off-stoichiometric local properties. Droplets with reduced stoichiometry may be expected to show plastic rather than brittle behaviour [35].

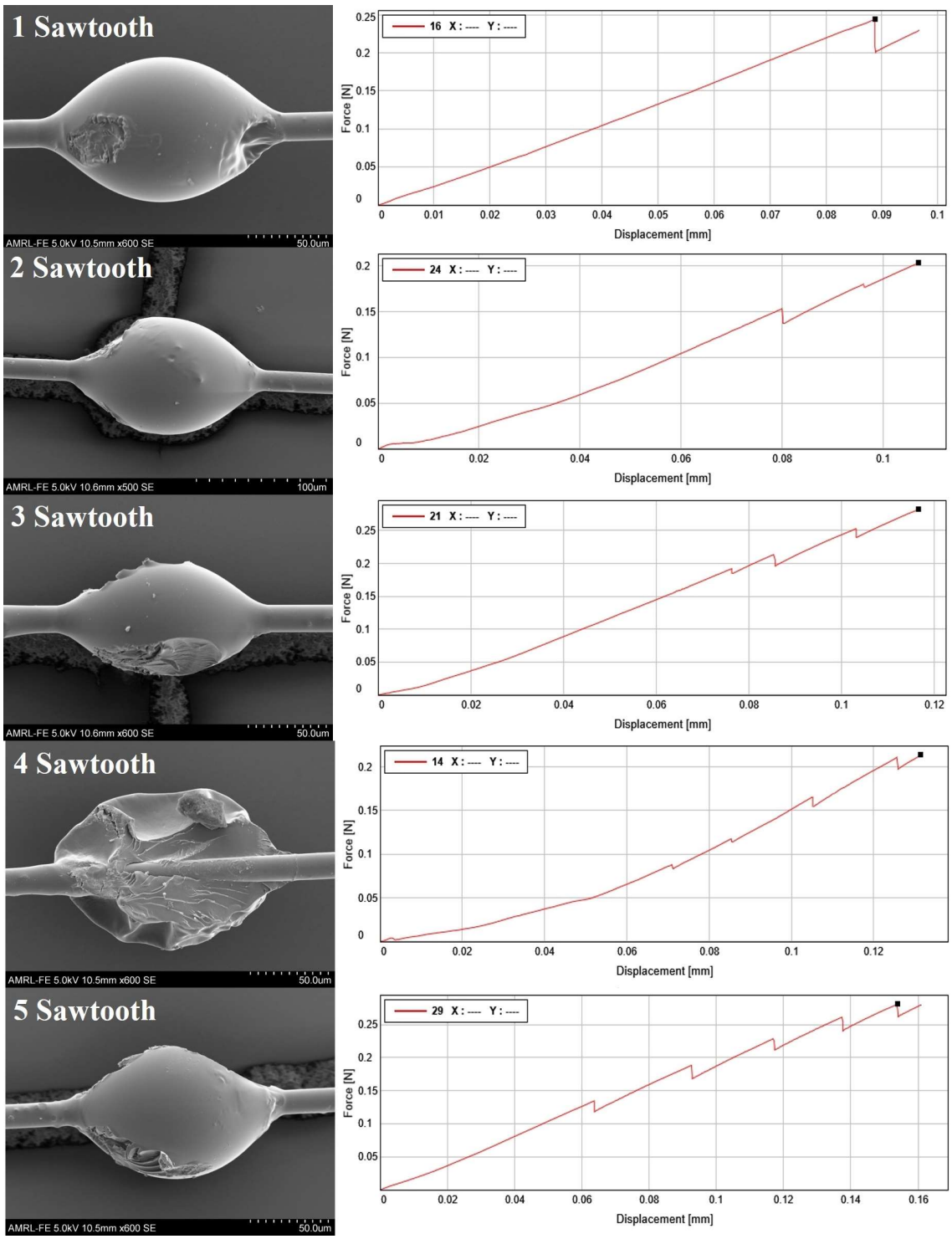

Figure 2:20: SEM micrographs and load versus displacement plots of epoxy coated microbond samples

Epoxy Solution Treatment of Sized Fibres

Glass fibres sized with GPTMS silane only and SE2020 full fibre sizing were treated with a 10 wt.% epoxy/acetone solution as shown in *Figure 2:21* and *Figure 2:22*. In all cases, IFSS was improved following epoxy treatment and the order of maximum IFSS achieved was reflected by the initial IFSS of the fibres before treatment (unsized < silane only < full sizing). Coating SE2020 fibres with a 10 wt.% solution, in fact, produced the largest IFSS values measured over the course of the round-robin investigation. Total sizing content measured by TGA LOI and subsequent layer thickness was lower for silane coated and fully sized fibres treated with the same solution concentration, despite solution concentration being the sole parameter that dictates layer thickness [114]. This behaviour is likely attributable to the pre-existing silane coupling agent inhibiting penetration of the fibre bundle by the epoxy solution. The effect was compounded by the pre-existing film former in the full SE2020 sizing. In any case, total epoxy sizing content and layer thickness achieved were over the apparent LOI threshold (around 1.3%) necessary to confer enhanced interfacial adhesion.

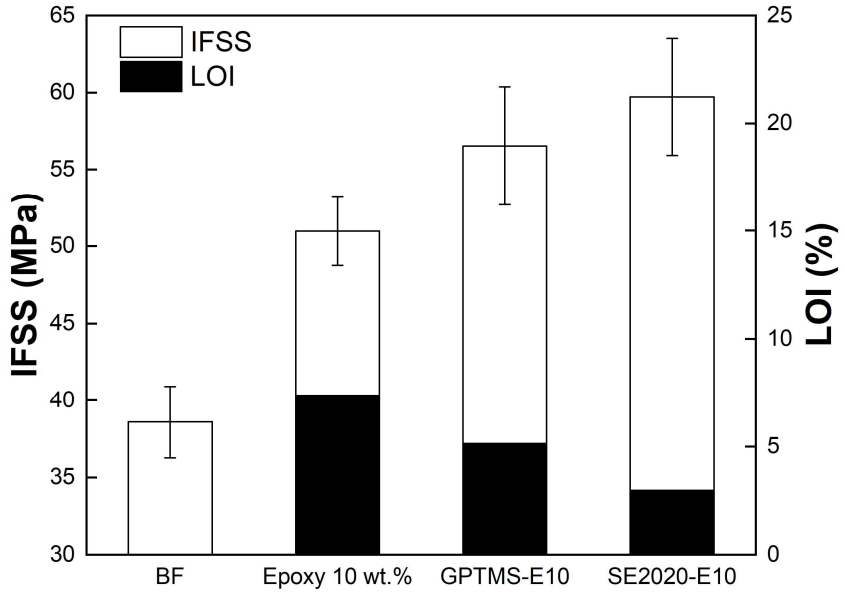

Figure 2:21: IFSS and sizing LOI of unsized, silane coated, and fully sized glass fibres after treatment with a 10 wt.% epoxy/acetone solution

Sawtooth behaviour was not observed in the load versus displacement plots of epoxy coated GPTMS and SE2020 fibres. This makes any hypothesis regarding alteration of droplet matrix properties problematic. It may be possible that the presence of the silane coupling agent (present in both GPTMS and SE2020) effectively isolates either the glass fibre surface or droplet from whatever factor is responsible for the apparent sawtooth behaviour. Definitive conclusions in this regard may not be determined within the scope of this work.

Increased IFSS following the application of an epoxy coating may, however, be attributed to a cumulative effect of increased adhesion by an epoxysilane coupling agent, interdiffusion of the epoxy sizing with the epoxy matrix material, and enhanced cross-linking at the interface between unreacted DGEBA in the sizing and the amine curing agent.

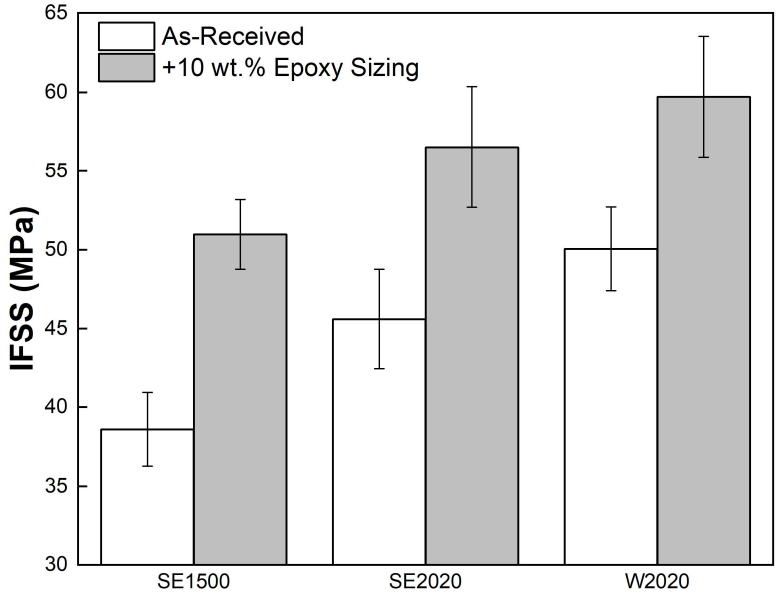

Figure 2:22: IFSS comparison of unsized, silane coated, and fully sized glass fibres after treatment with a 10 wt.% epoxy/acetone solution

Finally, the appearance of distinct circular formations not detectable by optical microscopy were observed on the surface of droplets with larger embedded lengths (>200 μm) as shown in *Figure 2:23*. The circular patterns observed may have been indicative of Marangoni flow behaviour to related to evaporation of curing agent at the droplet surface layer [139,140]. It is unclear the effect, if any, that this behaviour may have had on interfacial adhesion or microdroplet thermomechanical properties, as the effect only became apparent in microbond samples with excessively large embedded lengths that were not selected for microbond testing. The observation was generally not considered a concern, however. It has been reported previously that more significant structural deformations related to residual cure shrinkage did not have a significant influence on glass fibre/epoxy IFSS [141,142]. Nevertheless, the observation is interesting and does not appear to have been reported in previous literature.

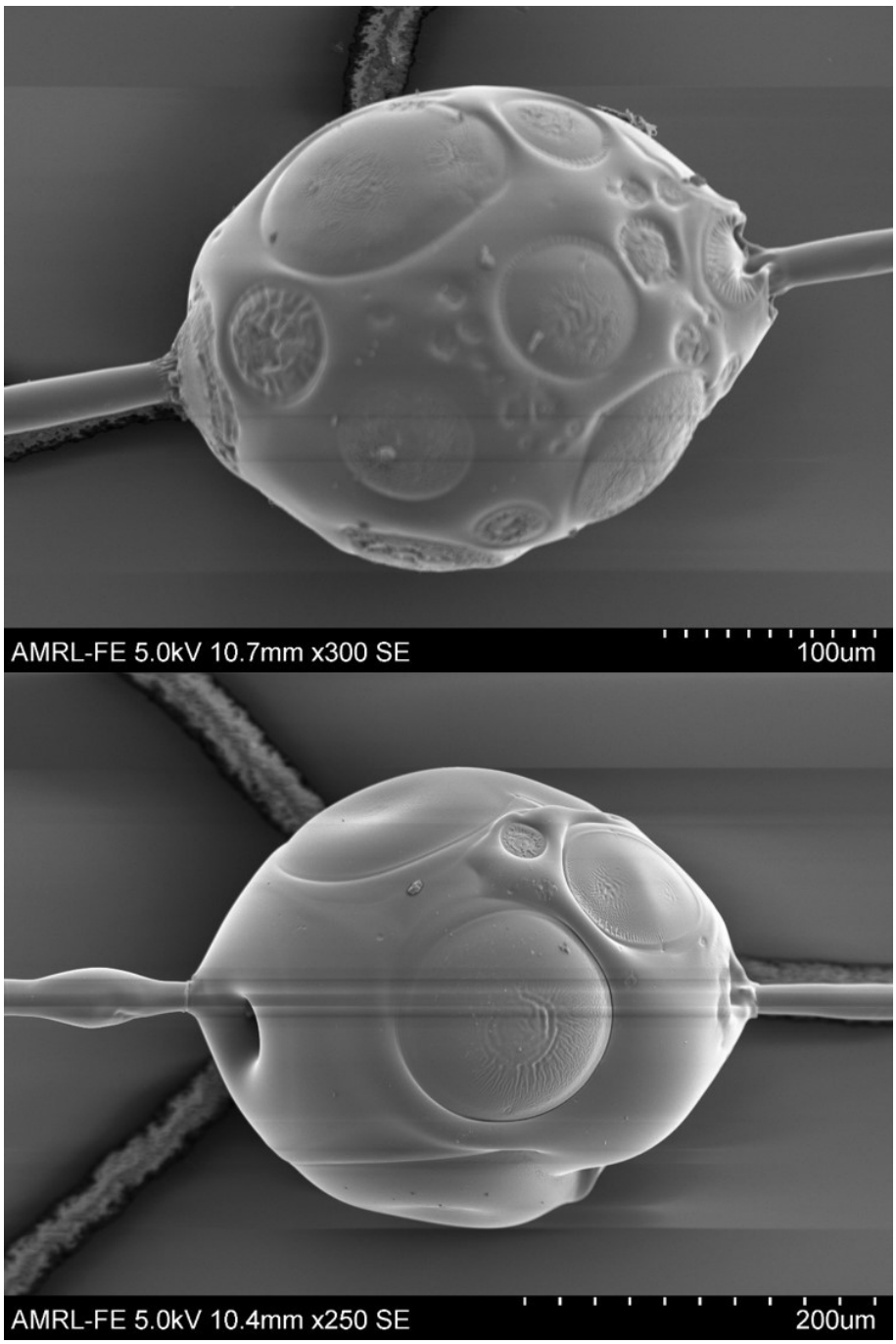

Figure 2:23: Epoxy microbond samples with possible surface Marangoni flow

2.5 CONCLUSIONS

The microbond testing results of the round-robin study of a range of current and experimental glass fibre sizings are summarised in *Table 2-4*. The unsized fibre (BF) is used as a comparative IFSS baseline for subsequent glass fibre sizings treatments. The matrix material used in the investigation was DER 332 DGEBA epoxy resin cured with a stoichiometric (14.3 phr) amount of TETA tetrafunctional amine curing agent.

Designation	Coupling Agent	Film Former	Other	IFSS (MPa)	IFSS Change
BF	-	-	Water	38.6	Baseline
APS	APS	-	-	46.0	↑ 19%
GPTMS	GPTMS	-	-	45.6	↑ 18%
MPTMS	MPTMS	-	-	45.2	↑ 17%
BF-GPTMS	GPTMS	-	-	50.1	↑ 30%
BF-GPMMS	GPMMS	-	-	47.3	↑ 23%
BF-GPMES	GPMES	-	-	53.0	↑ 37%
SE1500	Epoxy-compatible full sizing			51.2	↑ 33%
SE2020	Epoxy-compatible full sizing			50.1	↑ 30%
W2020	Epoxy-compatible full sizing			49.9	↑ 29%
Si-E1	Epoxy-compatible full sizing			48.2	↑ 10%
Si-E2	Modified epoxy-compatible full sizing			47.7	↑ 14%
Si-PP	Polypropylene-compatible full sizing			32.5	↓ 22%
SE1500 AW	SE1500		Acetone	53.5	↑ 39%
SE2020 AW	SE2020		Acetone	50.4	↑ 31%
W2020 AW	W2020		Acetone	54.0	↑ 40%
Epoxy 0.1 wt.%	-	Epoxy resin	-	40.6	↑ 5%
Epoxy 1 wt.%	-	Epoxy resin	-	40.9	↑ 6%
Epoxy 2 wt.%	-	Epoxy resin	-	49.3	↑ 28%
Epoxy 3 wt.%	-	Epoxy resin	-	48.8	↑ 26%
Epoxy 5 wt.%	-	Epoxy resin	-	50.4	↑ 31%
Epoxy 10 wt.%	-	Epoxy resin	-	51.0	↑ 32%
GPTMS-E10	GPTMS	Epoxy resin	-	56.5	↑ 46%
SE2020-E10	SE2020	Epoxy resin	-	59.7	↑ 55%

Table 2-4: Round-robin investigation of the effect of glass fibre sizing on IFSS

In Chapter 2, a round-robin study of the adhesion enhancing capabilities of a wide range of glass fibre sizing components, component combinations, and full sizing packages has been investigated. The application of a series of industrially silane coated fibres (APS/GPTMS/MPTMS) increased glass fibre/epoxy apparent IFSS by approximately 17–20% compared to unsized fibres. Little significant difference between the various silane coatings indicated that despite some measure of universal increase to adhesion properties, specific chemical interactions between the glass fibre and epoxy matrix were not changed much by the silane used. Investigation of the adhesion enhancing properties of silane coupling agents was extended to a range of epoxysilane chemistries using an in-house immersion coating process. The highest value of adhesion was achieved with a GPMES coupling agent. While it is not immediately clear why adhesion was increased by GPMES compared to the other epoxysilanes, the adhesion enhancing capabilities of this coupling agent may have been responsible for comparable IFSS values attainable in a series of epoxy-compatible full sizing formulations (SE1500, SE2020, W2020). Furthermore, the use of a matrix-incompatible full sizing resulted in adhesion properties lower than those of the unsized fibres despite the presence of an undisclosed coupling agent. An apparent adhesion-inhibiting effect of the thermoplastic film former appeared to counteract any improvement due to the silane.

Acetone extraction of fully sized fibres showed that IFSS was improved compared to the as-received fibres in all cases. High apparent IFSS following acetone extraction may be attributable to the bound portion of the sizing remaining on the fibre surface. This bound portion may consist primarily of a silane coupling agent, but the possibility of interaction with residual epoxy film former bound to the silane cannot be discounted. Increased IFSS compared to the as-received fibres may be related to removal of residual surface impurities or improved coupling agent homogeneity by removal of excessively bound silane aggregates. Alternatively, this behaviour may be related to the removal of sizing additives and processing agents whose contribution to the properties of the composite are not well defined.

Finally, glass fibres were treated with an unreacted DGEBA epoxy/acetone solution serving as both a model film former only sizing and post-sizing treatment. Interfacial adhesion values approximating and exceeding those of a number of silane coupling agents and full sizing packages were achieved by coating unsized fibres with epoxy/acetone solution concentrations of 2 wt.% to 10 wt.%. Lower concentration solutions produced adhesion values generally comparable to that of the unsized fibres. IFSS was improved following epoxy/acetone treatment and the order of maximum IFSS achieved was reflected by the initial IFSS of the fibres before treatment (unsized < silane only < full sizing). Coating SE2020 fibres

with a 10 wt.% solution, in fact, produced the highest IFSS values measured over the course of the round-robin investigation. Total sizing content was lower for silane coated and fully sized fibres treated with the same solution concentration due to pre-existing sizing components preventing penetration of the fibre bundles by the epoxy as effectively as unsized bundles. However, an apparent minimum LOI threshold necessary to confer enhanced adhesion properties appeared to have been reached. Increased IFSS as a result of the epoxy sizing application may have been attributable to interdiffusion of the epoxy sizing with the epoxy matrix material and enhanced cross-linking at the interface between unreacted DGEBA in the sizing and amine curing agent.

CHAPTER 3: CHARACTERISATION OF GLASS FIBRE SIZING DEGRADATION

3.1 INTRODUCTION

As a result of its location on the fibre surface, sizing plays a critical role in the formation and properties of the fibre/matrix interphase. Furthermore, glass fibre sizings have an important role in establishing and maintaining a high level of strength in glass fibre products. A number of authors have reported on the loss of strength and surface functionality when glass fibres are exposed to elevated temperature, suggesting that these phenomena are related to the loss of functionality of the fibre sizing and fundamental changes in both the flaw distribution density and severity on the fibre surface [143–147]. At high composite processing temperatures the thermal stability of organic materials, such as polymers and sizing components also becomes a concern. Such considerations are important due to an increase in research into the recycling of end-of-life composite products, with typical thermal recycling processes removing most, if not all, of the sizing layer from the glass fibre surface [146]. Furthermore, while glass fibre thermosetting composites are not typically processed at excessively high temperatures, the use of high temperature curing thermoset resin systems and local exotherm may contribute to spikes in local temperature.

Findings presented in Chapter 2 indicated that both silane coupling agents and polymeric film formers may contribute towards increased interfacial adhesion in glass fibre/epoxy microcomposites. It was also shown that an epoxy film former coating could confer favourable adhesion properties. As such, it is important to investigate how these sizing components respond to exposure to elevated temperature conditions and the resulting implications this holds for the interfacial adhesion of the system. The work presented in Chapter 3 details the thermal analysis, spectroscopic, and micromechanical testing methods used to characterise the thermal degradation of a range of commercial and experimental glass fibre sizings and the effect of sizing degradation on interfacial adhesion.

3.2 LITERATURE REVIEW

3.2.1 Thermal Degradation of Glass Fibre Sizings: Thermogravimetry

Gao *et al.* characterised the thermal stability of the fibre sizings using isothermal TGA between 200–330°C under air to simulate the temperatures used in a lamination process [148]. Apparent weight loss and degradation of components started at temperatures as low as 50°C and weight loss remained constant after 350°C. Thermogravimetric curves also showed that glass fibre sizing degraded within 15 min of isothermal heat treatment at 500°C. Furthermore, XPS data indicated that the organic finish and an APS silane coupling agent gradually desorbed as the glass surface became barer, evidenced by increased concentrations of glass fibre components. At 500°C, exceedingly low concentrations of carbon and nitrogen indicated that the organic finish and silane coupling agent had been almost completely removed.

Lenhart *et al.* have demonstrated that the thickness of the silane coupling agent layer in a model sizing may contribute to the decomposition temperature [129]. GPTMS coupling agent layers were grafted to glass microscope coverslips. Silane layer thickness was controlled by varying the concentration of the GPTMS/ethanol/water mixture and was measured using SEM. TGA of GPTMS grafted to high surface area silica power showed that higher concentration solutions corresponded to more material being present, but that a thicker silane coupling agent layer was removed at a temperature some 20–30°C below that of the thinner, lower concentration coating. The result was indicative that thinner sizing layers were more tightly bound to the silica surface.

Rudzinski *et al.* investigated the thermal behaviour of sizings in glass fibre reinforced polyamide composites [149]. Sizings contained either PU film former only or PU film former and APS coupling agent, to which additional polyacrylate or epoxy film formers were added. Thermogravimetric curves showed that sized fibres underwent a mass loss of up to 0.5% at 550°C, a value indicative of complete loss of glass fibre sizing. Differences in the degradation process were observed for fibres sized with formulations containing different components, indicating a dependence on sizing composition. The mass of the sizing containing a PU film former was reduced by 65% at 300°C and was degraded completely at 400°C. The inclusion of a silane coupling agent reduced mass loss by approximately 15% so that only 50% of the sizing was lost at 300°C. The addition of a second epoxy or acrylate film former further reduced thermal degradation and resulted in a mass loss of only 35% at 300°C. Pyrolysis-gas chromatography-mass spectrometry (Py-GC-MS) analysis showed that sizing components remained present at 400°C. Namely, isophorondiisocyanate (indicative of polyurethane) in all samples, bisphenol A (indicative of epoxy) in PU/epoxy/silane samples, and aliphatic ester

(indicative of a polyacrylic dispersion in the sizing). Ammonia, a characteristic degradation product of aminosilane, was also detected. Reduced interfacial adhesion was attributed to degradation of the silane coupling agent.

Pham and Chern reported on the thermal stability of organofunctional polysiloxanes [150]. Dilute aqueous solutions of APS, GPTMS, vinyltrimethoxysilane (VTMO), and MPTMS were hydrolysed and polycondensed to synthesize poly(aminopropyl)siloxane (ASLX), poly(glycidyloxypropyl)siloxane (GSLX), poly(vinyl)siloxane (VSLX) and poly(methacryloxypropyl)siloxane (MSLX) which were then cured and dried. TGA showed extremely different mass loss profiles for different polysiloxanes, with multiple-stage degradation observed over a temperature range of 150–800°C. GSLX and ASLX underwent significant weight loss between 200–300°C, while MSLX and VSLX showed only minor degradation. Further degradation and rapid mass loss was observed in GSLX, ASLX, and MSLX samples in the 300–600°C range, while VSLX showed increased thermal stability and little significant reduction at temperatures beyond 450°C. FTIR measurements indicated that thermal degradation did not occur in GSLX, MSLX, and VSLX samples subjected to treatment at 300°C, while the amino group-containing ASLX underwent degradation at the same temperature. Significant thermal degradation reactions were observed at temperatures of 400°C or higher.

Petersen *et al.* investigated processes for analysing glass fibre sizing [151]. Thermogravimetric analysis-mass spectrometry (TGA-MS) analysis of Soxhlet extracted glass fibre sizings (approximate residual mass 14 mg) showed a three-stage degradation process with a major mass loss peak at 372°C, a shoulder peak at 409°C, and a second peak at 551°C. The first peak corresponded to the loss of polymeric film former (either polyurethane or uncured epoxy resin). The smaller shoulder peak was also attributed to film former decomposition due to sizing formulations potentially containing a mixture of different polymeric components. The third peak was attributed to organosilanes(s) with thermal stability higher than that of APS. The authors reported that mass loss measurements showed good correlation with sizing component distribution. A combined mass loss of 67% from the first two peaks showed good correlation with 79% of the total sizing weight. Similarly, the mass loss of third peak, attributable to the silane coupling agent, accounted for 19% of the total loss. Clear differences in peak intensities at 390°C and 550°C confirmed that sizing components degenerated at different temperatures. Direct TGA measurements of sized glass fibre bundles (approximately 100 mg) showed good correlation with extracted sizings. A mass loss of 63% attributable to a film former occurred at around 320°C. Further degradation accounting for

35% of the total mass loss was observed at 420°C and 460°C and corresponded to organosilanes. Degradation peaks were generally lower for sized glass fibre samples due to differences in sample mass, surface-to-volume ratio, and relative component concentration.

Zhang *et al.* have investigated the thermal stability and mechanical properties of epoxy emulsion sizings [117]. A sizing mixture consisting of DER 331 epoxy resin, PEG 4000 and triphenylphosphine catalyst was stirred at elevated temperature before application to unsized carbon fibres as a 50 wt.% aqueous solution using a high-speed emulsifying machine. TGA performed on fibre samples of approximately 10 mg under nitrogen at heating rates of 10–30 °C/min indicated a sizing content of 1.2%. Onset of weight loss occurred at 300 °C and the sizing had fully degraded by 450°C.

Thermogravimetric analysis of APS particles by Sándor *et al*. indicated a three-step decomposition process [152]. Mass loss observed between 25–200°C corresponded to the release of water and other solvents. Further mass loss in the 250–400°C range was attributed to degradation of aminopropyl chains. The final decomposition stage (450–700°C) was due to dehydroxylation of Si-OH residual functions and formation of Si-O-Si groups. Thermal behaviour of silica hybrids was affected by both the nature and concentration of the organosilane and inorganic residual mass decreased with increasing organic content in the compounds.

Nagel *et al.* investigated the effects of thermal recycling temperatures on the reinforcement potential of glass fibres [147]. TGA results indicated that the organic fraction of the fibre sizing degraded under exposure to elevated temperature and that, under air, the majority of the mass loss occurred below 300°C. Under inert nitrogen atmosphere no significant mass losses were observed below 300°C and total mass loss reached parity with air at around 450°C (approximately 0.6% mass loss).

Belone resized thermally recycled glass fibres with an APS coupling agent and PP (Hydrosize PP2-01) film former at a range (1–5 wt.%) of different sizing solution concentrations and component ratios [153]. Inert atmosphere TGA of resized glass fibre bundles (approximately 50 mg) indicated that mass loss was a two-step process. Partial desorption of sizing and elimination of water from surface bonded silane occurred in the 180–230°C range and desorption of silane coupling agent and film former occurred in the 360–405°C range. Higher mass loss in 1 wt.% and 3 wt.% solutions corresponded to increased silane coupling agent content in the sizing. This behaviour was not observed for the 5 wt.% solution, in that mass loss and total sizing content were comparable for solutions containing 5% and 20% silane coupling agent, while mass loss of the 10% coupling agent sizing was

more than doubled. Higher coupling agent concentrations may have been more easily removed from the fibre surface during rinsing as a result of weaker interaction and self-polymerisation with ethoxy groups in water. Onset of mass loss of resized glass fibre bundles was some 15–50°C lower than that of dried sizing solutions due to differences in surface-to-volume ratio, sample size, and component concentration related to the small fibre diameter and sizing coating thickness. Sizings appeared less thermally stable under air due to thermo-oxidative degradation and the majority of the mass loss occurred at 180–220°C.

3.2.2 Thermal Degradation of Glass Fibre Sizings: Spectroscopy

Spectral characterisation of sized glass fibres and sizing extracts has been reported by Petersen *et al.* [154]. ATR-FTIR of extracted glass fibre sizing showed a broad band between 3600 and 3200 cm^{-1} attributable to the stretching in O-H bonded to C and Si. A triplet collection of bands from 2965–2873 cm^{-1} was attributed to the C-H stretching of CH, CH_2, and CH_3, both in aliphatic and aromatic compounds. A peak at 1735 cm^{-1} corresponded to the stretching of C=O in esters/carbonyl, potentially attributable to a surfactant or anti-static agent [111]. Bands identified at 1608, 1509, 1040, and 830 cm^{-1} were characteristic of an epoxy resin. Bands at 1248 and 1183 cm^{-1} were likewise thought to be associated with epoxy resin, though the former may have also been related to C-O-C in PEG or polyethylene oxide lubricants/surfactants. Bands around 1100 cm^{-1} were assigned to the stretching of C-O and Si-O, possibly indicating the presence of polyethylene or a silicon oxide component. Epoxysilane samples showed the characteristic epoxy peak attributable to the oxirane ring at 916 cm^{-1}. Furthermore, the C-O-C band identified may also have originated from a polyethylene oxide lubricant/surfactant. The authors concluded that the absorption bands observed in the spectra could plausibly be attributed to a sizing containing an epoxy resin film former and a polyethylene oxide lubricant/surfactant.

Direct spectral analysis of sized glass fibre bundle surfaces showed a broad high intensity band at 1200–800 cm^{-1} corresponding to Si-O-Si bonds that rendered the identification of sizing components with lower relative signal intensities difficult [111]. Low signal intensity was attributed to the penetration depth of infrared light exceeding the estimated sizing layer thickness. Visible bands in the 3600–1200 cm^{-1} range corresponded to those detailed for the sizing extracts. The disappearance of bands characteristic of the sizing (and reference silanes) after 565°C heat treatment indicated that the sizing had either been completely removed, or reduced to an amount below the detection limit of the instrument. Heat treated fibre surfaces may have shown spectra attributable to the inorganic portion of the sizing (Si-O from the silane

coupling agent) but it was indistinguishable from the Si-O signal of the glass fibre. Furthermore, silane could not be distinguished from physisorbed or bonded organosilane.

ATR-FTIR spectral details of aminosilane functionalised silica nanoparticles have been reported by Sándor *et al.* [152]. A broad band centred around 3440 cm^{-1} was assigned to hydrogen bonded and partially hydrated silanols (Si-OH). Aminopropyl samples showed symmetrical and asymmetrical stretching vibrations of CH_2 from aminopropyl segments in the 3000–2800 cm^{-1} range. A band at approximately 1630 cm^{-1} was characteristic of NH_2 deformation in primary amines and was overlapped by a band 1650 cm^{-1} attributable to C=O stretching in carbonyl compounds. A peak at 1491 cm^{-1} was assigned to bending mode N-H vibration in the primary amine group and 1390 cm^{-1} was assigned to C=O of bicarbonate species. Bands in the 1300–400 cm^{-1} region were associated with vibrations of a silica network.

Belone used ATR-FTIR to identify functional groups on unsized and resized glass fibres [153]. Spectra of resized glass fibres in the 3000–2800 cm^{-1} region corresponded to the stretching vibration of C-H bonds in CH_2 and CH_3 and were attributed to the presence of both a PP film former and a silane coupling agent (due to its aminopropyl segment). Peaks in the 1500–1300 cm^{-1} range were assigned to the bending vibrational mode of the C-H bond of the PP backbone in maleic anhydride grafted polypropylene (MAPP) and the N-H group of APS. Spectra of dried APS coupling agent showed a band at 3300 cm^{-1} corresponding to the N-H stretching vibration of primary amines, a doublet at 3000–2800 cm^{-1} corresponding to the stretching vibration of CH_2, and a peak at 1650–1580 cm^{-1} characteristic of an NH_2 bending mode in amines. Spectra below the dominating band at 1200 cm^{-1} were related to vibrational modes of polysiloxanes. Increased peak intensity appeared to correspond with increased sizing solution concentration.

Using ATR-FTIR, Bashir observed a substantial decrease in the doublet peaks around 2900 cm^{-1} after APS coated glass fibres were heat treated at 450°C, a result indicative of removal of the silane [155]. The characteristic silane peaks, however, became visible again following a sodium hydroxide treatment, with signal intensity exceeding that of the baseline as-received fibres. The author suggested this phenomenon may have been due to interaction between organic contaminants and alkali rather than residual silane. Hydrocarbon absorbance at 2900 cm^{-1} corresponded to strong carbonyl absorbance at 1750 cm^{-1}, indicating the possible presence of carboxylic species on the glass fibre surface. It was proposed that the limited penetration depth of ATR may have been the cause of some experimental error, though similar species were observed using alternate instrument interfaces (diffuse reflectance, specular reflectance) with greater penetration depths.

FTIR of sized glass fibre fabric by Sherif *et al.* indicated a major increase in a C=O peak at 1678–1683 cm^{-1} following compression moulding of composites, attributable to oxidation during the heating stage [156]. The same band was, however, also attributed to a solvent containing C=O in polymer solution samples. As-received glass fibres showed a C-H stretching triplet assigned CH, CH_2, and CH_3 between 2969 and 2831 cm^{-1} which was not present in samples pre-treated at 350°C. The authors suggested that the disappearance of this group in the heat treated fibres indicated that most of the sizing had been removed, though residual sizing may have remained below the detection limit of the instrument.

3.2.3 Thermal Degradation of Glass Fibre Sizings: Interfacial Adhesion

Thermosetting Matrices

Thomason has investigated the interface region in glass fibre reinforced epoxy resin composites [157]. It was shown that the removal of fibre sizing following heating at 500°C for 24 h resulted in a significant decrease in interfacial adhesion as measured by short beam shear test. Fibres that had been heated to 200°C showed a markedly less detrimental effect. Acetone extraction similarly removed the fibre sizing and decreased ILSS.

Kennerley *et al.* reported on the properties of glass fibres recycled from the thermal processing of scrap thermoset composites [158]. Samples of E-glass cloth were heat treated at temperatures of 375°C, 500°C, and 625°C for up to 1 h in an ashing furnace before composite samples were created using either wet lay-up or resin transfer moulding techniques. After treatment at 500°C, the reapplication of a silane coating made a significant contribution to composite material properties and was attributed to the improvement of the fibre/matrix interfacial bond. Improvements to interfacial properties were also responsible for significant increases in composite tensile strength following treatment at 500°C. Following treatment at 375°C, tensile strength was reduced with increasing treatment time, albeit to a lesser extent than that of 500°C and 625°C treatments. Furthermore, it was proposed that the original fibre sizing may not have been removed at a treatment temperature of 375°C.

Åkesson *et al.* performed microwave pyrolysis on scrap wind turbine blade thermoset material at 300–600°C for approximately 90 min under nitrogen atmosphere after which composites were prepared [159]. Tensile testing showed that fibres pyrolysed at 300°C were largely unaffected by the treatment. A decrease in tenacity of around 25% at 360°C compared to virgin fibres was observed, and no further reduction occurred by increasing treatment temperature to 440°C. Samples treated at 600°C were too brittle to test and had mostly been

destroyed by the process. The reduction in mechanical properties was attributed to the pyrolysis process causing changes in the surface properties of fibres. Degradation of the fibre sizing resulted in low interfacial tenacity between fibre and matrix and was evidenced by SEM. Micrographs showed clean fibres and fibre pull-out consistent with sub-optimal adhesion. The authors suggested that interfacial adhesion could be improved by heating under oxygen (removing char) and the reapplication of a new sizing.

Pender has investigated the tensile and interfacial properties of glass fibres recovered from a fluidised bed recycling process [160]. Glass fibre/epoxy IFSS was reduced to around to 60% of the initial value after APS coated fibres were exposed to a thermal recycling process. Poor adhesion was attributed to degradation of the silane coupling agent rendering the sizing ineffective. Post-treatment IFSS was comparable to that of unsized fibre using the same epoxy matrix material. Furthermore, significant weakening of fibre tensile strength made interfacial assessment difficult as both thermally conditioned and recycled fibres frequently fractured prematurely before debonding.

Thermoplastic Matrices

Yang *et al.* have reported that the IFSS of GF/MAPP decreased from 16 MPa to approximately 8 MPa after heat treatment at 500°C [161]. The loss in IFSS was attributed to the decomposition of the silane coating. IFSS values of heat treated fibres showed good correlation with that of previously measured values for an unsized fibre, indicating that the surface of the glass fibre had lost all functionality to react with the MAPP in the matrix. Further reductions in IFSS were predicted for fully sized glass fibres subjected to comparable heat treatments compared to a formulation containing a single component (silane). In a subsequent study by Thomason *et al.* IFSS of a GF/PP system dropped from 14.7 MPa to 9.2 MPa following heat treatment at 500°C removing the fibre sizing [162]**.** The value similarly approximated unsized glass fibre IFSS values. The tensile performance of composites containing the heat treated fibres reflected the lower strength of the individual fibres and poorer interfacial adhesion.

Nagel *et al.* reported that interfacial adhesion, as measured by the microbond test, showed that the compatibility of the glass fibre sizing to a PP matrix was lost after exposure to thermal treatment of 250°C in air and showed good correlation with mass loss due to sizing decomposition [147]. The loss in apparent adhesion was mirrored by a significant drop in the tensile strength of injection-moulded PP composites.

3.2.4 Conclusions of Literature Review

Thermogravimetric studies in the literature would indicate that glass fibre sizing decomposition may potentially onset at temperatures as low as 50°C [148], though the majority of sizing mass loss is typically recorded at temperatures in the 300-600°C range. At temperatures of 400–500°C and above, full thermal degradation of the sizing has been reported [117,147,149]. Polymeric film former and silane coupling agents may degrade at different temperature, and the composition [149] and concentration [129] of these components may affect the degradation temperature. Up to 80% of mass loss may be attributable to the film former in the 370–410°C range, while silane coupling agent accounting for the remainder of the sizing mass may not fully degrade until upwards of 550°C [151]. Sizings containing aminosilanes may degrade at lower temperatures, however [150,152,153]. Furthermore, glass fibre sizing content, characterised by LOI measurements is typically around 0.5–0.7% [147,149,151].

FTIR methods have previously been used to characterise the composition of glass fibre sizings [151] and silanes [152]. While spectra have been reported before and after extensive heat treatment or acetone extraction procedure, there appears to remain a gap in the knowledge as to how the composition of the sizing changes over the 25–500°C temperature range.

A number of authors have reported on interfacial adhesion between the fibres and the polymer matrix being a limiting factor in the strength of composites based on thermally degraded glass fibres. Both Bikiaris *et al.* [163] and Åkesson *et al*. [159] have cited fracture surfaces as proof of low interfacial adhesion while Roux *et al.* [164] and Yang *et al.* [161] measured changes in adhesion using micromechanical testing methods. While a number of authors have reported on fracture surface morphology as a qualitative assessment of the degree of fibre/matrix adhesion, Fu *et al.* have reported that conclusions drawn from such SEM observations may in fact be misleading [165]. Investigations of the relationship between sizing degradation and interfacial adhesion have typically been focused on thermoplastic matrices and few studies have employed direct methods of assessing the interfacial adhesion of epoxy-compatible glass fibres and thermoset matrices following exposure to elevated temperatures.

3.3 EXPERIMENTAL

3.3.1 Materials

Glass Fibres

Investigation of the thermal degradation of glass fibre sizings was performed on three fully-sized commercial glass fibres sized with epoxy-compatible formulations: SE1500, SE2020, and W2020. Fully sized glass fibres were produced by 3B and supplied by 3B (SE1500, SE2020) and Suzlon (W2020). Fibres sized with an epoxy film former alone were produced by coating unsized glass fibres with an unreacted epoxy resin/acetone solution. Epoxy coating thickness was controlled by using different concentrations of solution. Coating of epoxy coated fibres is detailed previously in 2.3.1. Sizing layer thickness calculations can be found in Appendix B. Fibres sized a with silane coupling agent alone were supplied by Owens Corning. Additionally, bare glass fibres were sized with 1 vol.% solutions of APS and GPTMS. The fibres used in the study were of the same approximate average diameter (17.5 μm) and nominal tex (1200 g/km) and are summarised in *Table 3-1*.

Designation	Coupling Agent	Film Former	Other	Manufacturer
BF	-	-	Water-spray	Owens Corning
APS	APS	-	-	Owens Corning
GPTMS	GPTMS	-	-	Owens Corning
MPTMS	MPTMS	-	-	Owens Corning
BF+APS	APS	-	-	In-house
BF+GPTMS	GPTMS	-	-	In-house
0.1–10 wt.% Ep-FF	-	Epoxy resin	-	In-house
SE1500	Epoxy-compatible full sizing			3B
SE2020	Epoxy-compatible full sizing			3B
W2020	Epoxy-compatible full sizing			3B

Table 3-1: Summary of glass fibres

Epoxy Resin

The matrix material used in the investigation was DER 332 DGEBA epoxy resin cured with a stoichiometric (14.3 phr) amount of TETA tetrafunctional amine curing agent, technical grade 60%. Both resin and curing agent were purchased from Sigma Aldrich/Merck. Microbond samples were cured at 60°C for 1 h followed by 120°C for 2 h with a 2°C/min temperature ramp used throughout and were allowed to cool overnight in the oven before being removed.

Silane Films

Pure silane was used to create GPTMS films. A dilute acetic acid solution was used to adjust the pH of deionised water to between pH 5 and 5.5 in order to promote hydrolysis of the silane in water. A 1 vol.% solution (100 mL) was hydrolysed for 24 h in a sealed volumetric flask. The solution was then poured into a petri dish and dried at 60°C for 12 h to create a film of approximate thickness 500–600 μm. GPTMS was purchased from Sigma Aldrich

3.3.2 Heat Treatment of Glass Fibres

In order to study the effect of heat treatment and subsequent thermal degradation of glass fibre sizing, three fully sized fibres were heat treated at 200–500°C in air atmosphere. Heat treatments were performed using a Carbolite CWF1200 electric furnace. Lengths of fibre bundle were removed from the larger roving and attached to a metal rig using a bolt and washer. All heat treatments were carried out for 25 min and consisted of a 10 min pre-heating step to reach the desired temperature followed by a 15 min heat treatment. The treatment time approximately reflects similar thermal recycling treatments found in the literature [158,166]. After treatment, samples were cooled immediately at ambient temperature. Individual filaments were extracted and microbond samples prepared according to the procedure detailed in 2.3.2.

3.3.3 Thermogravimetric Analysis of Sized Glass Fibres

Thermogravimetric analysis (TGA) was performed under air from 25–700°C with a heating rate of 10°C/min using a TA Instruments Q50 TGA. Gas flow rates were 40 mL/min and 60 mL/min for the balance and sample, respectively. The weight loss of glass fibres with different sizings were recorded as a function of the temperature in air atmosphere. A length of roving was extracted from the spool and one end held with tweezers while the other was cut with scissors. The small bundle of fibres was then placed into a platinum TGA pan, ensuring full coverage of the surface area, an adequate amount of fibre material (approximately 5–15 mg), and good contact with the pan surface. A baseline subtraction procedure and signal smoothing function was used to clarify thermograms with extraneous curve effects generated as a result of the small sample mass. Accordingly, three baseline measurements were performed by subjecting empty crucibles to the same temperature schedule. Once it was verified that the results were reproducible, a baseline subtraction was applied to sized fibre thermograms. Data were analysed using TA Universal Analysis software. Method details were as follows:

1. Equilibrate at 25°C
2. Data storage: On
3. Ramp 10°C/min to 700°C/min
4. Data storage: Off

The thickness of the glass fibre sizing and depletion of layer thickness following exposure to elevated temperature was calculated using TGA data as detailed in Appendix B

3.3.4 Fourier-Transform Infrared Spectroscopy

Fourier-transform infrared spectroscopy (FTIR) was used to analyse the surfaces of as-received glass fibre bundles and to characterise the thermal degradation of sizing following exposure to elevated temperature treatment. Analysis was performed using a 4100 ExoScan FTIR fitted with a spherical diamond attenuated total reflectance (ATR) interface, adjustable probe, and benchtop docking station. Sized glass fibre bundles were placed on the sample stage and the adjustable probe was fully lowered to ensure good fibre contact with the crystal. Spectra were collected from ten individual points (approximately 1 cm apart) along the length of 15 cm sections of each glass fibre roving. Background signal was measured after each spectra and the crystal was cleaned with acetone between measurements. Analysis was performed in the 4000 to 650 cm^{-1} range with a spectral resolution of 8 cm^{-1} and 64 scans per sample. OriginPro software was used to process spectral data and plot normalised average spectra. SpectraGryph software was used for peak identification and quantitative analysis. Spectra were generally insensitive to increased spectral resolution and scans collected at 4 cm^{-1} showed no significant differences compared to those collected at 8 cm^{-1}.

3.3.5 Micromechanical Testing: Microbond

The development [34] and utilisation of the microbond testing method used has been reported previously [167]. Microbond testing of fully sized glass fibres was conducted after exposure to 200–500°C thermal treatment to investigate the relationship between glass fibre sizing degradation and IFSS. Samples were prepared and tested as detailed in 2.3.2.

3.4 RESULTS AND DISCUSSION

3.4.1 Thermogravimetric Analysis of Glass Fibre Sizing

TGA was used to investigate the thermal degradation of glass fibre sizings. Silane coated, epoxy film former only, and fully sized commercial glass fibres were examined in order to determine the stability and decomposition temperatures of various sizing components.

Silane Coated Glass Fibres

Silane coupling agents are widely regarded as promoters of interfacial adhesion and the removal of them through a thermal treatment may significantly impact the interfacial strength of composite materials [149]. TGA thermograms of APS, GPTMS, and MPTMS silane sized glass fibres are shown in *Figure 3:1*.

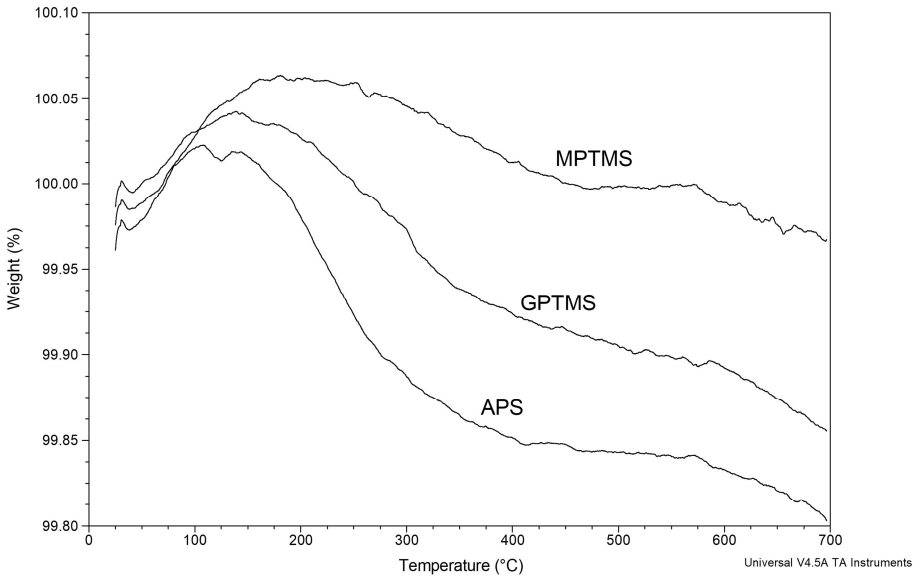

Figure 3:1: TGA thermogram of silane coated glass fibres

Silane coated fibre samples generally appeared thermally stable and underwent only an extremely small mass reduction, likely due to the fact that the mass of silane present is insignificant compared to the bulk fibre mass. The slight increase in sample mass observed in the 25–200°C range can be attributed to an artefact of the extremely small amount of material present. It is possible that the observed weight increase may be related to sample buoyancy caused by a heating pulse effect wherein purge gas density reduces following initial heating of the sample. Furthermore, decomposed silane mass was too small to allow a baseline subtraction procedure to be applied. From the TGA data it can be posited that either the silane component of the sizing is thermally stable, or that the instrument sensitivity was not sufficient

to accurately measure the mass loss of the silane. A large signal-to-noise ratio meant that the determination of degradation onset points and first derivative peak temperatures was not possible. Nevertheless, the LOI values generated for APS and GPTMS silane sizings showed good correlation with the values determined by an internal study of two different APS coated fibres conducted by the instrument manufacturer (0.1334–0.1370%). The LOI values of silane sized glass fibres are summarised in *Table 3-2*.

Fibre	TGA LOI (%)			
	1	2	3	Mean
APS	0.0777	0.1309	0.1978	0.1350
GPTMS	0.0163	0.2245	0.1456	0.1288
MPTMS	-	-	0.0378	0.0378

Table 3-2: TGA LOI of silane coated glass fibres

GPTMS polysiloxane films were examined due to the poor resolution of direct TGA of the decomposition of silane coated glass fibre bundles. A TGA thermogram and first derivative peak temperatures of a GPTMS silane film heated under air is shown in *Figure 3:2*.

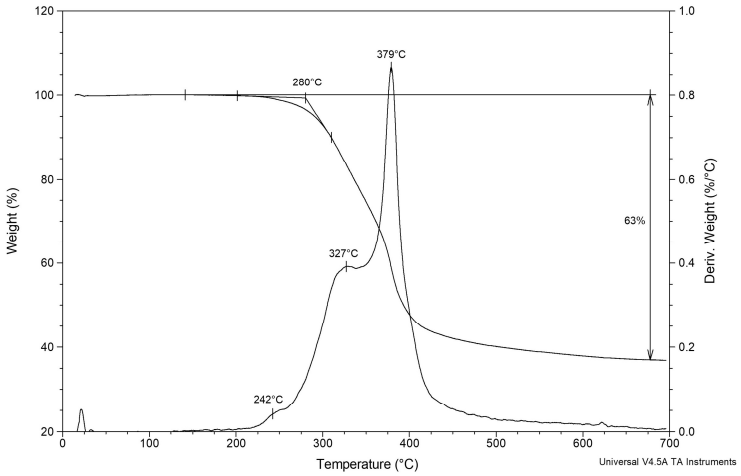

Figure 3:2: TGA thermogram of GPTMS polysiloxane film

Thermal decomposition of GPTMS polysiloxane films showed a primarily two-step degradation process with mass loss onset occurring at approximately 280°C. First derivative peak temperatures were located at around 327°C (corresponding to the smaller shoulder peak) and 379°C (corresponding to the larger sharp peak) and the majority of the mass loss occurred between 250–400°C. A second small shoulder peak located at around 242°C may be attributable to the decomposition of the epoxy group present in the silane. Mass loss appeared to stabilise at approximately 550°C and a 63% reduction in initial mass. The LOI values, onset temperature and first derivative peak temperatures of the GPTMS silane films are summarised in *Table 3-3.*

TGA LOI (%)				T_{onset} (°C)	$T_{shoulder}$ (°C)	T_{peak1} (°C)	T_{peak2} (°C)
1	2	3	Mean				
62.49	63.13	62.52	62.71	278	242	324	379

Table 3-3: TGA LOI of GPTMS silane films

Epoxy Coated Glass Fibres

It is well recognised in the literature that epoxy-compatible sizings may typically contain a large fraction of epoxy resin (typically DGEBA) as a film former, accounting for the majority of the sizing by weight [168]. Similarly, consideration is given to the findings presented in 2.4.5 which indicated that adhesion properties comparable to those of silane coupling agents and full sizings could be achieved by application of a model epoxy film former. *Figure 3:3* shows a typical epoxy coated glass fibre bundle thermogram.

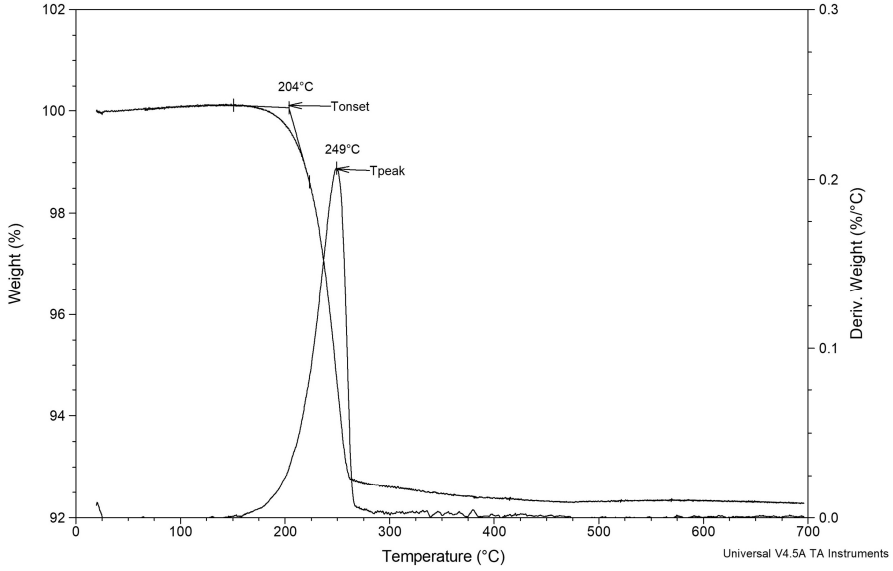

Figure 3:3: TGA thermogram of 10 wt.% epoxy coated glass fibres

A comparative overlay of glass fibres sized with a 0.1–10 wt.% unreacted epoxy resin/acetone solution film former is shown in *Figure 3:4*. A primarily single step degradation process with the majority of the mass loss occurring by 220–260°C was observed. A second smaller degradation was visible at approximately 260–400°C after which mass loss appeared to stabilise, indicating that the polymeric sizing had completely degraded. Further heating up to 700°C resulted in no further significant mass loss. The onset temperature and the position of the first derivative peak temperature increased linearly as the concentration of the epoxy/acetone solution and sizing layer thickness was increased. Fibres coated with a 10 wt.% epoxy/acetone solution, with a sizing layer thickness of approximately 735 nm, showed a mass loss onset temperature as much as 40°C higher than that of the fibres coated in a 0.1 wt.%

solution. Onset of degradation of unreacted epoxy resin coatings appeared to occur at temperatures around 100°C below that of a partially cross-linked epoxy sizing reported by Vautard and Drzal [114].

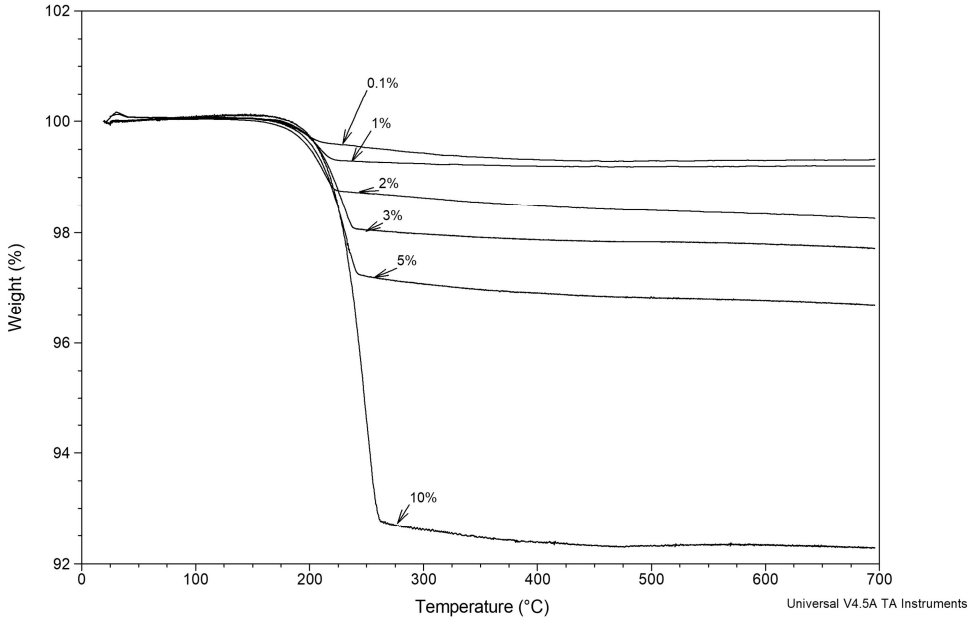

Figure 3:4: Thermogram overlay of epoxy coated glass fibres

Onset and first derivative peak temperatures are plotted against epoxy sizing layer thickness in *Figure 3:5*. Regardless of sizing layer thickness, the epoxy sizing was completely removed following treatment at 400°C and all sizings degraded at temperatures below that of bulk resin samples. Mass loss onset at approximately 256°C in the baseline bulk resin samples and a mass loss of approximately 95% in the 250–350°C range was observed. The remaining 5% mass was completely degraded by 500°C. It seems plausible to suggest that glass fibre sizing components, or certainly the polymeric film former, may be less thermally stable and degrade at temperatures markedly different to that of bulk samples, the extent of which is dependent on the thickness of the sizing layer. TGA performed on PU/APS-sized glass fibres and macroscopic film samples by Rudzinski *et al.* showed that the peak maxima position of the degradation of the sizing on the glass fibre surface was up to 100°C lower than that of a film [149]. Similarly, Petersen *et al.* reported that TGA of sized glass fibres and films cast from sizing extracted from the same fibres reflected a shift to decomposition at lower temperatures for the sizing on the fibres [151]. On the other hand, the results presented would appear to be contrary to those reported by Thomason, who showed that the T_g of a coating containing only epoxy resin applied to glass fibres decreased with increasing layer thickness [124]. Lenhart *et al.* reported a similar behaviour regarding the silane component of the sizing, in that a thicker GPTMS silane coupling agent layer in a model sizing was removed at a temperature 20–30°C

below that of the thinner, lower concentration coating [129]. A thinner layer was thought to be more tightly bound to the silica surface.

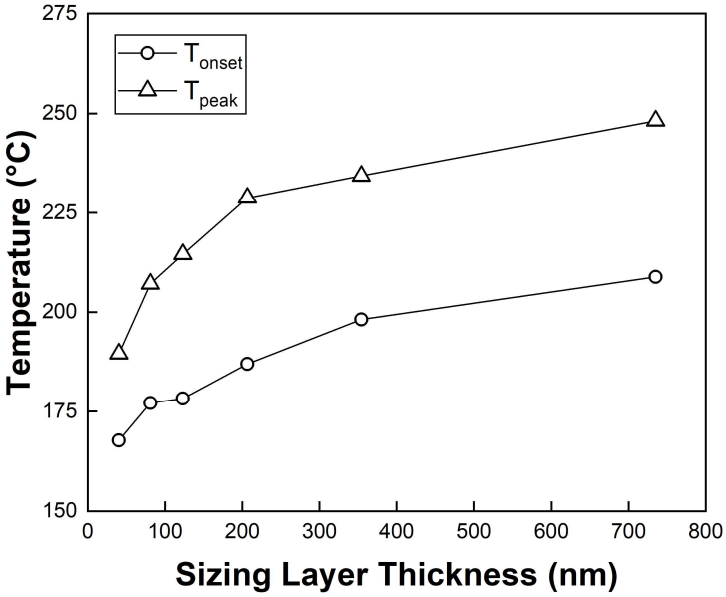

Figure 3:5: Onset and first derivative peak temperature versus epoxy layer thickness

Glass fibre LOI and sizing layer thicknesses were lower when the same 10 wt.% epoxy/acetone solution was used to coat fibres that were already sized with a silane (or a full sizing) compared to bare fibres. Silane coated fibres sized with a 10 wt.% epoxy solution produced a thicker sizing layer than the fully sized fibres. It is likely that the ability of the epoxy solution to effectively penetrate the fibre bundles and coat pre-sized fibres was limited by the existing sizing. This effect was more pronounced when a film former was already present in the sizing formulation (SE2020). Onset temperatures were generally somewhat lower than that of bare fibres sized with the same epoxy solution and were approximately the same for GPTMS and SE2020 fibres coated with a 10 wt.% solution despite lower layer thicknesses. Peak temperature measurements were similar for all 10 wt.% epoxy coated samples.

Care should, however, be taken in the interpretation of TGA data. Deviation between bulk resin and epoxy coated fibre onset temperatures became less apparent (≈10°C) when plotted over a fixed mass loss range (100–99%). Higher apparent onset and peak temperatures may also have been partially attributable to thicker sizing layers degrading more slowly than thinner ones. It is possible that a combination of this slowing effect and the dynamic temperature range used contributed to an apparent upwards shift in peak temperature. LOI values, onset temperatures (T_{onset}), first derivative peak temperatures (T_{peak}), and sizing layer thicknesses of epoxy film former coated glass fibres are summarised in *Table 3-4*.

Concentration	TGA LOI (%)				T_{onset}	T_{peak}	Sizing Thickness
	1	2	3	Mean	(°C)	(°C)	(nm)
0.1 wt.%	0.63	0.42	0.22	0.42	168	190	40
1 wt.%	0.86	0.80	0.87	0.84	177	207	81
2 wt.%	1.23	1.27	1.33	1.28	178	215	123
3 wt.%	2.28	1.98	2.13	2.13	187	229	207
5 wt.%	3.30	3.62	3.98	3.63	198	234	354
10 wt.%	7.70	7.00	7.50	7.40	209	248	735
GPTMS + 10 wt.%	5.10	4.95	5.42	5.16	194	240	507
SE2020 + 10 wt.%	2.92	3.02	3.03	2.99	198	242	291
Bulk resin	100%			-	256	325	-

Table 3-4: TGA LOI of epoxy coated glass fibres

Fully Sized Glass Fibres

While the mechanisms behind the improvements conferred by fibre sizing are not fully understood, it is well recognised in the literature that the optimal working of glass fibre sizings are necessary in order to maximise the performance of glass fibre reinforced composites. It is important that organic components in sizing formulations continue to function after exposure to the high temperatures that are often experienced during the processing of composites. Despite the fact that glass fibre thermosetting composites are typically processed at temperatures well below that of their thermoplastic counterparts, there exists a number of high temperature curing epoxy systems. Local exotherm during curing may also result in local temperature spikes. As a result, it is important that the thermal degradation of thermoset-compatible glass fibre sizings is considered. TGA thermograms of SE1500, SE2020, and W2020 glass fibre bundles are shown in *Figure 3:6*. LOI values and sizing layer thicknesses are summarised in *Table 3-5*. Fibres sized with a 1 wt.% epoxy/acetone solution with LOI sizing layer thickness approximating that of commercial fully sized fibres are also included for comparison.

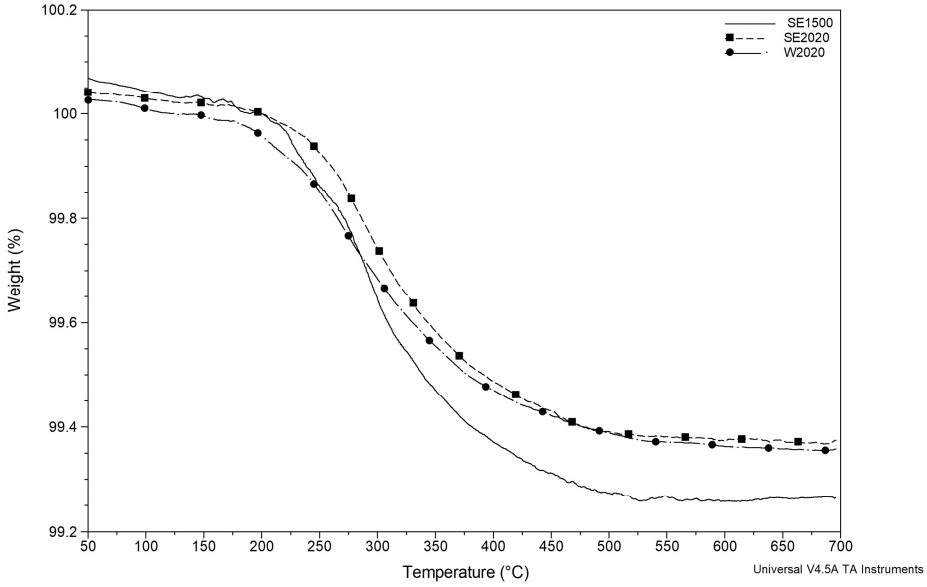

Figure 3:6: TGA thermograms of SE1500, SE2020, and W2020 glass fibre bundles

Fibre	TGA LOI (%)				T_{onset} (°C)	T_{peak} (°C)	Sizing Thickness (nm)
	1	2	3	Mean			
SE1500	0.87	0.74	0.74	0.78	228	296	87
SE2020	0.67	0.57	0.62	0.62	249	281	69
W2020	0.64	0.49	0.64	0.59	232	270	66
1 wt.% Epoxy	0.86	0.80	0.87	0.84	177	207	81

Table 3-5: TGA LOI of fully sized commercial glass fibres

Epoxy-compatible glass fibre bundles appeared to remain thermally stable up to approximately 200°C after which degradation of sizing components onset. A small weight increase in the 25–50°C temperature region can be attributed to an experimental artefact that was not entirely removed by the baseline subtraction procedure due to the extremely small sample mass [143]. E-glass is thermally stable in this temperature region, so it is reasonable to assume that the weight changes observed are caused primarily by the degradation of the organic components of the glass fibre sizing. The majority of the mass loss occurred in the 200–400°C range and was primarily attributable to the decomposition of the polymeric film former component of the sizing, given that film former accounts for the majority of the sizing by weight. Further mass loss at temperatures greater than 400°C may have been due to decomposition of the epoxysilane coupling agent present.

Mass loss stabilised around 500°C, indicating that the sizing had completely degraded, and TGA LOI measurements showed good correlation with values previously reported in the literature [102,149,151]. Onset of mass loss was generally higher, by some 20–60°C depending on layer thickness, than that of the fibres containing only an epoxy film former.

This behaviour may have been due to the inclusion of a silane coupling agent in the full sizing formulation. TGA analysis by Rudzinski *et al.* showed that the inclusion of a silane coupling agent reduced mass loss by approximately 15% at 300°C [149]. An apparent disparity between values for the full sizings (containing a film former and silane coupling agent) and the epoxy coated GPTMS/SE2020 fibres may be attributable to differences in sizing layer thickness and the fact that sizing components were applied sequentially. Sizings applied by an industrial kiss-rolling process may have been more tightly bound to the glass fibre surface than coated fibre bundles.

Thermal degradation of the glass fibre sizing appeared to be a primarily single-step process, rendering the exact decomposition temperature of individual components difficult. Conversely, Petersen *et al.* have reported a clear two-step degradation process [151]. It is possible that a combination of increased sensitivity (due to the TGA-MS technique employed) and increased fibre bundle mass (approximately 100 mg) accounted for the clarity between the peaks and identification of decomposition of individual sizing components. Despite this, the authors reported that even 10 cm fibre bundles may not have been sufficient for definitive determination of sizing content due to substantial variation in the amount of sizing present along the length of the fibres.

Finally, TGA data was used to quantify the depletion of the sizing layer thickness as treatment temperature was increased. An initial sizing layer thickness of 70–80 nm showed good agreement with those reported in the literature [128,168]. Sizing layer thickness was reduced by approximately 50% following 300°C heat treatment and removed almost entirely following treatment at 500°C. The depletion of the sizing layer thickness is summarised in *Table 3-6.*

Fibre	**Sizing Layer Thickness (nm)**						
	25°C	**200°C**	**250°C**	**300°C**	**350°C**	**400°C**	**500°C**
SE1500	82	74	62	38	21	11	2
SE2020	70	70	62	41	23	13	2
W2020	71	67	55	36	22	12	3

Table 3-6: Summary of glass fibre sizing layer thickness reduction

3.4.2 Spectroscopic Characterisation of Heat Treated Glass Fibres

Fully sized glass fibre surfaces were examined as-received and after being subjected to 200–500°C heat treatments. Furthermore, spectra were collected from the surfaces of glass fibres with sizings containing silane coupling agent only, or an epoxy resin solution film former only, in order to more easily identify these components, and the chemical changes thereof, in the full sizings. Thus, a spectral picture of glass fibre sizing is developed upwards from unsized to fully sized glass fibres.

Unsized Glass Fibres

FTIR spectra of unsized glass fibres are shown in *Figure 3:7*. The single high-intensity band in the 1200–800 cm^{-1} range is attributable to the Si-O-Si bonds in the glass fibres. Spectral noise in the 2650 to 1650 cm^{-1} range is attributable to the instrinsic absorption of diamond due to the ATR interface used and is unrelated to spectral characteristics of the sizing or the glass fibre surface.

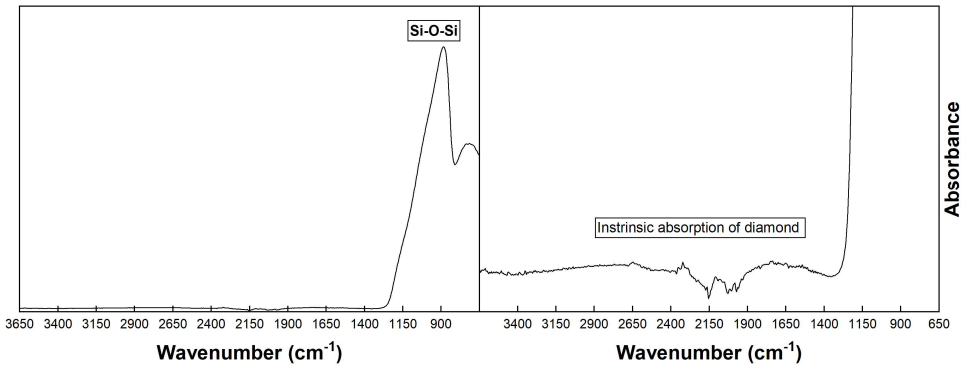

Figure 3:7: FTIR spectra of unsized glass fibres

Silane Coated Glass Fibres

Spectra of sized glass fibres showed a broad high-intensity band in the 1200–800 cm^{-1} range, attributable to the Si-O-Si bonds in the glass fibres, that masked much of the characteristic fingerprint region. The presence of the ubiquitous silica signal can be explained by the fact that the penetration depth of the ATR-FTIR interface used (500–3000 nm) exceeded that of the calculated sizing layer thickness (approximately 80 nm). Furthermore, the volume of the glass fibre was significantly larger than that of applied sizing. Indentification of bands associated with sizing components was complicated by the disparity in the signal intensity of the strong silica signal and the weaker bands indicative of sizing components such as silanes, polymeric film formers, and lubricants or surfactants. As a result, spectra of glass fibre surfaces

are hereafter presented with magnified views of key spectral regions. FTIR spectra of silane coated glass fibres are shown in *Figure 3:8*.

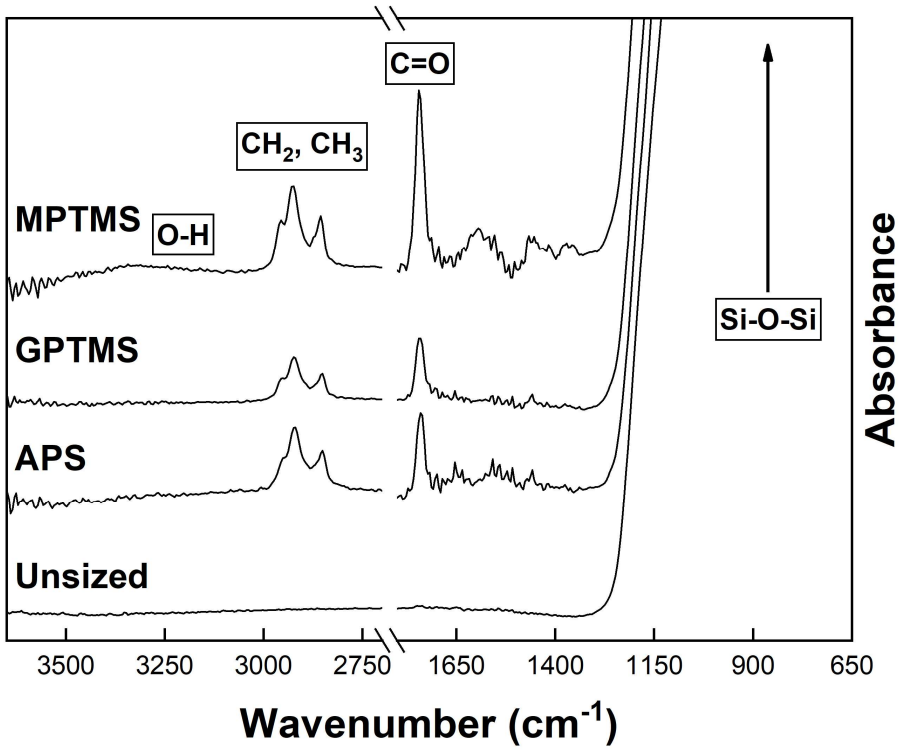

Figure 3:8: FTIR spectra of silane coated glass fibres

The primary spectral characteristic attributable to silane sized glass fibre samples was a doublet at 2926 and 2856 cm^{-1} indicating an alkoxy group, assigned to the C-H stretching of CH_2 and CH_3, respectively [169]. A peak attributable to the C=O stretching of carbonyls was also observed at around 1740 cm^{-1} in all samples. MPTMS FTIR spectra showed good correlation with that of Li *et al.* [170]. Bands at 2942/2850 cm^{-1} and 1720 cm^{-1} were identified as characteristics of a silane (MPTMS). Guo *et al.* have likewise observed strong C=O signal in MPTMS and MPTMS-treated alumina nanoparticles [171]. Petersen *et al*. have observed C=O stretching at 1735 cm^{-1} in sizing extracts but not in GPTMS coated fibres or pure APS and GPTMS samples [154]. An unidentified C=O containing compound has also been reported in NMR analysis of sizing extracts by Thomason [11]. While the C=O band was consistently reproducible, and is well reported in the literature for methacryl silanes [172], it is possible that the presence of this band in the GPTMS samples was related to a contamination effect due to the absence of carbonyl groups in epoxysilane. Bashir attributed the presence of C=O carbonyl group at around 1750 cm^{-1} visible in both baseline APS coated and heat treated fibres to potential interaction between organic contaminates and alkali forming carboxylic species or a halogenated ketone [155].

MPTMS sized fibres showed a weak intensity broad band at 3600–3200 cm^{-1} assigned to O-H that was not present in the other silane coated fibres and may have been attributable to silanol groups [132]. Salmon *et al.* have, however, observed an O-H band attributable to silanol in both APS and GPTMS films [169]. Petersen similarly observed the appearance of an O-H band in GPTMS coated fibres that was not present in pure GPTMS [111]. The fact that an O-H band was not visible in the GPTMS and APS coated fibre spectra may be attributed to poor signal intensity, uneven sizing distribution, and low concentration of sizing components on the fibre (in the range of 0.1% LOI). Conversely, Li *et al.* attributed the appearance of an O-H band at 3450 cm^{-1} to physically absorbed water [170].

Initial signal intensity of industrially kiss-rolled APS coated fibres was exceedingly low. It is possible that the uneven distribution of the silane resulted in spectra being collected from primarily bare glass sections, or that the amount of silane sizing present was below the detection limit of the FTIR instrument used. To address this, unsized glass fibres were sized with a 1 vol.% APS solution using the coating method described in 2.3.1. Signal intensity was improved and characteristic peaks were more easily identified. Spectra of GPTMS fibres sized at both laboratory and industrial scales were found to be comparable in peak behaviour and signal intensity. The spectral characteristics of silane sized glass fibres are summarised in *Table 3-7*.

Band (cm^{-1})	**Assignment**
3600–3200 (MPTMS)	O-H bonded to Si
2926, 2856	C-H stretching of CH_2, CH_3
1740	C=O stretching
1200–800	Si-O-Si

Table 3-7: Spectral characteristics of silane coated glass fibres

Epoxy Coated Glass Fibres

FTIR spectra of epoxy coated glass fibres and the DER 332 DGEBA epoxy resin used in the sizing solution are shown in *Figure 3:9.* Band assignments attributable to the epoxy coated fibres are a characteristic triplet showing peaks at 2965, 2929, and 2875 cm^{-1} assigned to the C-H stretching of CH, CH_2, and CH_3, respectively. The smaller shoulder peak located adjacent to the triplet at 3055 cm^{-1} is assigned to the C-H stretching of the oxirane ring of the epoxy resin. Peaks at 1608 and 1507 cm^{-1} are attributable to C=C and C-C stretching of the aromatic (benzene) ring, respectively. The 1200–800 cm^{-1} spectral region was dominated by the high-intensity Si-O-Si signal from the glass fibres. Accordingly, the fingerprint region was

generally eclipsed for epoxy sizing solutions with lower concentrations (0.1–5 wt.%) and layer thicknesses of 40–350 nm. Epoxy resin spectral bands in the 1200–800 cm^{-1} range became visible as the sizing layer thickness (700 nm) approached the minimum penetration depth of the instrument (500 nm) in the 10 wt.% solution samples. Spectral bands associated with epoxy resin visible in the 1200–800 cm^{-1} region are 1032 cm^{-1} (assigned to the C-O-C stretching of ethers), 910 cm^{-1} (assigned to the C-O stretching of the oxirane ring). The peak at 827 cm^{-1} may be assigned to C-O-C stretching of the oxirane ring [173] and a vibration of the aromatic ring [174]. Peaks at 910 and 827 cm^{-1} in the epoxy-sized fibres were marginally offset from those in the bulk epoxy resin samples (915, 830 cm^{-1}).

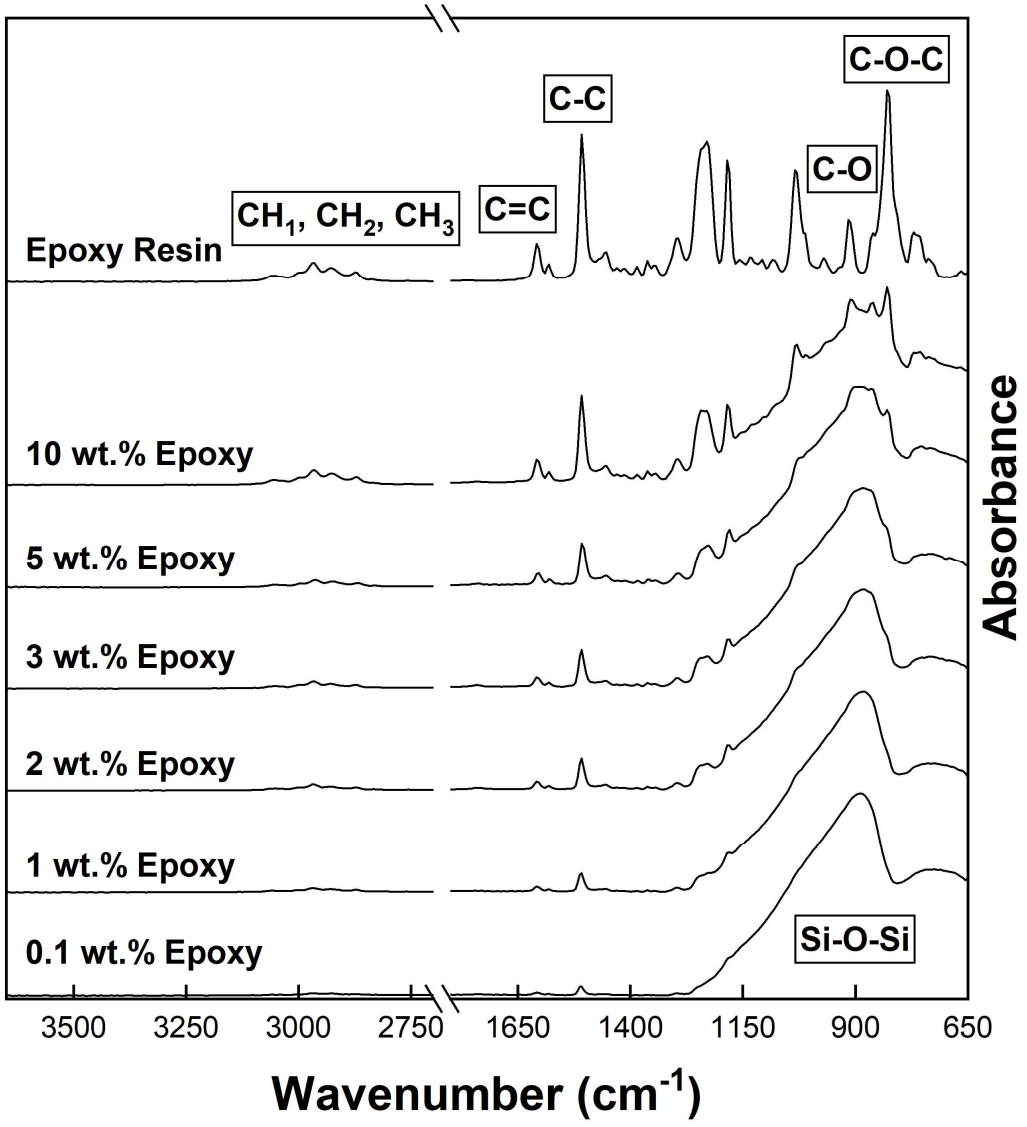

Figure 3:9: FTIR spectra of epoxy coated glass fibres

Figure 3:10 shows a magnified view of the key spectral regions associated with epoxy coated glass fibres. Concentration of chemical species and spectral bands at 1608 and 1508 cm^{-1} corresponding to the epoxy resin in the sizing increased linearly with solution concentration and sizing layer thickness and are summarised in *Table 3-8*.

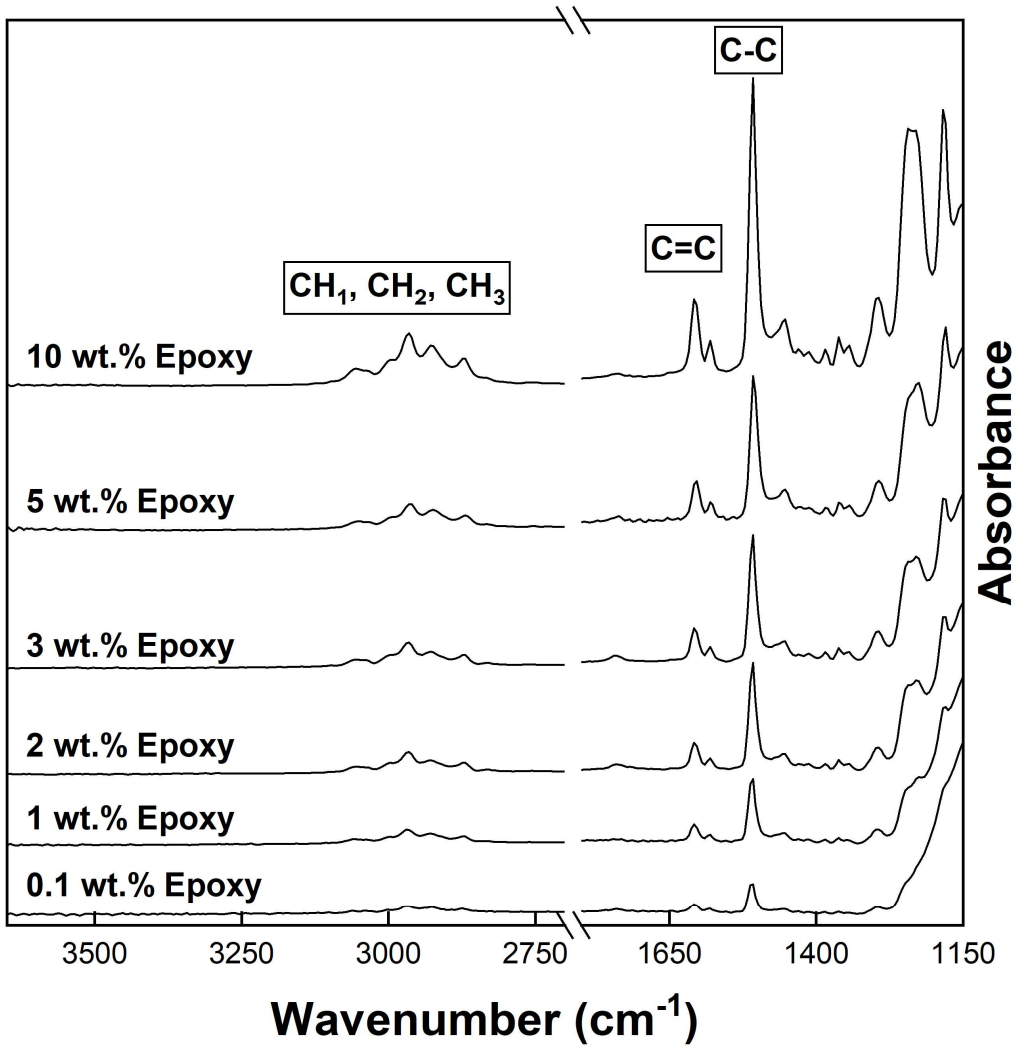

Figure 3:10: Magnified FTIR spectra of epoxy coated glass fibres

Solution Concentration (wt.%)	Sizing Layer Thickness (nm)	A_{1608}	A_{1508}
0.1	40	0.15	0.57
1	81	0.31	1.33
2	123	0.49	2.16
3	207	0.61	2.45
5	354	0.76	3.12
10	735	1.37	6.2
Bulk resin	-	2.34	10.29

Table 3-8: Summary of epoxy coated glass fibre species concentration

As a result of an eclipsing effect of the strong silica signal from 1200–800 cm^{-1} and overlap with silane spectra in the 3000–2800 cm^{-1} region, key band assignments for identification of epoxy film former are the peaks at 1608 and 1508 cm^{-1}. Spectral bands in the 1200–800 cm^{-1} region were not detectable on fibres coated with solution concentrations below 10 wt.%. The results show good correlation with the findings of Petersen *et al.* who likewise correlated bands at 1608, 1509, 1040, and 830 cm^{-1} to an epoxy film former in fully sized glass fibres and glass fibre sizing extracts [154]. The spectral characterises of epoxy coated glass fibres are summarised in *Table 3-9*.

Band (cm^{-1})	Assignment	Sized Fibre	Epoxy Resin
3055	C-H stretching of oxirane ring	✓	✓
2965,2929 2875	C-H stretching of CH, CH_2, CH_3	✓	✓
1741	C=O stretching of carbonyl	✓	X
1608	C=C stretching of aromatic ring	✓	✓
1508	C-C stretching of aromatic ring	✓	✓
1200–800	Si-O-Si	✓	X
1032	C-O-C stretching of ethers	X	✓
910	C-O stretching of oxirane ring	X	✓
827	C-O-C of oxirane ring/aromatic ring	X	✓

Table 3-9: Spectral characteristics of epoxy coated glass fibres

Fully Sized Glass Fibres

FTIR spectra of fully sized glass fibres are shown in *Figure 3:11.* The three epoxy-compatible full glass fibre sizings showed generally similar spectra indicating that the sizing formulations, containing at least a silane coupling agent and polymeric film former, were similar. The 1200–800 cm^{-1} spectral region was dominated by the strong Si-O-Si absorption from the glass fibres. Fully sized fibres showed a broad band corresponding to O-H and/or N-H between approximately 3600 and 3100 cm^{-1}, possibly attributable to silanol and indicating Si-OH in a coupling agent [169,175]. Petersen has similarly noted the presence of the same broad band in both fully sized fibres and acetone extracted fibres resized with GPTMS [111]. In this work, however, O-H group formation was only visible in MPTMS sized fibres. The O-H group may also be attributable to a lubricant such as PEG present in the sizing [132]. A triplet with peaks at 2965, 2929, and 2875 cm^{-1} corresponded to the C-H stretching of CH, CH_2, and CH_3, respectively [154]. Zhuang *et al.* [175] and Liu *et al.* [131] have, however, attributed increased intensity of the 2929/2875 cm^{-1} doublet to increased PEG content. A peak at 1731 cm^{-1},

assigned to C=O stretching of carbonyls, was visible in W2020 and SE2020 fibres and may be indicative of the presence of a silane coupling agent. FTIR spectroscopy of glass fibre sizing extracts by Thomason showed that C=O species were present in some sizing formulations and may have been related to amide or ester groups that were not present in the spectra of epoxy resin [11]. NMR analysis confirmed the presence of an ethoxylated compound and an unidentified compound containing C=O. Conversely, spectral analysis of carbon fibre sizing extracts by Yao *et al.* has attributed carbonyl group presence to a DGEBA epoxy component in the sizing [176]. Peaks at 1608 and 1508 cm^{-1} are assigned to the stretching of C=C and C-C of the aromatic ring and are indicative of the presence of an epoxy film former component in the sizing, as demonstrated by the spectra of epoxy coated fibres (*Figure 3:10*).

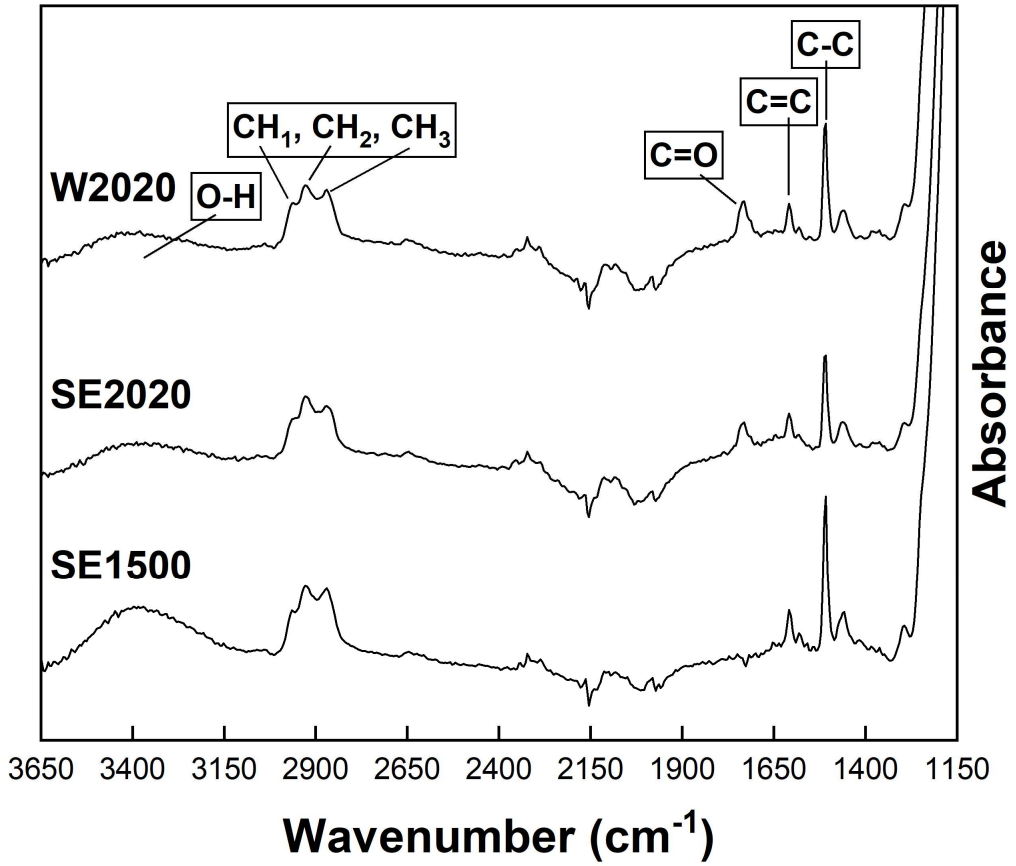

Figure 3:11: FTIR spectra of fully sized glass fibres

Analysis of glass fibre patent literature by Thomason [110] indicates the plausibility of patent EP 2 540 683 A1 describing the sizing formulation for SE2020. EP 2 540 683 A1 describes a formulation containing a silane coupling agent which is not an aminosilane, indicating that the coupling agent present is likely either GPTMMS or GPMES. The nature of the film former is specified as either epoxy or polyester resin, though compatibility with an epoxy resin matrix and the spectral bands observed would strongly indicate that the film

former present is an epoxy resin. A lubricant is also included in the sizing, which may have contributed to signal in the 1731 cm^{-1} range (due to the presence of carbonyl groups). The majority of the sizing components described are accounted for by the spectra presented despite poor signal strength due to low component concentration and a masking effect from the Si-O-Si signal strength. The spectral characteristics of SE1500, SE2020, and W2020 fully sized glass fibres are summarised in *Table 3-10*.

Band (cm^{-1})	**Assignment**	**Associated Component**
3600–3100	O-H bonded to Si	Surface hydroxylation/silane/lubricant
2965, 2929, 2875	C-H stretching of CH, CH_2, CH_3	Epoxy film former
2929, 2875	C-H stretching of CH_2, CH_3	Silane/lubricant
1731	C=O stretching of carbonyl	Silane/lubricant
1608	C=C stretching of aromatic ring	Epoxy film former
1508	C-C stretching of aromatic ring	Epoxy film former
1200–800	Si-O-Si	Glass fibre

Table 3-10: Spectral characteristics of fully sized glass fibres

Thermally Degraded Fully Sized Glass Fibres

FTIR spectra of thermally degraded SE1500, SE2020, and W2020 fibres are shown *in Figure 3:12*, *Figure 3:13*, and *Figure 3:14,* respectively. Spectra indicated that the three fully sized epoxy-compatible glass fibres contained similar sizing compositions including, at least, a silane coupling agent and an epoxy resin film former. Accordingly, the thermal behaviour of the three glass fibre sizings was relatively similar following exposure to elevated temperature heat treatment.

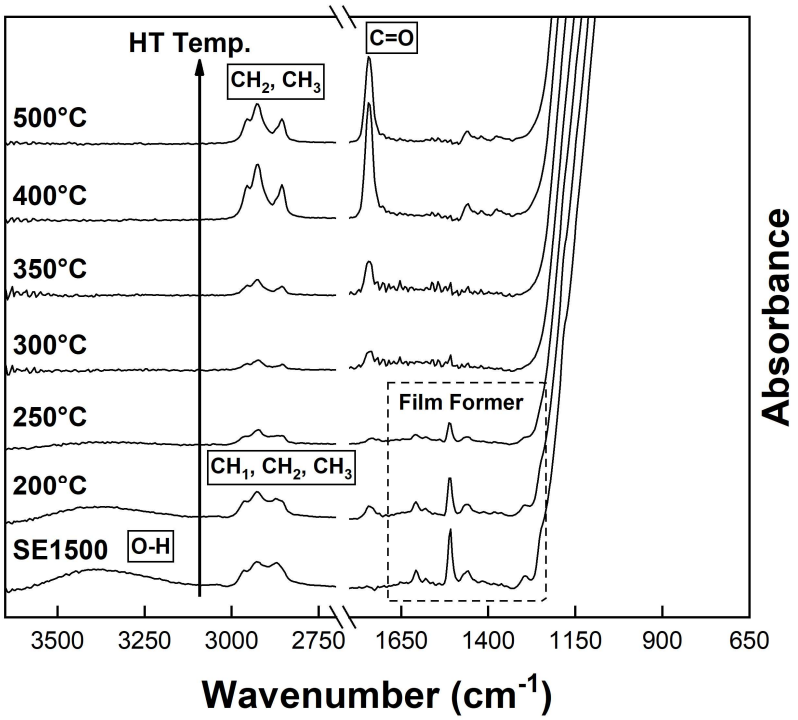

Figure 3:12: FTIR spectra of heat treated SE1500 glass fibres

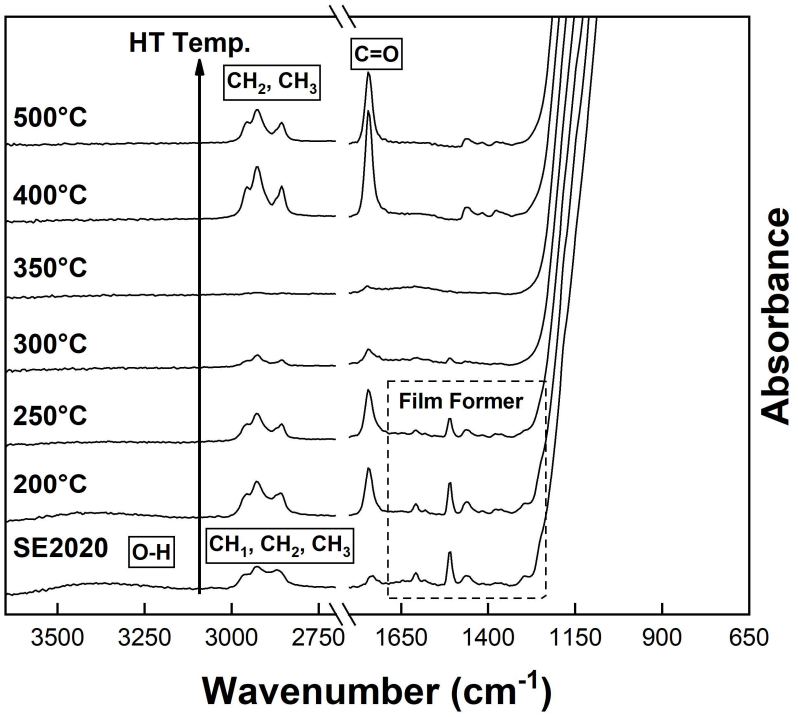

Figure 3:13: FTIR spectra of heat treated SE2020 glass fibres

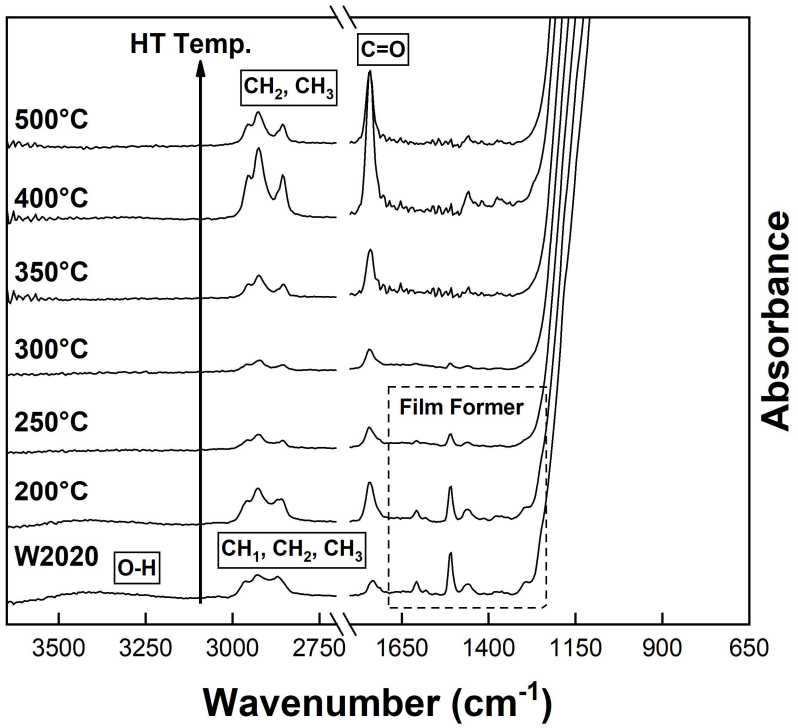

Figure 3:14: FTIR spectra of heat treated W2020 glass fibres

O-H group peak intensities with increasing heat treatment temperature are shown in *Figure 3:15*. The intensity of the broad band indicative of hydroxyl group (O-H) was reduced as temperature increased and was completely removed at 250–300°C. Reduced intensity of this band may be attributable to decomposition of a lubricant in the sizing with thermal stability lower than that of an epoxy film former or silane coupling agent. It is also possible that such a result indicates glass fibre surface dehydration and removal of initially present hydroxyl groups [177]. The differences in initial hydroxyl group intensity, and subsequent variance in decomposition temperature, of fully sized glass fibres may be attributable to variability in silanol group concentrations [178].

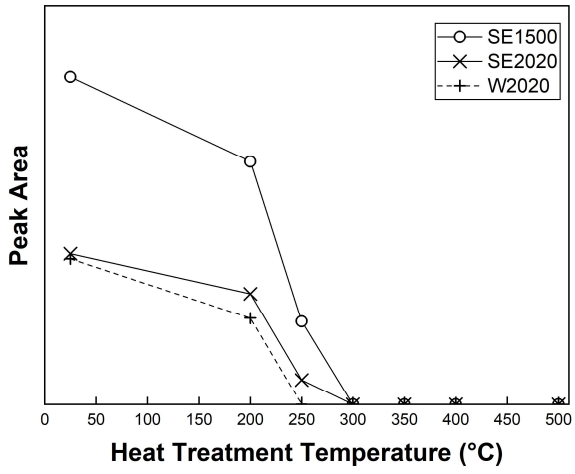

Figure 3:15: O-H peak intensity versus heat treatment temperature

Peak intensity of bands at 1608/1508 cm^{-1} are overlaid with TGA glass fibre sizing decomposition data in *Figure 3:*16. The peak intensity of spectral bands attributed to an epoxy resin film former (A_{1608}/A_{1508}) in the sizing decreased with increasing treatment temperature and were removed completely following treatment at 300–350°C. Reduction of peak intensity showed excellent correlation with TGA data that indicated that sizing mass loss in in the 200–400°C range was attributable to degradation of an epoxy film former. Reduced epoxy species concentration in the 25–200°C region observed in the spectral data is likely due to the higher sensitivity of the method compared to TGA of sized fibre bundles. Significant reduction in the concentration of epoxy species appeared to onset at a treatment temperature of 250°C. Thomason has reported that the soluble portion of epoxy-compatible sizings was thermally stable up to 150°C [11]. Furthermore, the soluble portion consisting primarily of an epoxy film former may have self-polymerised following treatment at 150°C. In this work, good correlation was shown with Thomason's findings, where the soluble portion (film former) of the fibre sizing began to degrade at temperatures greater than 150°C and degraded significantly in the 250–500°C range.

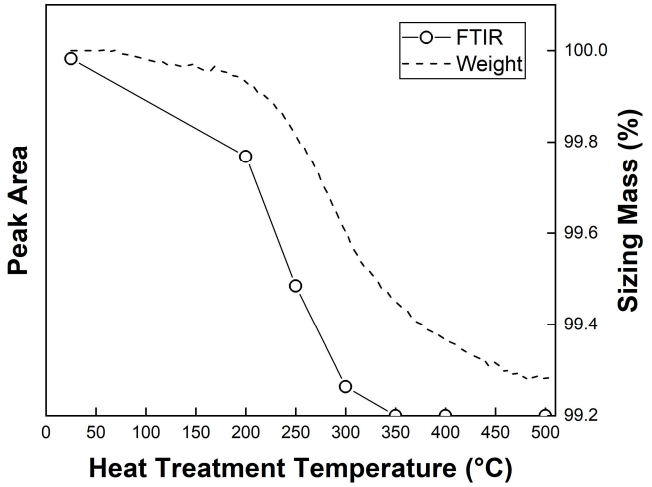

Figure 3:16: Overlay of epoxy film former peak intensity and TGA mass loss of sizing

The characteristic triplet peaks at 2965,2929, and 2875 cm^{-1} (also indicative of an epoxy film former) reduced in intensity at treatment temperatures of 250°C and above, and appeared to change to spectra consistent with a sizing containing only a silane coupling agent. Silane spectra was indicated by the doublet peaks at 2929 and 2875 cm^{-1} and peak intensity in this region appeared to increase in the 350–500°C range. Sherif *et al.* have likewise observed the disappearance of the CH, CH_2, CH_3 triplet at 350°C and correlated the disappearance of the spectral band to either a complete removal of the glass fibre sizing or to such an extent that the amount of sizing was below the detection limit of the instrument [156].

C=O group peak intensities versus increasing heat treatment temperature are shown in *Figure 3:17*. As a general trend, the intensity of the peak at 1740 cm^{-1} (C=O stretching of carbonyls) increased with treatment temperature to a maximum value at 400°C before reducing in intensity slightly following treatment at 500°C. It is not immediately clear why the SE2020 spectra appears to show a decrease in peak intensity in the 300–350°C range, though the apparent irregularities of the band have been reported previously [155]. Delor-Jestin *et al*. reported that increased intensity of a C=O spectral band could be correlated to the oxidation of epoxy resins as a result of thermal ageing [179].Similarly, Doblies *et al.* performed mIR FTIR analysis on 25–30 μm epoxy films heat treated at 130–200°C [180]. A carbonyl peak (1720 cm^{-1}) became apparent following treatment and peak intensity increased with time and temperature. Reduced intensity of epoxy backbone ether bonds at 1240 and 1040 cm^{-1} was also reported, though sized fibre spectra in this region are generally eclipsed by the strong Si-O-Si peak. Furthermore, the authors suggested that increased CH_3 peak intensity at 2964 cm^{-1} supported evidence of chain scission and polymer decomposition. It is possible that increased CH_3 peak intensity is related to some function of the polymeric component of the glass fibre sizing being decomposed at higher temperatures and the more strongly bound residual silane layer being exposed. It would seem plausible to suggest that increased carbonyl group peak intensity may be attributable to oxidation of the epoxy film former component in the sizing at temperatures greater than 200°C. Quantification of oxidation of sizing components, however, may be complicated by C=O spectral overlap with species related to the silane coupling agent as indicated by spectra of silane coated fibres (*Figure 3:8*).

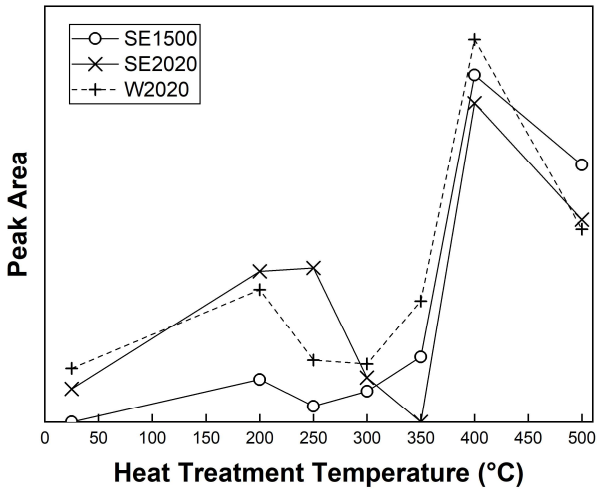

Figure 3:17: C=O peak intensity versus heat treatment temperature

Spectra of fibres treated at 400–500°C were comparable to those of fibres containing only a silane coupling agent, indicating that, while the polymeric film former had been completely removed, residues of degraded silane coupling agent material remained present on the glass fibre surface. TGA of GPTMS films indicated that the approximately 60% of the initial mass may be lost at a treatment temperature of 400°C. While residues of degraded silane coupling agent material were detected on the surface of thermally degraded glass fibres, the ability of the coupling agent to contribute to interfacial adhesion may have been significantly compromised.

It was also observed that the thermal degradation of the fibre sizing appeared to be non-uniform, though it must also be considered that the distribution of the initial sizing may be non-uniform before heat treatment [181]. Spectra were collected from ten points spaced approximately 1 cm apart along the length of heat treated sections of glass fibre roving. At a treatment temperature of 350°C, ATR-FTIR spectra of the SE1500 glass fibres indicated 80% of the spectra were consistent with a bare glass fibre and complete removal of all organic sizing components, while around 20% of the spectra showed a strong signal corresponding to residual silane coupling agent (CH_2,CH_3). A similar observation was noted for SE2020 fibres treated at 250°C. Spectra indicated that 60% of data points showed low intensity of the 2929/2875 cm^{-1} doublet and 1740 cm^{-1} band, while the remaining data points showed higher signal intensities in these regions.

The key spectral changes, characterised as the peak area, observed in the fully sized epoxy-compatible commercial fibres SE1500, SE2020, and W2020 are summarised in *Table 3-11*, *Table 3-12,* and *Table 3-13*, respectively.

SE1500				
Temperature (°C)	**$A_{3600–3100}$**	**A_{1740}**	**A_{1608}**	**A_{1508}**
25	4.11	0.00	0.13	0.52
200	3.05	0.26	0.09	0.38
250	1.05	0.10	0.05	0.19
300	0.00	0.18	0.00	0.04
350	0.00	0.39	0.00	0.00
400	0.00	2.09	0.00	0.00
500	0.00	1.55	0.00	0.00

Table 3-11: SE1500 key spectral absorption changes summary

SE2020				
Temperature (°C)	**$A_{3600–3100}$**	**A_{1740}**	**A_{1608}**	**A_{1508}**
25	1.90	0.20	0.08	0.33
200	1.40	0.91	0.08	0.31
250	0.31	0.93	0.05	0.19
300	0.00	0.27	0.00	0.05
350	0.00	0.00	0.00	0.00
400	0.00	1.92	0.00	0.00
500	0.00	1.22	0.00	0.00

Table 3-12: SE2020 key spectral absorption changes summary

W2020				
Temperature (°C)	**$A_{3600–3100}$**	**A_{1740}**	**A_{1608}**	**A_{1508}**
25	1.84	0.32	0.10	0.40
200	1.09	0.80	0.08	0.33
250	0.00	0.37	0.02	0.13
300	0.00	0.35	0.00	0.04
350	0.00	0.73	0.00	0.00
400	0.00	2.30	0.00	0.00
500	0.00	1.16	0.00	0.00

Table 3-13: W2020 key spectral absorption changes summary

3.4.3 Thermal Degradation of Glass Fibre Sizing and Interfacial Adhesion

Due to the significant role of fibre sizing in the determination of the level of apparent adhesion in composites, microbond testing was performed to provide a direct measurement of the interfacial shear strength of thermally conditioned glass fibres. The matrix material used was DER 332 DGEBA epoxy resin cured with a stoichiometric (14.3 phr) amount of TETA tetrafunctional amine curing agent. At least thirty samples were tested for each pre-treatment temperature with a success rate of generally 80–90%. Microbond testing results for SE1500, SE2020 and W2020 fibres are shown in *Figure 3:18*, *Figure 3:19*, *Figure 3:20*, respectively. IFSS is overlaid with corresponding glass fibre sizing decomposition data determined by TGA.

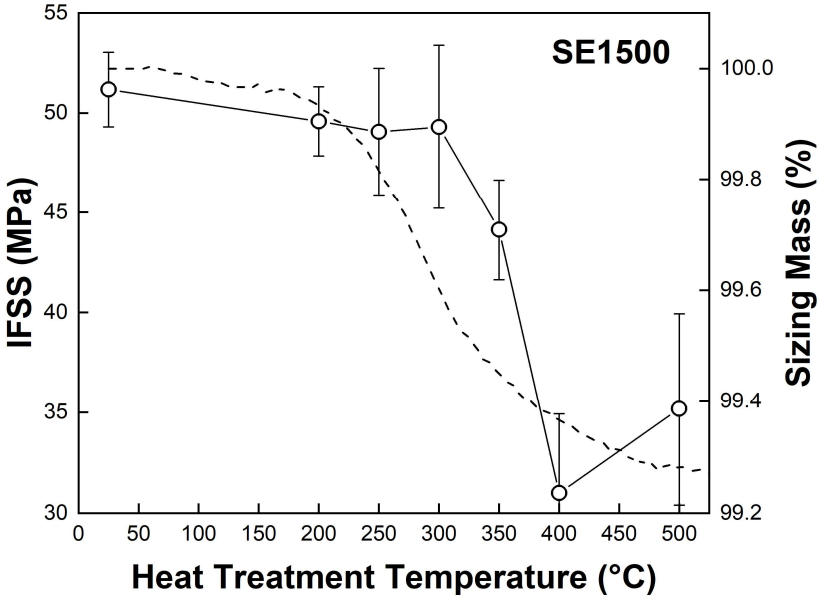

Figure 3:18: SE1500 IFSS versus heat treatment temperature

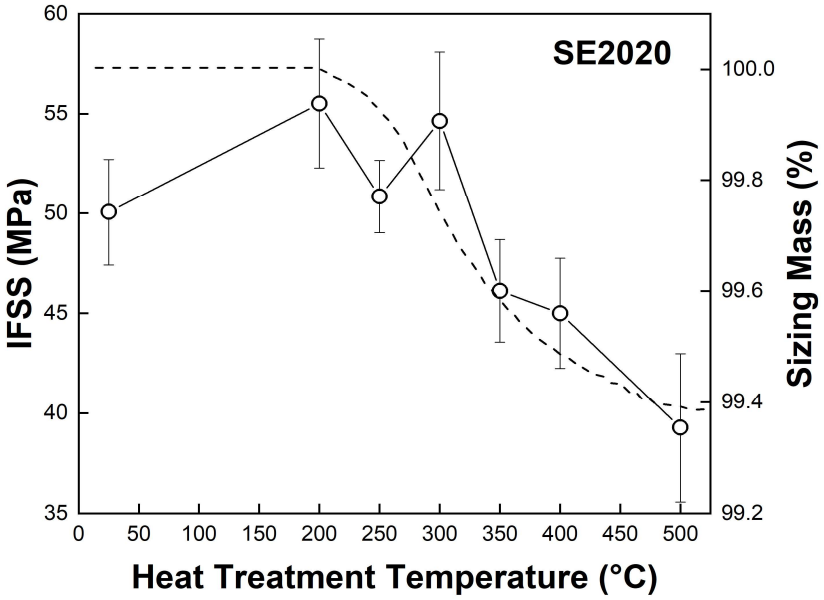

Figure 3:19: SE2020 IFSS versus heat treatment temperature

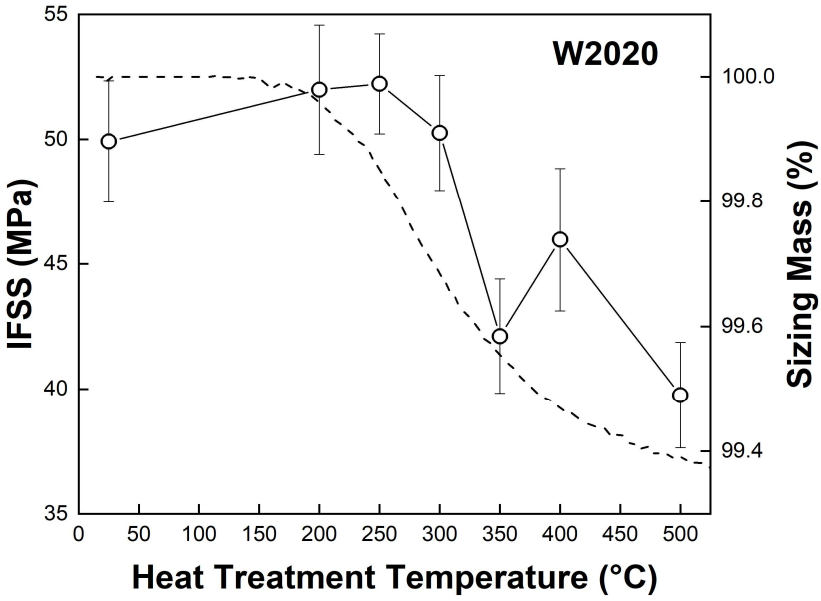

Figure 3:20: W2020 IFSS versus heat treatment temperature

IFSS of epoxy-compatible glass fibres was approximately constant (within confidence limits) up to a pre-treatment temperature of 300°C despite the fact that the sizing began to degrade at around 200°C. For the SE2020 and W2020 samples, IFSS appeared to increase slightly following treatment at 200–250°C compared to the untreated baseline. Above this temperature, 350°C marked the point that apparent fibre/matrix adhesion decreased significantly before levelling out above 400°C to a final value of approximately 35–40 MPa. SE2020 and W2020 sizings appeared to be generally slightly less sensitive to thermal degradation as IFSS values at the highest treatment temperatures were approximately 5 MPa greater than that of the SE1500 fibres. Samples treated at temperatures of 400–500°C showed IFSS approximating that of unsized glass fibres with no heat treatment using the same epoxy matrix, potentially indicating that the majority of the sizing components which influence IFSS had been removed. SE1500 fibres showed IFSS values even lower than that of unsized fibres. This may be due to the fact that some of the higher IFSS values are missing from the data set due to premature tensile failure of the weakened fibres after the 400–500°C heat treatment [145,146]. An alternative explanation is that there may be residual carbonised sizing material on the fibre surface, as indicated by FTIR results showing an increase in carbonyl group peak intensity at 1740 cm^{-1}. It is possible that such a surface results in poorer interaction with the epoxy resin matrix than the hydroxyl-rich surface of water sized fibres [182].

The loss in IFSS above 300°C showed good correlation with the weight loss of the fibre sizing at similar temperatures. It can thus be concluded that the loss in IFSS is associated with a loss of the adhesion-enhancing capability of the sizing. While the film former accounts for

the majority of the measured mass loss in the sizing, reduced IFSS did not onset until the epoxy film former had been completely removed (300–350°C), as indicated by FTIR results (*Figure 3:16*). It could be suggested that the complete removal of the film former is indeed detrimental to the chemical bonding potential of the sizing. On the other hand, no significant loss of IFSS was observed when the amount of film former present had been severely reduced at 250–300°C. It would seem possible to suggest that the loss in interfacial adhesion may be attributable to the degradation of the silane coupling agent [148,150]. While spectra of fibres treated at 500°C indicated that residues of degraded silane coupling agent material were present on the glass fibre surface, the silane coupling agent may have been degraded to an extent that the adhesion-enhancing capabilities were lost. It is also possible that interfacial adhesion was inhibited at higher treatment temperatures by the accumulation of weakly bound oxidised film former material on the glass fibre surface, evidenced by the carbonyl group growth in the spectral data (*Figure 3:17*).

The interfacial adhesion results for the epoxy-compatible fully sized fibres are summarised in *Table 3-14*.

Fibre	**IFSS (MPa)**						
	25°C	**200°C**	**250°C**	**300°C**	**350°C**	**400°C**	**500°C**
SE1500	51.2	49.6	49.1	49.3	44.1	31.0	35.2
SE2020	50.1	55.5	50.8	54.6	46.1	45.0	39.3
W2020	49.9	52.0	52.2	50.3	42.1	46.0	39.8

Table 3-14: IFSS of heat treated epoxy-compatible fully sized glass fibres

3.5 CONCLUSIONS

In this chapter the thermal degradation of a number of experimental and commercial glass fibre sizings has been investigated using thermal analysis, spectroscopic, and micromechanical testing methods. Silane sized fibres appeared generally thermally resilient, though extremely low LOI values and instrument sensitivity made accurate characterisation of mass loss difficult. TGA of GPTMS silane films indicated mass loss onset around 280°C and followed a two-step degradation progress. The majority of the mass occurred in the 250–400°C region before stabilising at approximately 550°C and a mass loss of 63%. Onset temperature and first derivative peak temperature of glass fibres sized with a DGEBA epoxy/acetone solution as a model film former increased with increasing solution concentration and sizing layer thickness. Mass loss onset was approximately 180°C for the lowest concentration coatings and was some 40°C greater following treatment with a 10 wt.% concentration solution. Regardless of layer

thickness, the epoxy coating was completely removed following treatment at 400°C and all sizings degraded at temperatures lower than that of the baseline bulk resin. Peak maxima position was approximately 75–135°C lower than that of the bulk resin specimen depending on sizing layer thickness.

TGA of three fully sized epoxy-compatible glass fibres indicated sizing LOI between 0.59% and 0.78%. The majority of the mass loss occurred at 200–400°C and was attributable to the decomposition of the polymeric film former component of the sizing. Mass loss stabilised at 500°C indicating that the sizing had been completely removed. TGA data was used to quantify the depletion of the sizing layer thickness as treatment temperature was increased. An initial 70–80 nm sizing layer was reduced by approximately 50% following 300°C heat treatment and removed almost entirely following treatment at 500°C.

ATR-FTIR spectroscopy was used to characterise glass fibre sizings and changes in composition following exposure to elevated temperature heat treatment. Spectra were typically dominated by a broad high-intensity peak at 1200–800 cm^{-1} attributable to the glass fibre silica signal. Analysis of fully sized fibres indicated that the formulations likely contained, at least, an epoxysilane (GPMES/GPMMS) coupling agent, an epoxy film former, and a lubricant. Silane coupling agent was characterised by doublet peaks at 2926 and 2856 cm^{-1} and a further band at 1745–1740 cm^{-1}, while an epoxy film former was primarily associated with bands at 1608 and 1508 cm^{-1}. Increasing the concentration of an epoxy/acetone solution and epoxy layer thickness resulted in a linear increase in intensity of species associated with the epoxy resin present on the glass fibre surface and corresponded to those identified as a film former in full sizings. As sizing layer thicknesses approached the minimum penetration depth of the instrument epoxy resin spectral bands in the 1200–800 cm^{-1} range became visible.

FTIR spectra of thermally degraded fully sized glass fibres indicated that an O-H group potentially attributable to surface hydroxyl groups or a lubricant was completely removed between 250–300°C. Furthermore, the intensity of spectral bands attributable to an epoxy resin film former (1608/1508 cm^{-1}) decreased with increasing treatment temperature and were removed completely at temperatures of 300–350°C. Reduction of peak intensities showed excellent correlation with TGA data that indicated that sizing mass loss in in the 200–400°C range was attributable to degradation of an epoxy film former. Reduction of epoxy species in the 25–200°C region observed in the spectral data was likely due to the higher sensitivity of the method compared to TGA of sized fibre bundles. Spectra of fibres treated at 350–500°C were comparable to those of silane sized fibres indicating that residue of degraded silane coupling agent may have remained present on the glass fibre surface. Increased peak intensity

of a carbonyl group (C=O) band at 1731 cm^{-1} following higher treatment temperatures may have been due to oxidation of the epoxy film former component in the sizing. Quantification of oxidation of sizing components was, however, complicated by spectral overlap with species related to the silane coupling agent.

Interfacial adhesion measurements showed that IFSS had an inverse relationship with fibre treatment temperature and was concurrent with decomposition of the glass fibre sizing measured by TGA. Reduced IFSS appeared to onset at 300–350°C and at treatment temperatures of 400°C and above interfacial adhesion was comparable to that of unsized fibres, suggesting that the majority of the sizing components which influence IFSS had been removed. While the film former component of the sizing accounted for the majority of the measured mass loss in the sizing, comparison of micromechanical and spectroscopic results indicated that reduced IFSS did not onset until the point at which the epoxy film former had been completely removed (300–350°C). This result could suggest that complete removal of the film former is detrimental to the chemical bonding potential of the sizing, though the fact that no significant loss of IFSS was observed when the amount of film former present had been severely reduced in the 250–300°C temperature range may suggest that degradation of the silane coupling agent is primarily responsible. Spectra of fibres treated at 500°C indicated that some residues of degraded silane coupling agent material were present at the glass fibre surface, though the silane coupling agent may have been degraded to the extent that the adhesion-enhancing capabilities were lost. Interfacial adhesion may also have been inhibited at higher treatment temperatures by the accumulation of weakly bound oxidised film former/sizing material on the glass fibre surface corresponding to the carbonyl group growth observed in the spectra of heat treated samples.

CHAPTER 4: MICROSCALE CURING PERFORMANCE OF EPOXY RESIN IN THE MICROBOND TEST

4.1 INTRODUCTION

The fibre/matrix interface region is critical to the mechanical performance of a composite, thus optimisation of the stress-transfer capability of this region is extremely important. Accordingly, it is essential to be able to characterise the interface and associated level of adhesion through a robust methodology in order to fully understand the composite performance. An accepted mechanically measurable value used to define the strength of the interface is the interfacial shear strength (IFSS), which can be assessed through a number of micromechanical methods such as the pull-out, fragmentation, or microbond tests [22]. Micromechanical testing methods can be useful in the economical and time-efficient development of fibre sizings and assessment of composite processing parameters by enabling screening and optimisation at the single fibre level without the need to scale up to fabric production, laminate processing, and macromechanical testing [24,25].

While the use of the microbond test to characterise the adhesion between various fibre and polymer systems has been widely reported in the literature, only a very few authors have commented on the difference in the behaviour of matrix materials at the microscale and the implications this holds for the applicability of the test and the interpretation of the results obtained. In fact, as the combined citations of Miller *et al.* [29] and Gaur and Miller's [71] seminal publications on the development of the technique approaches one thousand, it would appear that less than thirty studies have recognised microscale-related curing issues, with an even smaller number of detailed investigations reported. Microscale curing issues have been reported in the literature prior to the development of the microbond test [82] and have been identified as areas for improvement in some of the earliest critical reviews of microbond [74] and micromechanical [22] testing methods. In the intervening thirty years, however, there has been little significant effort to address the issue directly, despite the microbond test continuing to enjoy widespread usage.

Given the abundance of literature published on the apparently successful use of the microbond test with thermosetting matrices, it seems reasonable to suggest that not all material systems are susceptible to this effect, or at least not to the same degree. If the microbond test is to be presented as an efficient and robust methodology for effectively characterising the fibre/matrix interface it is essential for this phenomenon to be understood in greater detail.

It was found that, for a number of amine-cured epoxy systems, microdroplets exhibited properties different from those of the bulk matrix material subjected to the same processing conditions, the extent of which was dependent on the curing agent used. This behaviour had a significant influence on the degree to which these resins formed cured droplets suitable for microbond testing. Accordingly, Chapter 4 investigates the microscale curing performance of three epoxy resin systems using micromechanical and thermal analysis techniques to characterise the effect of these differences in relation to the use of the microbond test to measure interfacial adhesion.

4.2 LITERATURE REVIEW

4.2.1 Microscale Curing Performance in the Microbond Test

Some of the earliest issues related to microscale curing performance are reported by Järvelä *et al.* [82], predating Miller *et al.*'s seminal publications by some four years [29]. The authors developed a modified pull-out sample geometry based on the inability of low-viscosity resins to form droplets when applied directly to glass and polyamide fibres. A three-fibre method where supporting fibres were mounted horizontally parallel to the droplet on the initial vertical fibre was proposed. The authors concluded that the testing method was limited by an inability to control both droplet dimensions and the polymerisation process, factors that bond strength was highly dependent on. Despite changes to sample geometry, low viscosity and wetting of certain adhesives completely prevented the formation of droplets. Further issues were noted regarding the thermal history of the samples being undefinable due to the small droplet size, inability to measure the degree of polymerisation in the droplet, and evaporation of resin components essential for polymerisation during sample preparation.

Haaksma and Cehelnik conducted a critical evaluation on the use of the microbond method for the determination of composite interface properties [74]. The authors expressed concerns with material and experimental variables related to the testing method, including factors such as thermoset curing behaviour. The cure behaviour of the resin was investigated as a function of degree of mixing, resin/curing agent ratio, curing conditions, and droplet size. It was reported that it was "impossible to obtain an interfacial shear strength value" when using the same cure cycle conditions (75°C 2 h; 125°C 2 h) used to prepare fragmentation test specimens. Epon 828/m-PDA (meta-phenylenediamine) resin droplets did not cure on carbon, glass, or aramid fibres, indicating that microscale curing performance was independent of the fibre used. Incomplete cure was also observed for droplets placed on both aluminium and sodium chloride plates and was verified by an FTIR microscopy method. Droplets showed

spectra corresponding to the presence of unreacted resin and complete loss of curing agent. Droplet size had a notable effect on the extent of cure, which was lowest in smaller droplets. Samples with diameters larger than 1000 μm appeared to remain "tacky", hence below T_g at room temperature. Spectroscopic results and the inverse relationship between droplet size and degree of cure were both indicative that evaporation of curing agent from microbond specimens was a critical parameter that must be controlled. The authors concluded that prior to microbond testing an independent method must be employed in order to determine the extent of the cure in the droplets and a sample preparation method that produces cured droplets found.

Ozzello *et al.* reported on the interfacial shear strength of ion beam modified ultra-high-molecular-weight polyethylene (UHMW-PE) epoxy matrix composites using a DGEBA epoxy cured with m-PDA [41]. Immediate curing of microbond samples caused diffusion of the curing agent out of the droplets. Accordingly, an 18 h room temperature stage was introduced before curing at elevated temperature (75°C 2 h; 100°C 3 h) to successfully produce testable droplets of embedded length 100–1500 μm.

Rao *et al.* reported on a comparison of the fragmentation and microbond tests for determining IFSS [183]. Experiments were conducted using AS4 carbon fibres and a DGEBA epoxy resin (Epon 828) cured with two diamine curing agents (m-PDA/Jeffamine 700). DSC was used to characterise cured bulk matrix T_g and a novel thermomechanical analysis (TMA) technique was used to determine polymer droplet T_g. Samples with embedded length less than 600 μm were substituted for a cluster of similarly sized droplets in order to generate sufficient signal strength and checks between the two methods were carried out to ensure that T_g results were consistent. Attempts to perform the microbond test on DGEBA/m-PDA samples cured according to the standard schedule (75°C 2 h; 125°C 2 h) resulted in droplets deforming during the initial stages of testing. The TMA-T_g technique showed that T_g of smaller droplets (<150 μm) was around 60°C lower ($T_g \approx 80$°C) than that of the bulk cured matrix ($T_g \approx 140$°C) as droplets lost up to 40% of the curing agent due to diffusion and evaporation. Disparity between microdroplet and bulk matrix T_g was reduced to around 30°C when droplet size was increased to 600 μm.

Curing microbond samples under an amine-rich atmosphere or with double the stoichiometric amount of curing agent did not result in improved results, but allowing droplets to (partially) cure at room temperature for 24–36 h before exposing them to high temperatures caused the system to gel and appeared to prevent loss of curing agent. It was proposed that the inclusion of a room temperature step in the cure allowed for some reaction to occur between

the epoxy and amine which retarded the diffusion process. Despite diffusion being alleviated by a modified curing cycle, small still droplets lost up to 25% of the amine and agreement between interfacial testing methods remained poor. Conversely, samples cured with the less volatile Jeffamine 700 showed good agreement between microbond and fragmentation measurements without the inclusion of a room temperature stage or modification to the curing atmosphere. The authors concluded that microbond measurement of IFSS could produce artefacts at small droplets sizes in systems with volatile components due to changes in droplet stoichiometry.

In a subsequent publication Rao and Drzal investigated the loss of curing agent during droplet and thin film curing [184]. The study examined three different systems based on DGEBA epoxy resin cured with stoichiometric amounts of m-PDA, Jeffamine 403 (J403) and Jeffamine 700 (J700). Deviation from cured bulk matrix T_g, as measured by TMA/DSC, was used as a measure of how much curing agent was lost. TMA-T_g results showed that droplet T_g of even the largest m-PDA-cured specimens (> 800 μm) was approximately 20°C less than that of the bulk material, while smaller specimens deviated by around 70°C. Conversely, a comparison of the J403 and J700-cured systems showed only slightly reduced T_g at droplet sizes as low as 100 μm, with little discernible difference measured between the droplet and bulk matrix properties at embedded lengths greater than 200 μm. However, initial bulk matrix and droplet T_g were much lower in these systems, around 75 and 25°C, respectively.

A method to prepare thin films was described in which small aluminium hooks were repeatedly dip-coated in mixed resin solutions to create film thicknesses of up to 4 mm for DSC T_g measurements. Use of a thin film of thickness equivalent to droplet embedded length showed good correlation with the TMA results, wherein changes in T_g as a function of thickness/embedded length were generally the same. The Jeffamine-based systems (which had higher viscosity and lower volatility) showed consistent T_g across the range of thicknesses tested while T_g of DGEBA/m-PDA films deviated by some 10°C from the bulk cured matrix even at thicknesses of approximately 3000 μm.

Biro *et al.* considered the volatilisation of curing agent during microbond sample curing [185]. Epoxy/amine microdroplets were cured in three different ways. Firstly, under nitrogen atmosphere for 2 h at 90°C followed by 1 h at 120°C and a 2°C/min cool to room temperature. Secondly, with a small amount of curing agent in a pan in close proximity to the samples to increase the local concentration of curing agent vapours. Thirdly, with the resin samples placed in different DSC pans. It was reported that under the different curing conditions, all the samples exhibited similar material properties.

Liao and Tung investigated the properties of carbon fibre/polymer interfaces [120]. The authors reported that Epon 828 epoxy/m-PDA microbond samples failed to cure (75°C 2h; 125°C 2h) at the stoichiometric ratio (14.5 phr) and attributed the behaviour to adsorption of m-PDA onto the carbon fibre surface. Samples were instead prepared with an apparent excess of curing agent (18 phr) to alleviate the issue. Conversely, microbond curing issues did not appear to occur when the same epoxy system was cured with methylene dianiline (MDA). While microbond curing issues are not reported in detail, the observation confirms that m-PDA is the first and most consistently identified curing agent that proves problematic in the preparation and testing of microbond test samples. Furthermore, poor microdroplet curing performance at the stoichiometric ratio may imply a loss of curing agent and an off-stoichiometric microdroplet by some medium, as is further evidenced by the fact that curing issues were addressed by preparing samples with excess curing agent. It is possible that by preparing droplets with around 25% excess curing agent, amine loss was offset to an extent that droplets were no longer off-stoichiometric after curing.

Herrera-Franco and Drzal have commented on an apparent disparity in micro-/macroscale performance in their review of micromechanical techniques [22]. IFSS measured by the microbond test was consistently lower than values generated by fragmentation tests using an identical carbon fibre/DGEBA/m-PDA system. This behaviour was attributed to the mechanical properties of the epoxy microdroplets being lower than those of the matrix surrounding the embedded single fibre in the fragmentation test. Loss of curing agent in the microbond samples was caused by a large droplet surface-to-volume ratio. They acknowledged that other authors had performed the test, seemingly without issue, which could have been due to the use of a different curing agent.

Bartolomeo *et al.* investigated the micromechanical and microscopic effects of preprocessing on glass fibre/cyanate ester IFSS [186]. Microbond samples were prepared using D-glass fibres sized with an unspecified coupling agent and commercial cyanate ester matrices. FTIR spectroscopy was used to quantify degree cure using the cyanate band at 2270 cm^{-1} and T_g was determined by DMA. Good correlation was shown between the degree of conversion of bulk resin and microdroplet samples after 30 min ($\alpha_{resin} = 0.4$, $\alpha_{microdroplet} = 0.35$) and 1 h ($\alpha_{resin} = 0.52$, $\alpha_{microdroplet} = 0.51$) of isothermal curing at 180°C. At low degrees of conversion IFSS remained relatively constant (in the region of 8 MPa) before increasing significantly once the gel point of the system ($\alpha_{gel} = 0.6$) had been reached. The authors noted that it was not possible to measure IFSS at degrees of conversion higher than the gel point as the glass fibres consistently fractured prior to debonding. Substituting the glass fibres for

aramid showed low IFSS at low degrees of conversion and an S-shaped curve once the gel point had been surpassed. IFSS values remained approximately constant at degrees of conversion above the gel point. Increasing the curing temperature increased kinetic constant values, though no significant effect on the adhesion was observed, leading to the assertion that IFSS was dependent solely on the degree of monomer conversion. Furthermore, as IFSS values at low conversions were the same regardless of fibre used, it was proposed that IFSS was entirely matrix dependent at low degrees of conversion, while at high degrees of conversion both fibre and matrix interactions became apparent.

Zinck *et al.* reported that the physical and mechanical properties of microdroplets may differ significantly from that of the bulk matrix material [83]. DGEBA-based polyepoxies were cured with 4,40 methylenebis2,6-diethyleneaniline (MDEA) and anhydride cis 4-methyl 1,2,3,6-tetrahydrophtallic (MTHPA) to achieve different curing chemistries, namely epoxy/amine polycondensation and epoxy/anhydride chain polymerisation. Microdroplet properties were characterised by T_g measurements of thin films (thickness 100–200 μm) considered comparable models. The method was proposed as a simpler and more efficient alternative to the TMA-T_g droplet-cluster method used by Rao *et al* [183]. DSC thermograms of films showed residual exotherm attributable to unreacted species and an endothermic peak as a result of their volatilisation. Varying film thickness in the 100–200 μm range had no effect on T_g. Films subjected to 48 h pre-cure, however, showed T_g some 20°C (MDEA) or 50°C (MTHPA) below that of the bulk matrix material. It was thus recommended that a standing time should not be performed for chain polymerised microbond specimens due to a significant detrimental effect on droplet properties.

The authors suggested that poor curing behaviour could not be explained by existing curing agent evaporation hypotheses, and that differences in pre-curing effects indicated the presence of two distinct phenomena. Infrared analysis of amine-cured films (model microdroplets) showed two additional bands at 1661 cm^{-1} (C=N imine) and 1723 cm^{-1} (C=O carbonyl) not present in bulk matrix samples. Reduced T_g was attributed to the formation of imine groups and a resulting reduction in the number of amine functions available to react with the oxirane ring. It was concluded that epoxy/amine microbond samples should be cured under inert atmosphere and/or below 120°C. Reduced T_g in the anhydride-cured system was attributed to a phenomenon related to polymerisation during pre-cure. The chain polymerisation process may have been influenced by environmental parameters such as surface moisture on the fibres or hydrolysis of the anhydride.

Further concerns regarding interactions with standard atmosphere have been noted by Montgomery [10]. Epoxy microbond samples were cured under nitrogen in a vacuum oven in order to prevent blushing of the epoxy. Furthermore, both T_g and degree of cure increased with curing temperature and apparent IFSS increased linearly in relation to T_g. Samples cured at room temperature had a degree of cure of 79% which rose to 91-99% for samples that underwent a post-curing procedure. The author indicated that the change in measured IFSS values was likely a result of changes in residual stress.

Zinck and Gérard reported that extrapolation of microscale results to macroscopic behaviour must be considered with a great deal of caution [187]. Disparity between micro- and macroscale properties were important considerations due to deviations from the stoichiometric ratio playing an important role in the water absorption process. Off-stoichiometric formations resulted in significant alteration to sorption behaviour and degradation mechanisms. Accordingly, the ageing conditions of microcomposite samples may have differed significantly to macroscopic counterparts, potentially making micromechanical methods ill-suited to informing macroscale ageing effects. A comparison of the plasticisation of microscale and bulk specimens using thin films as model microcomposites revealed that T_g values were some 50°C below that of bulk matrices. Furthermore, T_g values for aged films were lower than the hydrothermal ageing temperature, resulting in a rubbery state, while macroscopic samples exposed to the same conditions remained glassy. Reduced T_g from curing agent loss was further exacerbated by higher water uptake at equilibrium resulting in plasticisation. The authors concluded that these observations effectively showed that plasticisation and ageing conditions at the microscale were more severe and the extent of degradation at the interface in microdroplet samples could be greater as a result.

Charlier *et al.* reported that processing and curing conditions had a significant effect on glass fibre/acrylic IFSS measured using the microbond test [188]. Without the addition of paraffin wax, radical polymerisation was not possible at high temperatures due to the rapid evaporation of MMA out of the droplets. With paraffin wax present, polymerisation time could be reduced by curing samples at higher temperatures. Higher IFSS was attributed to a combination of complete polymerisation of the droplet and increased physical/chemical adhesion to the fibre. The authors reported that the paraffin did not fully prevent evaporation of the solvent. Furthermore, evaporation of reactive components and ensuing changes to formulation composition may have been higher than expected due to the surface-to-volume ratio of the microdroplets and the wax may have had a plasticising effect. It was concluded

that the interfacial behaviour of microdroplets had to be carefully considered as it may not be relevant to the final composite part.

In a later publication, Charlier *et al.* investigated the multi-scale interfacial adhesion of glass fibre with acrylic and epoxy matrices [90]. Interfacial adhesion was evaluated at the microscale using the microbond test, while 15° off-axis tensile tests were performed to evaluate fibre/matrix tenacity at the macroscale. Microdroplet and tensile specimens were prepared using viscosity-adjusted polymethylmethacrylate (PMMA) acrylic and a reference thermosetting DGEBA-based epoxy system. All microbond samples were cured for 1 h at 80°C followed by 2 h at 160°C. Both cured bulk matrices exhibited similar mechanical properties at room temperature. The addition of paraffin wax to the acrylic resin was necessary to prevent the evaporation of acrylic monomers while preparing microbond samples. Furthermore, due to the microbond samples containing extremely low amounts of reactive mixture (in the range of a tenth of a milligram), an assumption was made that phenomena such as auto-acceleration/Trommsdorff's effect did not occur as it would in a bulk sample of several grams. Accordingly, microbond samples may have not reached comparable local temperatures, resulting in a lessened extent of reaction. Reference epoxy samples cured according to the supplier's recommendation were not fully cured and a higher post-curing temperature was necessary to produce fully cured droplets. Once a method that produced cured droplets was found, glass fibre/PMMA interfacial adhesion reached around 60% and 75% of the epoxy reference values at the micro- and macroscale, respectively. The authors concluded that good correlation between multi-scale methods indicated that micromechanical analysis relying on the microbond test was a reliable tool to estimate the fibre/matrix interfacial adhesion in practical composite parts.

A study by Ash *et al.* has proposed that varying degrees of stiffness observed in polyester microbond samples and subsequent data scatter may have been attributable to evaporation of reactive components [189]. Direct FTIR analysis of microbond samples appeared to confirm that 50–60% of the initial styrene content was lost in some samples due to the droplet surface-to-volume ratio, and was a cause of inconsistent curing.

Similarly, Dirand *et al.* commented on the curing of vinyl ester microbond samples and observed that "the mechanical properties of the microdroplets are inferior to those of the bulk matrix in a composite because of evaporation of styrene during the cure" [48]. The absence of a mould, high droplet surface-to-volume ratio, and the existence of a thick interphase stemming from a phase separation in the interfacial area due to interphase thickness approximating that of the droplet diameter were cited as possible causes of evaporation.

Laurikainen also reported significant problems in the preparation of vinyl ester microdroplets attributable to vaporisation of styrene from the resin causing poor curing [91]. Excessive post-cure treatments were unable to produce cured droplets due to insufficient styrene and samples continued to exhibit waxy plastic deformation under loading. Curing issues were, however, counteracted by sealing the droplets in sample holders in a high styrene content atmosphere.

A similar issue was also observed for Epon 828 epoxy droplets cured with Jeffamine D230. It was noted that the mixture contained no substances with significant vapour pressures, leading to the exclusion of evaporation hypotheses. During sample preparation, it was observed that resin droplets travelled along the fibre for a relatively long distance and that incomplete curing could be explained by phase separation of the resin and curing agent during sample preparation. This was supported by the observation that a similar resin system (Araldite 5052/polyamine mixture) did not exhibit curing issues due to the smaller difference in the viscosities of the resin and hardener compared to Epon 828/D230. It was found that cured Epon 828/D230 droplets could be prepared by allowing curing to advance until a significant increase in viscosity was observed before applying the droplets. Droplet samples prepared in such a way cured to a glassy state with mechanical properties conducive to micromechanical testing. In these cases, it was theorised that phase separation of the sample was no longer possible as significant covalent bonding existed between the resin and amine oligomers. Another proposed possible explanation to poor epoxy microdroplet curing was interaction of atmospheric moisture with the resin hindering the crosslinking reaction. This interaction was partially alleviated by allowing the curing reaction to progress in a sealed container.

Laurikainen *et al.* later used the Epon 828/D230 system in a further investigation of the microscale behaviour of aged glass fibre composites [190]. A 2 mL volume of epoxy and curing agent mixed at the stoichiometric ratio was held in an oven at 40°C for 2.5 h prior to applying droplets to the fibres in order to bring the mixture close to a gel state. Nevertheless, the curing of the microdroplets was concluded to be incomplete as post-curing was observed following ageing in elevated temperature water. Py-GC-MS analysis conducted on microbond samples showed huge emissions in the thermal desorption step compared to fully cured resin samples, a result indicative of the degree of cure in the microdroplet being significantly lower than a bulk matrix sample subjected to the same curing schedule.

4.2.2 Microstructural Effects

Mak *et al.* reported that monitoring the curing of thermoplastic reinforced epoxy samples was necessary as it proved problematic to obtain microdroplets of the same microstructure as the macroscale matrix composition cured under the same conditions [191]. Further examination of the microdroplet microstructure revealed that the curing temperature of microdroplet samples had to be significantly lower than that of the bulk matrix sample if the same microstructure was to be observed.

Conversely, Charlier *et al.* reported that a higher temperature was needed to fully cure both acrylic and epoxy droplets (despite the fact that the systems were able to polymerise at room temperature) compared to the schedule used for macroscale composite parts [90]. The authors proposed that as a result of the change in scale, phenomena such as auto-acceleration did not occur as in a bulk sample of several grams and accordingly, did not reach comparable local temperatures and the extent of reaction was reduced.

Patel *et al.* investigated the effect of curing rate on the microstructure and macroscopic properties of epoxy fibreglass composites [192]. Stoichiometric amounts of DGEBA and IPD were used to prepare composite and resin samples before curing according to three different temperature schedules. The first involved 12 h curing at room temperature (I) followed by 70°C for 6 h (II) and 140°C for 6 h (III) while subsequent schedules involved stages II–III and III only. Soxhlet extraction showed that samples that were allowed to gel completely prior to post-curing experienced no significant weight change, while samples cured immediately were considered less homogenous as microgels did not fully coalesce during the gelling stage. AFM showed no significant differences between samples at the microscale, but the inhomogeneous structure of samples cured immediately was readily observable at a scale of 250 nm. The authors suggested that the samples cured immediately at 140°C possessed large areas of partially unreacted network, had reduced mechanical properties, and that such samples exhibited a structure comparable to a non-stoichiometric epoxy/amine network. DSC analysis indicated both lower T_g and degree of conversion during the pre-curing stage for the fast-cured samples. Characterisation of the composite samples revealed that apparent changes in the microstructure as a result of differing heating rates did not translate into a change in the decomposition temperature of composite specimens as measured by TGA. Static flexural tests and the storage modulus were similarly unaffected. Fatigue testing, however, was reflective of the changes in matrix microstructure as samples cured immediately (possessing softer phases which acted as a stress concentration) failed after a significantly shorter number of cycles in comparison to the samples cured according to I–II and II–III, which failed after a similar

number of cycles. It was concluded that the curing cycle played a key role in the resin microstructure and that samples that were allowed to gel completely were comparable in both microstructure and mechanical properties, while immediately cured samples showed a low cross-link density region observable by a number of experimental techniques.

4.2.3 Conclusions of Literature Review

Analysis of the literature indicates that, while the issue of microdroplet curing is recognised by a relatively small number of authors, there is little agreement on the cause of this observed loss in performance, with studies in fact providing conclusions entirely contrary to one another. Microscale curing issues have been observed in epoxy, vinyl ester, polyester, and acrylic matrices and would appear to be related to both the surface-to-volume ratio of the microdroplet geometry and vaporisation of volatile components (curing agent, styrene) essential to the polymerisation process.

Investigations by Haaksma and Cehelnik [74], Rao *et al.* [183,184] and Ozzello *et al.* [41] examined the same epoxy/m-PDA system and attributed the reduction in microdroplet T_g to a stoichiometric imbalance due to evaporation of curing agent during elevated temperature curing. Liao and Tung, however, attributed poor epoxy/m-PDA curing behaviour to adsorption of m-PDA onto the fibre surface [120]. Dirand [48] and Laurikainen [91,190] agreed that diffusion and evaporation of curing agent was the cause of the problem in vinyl ester systems (due to the large surface-to-volume ratio) though the latter asserted that this could not have been the case for the same effect observed in an epoxy system due to insignificant vapour pressures. Poor curing was instead attributed to phase separation during sample preparation or interaction with atmospheric moisture. However, evaporation of essential components has likewise been observed in acrylic [188] and polyester matrices [189]. Zinck *et al.* [83] also refuted that evaporation was the cause of the issue in amine-cured epoxy samples and proposed instead that imine formation reduced the number of amine functions available to react with the oxirane ring. For an anhydride-cured epoxy they that suggested fibre surface moisture or hydrolysis of the anhydride during the pre-cure was the cause and that surface oxidation may also be a contributing factor.

Methods employed in order to overcome the issue are also discussed. Both Rao *et al.* [183] and Ozzello *et al.* [41] observed significant improvement by introducing a pre-cure/standing time (18–24 h), allowing comonomers to react at low temperature and, in theory, preventing vaporisation of curing agent. Zinck *et al.* [83] reported contradictory results, in that no change was seen after a 48 h pre-cure in an amine-cured system and that it had a significantly

detrimental effect on anhydride-cured samples. Liao and Tung were able to produce cured microdroplets by preparing samples with approximately 25% excess curing agent [120], while Rao *et al.* [183] reported no significant improvement when double the stoichiometric amount of curing agent was used. Some minor improvement was achieved by curing the samples in an amine-rich environment though Biro *et al.* [185] employed a similar procedure and observed no discernible effect on samples cured in the presence of curing agent vapours. However, Laurikainen [91] reported that curing under a styrene-rich environment alleviated curing problems in vinyl ester droplets. Zinck *et al.* [83] proposed that amine-cured systems should be cured under inert atmosphere (and at 120°C or below) to prevent loss of T_g from imine formation though Biro *et al.* reported no difference between samples cured under air or nitrogen using an epoxy and an aromatic amine. Laurikainen *et al.* [91,190] were able to produce cured epoxy microdroplets by allowing the resin viscosity to increase before application, amounting to much the same process as a protracted room temperature pre-cure.

Regarding matrix microstructure, Patel *et al.* [192] demonstrated that the inclusion of a standing time (and gelation) had a profound effect on composite fatigue performance. Mak *et al.* [191] showed that in order to achieve comparable microstructures, microdroplet samples had to be cured at considerably lower temperature compared to bulk samples. Conversely, Charlier *et al.* [90] proposed that a higher temperature was needed to fully cure both acrylic and epoxy droplets compared to the schedule used for macroscale composite parts due to reduced auto-acceleration at the microscale .

It becomes increasingly clear that there exists a need to be able to effectively characterise the degree of cure of microbond samples and to be able to determine droplet T_g. Järvelä *et al.* reported that incomplete control of polymerisation process constituted a significant source of uncertainty and data scatter in micromechanical test data [82]. Evaporation of components essential for the polymerisation process was theorised but the actual state of polymerisation in the droplet could not be measured. Haaksma and Cehelnik later advocated that “an independent method must be employed in order to determine the extent of the cure in the droplets” [74]. Biro *et al.* have similarly advocated that microbond testing investigations should involve a concurrent monitoring of matrix degree of cure via thermal analysis [193]. The development and use of a novel FTIR to assess microbond curing performance is discussed in Chapter 5. Microscale curing effects in the microbond test and proposed solutions are summarised and tabulated in Appendix C.

4.3 EXPERIMENTAL

4.3.1 Materials

Glass Fibres

In order to minimise the complexity of the interface, experiments were conducted using bare (water-sized) E-glass fibres taken from larger rovings supplied by Owens Corning. For microbond DSC measurements glass fibres were replaced with annealed AISI 302 steel wire of diameter 50 μm to increase droplet size and improve signal clarity. Steel wire was purchased from Goodfellow.

Epoxy Resin

Two multiple-component commercial epoxy resin systems designed for wind turbine blade applications were selected for investigation. Epotec YD-535 LV was cured with Epotec TH7257 hardener at a stoichiometric ratio of 35 phr. Olin Airstone 780E was cured with Olin Airstone 785H hardener at a stoichiometric ratio of 31 phr as per the manufacturers recommendation. Both Epotec and Olin epoxy resins are low-viscosity DGEBA-based systems containing a diluent. Epotec and Olin curing agents were comprised of 20–80% isophorondiamine (IPD), 30–65% polyoxypropylenediamine (PPD), less than 5% diethylenetriamine (DETA), and a proprietary copolymer (around 10%). Samples were cured at 65°C for 3.5 h followed by 75°C for 7 h with a 2°C/min temperature ramp used throughout and were allowed to cool overnight in the oven before being removed. The curing schedule was selected to coincide with the curing schedule used in the production of macroscale composite parts. Both resin systems were supplied by the project industrial partner Suzlon.

DER 332 DGEBA epoxy resin was cured with a stoichiometric (14.3 phr) amount of triethylenetetramine (TETA) tetrafunctional amine curing agent (technical grade 60%) and was used as a comparative control based on its ability to cure consistently at the microscale [36,141,182]. Samples were cured at 60°C for 1 h followed by 120°C for 2 h with a 2°C/min temperature ramp used throughout and were allowed to cool overnight in the oven before being removed. Epoxy resin and curing agent were purchased from Sigma Aldrich/Merck.

As key component amines of the curing agents IPD and PPD (M_w = 230 g/mol) were also examined independently. DER 332 DGEBA epoxy was cured with stoichiometric amounts of each amine according to the same schedule as the Epotec/Olin resins. To further investigate the effect of changing amine chemistry DER 332 DGEBA epoxy was also cured with stoichiometric amounts of diaminopropane (DAP), diethylenetriamine (DETA), and

tetraethylenepentamine (TEPA). Amines were selected based on varying hydrogen functionality. The epoxy resin systems and curing schedules used are summarised in *Table 4-1*.

Designation	Epoxy Resin	Curing Agent	Ratio (phr)	Curing Schedule
Epotec	YD-535 LV	TH 7257	35.0	65°C 3.5 h; 75°C 7 h
Olin	Airstone 780E	Airstone 785H	31.0	65°C 3.5 h; 75°C 7 h
332-TETA	DER 332	TETA	14.3	60°C 1 h; 120°C 2h
332-IPD	DER 332	IPD	25.0	65°C 3.5 h; 75°C 7 h
332-PPD	DER 332	PPD	33.8	65°C 3.5 h; 75°C 7 h
332-DAP	DER 332	DAP	10.9	60°C 1 h; 120°C 2h
332-DETA	DER 332	DETA	12.1	25°C 16 h; 60°C 1 h; 130°C 3 h
332-TEPA	DER 332	TEPA	15.9	60°C 1 h; 120°C 2h

Table 4-1: Epoxy resin, curing agent, and curing schedule details

4.3.2 Micromechanical Testing: Microbond

Microbond samples were prepared and tested as detailed in 2.3.2 following a number of modifications to the curing schedule, matrix composition, and curing atmosphere. Selected poorly cured droplets were examined using SEM according to the procedure detailed in 2.3.4.

4.3.3 Differential Scanning Calorimetry

Determination of Bulk Matrix T_g

Differential Scanning Calorimetry (DSC) was performed to characterise bulk matrix sample (approximately 20 mg) T_g according to ASTM standard E1356-08 *Standard Test Method for Assignment of the Glass Transition Temperatures by Differential Scanning Calorimetry* using a TA Instruments Q20 DSC and corresponding RCS90 cooling system. Specimens were prepared by measuring and mixing the appropriate pre-calculated ratios of resin and curing agent in a small container. The mixed system was then degassed for 10 min and approximately 20 mg syringed into an aluminium pan. Samples were cured according to the recommended macroscale curing schedule and following the addition of a 0-48 h room temperature pre-curing stage. Tests were performed under inert nitrogen atmosphere with a purge gas flow rate of 50 mL/min using open aluminium pans. Data was analysed using TA Universal Analysis software and T_g was estimated from the midpoint of step transitions. Method details were as follows:

1. Data storage: On
2. Ramp 10°C/min to –10°C
3. Isothermal for 5 min
4. Ramp 10°C/min to 180°C
5. Isothermal for 5 min
6. Ramp 10°C/min to –10°C
7. Isothermal for 5 min
8. Ramp 10°C/min to 180°C
9. Data storage: Off

Determination of Microbond Sample T_g

Microdroplet samples were cured on 50 µm lengths of steel wire to produce single larger microbond droplets of embedded lengths approximately 350 µm. Following a similar procedure used by Rao *et al.* involving a novel TMA technique for measurement of microbond T_g, a cluster of similarly sized droplets were placed in the crucible to increase the total sample mass and improve signal strength [183]. Individual droplets were also mounted on hole-punched discs of aluminium foil and applied directly to the heating elements. Silicone oil was also applied in order to improve signal strength. The resin system used was stoichiometric Epotec cured at 65°C for 3.5 h followed by 75°C for 7 h. DSC was performed to characterise microdroplet T_g according to ASTM standard E1356-08 using a TA Instruments Q20 DSC and corresponding RCS90 cooling system. Scans were made from –30 to 150°C at a rate of 10°C/min to account for low droplet T_g. DSC microbond samples and an optical micrograph at 100x magnification are shown in *Figure 4:1*.

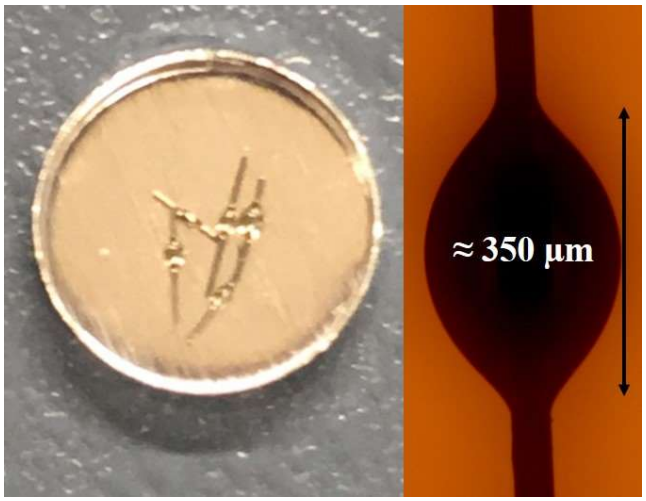

Figure 4:1: DSC microbond sample and 100x magnification optical micrograph

Determination of Gel Point and Pre-Cure Degree of Conversion

Gelation can be defined as the point during cure at which the viscous liquid matrix becomes a cross-linked gel or rubber. Gelation is constant in thermoset matrix systems and is not affected by parameters such as rate of cure, making determination of gel point difficult by direct DSC. It is, however, possible to determine the gel time by first calculating the theoretical degree of conversion of gelation (α_{gel}) at which a given thermoset reaches the gel point and measuring the time taken to reach α_{gel} using thermal analysis techniques such as dynamic rheology, dynamic mechanical analysis (DMA), or DSC. Thermoset gel point is dependent on the functionality, reactivity, and stoichiometry of the reactants and can be calculated for systems with known chemistries. The conversion at the gel point is given by *Eq. 4-1* [194].

$$(\alpha_1\alpha_2)_{gel} = \frac{1}{(f_1 - 1)(f_2 - 1)} \quad \text{(Eq. 4-1)}$$

Where: α_1 is the conversion of amine, α_2 is the conversion of epoxide, f_1 is the functionality of the amine, and f_2 is the functionality of the epoxy.

At the stoichiometric ratio (R = 1) gel point is given by *Eq. 4-2*

$$\alpha_{1,gel} = \alpha_{2,gel} = \alpha_{gel} \quad \text{(Eq. 4-2)}$$

The degree of conversion of gelation at stoichiometry can thus be defined by *Eq. 4-3*.

$$\alpha_{gel} = \sqrt{\frac{1}{(f_1 - 1)(f_2 - 1)}} \quad \text{(Eq. 4-3)}$$

DSC was performed to characterise the degree of cure according to ASTM Standard E2160-04 *Standard Test Method for Heat of Reaction of Thermally Reactive Materials by Differential Scanning Calorimetry* using a TA Instruments Q20 DSC. Scans from –50 to 300°C were made at a rate of 10°C/min in open aluminium pans under inert atmosphere. Total heat of reaction was calculated by integration of the exothermic peak area of an unreacted specimen (H_T) for each resin system. Subsequent samples were prepared and allowed to pre-cure at room temperature for 0–48 h before measuring residual curing heat after partial reaction (H). A typical DSC thermogram showing an exothermic peak area integration is shown in *Figure 4:2.*

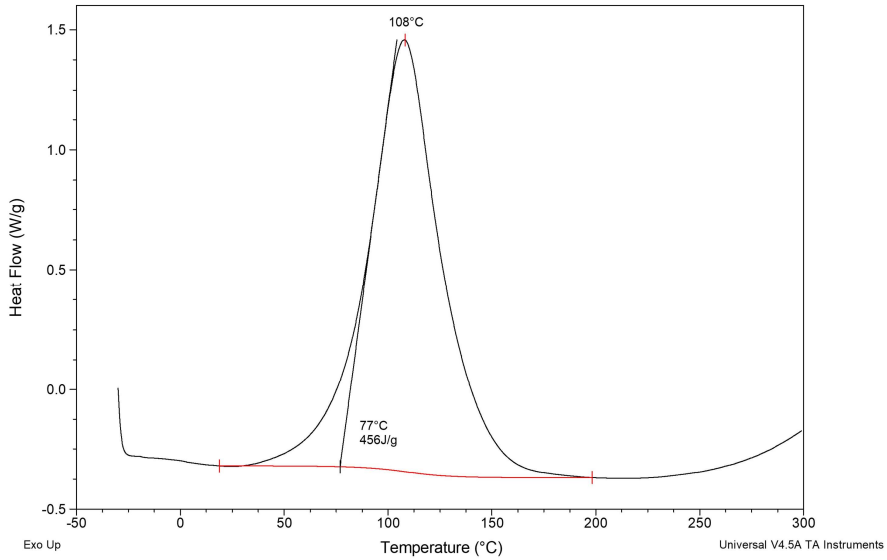

Figure 4:2: Exothermic peak of epoxy/amine curing reaction

Degree of cure was calculated using *Eq. 4-4*. Approximate gel time was defined as the pre-cure time required for experimental α to equal theoretical α_{gel}.

$$\alpha = \left(1 - \frac{H}{H_T}\right) \qquad \text{(Eq. 4-4)}$$

Where: α is degree of cure, H is heat of reaction of the sample, and H_T is total heat of reaction measured from an unreacted sample.

4.3.4 Hot-Stage Microscopy

Experimental Procedure

Hot-stage microscopy was performed using a Mettler Toledo FP90 hot-stage combined with an Olympus BX51 optical microscope (200x magnification) and digital camera. The inclusion of a hot-stage allowed a controlled temperature schedule matching that of the microbond specimen curing schedule to be programmed. The position of the hot-stage pinhole was initially marked on 1 mm rectangular glass microscope slides. Single bare glass filaments were then suspended above the slides using slow setting cement. The assembly was allowed to stand for 24 h to ensure full setting of the cement. Care was taken to ensure that glass fibres did not contact the surface of the glass cover slip in order to prevent contamination and ensure the droplet remained suspended once applied. The height of the cement was controlled in order to avoid contact with the hot-stage heating element and sample damage during set-up. Microdroplets were then applied using a thin length of steel wire and cured in the hot-stage at 65°C for 3.5 h followed by 75°C 7 h with a consistent 2°C/min temperature ramp either immediately or following a 24 h room temperature standing time.

An optical microscope was used to observe in-situ curing and photomicrographs were collected at 1 min intervals using a Nikon Coolpix P5100 digital camera mounted on the head of the microscope. Frequent manual adjustment was performed to counteract focal drift of the microscope and maintain image clarity. Due to the length of the curing schedules involved, the camera battery was replaced after approximately 5 h with a pre-charged secondary battery to minimise downtime between images. The development of the experimental technique and sample preparation procedure has been reported previously [195]. *Figure 4:3* shows a schematic diagram of a typical hot-stage microscope sample.

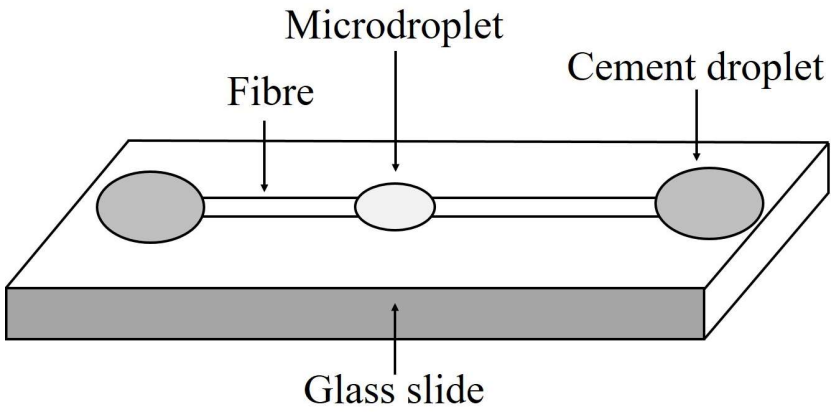

Figure 4:3: Schematic diagram of hot-stage microscope sample

Figure 4:4 shows an epoxy microdroplet hot-stage micrograph with the key dimensions labelled. Namely, the diameter of the fibre (D_f), the droplet diameter (D_d) and the embedded length (L_e). The dimensional change in the droplet was characterised by measurement of the embedded length and droplet diameter using an automated MATLAB script and manual image processing using ImageJ software.

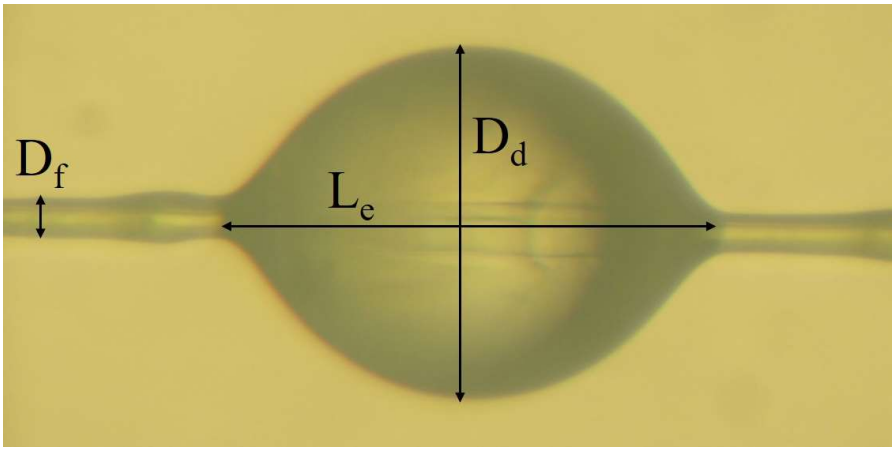

Figure 4:4: Hot-stage micrograph of epoxy droplet

Data Processing

As a result of the long curing schedules involved and large amount of micrographs produced, a MATLAB script was developed to enable automated measurement of droplet dimensions. A precision slide with divisions equal to 10 µm was used to calibrate the pixel/µm ratio of the script. Microscope magnification and digital camera zoom remained constant across all samples to ensure that images were analysed to a consistent and reproducible scale. A threshold operation was performed to generate a Boolean image with the fibre/droplet assigned a value of 1 and the background a value of 0 by detecting pixels with a red factor greater than (darker) or less than (lighter) approximately 155. As a result of image clarity and reflected light a close function was used to locate 0 value black pixels below a defined diameter placed between 1 value white pixels and render them white. A close operation was selected based on the short solving time and the fact that droplet dimensional parameters were unaffected by the function. Residual white corners in the image were removed using a region analyser function. The image processing progression from the raw micrograph following the application of threshold, close, and region analyser functions is shown in *Figure 4:5*.

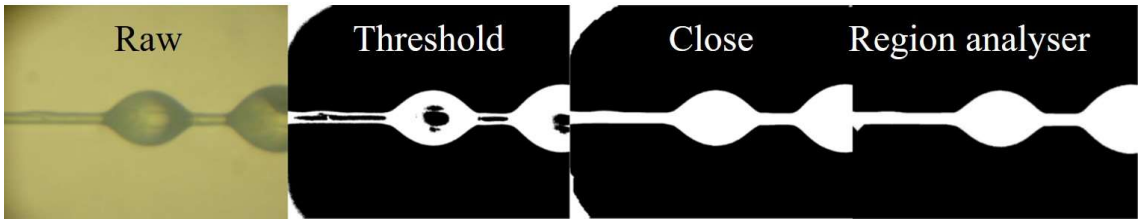

Figure 4:5: Hot-stage micrograph image processing procedure

Image analysis involved plotting the diameter of the fibre/droplet (white) region against the horizontal axis of the processed micrograph, effectively measuring the height of the white pixels across the width of the image. Pixel height was converted into a diameter using the pixel/µm calibration. Fibre diameter was assigned to the minimum consistent diameter. Droplet diameter and embedded length were determined by manual specification of a minimum diameter greater than that of the fibre diameter. Values below the minimum threshold were excluded and the droplet portion of the image effectively isolated by 0 value boundaries. A maximum diameter was also specified for cases where more than one microdroplet was present in the same image. Embedded length was defined as the length between 0 value boundaries and droplet diameter was defined as the maximum diameter measured. The volume of the microdroplet (V_d) was calculated according to *Eq. 4-5*. Droplets were modelled as ideal ellipsoids and it was assumed that the resin droplet remained symmetrical during the curing process. The volume of the fibre was also subtracted from the calculation.

$$V_d = \frac{4}{3}\pi \cdot \frac{L_e}{2} \cdot \left(\frac{D_d}{2}\right)^2 - \pi\left(\frac{D_f}{2}\right)^2 \cdot L_e \qquad (Eq.\ 4\text{-}5)$$

The MATLAB script sequentially performed the process on each image in a specified folder after which microdroplet dimensions were exported to an Excel spreadsheet. Results of automated droplet measurements were periodically compared to manual ImageJ measurements to ensure general consistency. Erroneous results induced by artefacts of optical effects were measured manually and updated. For droplets where a room temperature standing time was included, micrographs were collected immediately following the application of the droplet to the fibre, during the room temperature stage, and before hot-stage curing. The MATLAB script used is detailed in Appendix D.

4.4 RESULTS AND DISCUSSION

4.4.1 Micromechanical Testing: Microbond

Effect of Immediate Cure

Initial investigation of the Epotec and Olin resin systems showed exceedingly low IFSS values when microbond samples were cured according to the recommended macroscale schedule. Droplets did not appear to cure and immediately deformed plastically under applied load, a behaviour not observed previously with the TETA-cured 332 matrix reported in Chapters 2 and 3. Measurement of IFSS was not possible in such cases and the resulting forces generated during the test can be largely attributed to frictional effects during the crushing of the droplet and subsequent fibre pull-out from the soft and viscous matrix as opposed to any true measure of adhesion. Photomicrographs of a typical undercured microbond sample prior to, and during microbond testing with visible plastic deformation are shown in *Figure 4:6*.

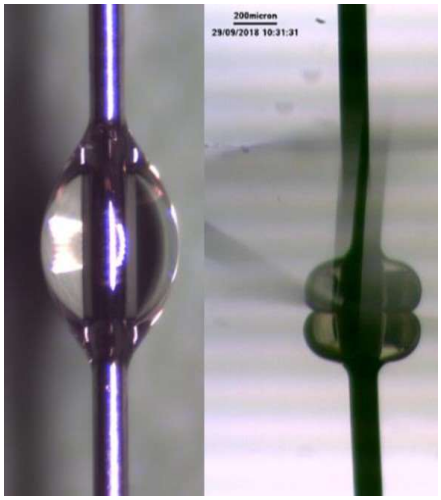

Figure 4:6: Plastic deformation of undercured microbond sample under loading

Microbond specimens that deformed during testing were also examined using SEM as shown in *Figure 4:7*.

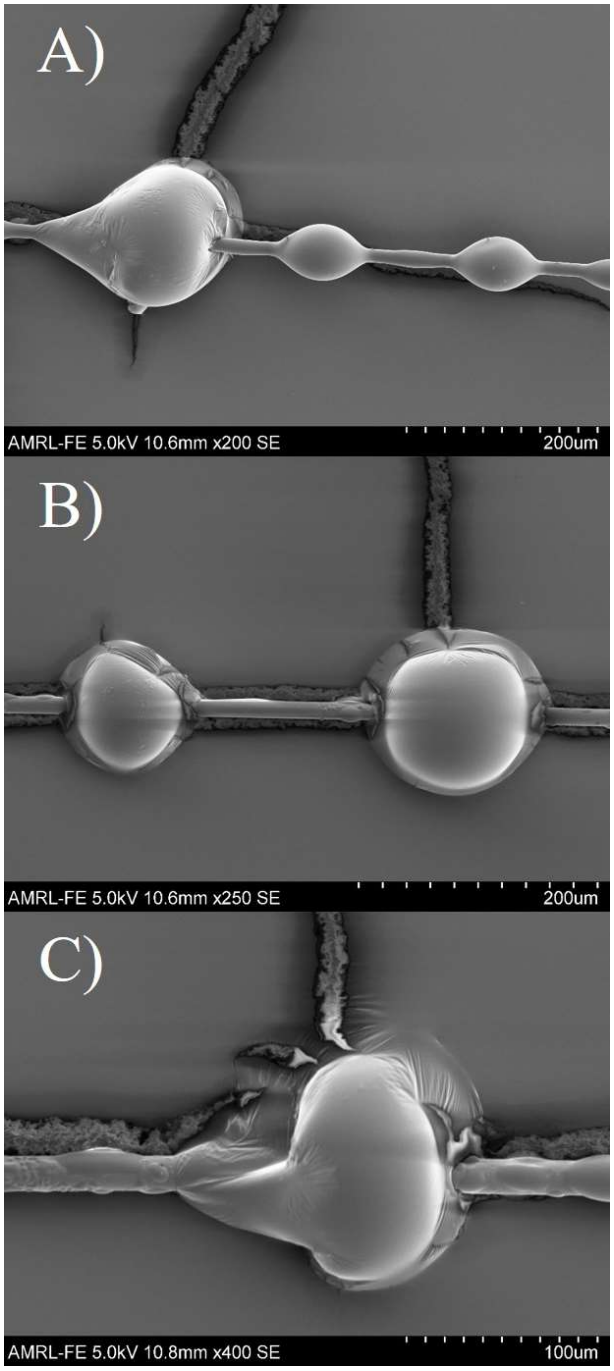

Figure 4:7: SEM micrographs of post-test plastically deformed microbond specimens

Plastic deformation of post-test microbond samples is readily visible in samples A) and C). Samples show an elongated meniscus at the point of contact with the shearing blades. Secondary smaller droplets formed as a result of the initial resin application that were not tested are visible in sample A). It is likely that these droplets retained an ideal ellipsoidal shape due to the larger post-test droplet preventing contact with the substrate. Both droplets shown

in sample B) were crushed from an initial axisymmetric ellipsoid to a sphere. All plastically deformed samples appeared to show a translucent outer layer surrounding the sample, though it was not possible to definitively attribute this behaviour to any specific phenomena. The translucent layer may have been related to evaporation of reacting components at the surface of the sample. Alternatively, it should also be considered that the behaviour may have been related to a charging artefact of the SEM procedure, as poorly cured sub-droplets in sample A) were not visibly affected by the cure state. However, the translucent surface layer was not observed in well-cured 332-TETA droplets prior to or after testing.

The deformation of microbond samples during testing would appear to suggest that microdroplet T_g was sub-ambient. Conversely, DSC of bulk matrix samples subjected to the same curing conditions showed T_g of approximately 90°C. This behaviour is most plausibly attributed to a stoichiometric imbalance due to diffusion and evaporation of components essential to the polymerisation reaction such as the curing agent. Curing agent evaporation appeared to result in insufficient amine groups necessary to produce a strongly cross-linked network structure in the droplet. Microdroplet cure state and corresponding T_g thus becomes an important parameter in the consideration of any microbond based experimental investigation due to the linear relationship between apparent IFSS and T_g [10,36] and the dependence of T_g on matrix stoichiometry [196,197]. Several authors have similarly attributed reduced epoxy/m-PDA microdroplet T_g to a stoichiometric imbalance due to evaporation of curing agent [41,74,183,184]. The results presented would appear to confirm that the behaviour is not limited to m-PDA but is prevalent in a number of diamine curing agents. Samples cured with TETA were, however, unaffected and cured successfully without the need for curing schedule modifications.

Microdroplet curing behaviour appeared to be entirely dependent on the curing agent used. It was observed that 332 resin cured with a stoichiometric amount of IPD or PPD failed to produce cured microbond specimens, while the same resin cured with TETA produced well-cured droplets suitable for testing. It is possible that the TETA-cured samples were less susceptible to microbond curing issues due to both lower vapour pressure and higher functionality. The epoxy/amine reaction may have progressed more quickly and effectively anchored curing agent molecules to epoxy groups. Previous hypotheses regarding curing agent volatility, however, do not appear to fully explain discrepancies in microbond curing behaviour [183,184]. Differences in data sheet vapour pressure (at 20°C) between TETA (<1 Pa), IPD (1.57 Pa) and Olin (<1.33 Pa) curing agents were not excessively large. Furthermore,

the Epotec (100 Pa) and Olin (<1.33 Pa) microdroplets showed similarly poor curing performance despite vapour pressure differing by a factor of 100.

Work by Zinck *et al.* has proposed that poor model droplet curing was attributable to an amine deficient stoichiometric imbalance caused by the formation of imine groups reducing amine functions available to react with oxirane groups, fibre surface moisture, or curing agent hydrolysis [83]. More recently, Laurikainen has similarly demonstrated both ideal and poor microdroplet curing in two epoxy resin systems where differences in curing agent vapour pressures were insignificant [91]. The ability to produce consistently cured droplets using an alternate epoxy system (Araldite 5052) was attributed to a smaller difference in viscosities between the resin and hardener compared to poorly cured samples. In the present work, however, cured droplets have been produced using high viscosity resins (332) and low viscosity hardeners (TETA). Pre-heating the 332 resin for 1 h at 60°C before mixing to reduce resin viscosity had no effect on curing performance. This behaviour may be interpreted as further confirmation that microdroplet curing performance depends on curing agent behaviour to a greater extent than factors related to the unreacted epoxy resin. It is worth noting that the Jeffamine D230 curing agent that resulted in undercured droplets is a trade name for Huntsman PPD. In this work, PPD-cured epoxy failed to produce cured droplets, and was a component of the Epotec and Olin curing agents. Early investigations identify poor microdroplet curing with epoxy/m-PDA combinations [41,74,120,183,184]. A recommendation is proposed that the microbond test be used with a degree of caution when using IPD or PPD curing agents, or commercial blends thereof, and that a modification to the comparable macroscale curing schedule may be necessary to produce droplets suitable for micromechanical testing.

Effect of Pre-Cure Standing Time

A number of previous studies have addressed similar microdroplet curing issues through the introduction of an 18–24 h standing time [41,183]. Accordingly, it was initially verified that a 24 h standing time was sufficient to produce cured microbond samples. Standing times lower and higher than those reported in the previous literature have been investigated in order to determine a threshold value at which microbond samples cured in these systems. Microbond testing results for the Epotec, Olin, and 332-TETA droplets cured after a 0–48 h pre-cure standing time are shown in *Figure 4:8*.

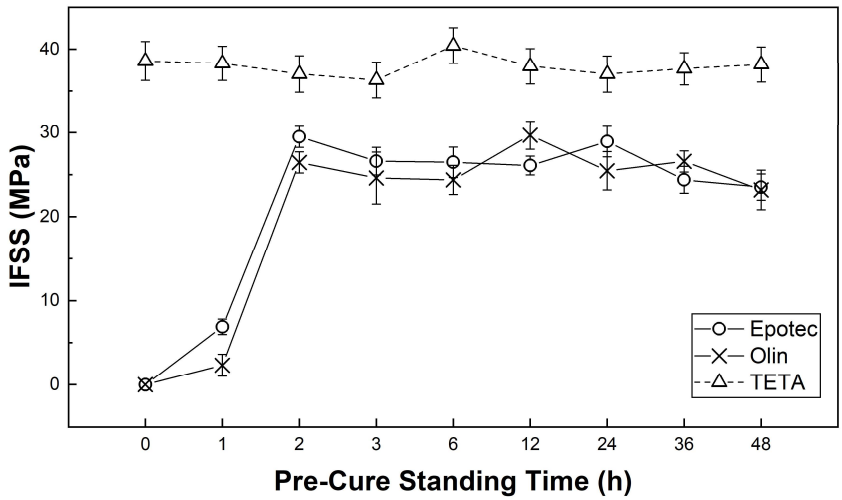

Figure 4:8: IFSS versus room temperature pre-cure standing time

Microbond testing results indicated that the inclusion of a room temperature pre–cure stage had a profound effect on the apparent IFSS of both Epotec and Olin resins. It was not possible to accurately measure the IFSS of samples cured immediately due to plastic deformation of the samples during microbond testing. A standing time of 1 h was insufficient to ensure good curing and such samples showed only some tackiness while still deforming under load. The IFSS values of approximately 6 MPa can largely attributed to frictional effects during deformation of the sample. It was found that a 2 h room temperature standing time was sufficient to ensure good curing and interfacial adhesion, and that further standing times of up to 48 h showed no significant improvement. Improved curing performance after 2 h would indicate that the pre-cure standing time necessary to produce cured droplets is notably lower than the gel time, as has been proposed in previous literature [41,183]. Improved curing performance may be attributable to comonomers reacting at low temperature and subsequently preventing diffusion and vaporisation of the curing agent.

No significant travel distance along the fibre was observed following resin application as in [91], indicating that no discernible phase separation occurred during sample preparation. The results in this work, however, show good correlation with the fact that microdroplet curing performance was improved by allowing mixed resin to partially gel for 2 h before applying the microbond samples. Furthermore, the results are contradictory to those of Zinck *et al.*[83], who reported that a pre-curing time had no effect on amine-cured samples and a detrimental effect on anhydride-cured droplets. IFSS of 332-TETA samples was entirely independent of pre-cure standing time and microdroplets cured consistently across the range of immediate and pre-cure standing time schedules investigated. Higher IFSS values observed for the 332-TETA may also be due to higher cured matrix T_g.

Plastic deformation of microbond samples under applied load during the microbond test and increased IFSS after a room temperature pre-cure can be plausibly attributed to whether the samples were allowed to partially gelate prior to exposure to elevated temperature. The deformation of the 0 and 1 h samples observed would indicate that T_g of these samples was significantly lower than that of bulk matrix samples cured according to the same temperature schedule. IFSS in all three systems appeared to depend strongly on microdroplet cure state and corresponding T_g. According to Haaksma and Cehelnik, it is essential that an independent test method be developed to determine the extent of cure of thermoset matrix droplets [74]. An FTIR technique to address this directly will be presented in Chapter 5. The effect of a room temperature pre-cure standing time on IFSS in three amine-cured epoxy resins is summarised in *Table 4-2*.

	IFSS (MPa)		
Pre-Cure Time (h)	**Epotec**	**Olin**	**332-TETA**
0	-	-	38.6
1	6.9	2.3	38.3
2	34.7	33.5	37.0
3	26.6	24.6	36.3
6	26.5	24.3	40.4
12	26.0	29.7	38.0
24	28.9	25.5	37.0
36	24.4	26.6	37.7
48	23.5	23.2	38.2

Table 4-2: Summary of IFSS versus pre-cure standing time

Effect of Post-Curing

In addition to a room temperature pre-cure standing time, a number of microbond sample processing methods were investigated. It seems plausible to suggest that the undercured microbond samples exposed to immediate elevated temperature curing had different thermomechanical properties to those that showed high apparent IFSS. Most notably, a low T_g due to a stoichiometric imbalance caused by evaporation of curing agents during the early stages of curing. A post-curing study was undertaken for a number of reasons. Firstly, so that the lower curing temperature (65–75°C) of the Epotec/Olin samples and potential reduction of auto-acceleration and reaction extent related to a droplet dimensional effect could be effectively discounted [90]. Secondly, if evaporation of curing agent did occur in the early stages of the heating process, the lost amine would be irrecoverable and curing at higher

temperature should still result in an amine-deficient mixture. A set of sixty Epotec microbond samples were cured according to the standard macroscale schedule (65°C 3.5 h; 75°C 7 h). After the initial curing, half of the samples were tested. The other half were post-cured at 120°C for 2 h prior to testing.

Post-curing increased apparent IFSS from around 2 MPa to approximately 10.5 MPa. Despite some measure of improvement, IFSS was less than half that of well-cured samples with a 2–48 h pre-cure and full debonding was not observed. Droplets appeared to be tackier than those cured immediately, though a degree of plastic deformation remained evident, indicating incomplete cure and sub-optimal droplet T_g. Furthermore, peak areas of load versus extension plots generated during microbond testing were significantly broader than those of well-cured specimens due to plastic deformation of the droplet. Sub-optimal properties of post-cured droplets would appear to confirm an irreversible amine deficiency as a result of the initial curing schedule. Higher post-curing temperature, however, may result in increased cross-linking and etherification of off-stoichiometric droplets, allowing an overall higher degree of cure and T_g to be achieved [198]. Increased IFSS may thus be attributable to improved microdroplet T_g. Finally, the results presented show good correlation with a similar behaviour reported for vinyl ester microdroplets [91]. Excessive post-curing treatments are not suitable to produce optimal droplet with comparable bulk matrix properties due to irreversible vaporisation of reactive components essential for polymerisation. Charlier *et al.* reported improvement to droplet cure state by using higher curing temperatures, though comparisons are complicated by undisclosed epoxy and curing agent compositions [90].

Effect of Excess Curing Agent

Microbond samples were prepared that contained an excess of curing agent. It was theorised that an initial excess of curing agent could counterbalance amine evaporation effects and allow an ideal droplet stoichiometry to be retained following immediate curing. Epotec and Olin droplets were prepared with double the stoichiometric amount of curing agent and cured according to the standard macroscale curing schedule (65°C 3.5 h; 75°C 7 h) without any pre-cure modification.

The addition of excess curing agent appeared to counteract amine evaporation and produced cured microdroplets with measurable IFSS. Furthermore, values were generally higher than when a pre-cure standing time was included. IFSS of samples cured with twice the stoichiometric amount of curing agent was around 31–33 MPa. Liao and Tung reported that epoxy/m-PDA microbond curing issues appeared to be successfully mitigated and testable

droplets produced by the addition of around 25% excess curing agent [120]. Conversely, Rao *et al.* reported no significant increase in IFSS when the resin mixture contained twice the stoichiometric amount of m-PDA [183].

It must be considered, however, that the goal of the investigation is not to simply produce a sample preparation and processing procedure that generates the highest apparent IFSS, but a methodology wherein best correlation is found between the thermomechanical properties of microbond samples and comparable bulk matrix specimens. Microbond samples prepared at the stoichiometric ratio and cured according to the unmodified macroscale curing schedule resulted in microbond specimens with thermomechanical properties far below that of the bulk cured matrix. Conversely, DSC measurements indicated that T_g of the bulk matrix was reduced by approximately half when samples were prepared with twice the stoichiometric amount of curing agent and cured according to the standard temperature schedule. Amine-rich bulk scale DSC samples likely had low T_g due to the fact that curing agent did not evaporate out of the sample to produce a near-stoichiometric formulation. Microbond data, however, appears to provide further evidence of loss of curing agent in droplet samples. Cure state and apparent IFSS may be enhanced by the addition of excess curing agent when cured according to the macroscale temperature schedule. This method cannot be proposed as a viable solution to alleviate microscale curing issues, however, based on deviation of bulk matrix T_g produced by a comparable procedure and resultant IFSS being measured in a material with undefined system chemistry.

Effect of Curing Atmosphere

Reduced T_g of amine-cured epoxy microdroplets has previously been attributed to imine formation reducing the number of amine functions available to react with the oxirane ring [83]. A recommendation that epoxy/amine droplets should be cured under inert atmosphere was proposed. To investigate the effect of curing atmosphere and potential imine formation, microbond samples were pre-cured under inert nitrogen atmosphere in a vacuum oven at room temperature for 24 h before curing for 3.5 h at 65°C and 7 h at 75°C in a standard fan oven. Results were compared with IFSS values from the pre-cure standing time study with a 24 h pre-curing time under standard laboratory atmosphere.

Apparent IFSS appeared to depend solely on pre-curing time rather than atmosphere. IFSS of Epotec and Olin samples following pre-curing under air (≈ 25–29 MPa) or nitrogen (≈ 28–29 MPa) were approximately the same. The results show good correlation with those of Biro *et al*. who similarly observed that curing under inert and amine-rich atmospheres had no

significant effect on microdroplet properties [193]. Montgomery, however, cured epoxy microbond samples under nitrogen to prevent blushing of the epoxy, though no comparable data for samples cured otherwise was available [10]. Spectroscopic analysis of potential imine formation is investigated further in Chapter 5.

Effect of Fibre Type

The curing performance of both Epotec and Olin resin systems was shown to be independent of the type of fibre used. Microbond samples subjected to the same macroscale curing schedule failed to cure when applied to glass, carbon, and steel wire filaments. Haaksma and Cehelnik have similarly reported that Epon 828/m-PDA resin droplets failed to cure on carbon, glass, or aramid fibres [74]. It can be concluded that fibre selection did not play a significant role in the curing performance of these resin systems. Microbond curing behaviour appeared to be independent of fibre type and should be a consideration for all practitioners of the microbond method.

Effect of Droplet Size

Haaksma and Cehelnik observed that droplet size had a notable effect on cure state [74]. Curing performance was poorest for small droplets and even specimens with diameters exceeding 1000 µm appeared incompletely cured. FTIR microscopy appeared to confirm an inverse relationship between droplet size and degree of conversion. Similarly, Rao *et al.* reported that T_g of smaller droplets (<150 µm) was around 60°C lower than that of the bulk cured matrix, while deviation was reduced to around 30°C when droplet embedded length was increased to 600 µm [183]. Droplets larger than 800 µm likewise showed a T_g reduction of around 20°C [184]. Conversely, Zinck *et al.* reported that varying film thickness (considered a comparable microdroplet model) in the 100–200 µm range had no effect on T_g [83].

Glass fibres were substituted by steel wire of diameter 50–150 µm in order to investigate the effect of droplet size on microscale curing behaviour. Average microdroplet embedded length was increased by a factor of approximately 2 and 5 by substituting glass fibres with steel wire of diameter 50 and 125 µm, respectively. Epotec and Olin microbond samples with embedded lengths up to approximately 700 µm failed to cure when exposed to the immediate elevated temperature curing schedule. Curing performance of exceedingly large droplets was generally indicative that evaporation of curing agent still occurred in these specimens. The maximum embedded length to achieve debonding for glass fibre/epoxy is around 150 µm, with

larger specimens typically resulting in premature fibre fracture. Accordingly, increasing droplet size would not appear to be a viable method to address poor microbond curing performance in any case. This behaviour may be attributable to microbond droplet surface-to-volume ratio. Given that curing performance appeared consistent in the bulk matrix specimens, it would seem plausible to suggest that there exists a critical surface-to-volume ratio that results in evaporation of some portion of the curing agent out of the droplet, that may be defined by both the droplet size and the curing agent used [83,183,184].

Summary of Curing Condition Modification

Modifications to the recommended macroscale curing schedule for the Epotec and Olin epoxy resin systems and resulting effect on microdroplet curing performance and interfacial adhesion are summarised is *Table 4-3*.

Parameter	**IFSS (MPa)**	**Comment**
Immediate cure (macroscale schedule)	No cure	Microbond samples failed to cure when subjected to the recommended macroscale curing schedule. Plastic deformation under applied load.
Addition of pre-cure standing time	≈ 25.0	Inclusion of a room temperature pre-cure stage improved droplet curing and IFSS. IFSS constant after 2–48 h standing time.
Post-curing (120°C)	≈10.5	Some improvement despite incomplete cure and sub-optimal droplet T_g. Irreversible amine deficiency as a result of the initial heating. Increased cross-linking and etherification of off-stoichiometric droplets.
Excess curing agent	≈ 32.0	Excess curing agent (double the stoichiometric amount) counteracted amine evaporation and produced cured microdroplets with measurable IFSS. T_g of the bulk matrix was reduced by approximately half.
Standing time under nitrogen	≈ 28.0	Microbond curing performance independent of pre-curing atmosphere.
Change reinforcement fibre	No cure	Microbond curing performance independent of reinforcement fibre type.
Increased droplet size	No cure	Microbond curing performance not improved by increasing embedded length up to 700 μm.

Table 4-3: Summary of the effect of Epotec/Olin curing modification

Effect of Curing Agent Chemistry

Investigation of microscale curing behaviour was extended to a range of epoxy/amine chemistries. DER 332 epoxy resin was cured with stoichiometric amounts of isophorondiamine (IPD), polyoxypropylenediamine (PPD), diaminopropane (DAP), diethylenetriamine (DETA), triethylenetetramine (TETA), and tetraethylenepentamine (TEPA). Curing agents were selected to include a range of molecular and amine equivalent weights and varying numbers of reactive hydrogen atoms and functionality. All diamines, the Epotec and Olin curing agents, IPD, PPD, and DAP had a functionality of 4. The functionality of DETA, TETA, and TEPA curing agents was 5, 6, and 7, respectively.

Microbond samples cured with IPD and PPD diamines deformed under applied load when exposed to immediate elevated temperature curing. Curing behaviour appeared generally comparable to that of the Epotec and Olin droplets and was improved by the introduction of a 24 h pre-cure standing time. Improved curing performance was less apparent in the IPD-cured samples. IFSS was increased from around 4 MPa to approximately 15 MPa. Furthermore, load versus displacement plots indicated that curing performance was relatively inconsistent across the data set. A number of immediately cured samples deformed under extremely low loads, while others did not deform immediately and had approximate IFSS of 8–10 MPa. Improved curing performance following the standing time was likewise inconsistent. For PPD-cured samples, a 24 h standing time increased IFSS from around 2 MPa to approximately 27 MPa, a value approximating that of the well-cured Epotec and Olin droplets.

A DAP-cured epoxy did not produce cured droplets when exposed to immediate elevated temperature curing. Despite curing agent functionality similar to IPD and PPD, microdroplet cure state was not improved following the inclusion a 24 h pre-curing stage. Poor curing performance may have been attributable to the combination of lower functionality and lower molecular weight. A stoichiometric 332-DAP formulation had an initial curing agent content considerably lower (10.9 phr) than Epotec (35 phr), Olin (31 phr), IPD (25 phr), and PPD (33.8 phr) samples. Accordingly, samples may have been more strongly affected by evaporation of some portion of the curing agent in the microdroplet samples. It is also possible that the curing temperature used was insufficient [199,200].

Similarly, DETA-cured samples failed to produce droplets suitable for testing when cured according to a macroscale temperature schedule that included a 16 h standing time (25°C 16 h; 1h 60°C; 3 h 130°C) previously reported in the literature [201]. Higher curing temperatures have, however, been reported by De Nograro *et al.* [202]. As reported previously in this work,

and in the literature [36,141], 332-TETA samples cured consistently when cured immediately and appeared unaffected by a pre-curing stage.

TEPA-cured microbond samples appeared to cure well and were suitable for microbond testing when subjected to the same curing schedule as TETA samples (1 h 60°C; 2 h 120°C). The inclusion of a 24 h standing time prior to the curing schedule similarly produced droplets that appeared to be well-cured and did not deform plastically under load. However, samples appeared to be significantly deformed after curing and the formation of axisymmetric samples was generally not possible. While samples appeared more resilient to loss of curing agent, the inability to form axisymmetric microdroplets limited the use of this system with the microbond test. Furthermore, samples appeared visibly discolored following the inclusion of a pre-curing stage that may have indicated sample oxidation [177].

The microscale curing performance of a range of epoxy/amine chemistries is summarised in *Table 4-4*.

Amine	Functionality	Ratio (phr)	Vapour Pressure (Pa)	Standard Schedule	With Standing Time
Epotec	4	35.0	100 (@ 20°C)	No cure	Cured
Olin	4	31.0	<1.33 (@ 20°C)	No cure	Cured
IPD	4	25.0	1.57 (@ 20°C)	No cure	Cured (inconsistent)
PPD	4	33.8	100 (@ 100°C)	No cure	Cured
DAP	4	10.9	<1100 (@ 20°C)	No cure	No cure
DETA	5	12.1	No data available	-	No cure
TETA	6	14.3	<1 (@ 20°C)	Cured	Cured
TEPA	7	15.9	No data available	Cured	Cured (non-axisymmetric)

Table 4-4: Summary of curing agent chemistry and microbond curing performance

The results discussed have clear implications for the applicability of the microbond test, in that the range of curing agents that are capable of producing cured droplets with properties comparable to that of the bulk matrix may be limited. The findings further reinforce the need for the development of a method to characterise the cure state and glass transition temperature of microbond samples. Curing samples with amines with a higher number of reactive hydrogen atoms and increased functionality (TETA = 6, TEPA = 7) appeared to play a role in the ability of microbond samples to cure to a high degree and retard the effects of curing agent evaporation. It is possible that increased reactivity at room temperature promoted faster bond formation, increased molecular weight, and formation of a more highly cross-linked structure during the earliest stages of cure [202]. Constraining of molecular chains due to reduced gel time may have also had a preventative effect on curing amine evaporation. Conversely,

pendant methyl groups may have hindered intermolecular interactions between chains in epoxy/amine formulations containing IPD or PPD.

4.4.2 Differential Scanning Calorimetry

Bulk Matrix Glass Transition Temperature

DSC was performed on bulk matrix samples cured in open aluminium pans according to the macroscale curing schedule and with the inclusion of a 0–48 h pre-cure standing time. No significant difference in T_g between the different curing schedules was observed. Material properties of the bulk matrix samples (in the range of 20 mg) appeared unaffected by the inclusion of a standing time, indicating that the improvements observed during interfacial testing are limited to the microscale range. Bulk cured matrix properties determined by DSC are summarised in *Table 4-5*.

	T_g (°C)		
Standing Time (h)	**Epotec**	**Olin**	**332-TETA**
0	87	79	124
1	86	79	122
2	87	78	125
3	87	80	125
6	89	82	127
12	88	81	127
24	87	81	127
36	88	79	128
48	87	77	128

Table 4-5: Glass transition temperature of bulk matrix resin samples

Microbond Droplet Glass Transition Temperature

DSC was used to characterise the glass transition temperature of poorly cured microdroplet samples that had been cured immediately at elevated temperature. Micromechanical testing results indicated that droplet curing remained poor when embedded length was increased by a factor of around 2 by substituting glass fibres for lengths of 50 µm steel wire. Steel wire was thus considered an appropriate substitution for glass fibres as a dimensional effect alone was not responsible for discrepancies in curing behaviour. Curing droplets on steel wire allowed for easier sample handling and ensured consistent application of a single droplet per specimen.

Direct DSC of individual microbond samples was complicated by the lack of a clear step change in the heat flow versus temperature data. Poor signal was likely due to insufficient sample mass in the range of hundreds of nanograms to a few micrograms. Attempts were made to improve signal clarity by mounting individual droplets on hole-punched discs of aluminium foil applied directly to the instrument heating elements. Silicon oil was also applied in order to improve signal strength. This was, however, insufficient to generate reliable signal and clear step transitions using single droplets.

Total sample mass and signal clarity was improved by using a cluster of similarly sized droplets, similar to the TMA-T_g method used by Rao *et al.* [183]. It was found that four droplets were necessary to generate sufficient signal to discriminate a clear step transition. A microdroplet T_g of approximately 40°C was measured. Subsequent tests using clusters of 7, 10, and 20 microbond samples similarly showed clear step transitions and T_g of 30–40°C. Microdroplet T_g generally appeared unaffected by increasing the number of droplets once sufficient sample mass had been reached to register a clear step change and was relatively consistent between droplet clusters from the same specimen set. Variation of T_g between specimen sets was around 10°C. Droplet T_g was around 50 to 60°C lower than that of the bulk matrix samples (≈ 90°C) when cured according to the same temperature schedule. The reduction in T_g observed was indicative of a significant loss of curing agent out of the droplets

The microbond DSC data is summarised in *Table 4-6*.

Number of Droplets	T_g (°C)
1	No clear step change
2	No clear step change
3	No clear step change
4	44^A
4	37^A
7	42^A
10	32^B
20	31^B

Table 4-6: Microbond droplet T_g DSC summary

$^{A/B}$ = droplets from the same sample set

Matrix Gel Point and Pre-Cure Conversion

The degree of conversion at the gel point for each epoxy/curing agent combination was calculated using *Eq. 4-3*.

$$\alpha_{gel} = \sqrt{\frac{1}{(f_1 - 1)(f_2 - 1)}} \quad \text{(Eq. 4-3)}$$

Epotec and Olin samples had a functionality (f_1) of 4, while TETA-cured samples had a functionality of 6. The epoxy resins used shared a common functionality (f_2) of 2. Degree of conversation at the gel point (α_{gel}) was 0.58 for the Epotec and Olin samples and 0.45 for the TETA cured samples.

The degree of cure for Epotec, Olin, and 332-TETA matrices after a 0–48 h room temperature standing time was calculated by *Eq. 4-4*.

$$\alpha = \left(1 - \frac{H}{H_T}\right) \quad \text{(Eq. 4-4)}$$

Residual exotherm was reduced as the samples were allowed to pre-cure for longer standing times. DSC thermograms of residual exotherm after a 0–48 h pre-curing time for Epotec, Olin, and 332-TETA epoxy resins are shown in *Figure 4:9*, *Figure 4:10*, and *Figure 4:11*, respectively. Comparison of DSC data and theoretical degree of cure at the gel point was used to determine the gel time of each of the systems. The gel time was approximately 18 h for the Epotec and Olin systems and 2.5 h for the 332-TETA system. DSC degree of cure measurements after a protracted room temperature standing time are summarised in *Table 4-7*.

		α	
Standing Time (h)	**Epotec**	**Olin**	**332-TETA**
0	0.00	0.00	0.00
1	0.03	0.03	0.18
2	0.04	0.09	0.34
3	0.07	0.14	0.50
6	0.18	0.18	0.67
12	0.50	0.51	0.79
24	0.70	0.69	0.80
36	0.82	0.80	0.80
48	0.85	0.84	0.81

Table 4-7: Summary of degree of cure versus standing time

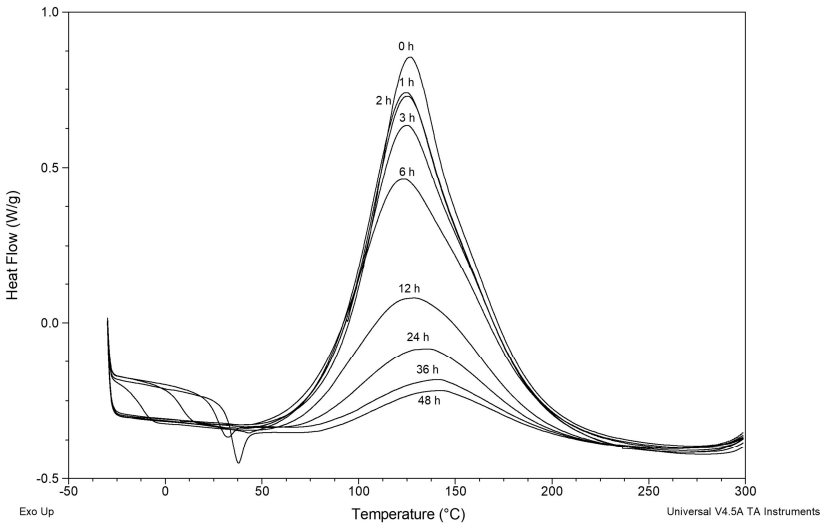

Figure 4:9: Epotec residual exotherm with 0–48 h standing time

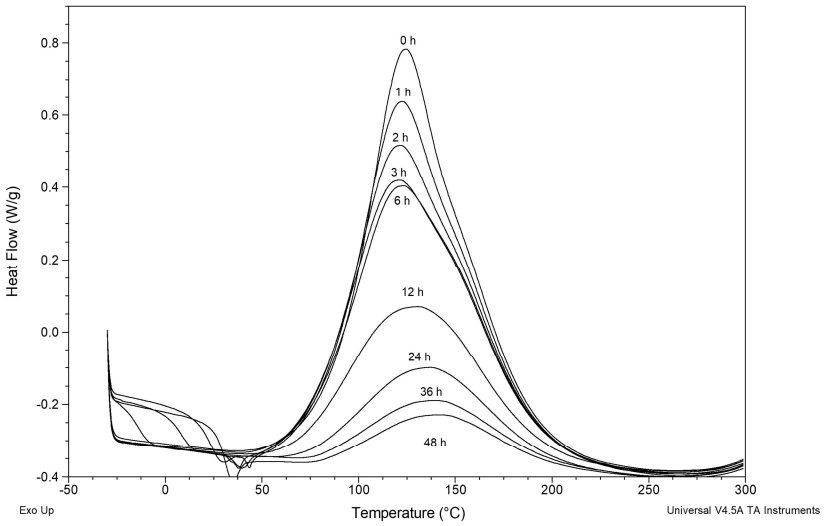

Figure 4:10: Olin residual exotherm with 0–48 h standing time

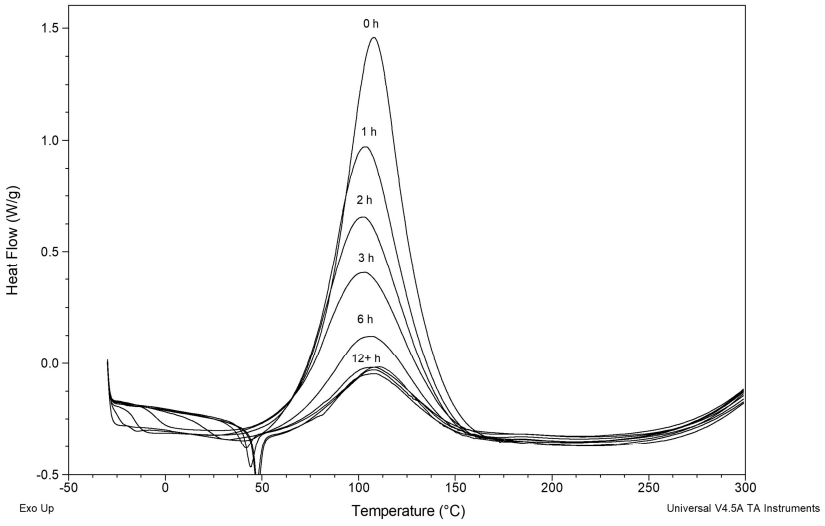

Figure 4:11: 332-TETA residual exotherm with 0–48 h standing time

IFSS of microbond samples cured after a 0–48 h pre-cure standing time is plotted against the degree of cure that samples reached prior to being exposed to elevated temperature curing. Epotec, Olin, and 332-TETA are shown in *Figure 4:12*, *Figure 4:13*, and *Figure 4:14*, respectively.

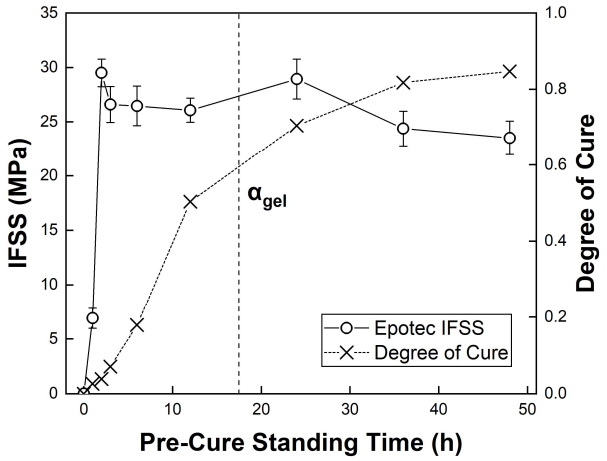

Figure 4:12: Epotec IFSS versus pre-cure α

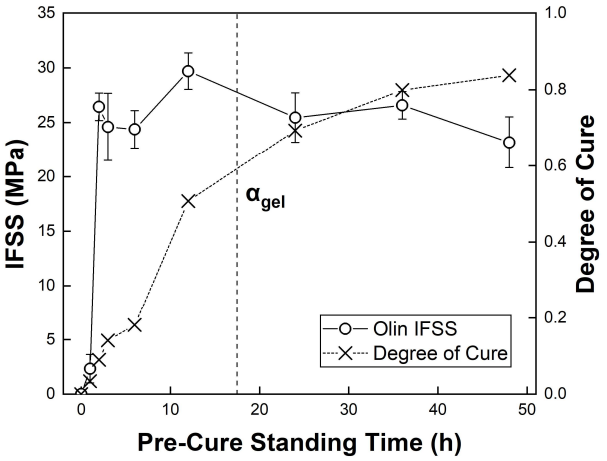

Figure 4:13: Olin IFSS versus pre-cure α

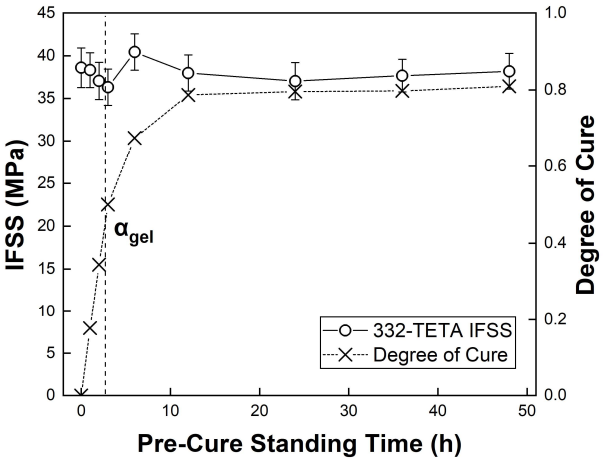

Figure 4:14: 332-TETA IFSS versus pre-cure α

Comparison of pre-cure α and IFSS data indicated that the standing time necessary in order to produce cured droplets was significantly lower than the gel time. The results show good correlation with those presented in previous literature, in that the inclusion of a room temperature stage in the curing schedule appeared to retard the effects of curing agent evaporation in the Epotec and Olin microbond samples. The standing time of 2 h necessary to create cured droplets, however, was significantly lower than previous investigations [41,183]. Similar correlation has, however, been observed by Laurikainen *et al.* when mixed resin was allowed to approach the gel point by heating at 40°C for 2.5 h prior to applying microbond samples to the fibres [190]. It would seem possible to suggest that while evaporation of volatile curing agents may occur in the early stages of curing, the pre-curing time necessary to prevent this evaporation is related to the time taken for each curing agent molecule to form a single intermolecular bond, which is significantly less than the gel time. In the 332-TETA system, microbond samples cured well regardless of the extent of the curing reaction prior to exposure to elevated temperature curing.

4.4.3 Hot-Stage Microscopy

Hot stage microscopy was used to monitor microbond sample curing in-situ. Samples were cured at 65°C for 3.5 h followed by 75°C 7 h with a consistent 2°C/min temperature ramp either immediately, or following a 24 h pre-curing time. In-situ volumetric cure shrinkage results for Epotec and Olin droplets are shown in *Figure 4:15* and *Figure 4:16,* respectively.

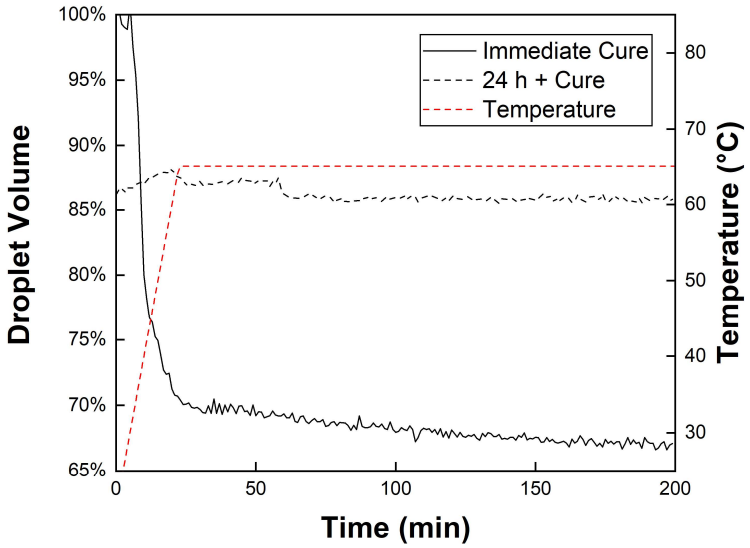

Figure 4:15: In-situ volumetric shrinkage of Epotec microbond samples

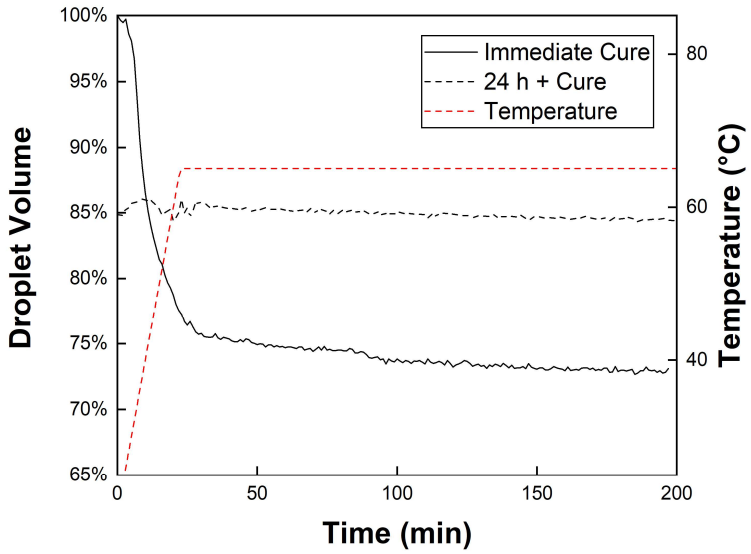

Figure 4:16: In-situ volumetric shrinkage of Olin microbond samples

In-situ monitoring of volumetric shrinkage during cure showed that the dimensional change of the droplet was significantly affected by modification of the curing schedule and inclusion of a pre-cure standing time. Droplets exposed to immediate elevated temperature curing underwent a significant volumetric reduction. The majority of the reduction occurred early in the curing schedule during the ramping stage. Droplets cured immediately appeared to shrink by around 25–30% during this stage, after which droplet volume remained consistent for the duration of the schedule. Measurement of droplets before and after a 24 h standing time showed that a volumetric reduction of some 15% occurred during the room temperature pre-curing stage. Once subjected to curing at elevated temperature, however, droplet size was unaffected by further heating and no discernible reduction in droplet volume was observed.

Increased cure shrinkage when droplets were cured immediately may be indicative of evaporation of curing agent out of the droplets and appeared to show good correlation with the hypothesis that droplet properties could be significantly altered by a pre-curing stage. If it is assumed that both poorly and well-cured droplets underwent a volumetric shrinkage of around 15% due to cure shrinkage, the additional 10–20% may be attributable to loss of the curing agent and constitutes a significant deviation from initial droplet stoichiometry. Furthermore, since cure shrinkage may be reduced in off-stoichiometric formulations, loss of amine may, in fact, be even higher than the reduction in volumetric shrinkage would indicate [195]. Conversely, the droplets that were allowed to react for 24 h appeared to retard amine evaporation.

4.5 CONCLUSIONS

In this chapter, the microscale curing performance of a number of amine-cured epoxy resins and the influence of processing parameters has been investigated using micromechanical testing and thermal analysis methods. Micromechanical testing results showed that, for two commercial amine-cured epoxy systems, the degree to which these resins formed cured axisymmetric droplets suitable for microbond testing was dependent on the inclusion of a room temperature pre-curing stage. Microbond samples showed exceedingly low IFSS values (<1 MPa) when subjected to immediate heating according to the recommended macroscale curing schedule. Droplets did not appear to cure correctly and immediately deformed plastically under loading. Plastic deformation was observed in-situ using optical microscopy and post-test samples were examined using SEM. Deformation of microbond samples during testing was indicative of poor microdroplet curing and low T_g and is plausibly attributable to a stoichiometric imbalance caused by evaporation of components essential to the polymerisation reaction. Evaporation of curing agent appeared to result in insufficient amine groups necessary to produce a strongly cross-linked network structure in the droplet.

Modification of the recommended macroscale schedule was necessary to produce cured droplet samples. The inclusion of a room temperature pre-curing stage had a profound effect on apparent IFSS. A standing time of 1 h prior of elevated temperature cure was insufficient to ensure good curing and such samples showed only some tackiness while still deforming under load. A 2 h room temperature standing time was sufficient to ensure good curing and interfacial adhesion and increasing pre-curing time up to 48 h showed no further improvement. Microbond samples cured with TETA appeared unaffected by this microscale curing issue and cured successfully without the need for modification to the curing schedule. Conversely, the glass transition temperature of cured bulk matrix samples of all three resin systems were generally independent of curing cycle modification and was unaffected by immediate curing or the inclusion of a pre-curing stage.

The results of a DSC gelation study and IFSS data indicated that the standing time necessary in order to produce cured droplets was significantly lower than the gel time. Accordingly, while evaporation of volatile curing agents appears to occur in the early stages of curing, the pre-curing time necessary to prevent evaporation may be related to the much shorter time taken for each curing agent molecule to form a single intermolecular bond during the pre-gelation stage.

Evaporation of curing agent out of the microdroplets was further evidenced by a number of modifications to the curing schedule and sample preparation methodology. Post-curing

droplets at higher temperatures increased apparent IFSS to around 10.5 MPa, less than half of what was achievable with a pre-curing stage. Sub-optimal droplet properties were indicative of an irreversible amine deficiency as a result of the initial curing schedule. Increased IFSS was attributable to increased cross-linking and etherification of off-stoichiometric droplets, allowing an overall higher degree of cure and droplet T_g to be achieved. Furthermore, microbond samples prepared with double the stoichiometric amount of curing agent showed good curing performance and IFSS values indicative of high droplet T_g. Initial excess curing agent appeared to counterbalance amine evaporation effects and allowed a more balanced droplet stoichiometry to be retained following immediate elevated temperature exposure. Conversely, T_g of the bulk matrix was reduced by approximately half when samples were prepared with twice the stoichiometric amount of curing agent and cured according to the standard temperature schedule. However, neither method could be proposed as a viable solution to alleviate microscale curing issues due to irreversible vaporisation of reactive components, deviation of bulk matrix properties, and resultant IFSS being measured in a material with undefined system chemistry.

Microdroplet curing performance was generally comparable when pre-curing took place under standard or inert atmospheres. Increasing microdroplet embedded length up to approximately 700 μm without modification to the curing schedule still resulted in sub-optimal droplet properties. Poor curing may have been indicative of a critical droplet surface-to-volume ratio that could not be compensated for by increasing droplet size within an embedded length range where glass fibre/epoxy debonding is achieved before fibre fracture. Furthermore, analysis of a range of curing agent chemistries indicated that microscale curing issues were prevalent in a number of amine-cured epoxy resins and the ability to produce cured droplets according to a comparable macroscale schedule appeared limited to hardeners with lower volatility or higher functionality.

DSC was used to characterise T_g of undercured microdroplet samples using a cluster of similarly-sized droplets cured on lengths of 50 μm steel wire to increase sample mass and produce a visible step transition. It was found that four droplets (total weight less than 1 mg) were necessary to generate sufficient signal to discriminate a clear step transition. A microdroplet T_g of approximately 40°C was measured, a value around 50 to 60°C lower than that of the bulk matrix samples cured according to the same temperature schedule. Subsequent tests using clusters of 7, 10, and 20 droplets suggested that T_g was unaffected by increasing the number of droplets once sufficient sample mass had been reached to register a clear step

change. However, sample masses were still significantly lower than typical 15–20 mg DSC specimens.

In-situ monitoring of volumetric shrinkage during cure using a hot-stage microscopy method showed that droplets exposed to immediate elevated temperature curing underwent a significant volumetric reduction of around 25–30%, after which droplet volume remained consistent for the duration of the schedule. Measurement of droplets before and after a 24 h standing time showed that droplets underwent a volumetric reduction of around 15% attributable to cure shrinkage during the room temperature pre-curing stage. Afterwards, droplet size was unaffected by further heating and no discernible reduction in droplet volume was observed. Increased droplet shrinkage may have been indicative of evaporation of curing agent and constituted a significant deviation from initial droplet stoichiometry.

Interfacial testing methods are often employed to measure the influence of factors such as fibre surface treatment, application and screening of sizings, and degradation thereof. Changes in IFSS as the result of such alterations may be significantly smaller than the influence of the cure state of the matrix microdroplet. Accordingly, the route taken in creating microbond samples and the potential effect of discrepancies in microscale curing behaviour must be carefully considered. The literature review presented in this chapter, and the present work, casts reasonable doubt on the literature published on the utilisation of the microbond test in works where no apparent problem was detected or discussed. Though the testing method has been employed in conjunction with a number of different fibre and matrix materials, whether these works make successful use of the microbond test must be carefully considered. Microbond samples that undergo loss of curing agent show thermomechanical characteristics typical of off-stoichiometric compositions such as significantly reduced T_g and stiffness compared to macroscale composite specimens subjected to the same curing schedule or processing parameters. This behaviour may make microbond tests: I) poor in informing macroscale decisions regarding composite processing parameters, or II) impossible to perform due to droplet deformation such that certain matrix and curing agent combinations cannot be evaluated at the single fibre level without significant changes to the recommended cure cycle for macroscopic specimens. Unanswered questions appear to remain in regards to how much curing agent evaporation is effectively locked in place prior to partial gelation and a greater understanding of the relationship between gel point, T_g, residual stress, and interfacial shear strength in the microbond test needs to be developed.

CHAPTER 5: A NOVEL FTIR METHOD TO CHARACTERISE MICROBOND SAMPLE CURE STATE

5.1 INTRODUCTION

The microscale curing performance of two commercial epoxy resin systems was investigated in Chapter 4. It was shown that the degree to which these resins formed cured axisymmetric droplets suitable for microbond testing was influenced by the inclusion of a room temperature pre-curing stage. Immediate curing at elevated temperature resulted in the formation of under-cured soft droplets that showed plastic deformation under loading. The introduction of a protracted room temperature standing time increased the apparent interfacial shear strength substantially. The implication of this result was that micro- and macroscale samples subjected to the same curing schedule had different material properties. Namely, that microbond samples exposed to immediate elevated temperature curing were incompletely cured and had a T_g significantly lower than that of the samples that were first allowed to partially gelate. Incomplete cure was plausibly attributed to evaporation of curing agent out of the microbond samples. Conversely, the curing performance and IFSS values of DGEBA/TETA microbond samples used as a comparative control appeared to show no dependence on pre-cure standing time.

These results, combined with the review of the literature undertaken in the previous chapter showed a clear indication that there exists a need to be able to effectively monitor the degree of cure of micromechanical samples [82] and to be able to characterise droplet T_g [74]. While the issue of microdroplet curing is recognised by only a relatively small number of authors, there has been little significant development towards a method to address this fundamental concern regarding the validity of the microbond test and thermosetting epoxy matrices. As shown in the previous chapter, some measurement of undercured droplet T_g was possible using a DSC technique and cluster of similarly sized microdroplets. However, a higher throughput and more precise evaluation of the cure state of droplets subjected to a range of curing condition modifications is desirable.

The ability of micromechanical testing methods to inform macroscale materials selection and processing parameters is predicated on comparable polymer chemistry and material properties across both scales. Determination of droplet cure state would thus appear to be an essential component of any microbond investigation. It should be carefully considered that even matrix and curing agent combinations that do not appear to show excessively poor droplet curing may still have material properties significantly different from those of comparable

macroscale specimens [22,184]. In such cases, the validity of the test results may be questioned due to interfacial adhesion being assessed on an undefined system chemistry and values of interfacial shear strength may not be truly representative.

Chapter 5 details the development and implementation of a spectroscopic method to directly characterise the cure state of microbond/microdroplet samples. The method proposed enables the accurate measurement of individual microbond sample cure states using a conventional benchtop FTIR instrument without the need to employ complex thermal analysis methods [183] or model microdroplet samples as thin films [83], which may not be directly comparable. Spectra of microbond samples exposed to a range of curing and sample preparation conditions are correlated with DSC stoichiometry data to determine approximate curing agent loss and microdroplet T_g. Finally, a relationship between microdroplet cure state, T_g, and apparent IFSS is demonstrated.

5.2 LITERATURE REVIEW

5.2.1 Curing Reaction of Epoxy Resins

The term "cure" can be broadly described as a reaction in which a thermosetting resin converts from a soluble, fusible state into an insoluble and infusible state. The curing process can be subdivided into two components, namely conversion and cross-linking. Conversion involves chemical reaction during cure and is expressed as the disappearance of reactive epoxy groups. A conversion of 50% equates to the point at which 50% of the initially present epoxy groups have been depleted in the formation of a polymer. Cross-linking involves the formation of a three-dimensional network during curing. The extent of cross-linking is dependent on both the chemical reaction, the conversion, and the functionality of the compounds involved in the reaction [203].

Epoxy resin can be described as an ether containing highly active three-member rings in which two carbon atoms are connected to a single oxygen atom forming an oxirane ring (also known as an epoxy group [204]). As the ultimate properties of the epoxy polymer are largely defined by the curing process, being able to accurately monitor this process can be highly beneficial. Epoxy resin is highly reactive compared with other ethers as a result of the different electronegativities of the carbon and oxygen atoms present in the oxirane ring, rendering the carbon atom electrophilic in nature. High reactivity is predominantly related to straining of the oxirane ring and bonds surrounding the carbon atoms being forced into an unstable geometry.

Linkage between the aromatic ring and oxygen shows a higher electron withdrawing effect which attracts nucleophilic compounds, such as amines, to the oxirane group [205].

The most commonly used epoxy resin is based on diglycidyl ether of bisphenol A (DGEBA) with the oxirane rings present at either end of the chains serving as reactive sites to facilitate the cross-linking reaction. The synthesis of DGEBA typically involves the oxidation of bisphenol A and epichlorohydrin at a stoichiometric ratio. It can be cured with a wide variety of chemicals including: alcohols, amines, anhydrides, carboxylic acids, and phenols. Amines are the most commonly used hardeners and have more than three reactive sites per molecule, allowing a three-dimensional network to be formed following a reaction with epoxy resin at both ambient and elevated temperature curing. It is possible for this reaction to take place at room temperature provided the correct curing agent is chosen in order to ensure a complete reaction. The curing agent is a determining factor in the kinetics of the curing reaction which greatly influences the final performance of epoxy polymers.

In epoxy/amine systems, the curing is largely defined by three main reactions that either take place simultaneously or sequentially based on factors such as component reactivity and temperature. These reactions are the addition of both primary and secondary amines to the oxirane ring and the etherification of the epoxy group with a pendant hydroxyl group. The presence of hydroxyl functionalities, either added as accelerants or created during epoxy-amine reactions, catalyse the addition of the primary and secondary amines. This effect can contribute towards the autocatalytic nature of curing. A diagram of the epoxy/amine curing reaction is shown in *Figure 5:1* [206].

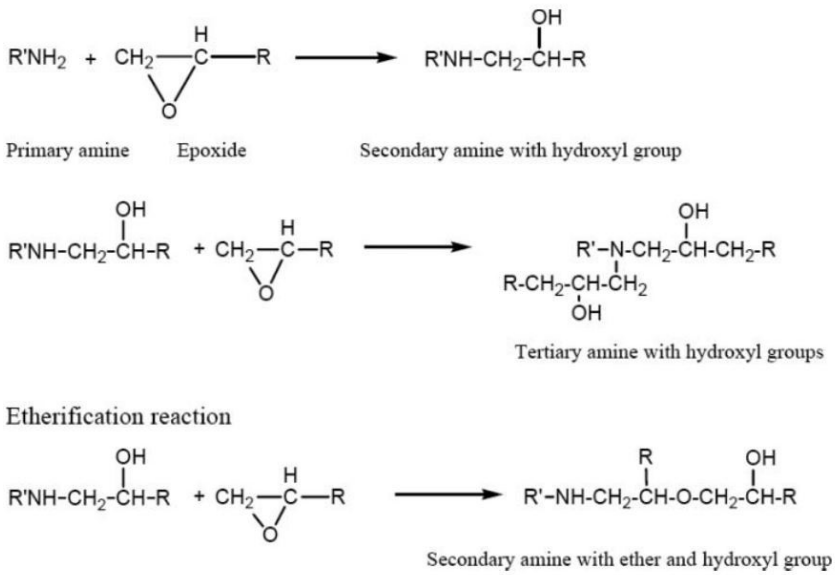

Figure 5:1: Diagram of the epoxy/amine curing reaction

The development of the polymer network in epoxy systems can be subdivided into three discrete stages. Prior to the gel point, the system is comprised of both unreacted monomer and low molecular weight oligomers. The formation of the network during the pre-gelation stage is largely governed by chemical factors as unreacted species are able to diffuse freely to reactive sites. The gel point marks the first appearance of an infinite molecular weight network. Network growth restricts diffusion of unreacted species and inhibition of diffusion increases as the sample nears vitrification [207]. During gelation viscosity is increased substantially and the material transitions from a liquid to a rubbery state. The onset of vitrification can be defined as the point at which network growth ends as the cross-linked structure prevents diffusion of unreacted species to active reaction sites. During vitrification the material transitions from a rubbery state to a glassy solid. Further reaction at elevated temperature is often required in order to facilitate further monomer conversion and achieve complete curing.

5.2.2 Fourier-Transform Infrared Spectroscopy

Background

A number of techniques can be used to monitor the curing reaction of epoxy systems and can be broadly divided into direct and indirect methods. Direct methods involve evaluation of the concentration of one or more reactive groups as a function of time and includes methods such as gel permeation chromatography [208], nuclear magnetic resonance (NMR) [209], electron paramagnetic resonance [210], Fourier-transform infrared spectroscopy [211], and Raman spectroscopy [212]. Conversely, indirect methods of analysis assess the degree of cure by monitoring a physical property correlated with reactant conversion as a function of time and includes techniques such as DSC [213]. In such methods the degree of cure is assessed by monitoring the heat released as a function of time under the assumption that it is in proportion to the rate of polymerisation. Other indirect methods of assessment include rheology [214], dielectric spectroscopy [215], ultrasound [216], and fluorescence techniques [217]. FTIR offers a number of advantages in that it allows the curing process to be monitored over the entire conversion range. Despite the fact that the material undergoes a number of state transitions during curing, these have little influence on the vibrational spectrum. By selecting appropriate absorption bands, it is possible to simultaneously monitor the concentration of various reacting components in the system.

FTIR in the mid (mIR) and near (nIR) ranges show characteristic peaks corresponding to oxirane groups and amines in the 4000–600 cm^{-1} and 7000–4000 cm^{-1} spectral ranges, respectively. The conversion of DGEBA from a liquid to a hard and infusible 3D network

during the curing process generally consists of gelation followed by vitrification. In the former stage, the nucleophile primary amine attracts the electrophilic carbon atoms. This leads to the formation of a secondary amine which leads to a tertiary amine by forming branches. Subsequent monomers added attach to the active ends of the chain and the molecular weight increases until a single molecule is formed. As a rule, the kinetics of the curing reaction involves changes in the concentration of four main species. Those being the oxirane ring and primary, secondary, and tertiary amines. Accordingly, monitoring of the degree of chemical crosslinking is achieved by observation of the concentration of one or more these species by infrared spectroscopy.

Spectroscopic Characterisation of the Epoxy/Amine Curing Reaction

Dannenberg and Harp reported on the determination of cure in thin film (approximate thickness 25 μm) samples of DGEBA epoxy resin cured with three different amines [203]. Transmittance FTIR was used to determine epoxy group content by examining the absorption band associated with the fundamental vibration of the oxirane ring at 915 cm^{-1}. As the epoxy curing reaction progressed the oxirane ring opened and the associated band reduced with increasing epoxy conversion, then disappeared entirely, resulting in a clear difference in spectra for uncured, partially cured, and fully cured samples. Epoxy content was determined using the 915 cm^{-1} oxirane absorbance band and a correction based on the intensity of phenyl group absorbance bands to account for variation in film thickness between samples. The authors concluded that the degree of conversion of epoxy samples determined by FTIR showed good correlation with results determined by a chemical analysis technique.

Cañavate *et al.* investigated the influence of epoxy:hardener ratio, temperature, and time on epoxy/IPD curing using FTIR [218]. Spectral bands at 1610 and 1508 cm^{-1} were assigned to the C=C tension vibration of benzene rings in the epoxy, the intensity of which did not vary during the curing reaction. Bands at 917 and 863 cm^{-1} were assigned to epoxy and anhydrous rings, the intensity of which decreased as the curing reaction progressed due to the opening of the epoxy ring. Reduction of epoxy peak intensity was normalised against reference signals of the benzene ring with best correlation found between 863/1508 cm^{-1} and 917/1610 cm^{-1}. Furthermore, good agreement between the results determined by both band selections was reported.

Fraga *et al.* reported on the cure kinetics of DGEBA epoxy resin cured with IPD [219] and diaminocyclohexane (DCH) [220] using FTIR. Quantitative analysis was performed by measuring the reduction of the epoxy peak at 915 cm^{-1} (also visible at 970 and 760 cm^{-1}) using the p-phenylene band at 830 cm^{-1} as an internal standard. An increase in the O-H group at 3450 cm^{-1} as curing progressed was also observed. The authors reported that degree of conversion, reaction rate, and activation energies determined by FTIR showed good correlation with those obtained using DSC. Peaks located at 915 and 3450 cm^{-1} were deemed suitable for quantitative and kinetic analysis, respectively.

Fouchal *et al.* reported on the online monitoring of the curing process of DGEBA/2,2'-dimethyl-4.4'methylenebis(cyclohexylamine) using FTIR and DSC [221]. The authors reported an increase in the broad band at 3400–3200 cm^{-1} as curing progressed, attributable to a combination of O-H and N-H groups. Degree of epoxy conversion was quantified using the disappearance of the peak at 1131 cm^{-1} related to the C-O bond of the oxirane ring present only in unreacted epoxy. The peak at 915 cm^{-1} was considered potentially unreliable due to hydroxyl vibration at the same frequency. A progressive shift in peak positon from 1131 to 1135 cm^{-1} was also observed. The C-H peak attributable to the benzene ring at 1603 cm^{-1} was used as a reference band as the intensity did not change over the course of the curing reaction. Weak peak intensity at 1131 cm^{-1} and the crowding of neighbouring peaks, however, complicated collection of reliable data [222]. DSC was used to measure T_g of epoxy samples and degree of epoxy conversion was calculated based on the reduction of residual exotherm. It was, however, noted that residual exotherm became increasing difficult to quantify at high conversion rates. Furthermore, quantification of degree of conversion by FTIR was translated to measurement of T_g using a fitting polynomial produced from DSC data. The authors concluded that comparison of degree of conversion calculated by FTIR and DSC showed good agreement (up to approximately 75% conversion) and that the area under an infrared band of a given FTIR spectrum was proportional to the number of atoms involved in the reaction

Karayannidou *et al.* investigated the cure kinetics of DGEBA-based Araldite 2020 cured with IPD using FTIR spectroscopy [223]. Samples were prepared at 20, 25, and 30 phr ratios (corresponding to 5, 25, and 58% excess curing agent) before casting thin films and curing. The oxirane ring was identified at 915 cm^{-1}. Absorptions at 3369, 3298, and 3174 cm^{-1} were attributed to the stretching vibration of the primary amino group ($N\text{-}H_2$) of the curing agent. A strong peak at 1608 cm^{-1} was similarly associated with the primary amino group. A peak at 2920 cm^{-1} was the result of the stretching vibration of $C\text{-}H_2$ groups. Ether groups of the DGEBA molecule were identified at 1250 (aromatic C-O stretching), 1038

(aliphatic C-O stretching) and 950 cm^{-1} (epoxy ether group). Bands at 1510 cm^{-1} and 833 cm^{-1} were assigned to p-phenylene groups. After curing, the intensity of epoxide (915 cm^{-1}) and primary amine (3369, 3298, 3174 cm^{-1}) groups decreased and new absorptions appeared around 3400 cm^{-1} as a result of secondary amine (N-H) and hydroxyl (O-H) group formation. Reference bands at 1510 and 833 cm^{-1} remained constant during the curing process. Epoxy group conversion (degree of cure) was calculated by peak area measurement of the oxirane ring at 915 cm^{-1} using the invariant band at 833 cm^{-1} as an internal standard. Results of quantitative measurements using 1510 and 833 cm^{-1} as reference peaks yielded approximately the same results. The authors concluded that higher degrees of cure were achieved both at higher temperatures and with increased amounts of curing agent.

Nikolic *et al.* reported on FTIR characterization of DGEBA epoxy cured with both aliphatic and cycloaliphatic polyamines [174]. Spectral bands associated with epoxy groups identified at 3056 and 915 cm^{-1} decreased as curing progressed (indicating the opening of epoxy rings) and the appearance of a peak at 1109 cm^{-1} was characteristic of C-N stretching vibrations. Further confirmation of curing was evidenced by the presence of O-H and C-N groups manifesting as a result of the cross-linking process and conversion of epoxy groups into the corresponding polymer. The authors calculated epoxy group content using the peak at 915 cm^{-1} and the C-O stretching absorption of DGEBA aromatic ring at 1182 cm^{-1} as a reference peak. A method for calculating the epoxy conversion using the peak at 3056 cm^{-1} was also presented and a subtraction procedure to remove nearby peaks was performed to improve signal clarity in both calculations.

Fu *et al*. investigated the curing process of epoxy resin and aliphatic (TEPA) and aromatic (polyamide, T-31) amine curing agents using FTIR [224]. Degree of cure was calculated using an internal standard method using the ratio of the absorbance values of the peak at 914 cm^{-1} (epoxy) and the invariant peak at 1607 cm^{-1} (benzene ring) before and after curing. The authors reported that when aromatic rings were present in the curing agent (polyamide, T-31), the 1607 cm^{-1} absorption band of the benzene ring could hinder FTIR analysis of the curing process as peak intensity appeared to increase with increased amounts of curing agent. Accordingly, a modified equation accounting for a correction was introduced. Maximum degree of cure in all three systems was between 96.98 and 98.49% when using theoretical stoichiometric amounts of curing agent and degree of cure was increased by adding excess curing agent (up to 180% of the theoretical stoichiometric value).

Li *et al.* investigated the effects of epoxy/amine stoichiometry on the structure and properties of DGEBA epoxy cured with diethanolamine (DEA) at ratios ranging from 8–20

wt.% [225]. ATR-FTIR spectra collected before and after curing showed changes in three major absorptions at 3400, 1109, and 913 cm^{-1}, corresponding to hydroxyls in hydrogen bonding states, aliphatic ether formation, and depletion of epoxy groups, respectively. Spectra were normalised against the invariant peak area at 1506 cm^{-1} as an internal standard. The absorption at 3400 cm^{-1} increased with increasing amine content and the absorption at 1109 cm^{-1} reached a maximum in 14 wt.% samples, implying the highest degree of ether linkage. Degree of cure was calculated based on the reduction of the 913 cm^{-1} peak and at 18–20 wt.% amine no epoxy signal could be detected, indicating complete cure. Conversely, amine deficient formulations showed spectra indicative of reduced epoxy conversion.

Mijović and Andjelić reported that a correction may be necessary to the standard epoxy peak at 915 cm^{-1} [226]. A new absorption in the immediate vicinity (905 cm^{-1}) of the epoxy peak emerged in the late stages (after approximately $\alpha = 0.6$) of the curing schedule. The authors posited that the new peak arose as a result of gelation and that a simultaneous increase in this well-hidden peak alongside the widely reported decrease in the epoxy/oxirane peak at 915 cm^{-1} may result in a partial overlap of the two, giving rise to an apparent false slowing and premature levelling off in the reaction. Dannenberg and Harp have reported similar concerns regarding overlap with an unknown absorption unrelated to epoxy groups in this region [203]. Escola *et al.* [227] and González *et al.*[173] have likewise reported uncertainty in using 915 cm^{-1} as a reliable peak, especially in the later stages of cure.

In their investigation of curing mechanisms and review of the literature, however, Cholake *et al.* concluded that the absorption of the oxirane ring at 915 cm^{-1} is the most reliable peak, gives the most accurate result in the medium infrared range and can be normalised with a number of different reference peaks [205]. The potential overlap in the close 905 cm^{-1} band and false levelling off could be accounted for by close inspection of the spectra and careful measurement of the peak area, or alternatively, the use of a peak height method. Alternative peaks, however, generally had lower signal intensity and other potential overlaps that may render quantitative analysis inaccurate.

5.2.3 FTIR at the Microscale

Direct spectral analysis of microbond samples is not widely reported in the literature, though there are a number of studies of note. In their critical review of the microbond test, Haaksma and Cehelnik performed FTIR microscopy on droplets of resin applied to sodium chloride plates, carbon, glass, and aramid fibres, and obtained spectroscopic results before and after curing [74]. Incomplete cure was observed in all cases and an inverse relationship between droplet size and degree of cure was shown.

Fondeur and Koenig utilised a reflection-absorption FTIR microscopy technique to study compositional differences in thin (0.4–11 μm) epoxy adhesive films [228]. Thin film samples were prepared by spin-casting dilute epoxy/dimethyl formamide (DMF) solutions onto aluminium coupons. FTIR microscopy was used to examine multiple 30 μm sections on the same sample to check for compositional differences on the same films. Unreacted epoxy was found at the surface and a reduction in carbonyl groups consistent with reduced curing agent was observed.

A study by Ash *et al.* has proposed that varying degrees of stiffness observed in polyester microbond samples and ensuing data scatter may have been attributable to evaporation of reactive components [189]. Direct FTIR analysis of the microbond samples appeared to confirm that 40-50% of the initial styrene content was lost in some samples and was a cause of inconsistent curing.

5.2.4 Conclusions of Literature Review

Through the use of infrared absorption spectroscopy, it is possible to obtain valuable information about the chemical structure and composition of epoxy polymers. The method is particularly adept in the examination of cross-linking and can be used to characterise hydroxyl and epoxy functional group conversion in polymeric materials. Changes in the concentration of species related to the curing process in the mIR range is primarily concerned with the depletion of epoxy/oxirane groups and corresponding formation of hydroxyl (O-H) and reaction with secondary amine groups (N-H). As the epoxy curing reaction progresses the oxirane ring opens and associated bands reduce in intensity and eventually disappear (indicating complete cure). Furthermore, quantitative analysis of degree of cure can be performed by measurement of the peak area of a range of characteristic epoxy group peaks normalised against an invariant reference band typically associated with a benzene ring. Finally, despite the long-standing need for a method to effectively characterise the degree of cure of microbond samples, very few studies in the literature report on methods (spectroscopic or otherwise) to assess droplet cure state and no standard testing procedure has been established. The fact that FTIR microscopy methods have been used to detect unreacted epoxy groups and evaporation of reactive components in microbond samples in published investigations would imply that spectroscopic method sensitivity is sufficient to warrant development of a reproducible novel FTIR method to coincide with micromechanical testing investigations.

Changes in spectral bands attributable to the epoxy/amine curing reaction used for the determination of degree of cure are summarised in *Table 5-1*.

Band (cm^{-1})	Assignment	Behaviour During Cure	Ref.
3600–3100	O-H of hydroxyl	Increase. Qualitative.	[220,221,223,225]
≈ 3400	N-H of secondary amine	Increase. Qualitative.	[223]
3369, 3298, 3174	N-H_2 stretching of primary amine	Decrease. Qualitative.	[223]
≈ 3056	C-H stretching of oxirane ring	Decrease. Qualitative.	[174]
2920	C-H_2 stretching	Invariant.	[223]
≈ 1608	C=C stretching of aromatic ring	Invariant reference.	[218,221,223,224]
≈ 1507	C-C stretching of aromatic ring	Invariant reference.	[218,223]
1250	C-O stretching of aromatic ring	Invariant.	[223]
1182	C-O stretching of aromatic ring	Invariant reference.	[174]
≈ 1132	C-O stretching of oxirane group	Decrease. Qualitative.	[221,222]
≈ 1100	C-N stretching/stretching of C-O-C	Increase. Qualitative.	[174,225]
1038	C-O stretching of aliphatics	Invariant.	[223]
970	Epoxy group	Decrease. Qualitative.	[220]
950	Epoxy ether group	Invariant.	[223]
≈ 915	C-O stretching of oxirane group	Decrease. Quantitative.	[203,218,220,224,225]
905	Related to gelation	Increase. Overlap.	[205,226]
863	C-O-C stretching of oxirane group	Decrease. Qualitative.	[218]
830	C-O-C of oxirane ring/aromatic ring	Invariant reference.	[220,223]
760	Epoxy group	Decrease. Qualitative.	[220]

Table 5-1: FTIR band assignments for the epoxy/amine curing reaction

5.3 EXPERIMENTAL

5.3.1 Materials

Glass Fibres

In order to minimise the complexity of the interface, experiments were conducted using bare (water-sized) E-glass fibres taken from larger rovings supplied by Owens Corning. For Fourier-transform infrared spectroscopy (FTIR) measurements of microbond samples, glass fibres were replaced with annealed AISI 302 steel wire of diameter 50 μm to improve signal clarity due to consistent and controllable increased microdroplet size. Signal strength may also have been improved by a favourable mirroring effect related to the reflective steel surface. Steel wire was purchased from Goodfellow.

Epoxy Resin

Two multiple-component commercial resin systems designed for use in wind turbine blade applications were selected for investigation. Epotec YD-535 LV was cured with Epotec TH7257 hardener at a stoichiometric ratio 35 phr. Olin Airstone 780E was cured with Olin Airstone 785H hardener at a stoichiometric ratio of 31 phr as per the manufacturers recommendation. Both resin systems were supplied by the project industrial partner Suzlon.

DER 332 DGEBA epoxy resin was cured with a stoichiometric (14.3 phr) amount of TETA tetrafunctional amine curing agent (technical grade 60%) and used as a comparative control based on its ability to cure consistently at the microscale. IPD is a key component amine of both the Epotec and Olin curing agents. Accordingly, 332 epoxy resin was also cured with a stoichiometric (25 phr) amount of IPD. Resin and curing agents were purchased from Sigma Aldrich/Merck.

5.3.2 Differential Scanning Calorimetry

Determination of Off-Stoichiometric Matrix T_g

Off-stoichiometric cured matrix formulations were used to model increasing loss of curing agent by evaporation in microdroplet specimens. Samples were prepared by measuring and mixing pre-calculated ratios of epoxy resin and curing agent at the stoichiometric ratio (R=1) and 10% decrements in curing agent up to a maximum reduction of 80% (R=0.2). The mixed resin was then degassed for 10 min and approximately 20 mg syringed into an open aluminium pan before curing in an oven at the appropriate temperature schedule. Epotec, Olin, and 332-IPD samples were cured at 65°C for 3.5 h followed by 75°C for 7 h. The curing schedule was selected to coincide with the curing schedule used in the production of macroscale composite parts. 332-TETA samples were cured at 60°C for 1 h followed by 120°C for 2 h. Samples were allowed to cool overnight then removed from the oven and tested the following day. DSC was performed to determine T_g of off-stoichiometric cured matrix formulations according to ASTM standard E1356-08 *Standard Test Method for Assignment of the Glass Transition Temperatures by Differential Scanning Calorimetry* using a TA Instruments Q20 DSC and corresponding RCS90 cooling system. Tests were performed under inert nitrogen atmosphere with purge gas flow rate of 50 mL/min. Data were analysed using TA Universal Analysis software and T_g was estimated from the midpoint of step transitions.

5.3.3 Fourier-Transform Infrared Spectroscopy

Fourier-transform infrared spectroscopy was used to characterise the degree of epoxy conversion of bulk cured matrix samples with variable curing agent content and microbond samples subjected to a range of curing schedules. Analysis was performed using a 4100 ExoScan FTIR fitted with a spherical diamond attenuated total reflectance (ATR) interface, adjustable probe and benchtop docking station. Background signal was measured after each spectra and the crystal was cleaned with acetone between measurements. Analysis was performed in the 4000 to 650 cm^{-1} range with a spectral resolution of 8 cm^{-1} and 64 scans per sample. OriginPro software was used to process spectral data and plot normalised average spectra. SpectraGryph software was used for peak identification and quantitative analysis.

Determination of Off-Stoichiometric Matrix Degree of Conversion

Off-stoichiometric cured matrix formulations were prepared by measuring and mixing pre-calculated ratios of epoxy resin and curing agent at the stoichiometric ratio (R =1) and 10% decrements in curing agent up to a maximum reduction of 80% (R=0.2). After mixing and degassing, samples were syringed onto a section of composite release film to allow for easy removal. In each case, two drops were applied in order to maintain a consistent sample size. Samples were cured according to the appropriate temperature schedule and allowed to cool overnight before being removed from the oven. At low curing agent contents, undercured gel-state samples were too tacky to be removed from the release film. In these cases, a scalpel was used to cut around the resin and the sample was inverted before clamping in place. The low penetration depth (around 0.5–2 μm) of the ATR instrument ensured that spectra related to the release film material were not present. Nevertheless, spectra of the film were collected and compared to verify that additional bands unrelated to the epoxy/amine curing reaction were not produced as artefacts. Due to consistent reproducibility of the spectra, results were plotted as a normalised average of approximately ten samples.

Determination of Microbond Specimen Degree of Conversion

Glass fibres were substituted by lengths of 50 μm diameter steel wire to produce larger droplets of consistent dimensions. Steel wire was considered an appropriate substitution for glass fibres based on microbond data reported in 4.4.1. It was confirmed that microbond curing issues were prevalent across both glass fibre ($L_e \approx 120$ μm) and steel wire ($L_e \approx 380$ μm) samples to verify that a dimensional effect alone was not responsible for discrepancies in curing behaviour. Furthermore, the use of steel wire allowed for accurate application of a single droplet per

sample by preventing the applied droplet splitting into multiple smaller droplets as was observed with deposition onto glass or carbon filaments. Signal strength when collecting spectra was improved both by the use of a larger droplet and a reflectance effect of the steel wire, allowing for conventional FTIR apparatus to be used in the analysis of microscale samples. Lengths of steel wire were applied to a card mounting template containing numbered sample tabs with 10 mm gauge length windows cut out. FTIR microdroplet samples were prepared, applied, and cured alongside corresponding unsized glass fibre microbond samples used for interfacial testing. Samples were either cured immediately or allowed to partially gelate by pre-curing at room temperature for 0 to 48 h before curing. Cutting the surrounding card to retain a holding tab while leaving the steel wire attached allowed individual droplets to be positioned on the ATR interface of the apparatus and the probe was fully lowered to ensure maximum contact with the sample. Spectral results were plotted as a normalised average of thirty independent samples for each data set. The FTIR microbond sample preparation methodology and experimental configuration is illustrated in *Figure 5:2* and *Figure 5:3*, respectively. A typical optical micrograph of a steel wire-mounted epoxy droplet at 100x magnification is also shown in *Figure 5:3*.

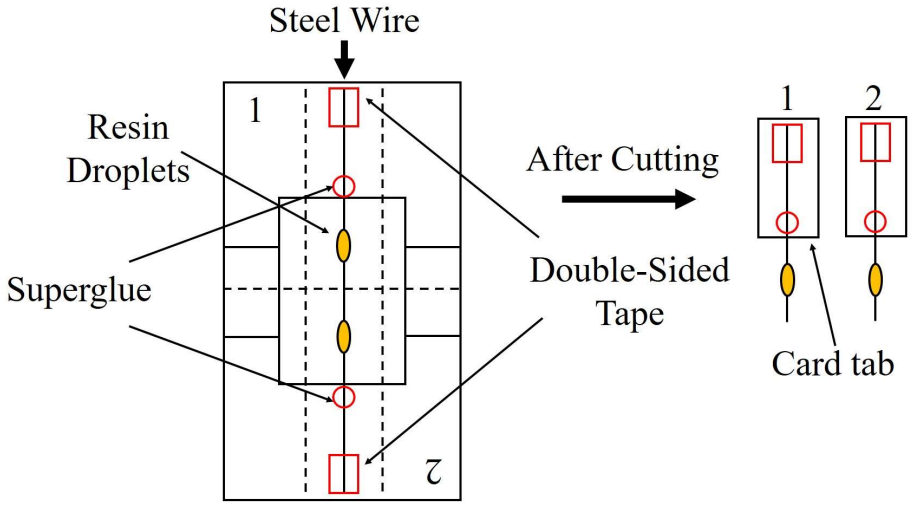

Figure 5:2: FTIR microbond sample preparation schematic diagram

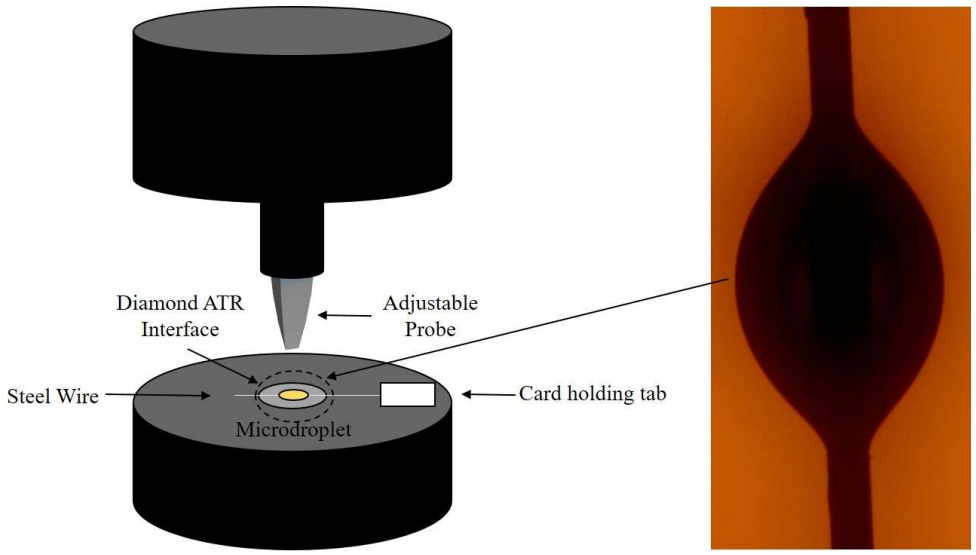

Figure 5:3: Schematic diagram of microbond ATR-FTIR experimental configuration

Calculation of Degree of Epoxy Conversion

The Beer-Lambert law relates absorbance (A), absorptivity (a), sample thickness (d), and concentration of absorbing species (c) according to *Eq. 5-1* [221,229].

$$A = adc \qquad \text{(Eq. 5-1)}$$

As a result of the relationship between concentration and absorbance, the extent of epoxy conversion can thus be determined from FTIR spectra. The fractional conversion of epoxy groups (α) is expressed by *Eq. 5-2*.

$$\alpha = 1 - \frac{A_{t=t}}{A_{t=0}} \qquad \text{(Eq. 5-2)}$$

To account for a non-zero baseline absorbance in experimental spectra, a reference band is introduced. The use of a reference band also accounts for variations in sample thickness and peak integration errors related to cure shrinkage and the initial thermosetting reaction [205]. Fractional degree of epoxy conversion is expressed by *Eq. 5-3*. Where α is the degree of epoxy conversion (degree of cure), A is the absorbance peak area, and the subscripts "0" and "t" denote zero (unreacted epoxy monomer) and reaction time t (cured sample), respectively. The subscripts "epoxy" and "ref" are used to denote characteristic epoxy and reference peaks, respectively.

$$\alpha = 1 - \frac{(A_{epoxy}/A_{ref})_t}{(A_{epoxy}/A_{ref})_0} \qquad \text{(Eq. 5-3)}$$

It is therefore possible to determine the extent of cure by measuring the peak area indicative of unreacted epoxy groups at 915 cm^{-1} in relation to an invariant reference band that is not involved in the epoxy/amine curing reaction, such as that of the benzene ring located at 1507 cm^{-1} [218]. Further suitable analytical peaks (related to the oxirane ring) to monitor the epoxy/amine curing reaction are located at approximately 3056 [230], 1131 [221], 970 [231] and 861 cm^{-1} [218]. Additional invariant reference peaks are located at approximately 1607 [221] and 833 cm^{-1} [223]. Degree of cure/monomer conversion was quantified using the reduction of the area of the oxirane/epoxy group at 915 cm^{-1} against the invariant peak at 1507 cm^{-1} (C=C stretching) as an internal standard as expressed in *Eq. 5*-4. Peaks were selected due to stronger relative signal intensities compared to other analytical and reference peaks, making consistent peak area measurements easier. Absorbance peak areas were calculated using a baseline integration function between the values of 927–893 cm^{-1} and 1526–1489 cm^{-1}. Manual adjustments were performed to account for minor peak shifting effects.

$$\alpha = 1 - \frac{(A_{915}/A_{1507})_t}{(A_{915}/A_{1507})_0} \qquad \text{(Eq. 5-4)}$$

5.4 RESULTS AND DISCUSSION

5.4.1 Characterisation of Epoxy/Amine Curing Reaction

FTIR was used to determine the characteristic spectral changes associated with the epoxy/amine curing reaction of four epoxy resin systems. FTIR spectra of unreacted and fully cured Epotec, Olin, 332-TETA, and 332-IPD resins are shown in *Figure 5:4*, *Figure 5:5*, *Figure 5:6*, and *Figure 5:7*, respectively. Unreacted resin spectra were collected before the curing agent was added.

Changes in the concentration of species related to the curing process in the mIR range are primarily concerned with the depletion of epoxy groups related to the oxirane ring and the corresponding formation of hydroxyl (O-H) groups. As the epoxy curing reaction progresses the oxirane ring opens and associated bands reduce in intensity and eventually disappear (indicating complete cure) [218]. Furthermore, direct spectral characterisation of the concurrent changes relating to primary, secondary, or tertiary amines is generally not accurate in the mIR range due to overlap with the broad hydroxyl band. Characteristic isolated amine bands are only visible in the nIR range at 6535 and 4623 cm^{-1} [205].

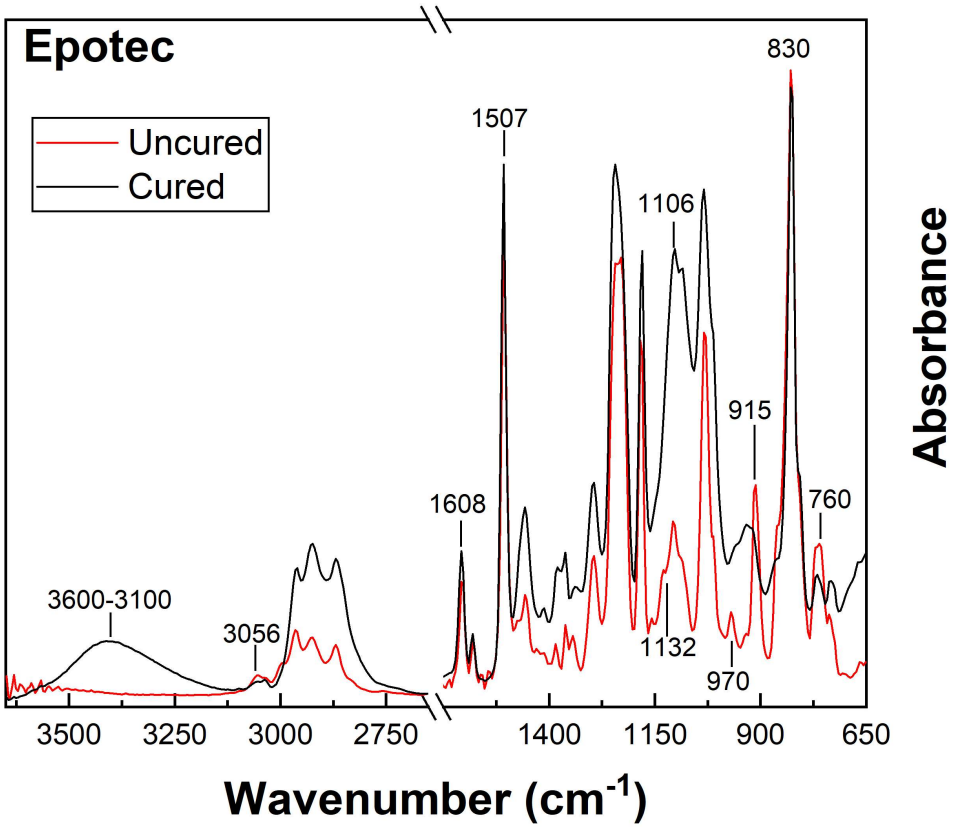

Figure 5:4: FTIR spectra of Epotec epoxy/amine curing reaction

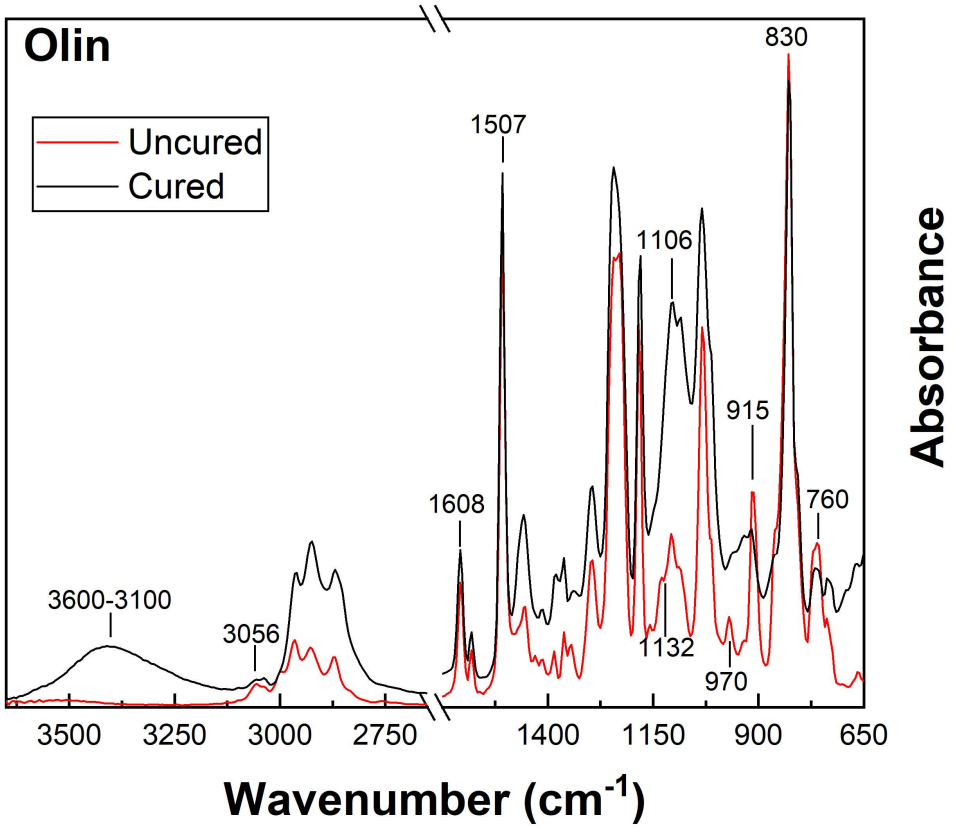

Figure 5:5: FTIR spectra of Olin epoxy/amine curing reaction

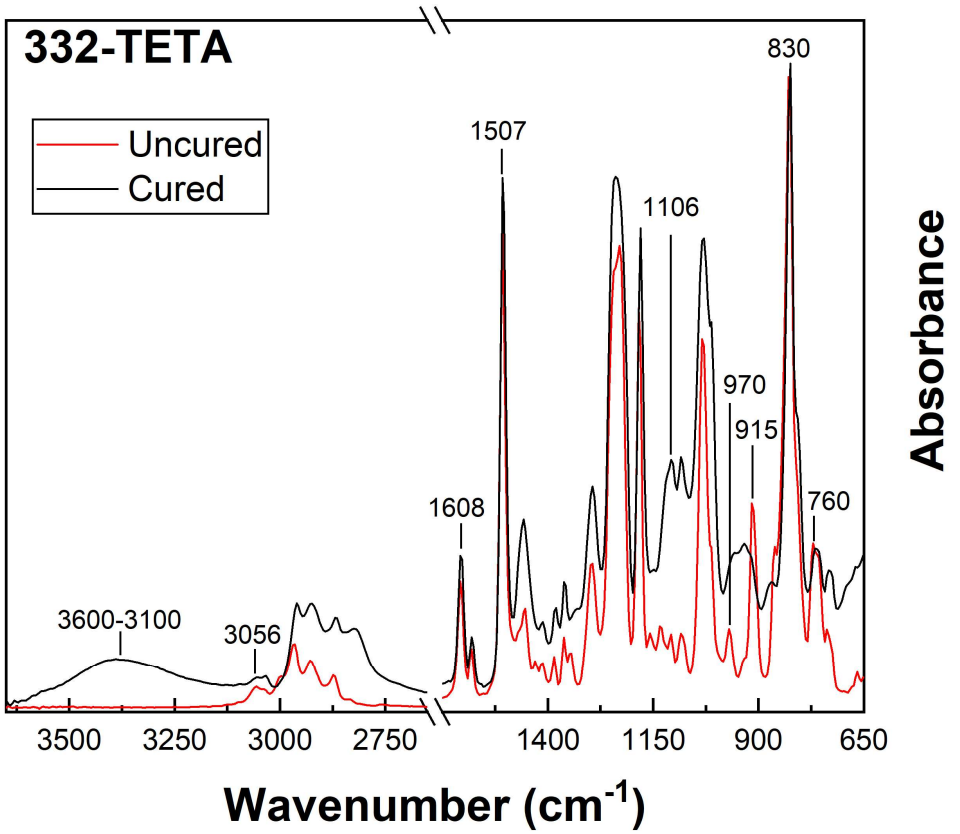

Figure 5:6: FTIR spectra of 332-TETA epoxy/amine curing reaction

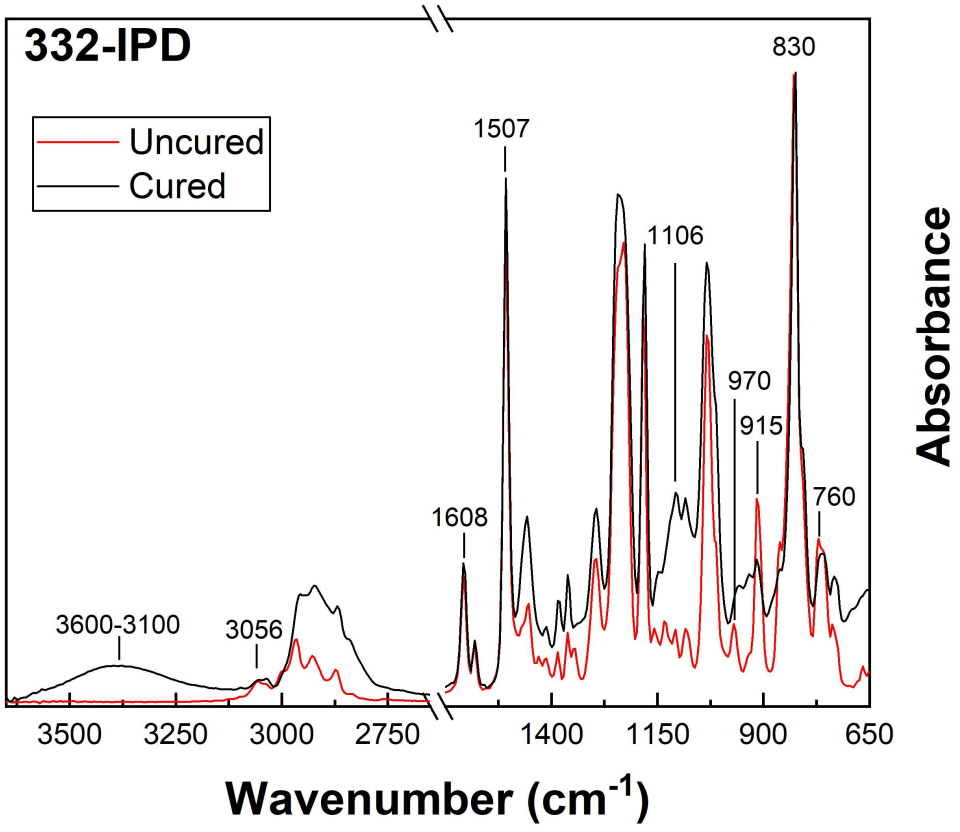

Figure 5:7: FTIR spectra of 332-IPD epoxy/amine curing reaction

An apparent baseline shifting effect between uncured and cured may be attributable to variability in sample point of contact with the diamond ATR interface. Uncured resin spreads more easily and may establish better contact than the approximately 20 mg cured samples despite the use of an adjustable sample probe. The increase in the broad band between 3600–3100 cm^{-1} is assigned to hydroxyl group accumulation [221]. Development of the hydroxyl band can be considered a qualitative indicator of extent of reaction, though use in quantitative analysis is limited as a result of the shape (clear boundaries are difficult to establish in broader peaks) and the presence of overlapping bands. Band growth in the overlapping region around 3300 cm^{-1} is also attributable to the formation of secondary amine groups [221,223].

A small peak located at approximately 3056 cm^{-1} is attributable to the C-H stretching of the oxirane ring [174]. Peaks located at 970, 915, 863, and 760 cm^{-1} are similarly assigned to epoxy groups related to vibrations of the oxirane ring [220]. Bands at 1608 and 1507 cm^{-1} are attributable to C=C and C-C stretching of the aromatic (benzene) ring, respectively [205]. The peak at 830 cm^{-1} is likewise assigned to vibration of the aromatic ring and C-O-C of the oxirane ring [173,174]. Clear overlap in the spectra related to the benzene ring confirmed that peak intensities were unaffected by the epoxy/amine curing reaction and were suitable invariant reference peaks. The shoulder peak at 1132 cm^{-1} is assigned to the C-O bond of the oxirane ring, which disappeared after curing [221].

A peak at around 1106 cm^{-1} became apparent following cure. The appearance of this peak is attributable to the crosslinking process and conversion of epoxy groups in a polymer [232]. Nikolic *et al.* have attributed the appearance of a similar peak at 1109 cm^{-1} to C-N stretching vibrations [174]. Li *et al.* have attributed increased intensity in this region to formation of aliphatic ethers and reported that it was maximised at the highest degree of cure [225]. The 332 epoxy resin cured with TETA and IPD showed comparatively lower signal intensity in the 1106 cm^{-1} region compared to cured Epotec and Olin resins. This behaviour is likely attributed to the absence of a reactive diluent present in the other resins. Increased peak intensity attributable to the diluent is apparent in the Epotec/Olin unreacted resin monomers. Furthermore, an additional shoulder peak around 2815 cm^{-1} assigned to $O\text{-}CH_3$ became visible in cured 332-TETA samples. The appearance of this peak may have been related to surface oxidation due to the higher curing temperature used to cure these specimens.

Degree of cure was calculated according to *Eq. 5-4*. Bands at 915 and 1507 cm^{-1} were selected as analytical and reference peaks, respectively, due to relative separation from neighbouring peaks higher signal intensity enabling accurate peak area measurements. Good agreement was found using either 1608 or 1507 cm^{-1} as an internal standard, however. Further

qualitative indicators of complete cure were reduced peak intensity of signals corresponding to epoxy groups located at 3056 [174], 1132 [221], 970 [231], 863 [218], and 760 cm^{-1} [220].

Degree of conversion of cured samples was 0.88–0.93 for the Epotec and Olin resins. Maximum degree of conversion was observed in 332-TETA samples (0.95), possibly due to a combination of increased curing agent functionality and higher curing temperature. Degree of cure was lowest in 332-IPD samples (0.83). It is possible that the use of the Epotec/Olin curing schedule did not produce complete cure in the 332-IPD samples, evidenced by lower degree of conversion and reduced hydroxyl band intensity, due to lower curing temperatures compared to cured matrix T_g.

Full conversion of epoxy groups to hydroxyl groups should result in the complete disappearance of the band at 915 cm^{-1}. While significant reductions in this peak area were observed as the curing reaction progressed, all cured spectra appeared to show a small residual hump at 915 cm^{-1}, indicating an immeasurable fraction of unreacted epoxy. Meyer *et al.* have suggested that topological constraints in highly crosslinked networks may render a small fraction of the epoxy groups inaccessible during the final stages of the curing process [233]. Similarly, Carothers proposed that due to the availability of the six bonding sites on the TETA molecule, oxirane/amine groups are not completely consumed during cure [234]. A small amount of unreacted amine and oxirane groups may remain within the epoxy network following even extensive post-curing.

Alternatively, this behaviour may also arise as a result of spectra in the mid-range providing an underestimation of cure state [235]. Mijović and Andjelić reported the emergence of a new absorbance peak at 905 cm^{-1} as a result of gelation [226]. Simultaneous increase in this peak alongside the decrease in the epoxy/oxirane peak at 915 cm^{-1} may result in a partial overlap of the two, giving rise to an apparent false slowing and premature levelling off in the reaction. Dannenberg and Harp have reported similar concerns regarding overlap with an unknown absorption unrelated to epoxy groups [203].

Band assignments associated with the epoxy/amine curing reaction are summarised in *Table 5-2*.

Band (cm^{-1})	Assignment	Behaviour During Cure
3600–3100	O-H of hydroxyl/N-H of secondary amine	Increase. Qualitative.
3056	C-H stretching of oxirane ring	Decrease. Qualitative.
1608	C=C stretching of aromatic ring	Invariant reference.
1507	C-C stretching of aromatic ring	Invariant reference.
1132	C-O stretching of oxirane group	Decrease. Qualitative.
1100	C-N stretching/stretching of C-O-C ethers	Increase. Qualitative.
970	Epoxy group	Decrease. Qualitative.
915	C-O stretching of oxirane group	Decrease. Quantitative.
863	C-O-C stretching of oxirane group	Decrease. Qualitative.
830	C-O-C of oxirane ring/aromatic ring	Invariant reference.
760	Epoxy group	Decrease. Qualitative.

Table 5-2: Epoxy/amine curing reaction band assignment

5.4.2 Relationship Between Stoichiometry, Degree of Conversion, and T_g

Off-stoichiometric formulations were used to model the proposed loss of curing agent by evaporation and FTIR and DSC were used to characterise the ensuing effect on degree of cure and T_g, respectively. FTIR spectra of unreacted, off-stoichiometric, and fully cured Epotec, Olin, 332-TETA, and 332-IPD resins are shown in *Figure 5:8*, *Figure 5:9*, *Figure 5:10*, and *Figure 5:11*, respectively. The relative extent of epoxy conversion of off-stoichiometric matrix formulations was monitored by the reduction of epoxy peak at 915 cm^{-1}. The accumulation of hydroxyl groups, produced from the reaction of epoxy groups, was monitored using the broad band at 3600–3100 cm^{-1}. Spectra of off-stoichiometric formulations with reduced amine content showed increased intensity in peaks attributable to unreacted epoxy groups (3056, 970, 915, 863 cm^{-1}). Reduced hydroxyl/N-H group accumulation, and a weaker etherification peak were also observed. Degree of cure in off-stoichiometric samples was thus lowered as curing agent was reduced.

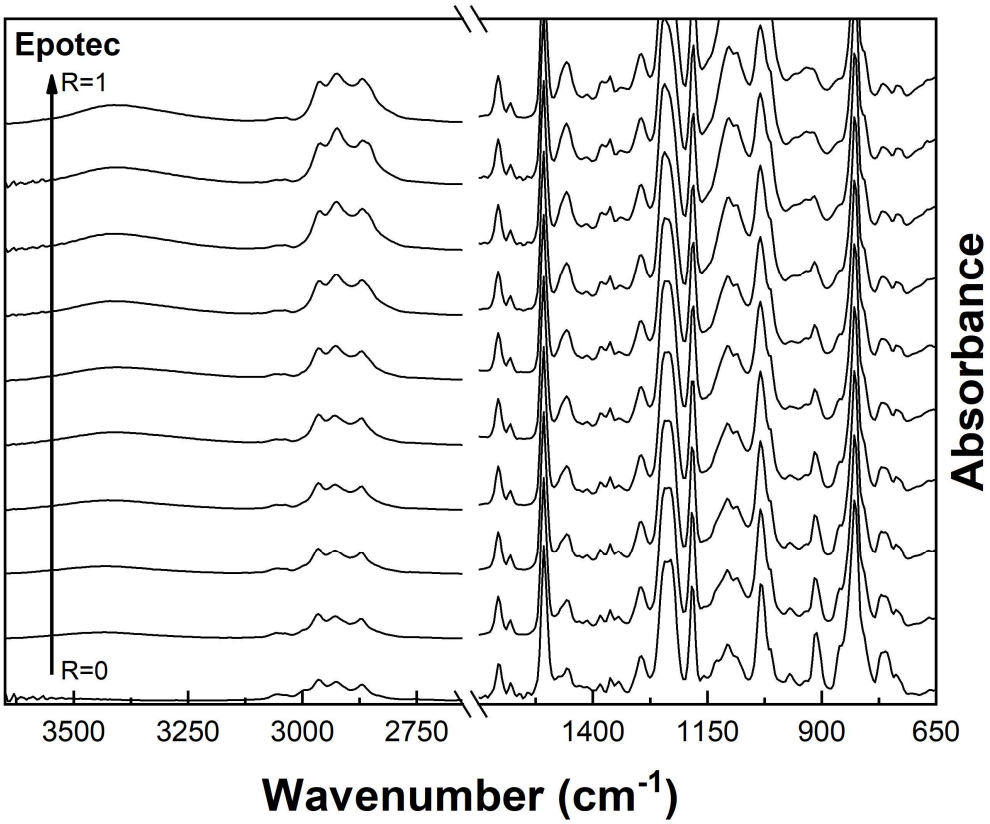

Figure 5:8: FTIR spectra of Epotec stoichiometry study

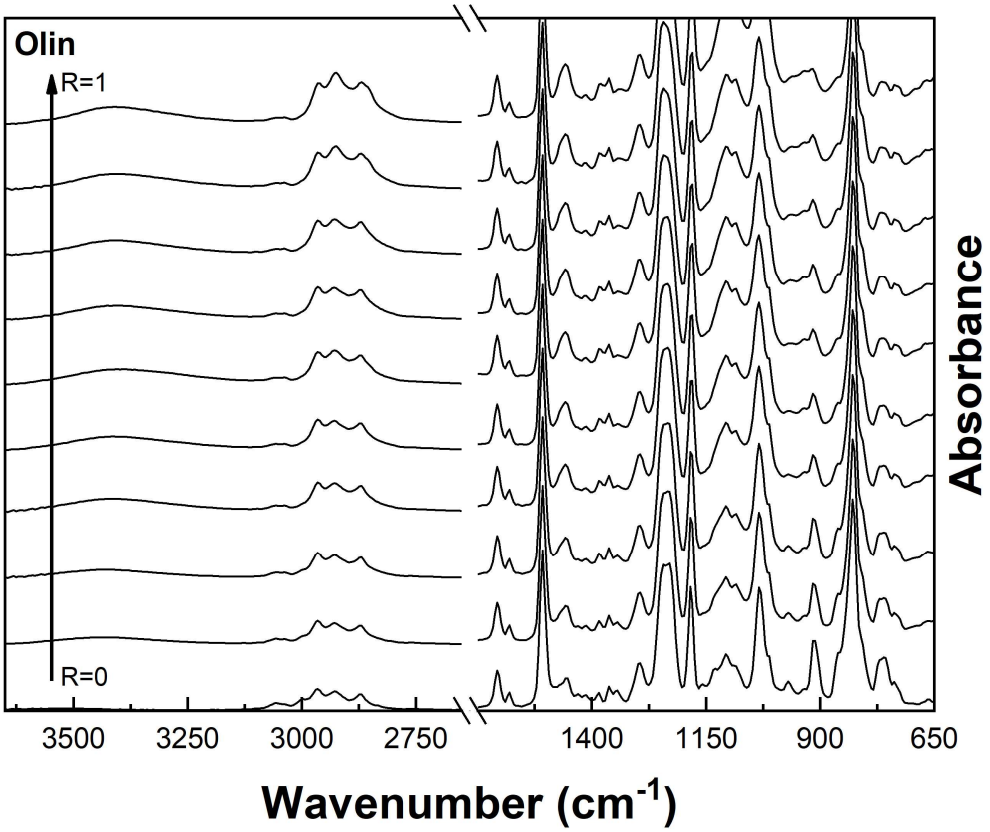

Figure 5:9: FTIR spectra of Olin stoichiometry study

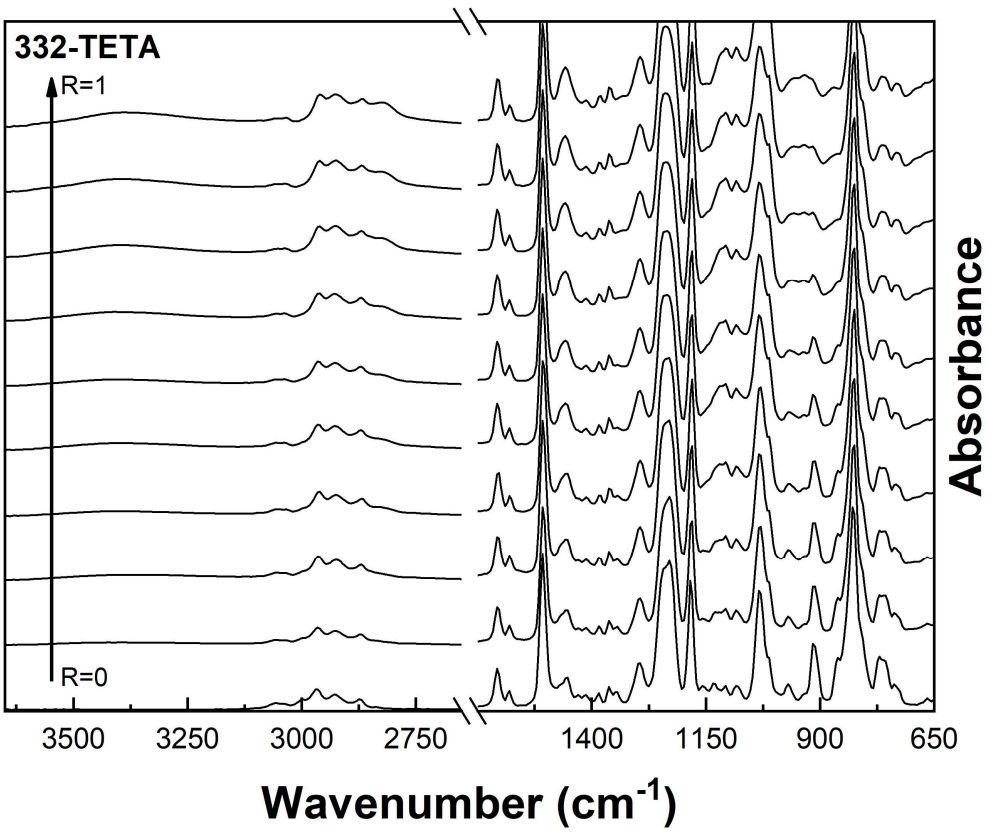

Figure 5:10: FTIR spectra of 332-TETA stoichiometry study

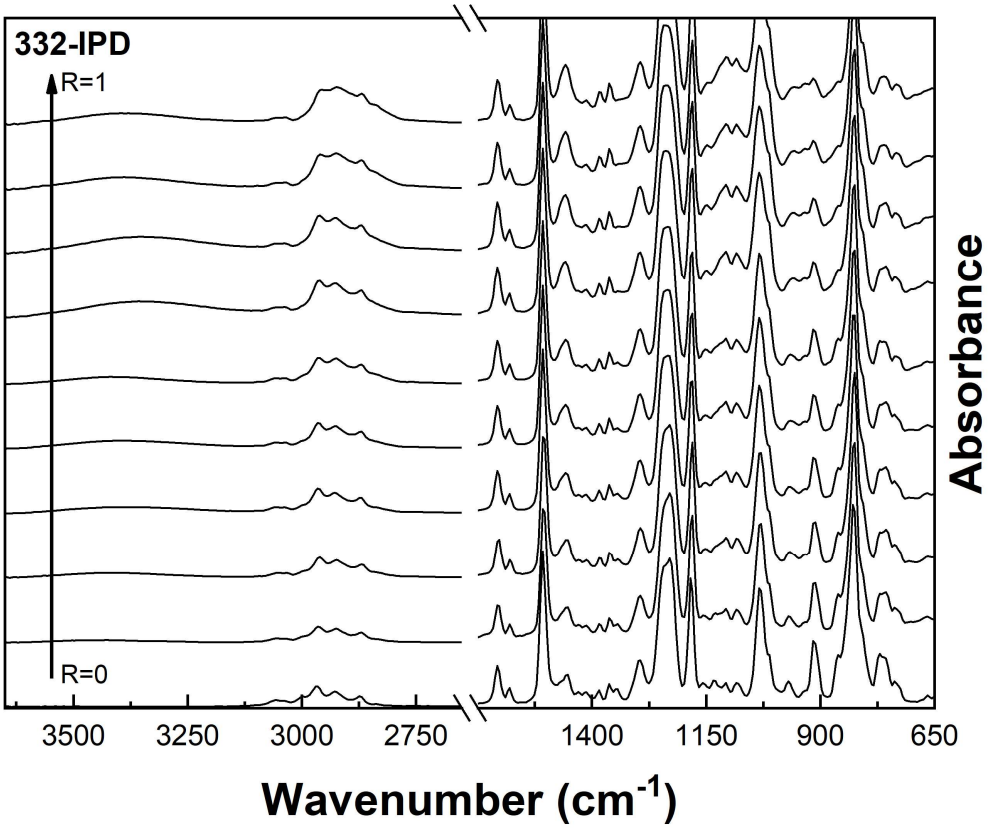

Figure 5:11: FTIR spectra of 332-IPD stoichiometry study

Comparison of FTIR degree of conversion and DSC T_g measurements are shown in *Figure 5:*12. DSC results showed that glass transition temperature was highest at the stoichiometric ratio and decreased with reduced amine content. T_g of the epoxy/amine systems investigated was strongly influenced by the cure state of the matrix. Epotec and Olin resin systems, that were shown to be susceptible to curing agent loss at the microscale, had initial stoichiometric T_g values of approximately 87°C and 80°C, respectively. Conversely, 332-TETA and 332-IPD samples had significantly higher stoichiometric T_g values of 124°C and 159°C, respectively. Higher T_g was likely due to the absence of a reactive diluent in these two resin systems.

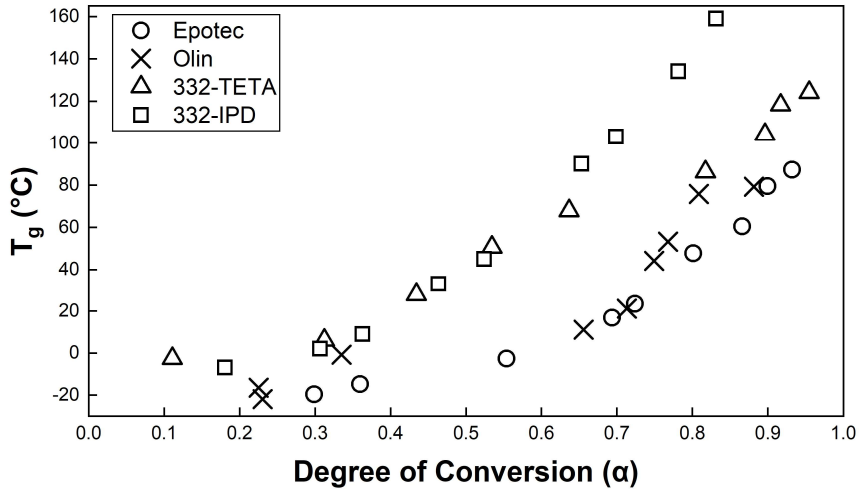

Figure 5:12: Degree of conversion (α) versus glass transition temperature (T_g)

The results of the FTIR and DSC stoichiometry study are summarised in *Table 5-3*.

		FTIR α				DSC T_g (°C)			
CA Reduction	**R (amine/epoxy)**	**Epotec**	**Olin**	**332-TETA**	**332-IPD**	**Epotec**	**Olin**	**332-TETA**	**332-IPD**
0	1	0.93	0.88	0.95	0.83	87	79	124	159
10%	0.9	0.90	0.81	0.92	0.78	80	76	118	134
20%	0.8	0.87	0.77	0.90	0.70	61	53	104	103
30%	0.7	0.80	0.75	0.82	0.65	48	44	86	90
40%	0.6	0.72	0.71	0.64	0.52	24	21	68	45
50%	0.5	0.69	0.66	0.53	0.46	17	11	51	33
60%	0.4	0.55	0.34	0.43	0.36	-3	-1	28	9
70%	0.3	0.36	0.23	0.31	0.31	-15	-16	6	2
80%	0.2	0.30	0.23	0.11	0.18	-20	-22	-3	-7

Table 5-3: Summary of FTIR (α) and DSC (T_g) stoichiometry study

Microbond data presented in Chapter 4 plausibly attributed the inability to measure IFSS in immediately cured microbond samples to evaporation of curing agent out of the droplets. Furthermore, plastic deformation of samples under applied load would suggest that any curing agent loss would have to be sufficient to induce a sub-ambient microdroplet T_g. DSC results showed that in the Epotec and Olin resin systems, a curing agent reduction of 40% was sufficient to reduce matrix T_g to a value approximating room temperature. It can be proposed that such a reduction in amine content in microbond samples would correspond to the plastic behaviour observed during microbond testing of these systems. Rao *et al.* have proposed a similar loss of curing agent in the range of 40% in a TMA study of epoxy/m-PDA microbond samples [183]. Curing agent loss corresponded to a reduction of some 60°C in microdroplet T_g.

In the 332-TETA system, where microscale curing was consistent regardless of pre-cure standing time, it is important to note that a loss of 40% of the initial curing agent had a significantly less detrimental effect. While T_g was markedly reduced from an ideal stoichiometric value of 136°C to 68°C, a loss of more than 60% of the curing agent was necessary to induce a sub-ambient T_g. Comparison with 332-IPD data indicates that a high initial T_g is not the only parameter involved in successful microdroplet curing. Despite highest initial T_g, 332-IPD microbond tests were unsuccessful. Curing agent loss of more than 50% would thus be needed to produce sub-ambient T_g in these specimens.

It would seem possible to suggest that the ability to produce well-cured microbond samples suitable for testing (without modification to sample preparation methodology) may be related to both initial stoichiometric T_g and the ability of the matrix material to retain moderately high T_g following a loss of 40% (or more) of the curing agent by evaporation during cure. Such a result would imply that instead of solely investigating which resin and hardener combinations are susceptible to microbond curing issues, any microbond investigation should involve a commensurate study of the off-stoichiometric properties of the matrix material and some form of direct assessment of the droplet cure state.

5.4.3 Effect of Pre-Cure Standing Time

Evaluation of Microbond Sample Cure State

Microbond testing results showed that it was not possible to measure the IFSS of Epotec/Olin droplets when samples were cured immediately. A pre-cure standing time of 2 h was sufficient to ensure good curing, after which IFSS was relatively constant up to pre-curing times of 48 h. FTIR was used to assess the cure state of microbond samples cured after varying lengths of pre-cure standing time. FTIR spectra of Epotec, Olin, and 332-TETA microbond samples cured immediately and with pre-cure standing times are shown in *Figure 5:13, Figure 5:14*, and *Figure 5:15* respectively.

Spectra were plotted as a normalised average of thirty microbond specimens in order to match the number of samples in the corresponding microbond test data set. Furthermore, examining a larger number of samples accounted for sample to sample variation not typically observed in the spectra of bulk scale samples. Degree of cure/monomer conversion (α) was quantified using the reduction of the area of the oxirane/epoxy group at 915 cm^{-1} against the invariant peak at 1507 cm^{-1} as an internal standard. Microdroplet degree of cure was collated to off-stoichiometric data in *Table 5-3* to estimate loss of curing agent and microdroplet T_g.

Epotec and Olin microbond samples cured immediately and with a standing time of only 1 h clearly showed unreacted epoxy groups (as indicated by increased peak intensity at 970, 915, 863, and 760 cm^{-1}), reduced hydroxyl and secondary amine group accumulation (3600–3100 cm^{-1}) and a weaker etherification peak (1106 cm^{-1}), commensurate with spectra indicating an off-stoichiometric matrix formulation. Accordingly, droplet spectra would appear to lend significant credence to the hypothesis that reduced curing and poor IFSS in these samples is attributable to a loss in curing agent.

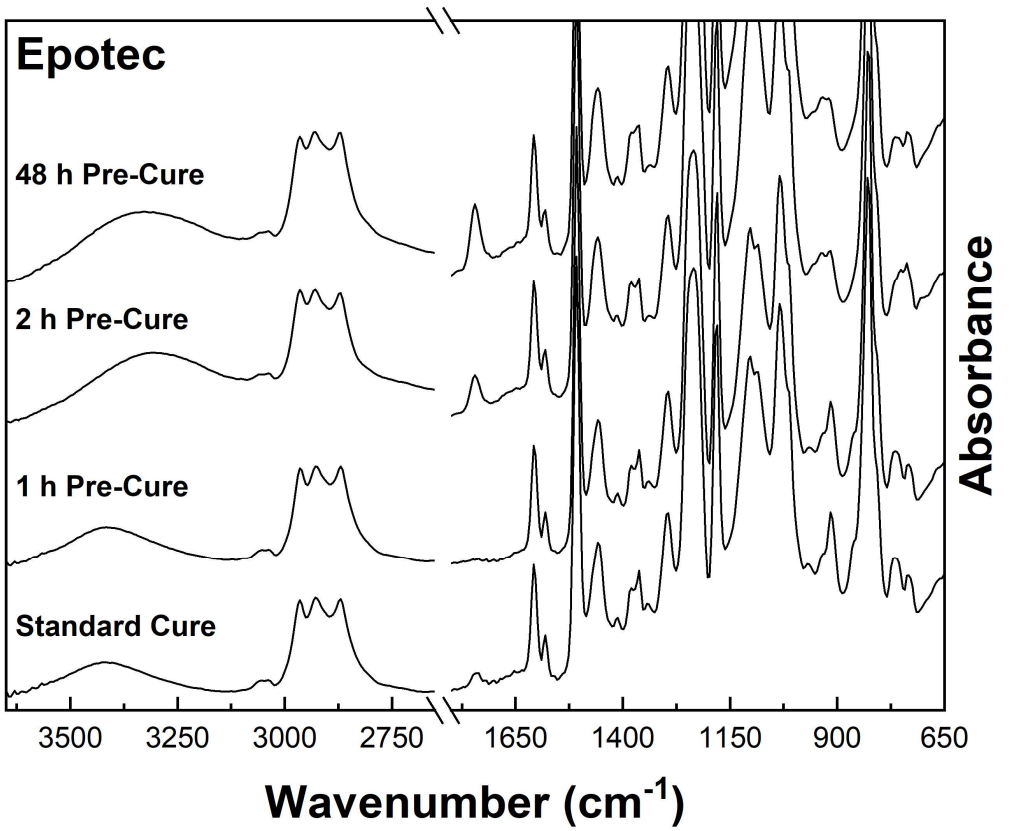

Figure 5:13: FTIR spectra of Epotec microbond samples with 0–48 h pre-cure

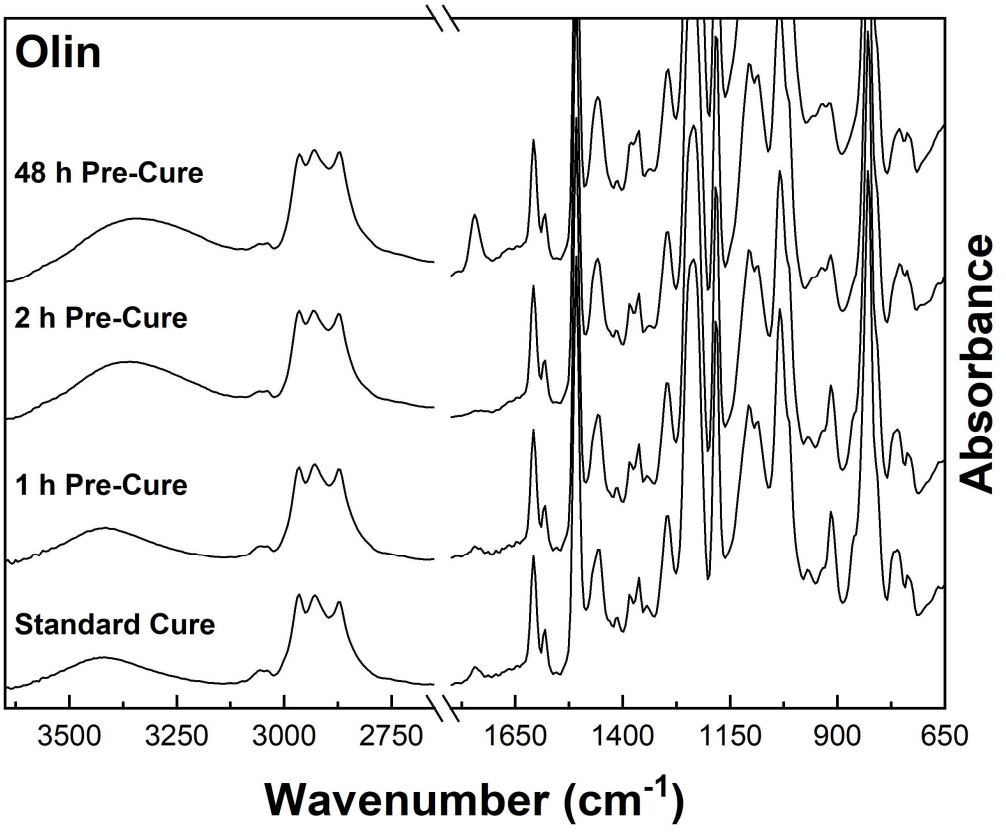

Figure 5:14: FTIR spectra of Olin microbond samples with 0–48 h pre-cure

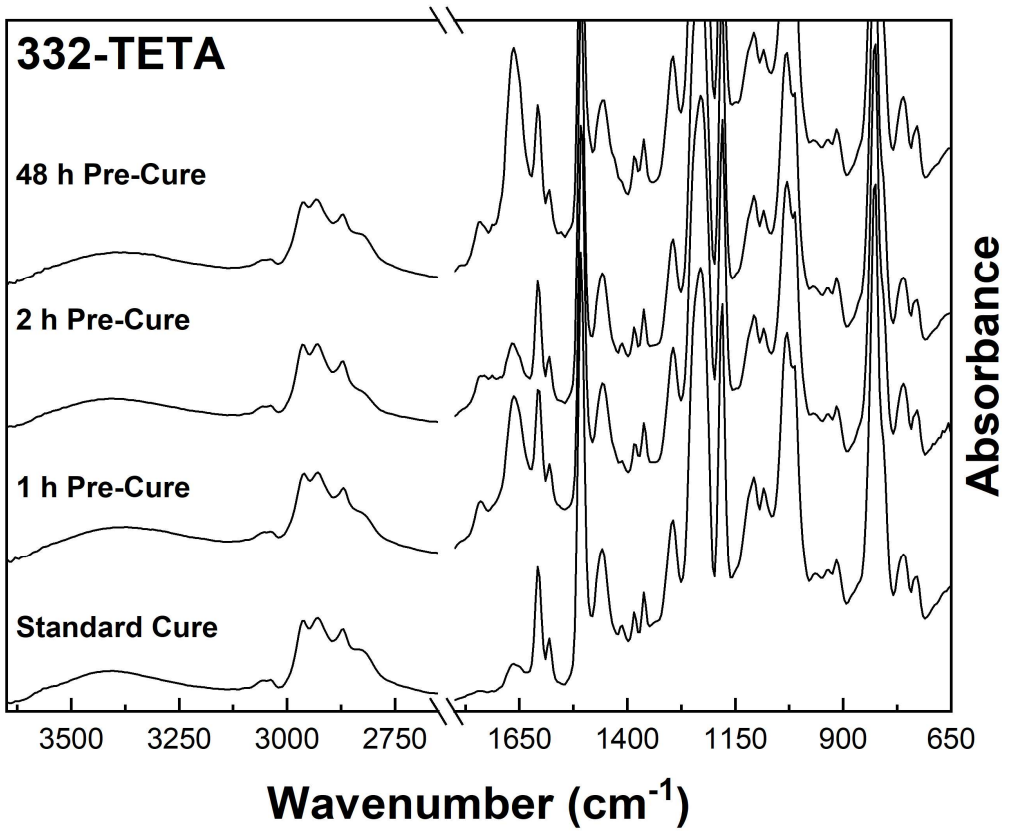

Figure 5:15: FTIR spectra of 332-TETA microbond samples with 0–48 h pre-cure

Quantitative analysis of unreacted epoxy groups and determination of droplet cure state indicated that samples cured immediately had degrees of conversion in the region of 0.55, a value commensurate with a loss of up to 60% of the initial curing agent and a sub-ambient T_g. Samples with a standing time of only 1 h showed increased degree of cure of 0.60–0.68, commensurate with a loss of approximately 50% of the initial curing agent. Degree of cure appeared to have increased to the extent that some measure of IFSS was possible with the Epotec specimens. However, plastic deformation remained present and IFSS values were exceedingly low (2–7 MPa). Droplet T_g was marginally improved to a value of around 15°C for the Epotec samples, while Olin samples showed little improvement in cure state. Conversely, samples that were allowed to pre-cure at room temperature for 2–48 h and partially react prior to curing produced spectra much closer to a stoichiometric mixture and had degree of cure between 0.87 and 0.93. High degree of cure corresponded to T_g of approximately 80°C or greater and was generally closely comparable to that of bulk matrix samples.

For the 332-TETA microbond samples, degree of cure was generally consistent regardless of whether a standing time was included. Degree of conversion was lowest (0.77) following a 36 h pre-cure and was, in fact, highest when samples were cured immediately (0.87). It is thus possible to suggest that a curing agent loss in the region of 10–30% occurred in these samples. While maximum degree of cure was lower in the reference system than the commercial resins, higher initial T_g at ideal stoichiometry and the ability to maintain high T_g following some degree of curing agent evaporation ensured a higher overall microdroplet T_g and consistent curing performance in the microbond test. It can be noted that off-stoichiometric 332-TETA T_g following a 30% loss in curing agent approximated that of the Epotec/Olin resins at ideal stoichiometry. The appearance of an additional peak at 1663 cm^{-1} may suggest distinct phenomena for the reduced 332-TETA droplet cure state. It is also possible that peak growth at 1663 cm^{-1} is attributable to imine formation [83] or an interaction with atmospheric moisture [236]. In either case, active amine sites available to react with the oxirane ring may be depleted

Degree of Cure and IFSS

Microdroplet degree of cure determined by FTIR and apparent IFSS measured by the microbond test were compared. Microbond droplets were prepared and cured on unsized glass fibres. FTIR droplets were prepared and cured on lengths of 50 µm steel wire. Embedded lengths were approximately double that of the glass fibre microbond samples. Epotec, Olin, and 332-TETA results are shown in *Figure 5:16*, *Figure 5:17*, and *Figure 5:18*, respectively.

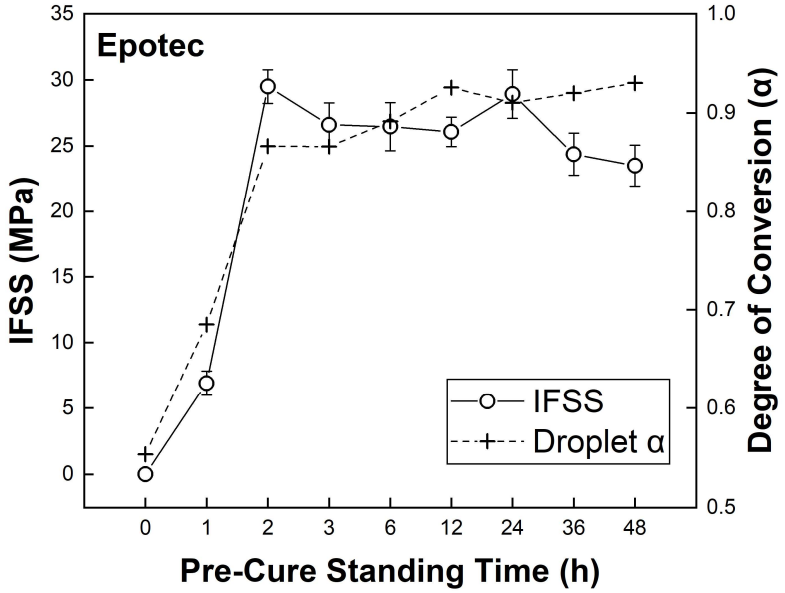

Figure 5:16: Epotec IFSS and microdroplet α versus pre-curing time

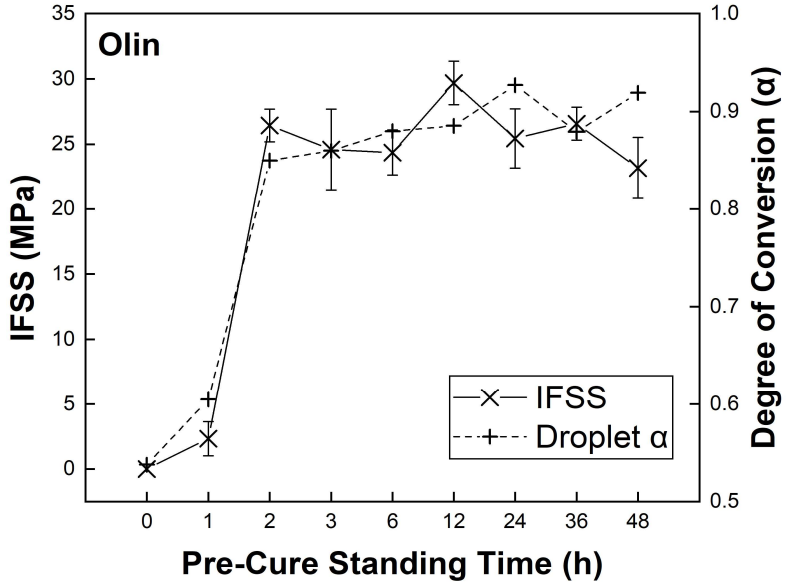

Figure 5:17: Olin IFSS and microdroplet α versus pre-curing time

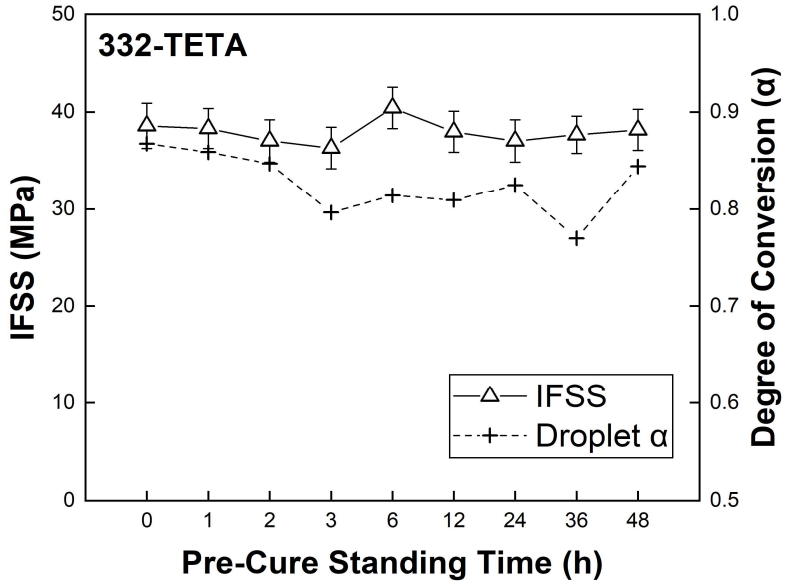

Figure 5:18: 332-TETA IFSS and microdroplet α versus pre-curing time

Excellent correlation was shown between micromechanical and spectroscopic methods, in that an increase in IFSS was commensurate with spectra indicating droplets were closer to the stoichiometric ratio and had higher degrees of cure. IFSS appeared to show a linear relationship with microdroplet degree of cure (and droplet T_g) up to conversion of approximately 0.8, after which further increases in droplet cure state were not reflected in increased IFSS. It is possible that an upper threshold IFSS value limited by the adhesion properties and tensile strength of the unsized fibres was reached in such cases. Due to the absence of sizing on the fibres, however, it may be possible to suggest that IFSS was largely dependent on the cure state of the droplet. Bartolomeo *et al.* have similarly proposed that IFSS in a cyanate ester was dictated solely by the degree of monomer conversion [186].

Microbond versus Bulk Glass Transition Temperature

Droplet degree of cure (α) was determined by direct ATR-FTIR of epoxy droplets cured on 50 µm steel wire filaments. Droplet T_g was estimated by curve intersection of droplet degree of cure values with off-stoichiometric data (*Figure 5:12*) that established the relationship between degree of epoxy conversion and glass transition temperature for each matrix material. Bulk cured matrix T_g was measured on DSC samples allowed to pre-cure for identical standing times before curing. Epotec, Olin, and 332-TETA results are shown in *Figure 5:19*, *Figure 5:20*, and *Figure 5:21*, respectively.

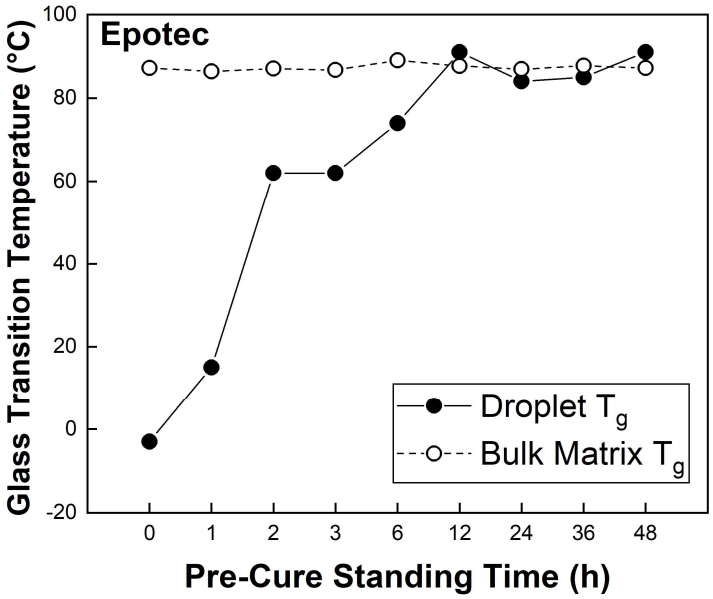

Figure 5:19: Epotec microbond versus bulk T_g

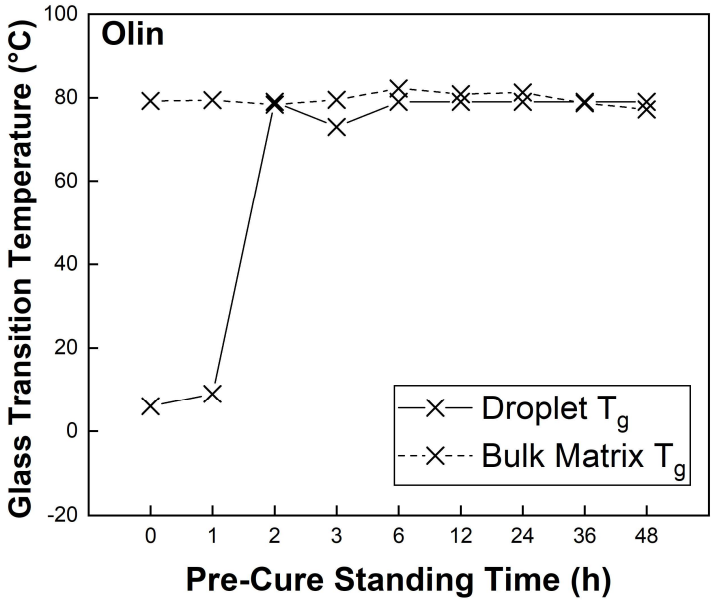

Figure 5:20: Olin microbond versus bulk T_g

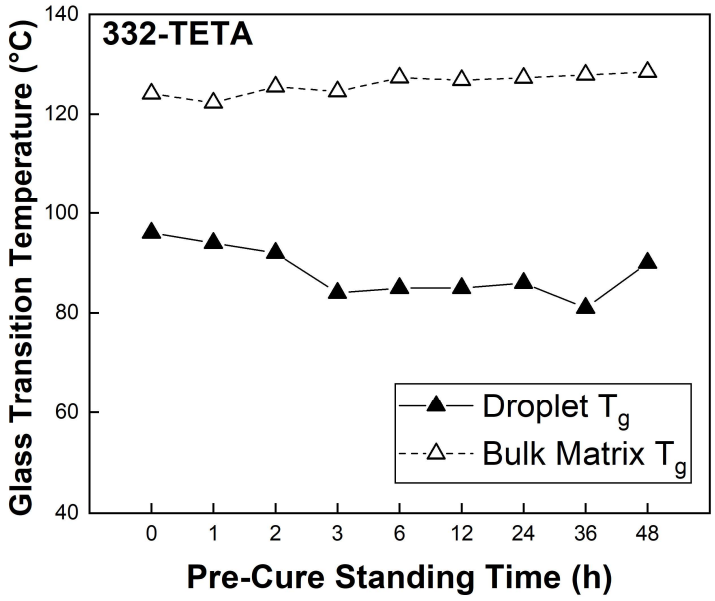

Figure 5:21: 332-TETA microbond versus bulk T_g

Microscale T_g of the Epotec and Olin commercial resin systems was sub-ambient when samples were cured immediately, a behaviour which accounts for the droplet plastic deformation observed during micromechanical testing. Samples with a 1 h standing time showed marginally improved T_g and good correlation with the observation that microbond samples were visibly tackier than droplets cured immediately and had a measurable IFSS of 2–6 MPa. Epotec microbond samples appeared to reach a T_g comparable to that of the bulk matrix sample following a 12 h standing time, despite evidence that IFSS was not increased to any significant degree in the 2–12 h region. Closest correlation between microdroplet T_g and micromechanical data was found with the Olin resin system. Measurements correlated well to IFSS data, in that microbond sample T_g achieved parity with bulk matrix DSC measurements following a 2 h standing time, after which microbond and bulk T_g values remained generally comparable.

A particularly interestingly behaviour can be observed in the 332-TETA samples. Despite consistently high IFSS values and invariant cure state with respect to standing time, microbond sample T_g was consistently some 30–40°C lower than that of bulk matrix and was commensurate with a loss of approximately 25–30% of the initial curing agent. Loss of some portion of the initial curing agent and a deviation from macroscale T_g properties would thus appear to occur in resin systems with no apparent microscale curing issues, and may potentially go unrecognised in experimental investigations.. Furthermore, curing performance and amine evaporation did not appear to be offset by the introduction of a pre-curing time.

The ability of micromechanical testing methods to inform macroscale materials selection and processing parameters is predicated on comparable polymer chemistry and material properties across both scales. Determination of droplet cure state would appear to be an essential component of any microbond investigation. It should be carefully considered that 332-TETA data would appear to indicate that droplets with "ideal" curing behaviour, may in fact have material properties different from those of the bulk cured matrix and comparable composite part. By extension, a number of matrix and curing agent combinations in the previous microbond literature that do not appear to show excessively poor droplet curing may still have unrecognised sub-optimal material properties. In such cases, the validity of the testing method may be questioned due to interfacial adhesion being assessed on an undefined system chemistry.

Given the demonstrable relationship between droplet cure state and apparent IFSS, it seems reasonable to suggest that any assessment of changes in interfacial adhesion as a result of sizing application or processing parameters must carefully consider the cure state of the droplet. Some form of modification to the curing procedure is advised in epoxy systems with lower initial T_g and a sub-ambient T_g following loss of 40% or more of the initial curing agent. Furthermore, T_g of successfully cured microbond samples may deviate by some 30–40°C compared to bulk matrix specimens subjected to the same curing schedule. Microdroplet degree of cure determined by FTIR, approximate droplet T_g (calculated from α), and apparent IFSS determined by the microbond test are summarised in *Table 5-4*.

	Degree of Cure (α)			**≈ T_g(°C)**			**IFSS (MPa)**		
Pre-Cure (h)	**Epotec**	**Olin**	**332-TETA**	**Epotec**	**Olin**	**332-TETA**	**Epotec**	**Olin**	**332-TETA**
0	0.55	0.54	0.87	–3	6	96	-	-	38.6
1	0.68	0.60	0.86	15	9	94	6.9	2.3	38.3
2	0.87	0.85	0.85	62	79	92	29.5	26.4	37.0
3	0.87	0.86	0.80	62	73	84	26.6	24.6	36.3
6	0.89	0.88	0.81	74	79	85	26.5	24.4	40.4
12	0.93	0.89	0.81	91	79	85	26.1	29.7	38.0
24	0.91	0.93	0.82	84	79	87	28.9	25.5	37.0
36	0.92	0.88	0.77	85	79	81	24.4	26.6	36.7
48	0.93	0.92	0.84	91	79	90	23.5	23.2	38.2

Table 5-4: Summary of microbond degree of cure, T_g, and IFSS with increasing pre-cure standing time

5.4.4 Effect of Excess Curing Agent

Microbond test data presented in Chapter 4 showed that Epotec and Olin commercial resins could be cured immediately according to the macroscale schedule when twice the stoichiometric amount of curing agent was added to the mixture. The effect of adding curing agent as a means of compensating for the stoichiometric imbalance observed in immediately cured samples was investigated. Epotec and Olin microbond samples were prepared with matrix formulations containing 25–100% (R=1.25 to R=2) excess curing agent and were cured immediately according to the recommended macroscale schedule (without a pre-curing modification). Glass transition temperature of microbond samples was determined from FTIR degree of cure measurements and DSC was used to characterise T_g of bulk matrix samples directly. FTIR spectra of the Epotec and Olin droplets cured with excess curing amine are shown in *Figure 5:22* and *Figure 5:23*, respectively.

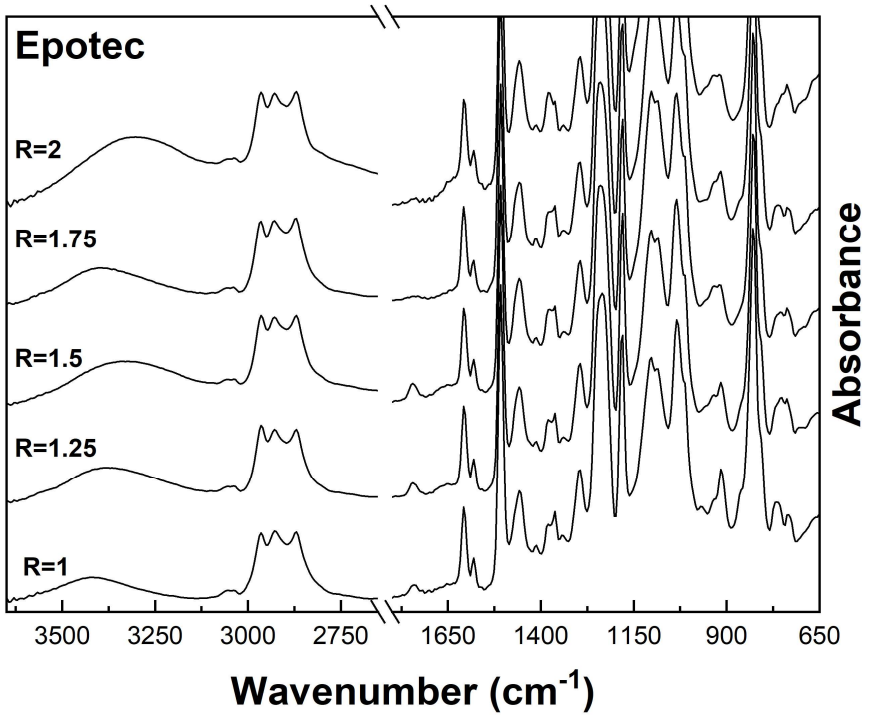

Figure 5:22: FTIR spectra of Epotec microbond samples cured with excess amine

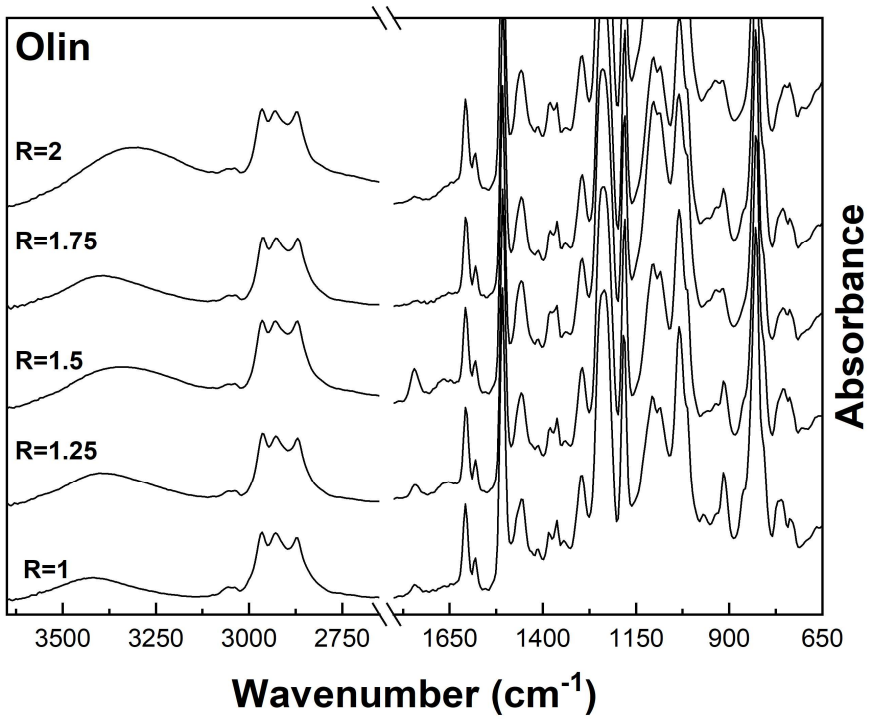

Figure 5:23: FTIR spectra of Olin microbond samples cured with excess amine

Spectra of droplets with up 25% excess amine appeared to show unreacted epoxy groups. While good curing appeared to have been achieved at R = 1.5, unreacted epoxy was visible in both spectra when 75% excess curing agent was used. With double the stoichiometric amount of curing agent (R = 2), epoxy groups appeared fully reacted in both resins. Furthermore, increased peak intensity around 3300 cm^{-1} in these samples may have been indicative of increased N-H due to increased amine interaction [232].

Comparison of microbond and bulk T_g measurements for Epotec and Olin resins are shown in *Figure 5:24* and *Figure 5:25*, respectively.

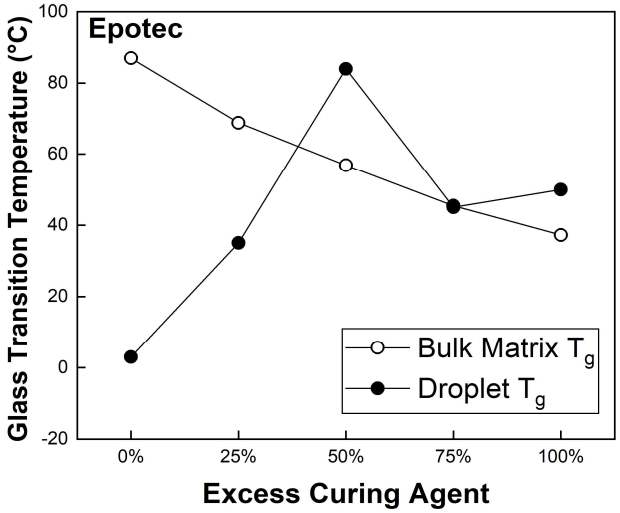

Figure 5:24: Epotec microbond versus bulk T_g with excess curing agent

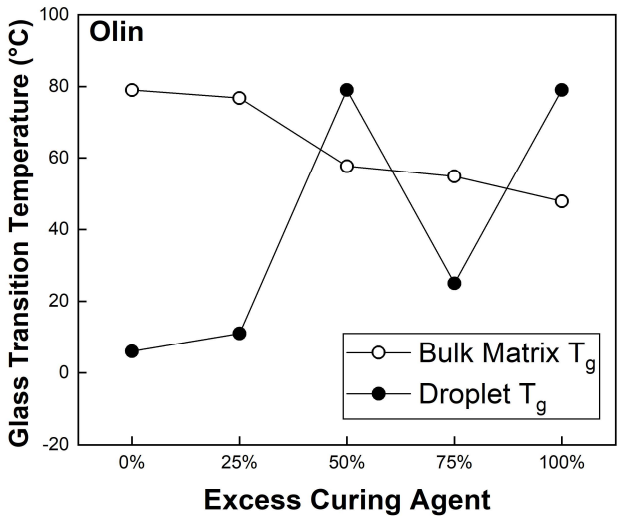

Figure 5:25: Olin microbond versus bulk T_g with excess curing agent

Microdroplet T_g appeared to increase when samples contained excess curing agent. Disparity between microscale and specimen T_g was most prevalent at ideal stoichiometry due to loss of 40–60% of the curing agent at the microscale. Similarly, samples containing only a 25% excess had notably poor microdroplet T_g, implying that the excess curing agent was not sufficient to offset the loss due to evaporation. Evaporation of curing agent appeared to be offset with 50–100% excess curing agent, though T_g was reduced following a 75% increase in curing agent. In both systems, microbond and bulk T_g achieved approximate parity at75% excess curing agent added, however.

Liao and Tung reported that poor epoxy/m-PDA microbond curing (attributed to adsorption of m-PDA onto the fibre surface) appeared to be successfully mitigated by oversaturating the droplets with around 25% excess curing agent [120]. In this work, the two diamine-based commercial resin systems required a minimum excess of 50% curing agent. Conversely, Rao *et al.* reported no significant increase in IFSS when the resin mixture contained twice the stoichiometric amount of amine [183].

It should, however, be reasserted that the goal of the investigation is not to simply produce a sample preparation and processing procedure that generates the highest apparent IFSS, but a methodology wherein best correlation is found between the thermomechanical properties of microbond samples and comparable bulk specimens. If the goal of micromechanical methods is the economical and time-efficient development of fibre sizings and assessment of composite processing parameters by enabling screening and optimisation, some form of verification that microbond parameters approximate to those of the macroscale specimen is desired. To this end, the experimental data generated by the curing agent saturation investigation provides

further evidence towards the theory that loss of curing agent to evaporation is prevalent in these microbond samples.

The addition of excess curing agent to bulk matrix specimens, however, resulted in a linear decrease in T_g with increasing amine content. Poor T_g at such epoxy/amine ratios may be attributable to primary amines dominating the curing reaction. Reduced secondary amine bonding (around a third at R =1.5) may result in a branched polymer structure and give rise to rings consisting of partially reacted molecules at the end of the epoxidic chain. Both of these structures may contribute to increased free volume in the system and subsequent reduced T_g compared to the stoichiometric formulation [196]. Furthermore, assessment of droplet cure state in samples with excess curing agent is complicated by the fact that at ratios greater than R = 1, quantitative analysis in the mIR range is limited to epoxy group depletion, which may not be an accurate representation of the cure state in the presence of excess amine. While microdroplet T_g (and IFSS) may be enhanced by the addition of excess amine, this method cannot be proposed as a solution to alleviate microscale curing issues based on resultant deviations to bulk matrix T_g using a comparable procedure and IFSS being measured in a material with undefined system chemistry.

5.4.5 Effect of Curing Atmosphere

Reduced droplet T_g in an amine-cured epoxy has previously been attributed to imine formation. It has been suggested that the formation of imine groups may reduce the number of amine functions available to react with the oxirane ring and contribute to a reduced cure state [83]. A diagram of the reaction process of amine to imine is shown in *Figure 5:26* [237]. Accordingly, it has been suggested that amine-cured microbond samples should be cured under inert atmosphere. FTIR spectra of Epotec and Olin droplets cured following a 24 h pre-curing time under both air and nitrogen is shown in *Figure 5:27* and *Figure 5:28*, respectively.

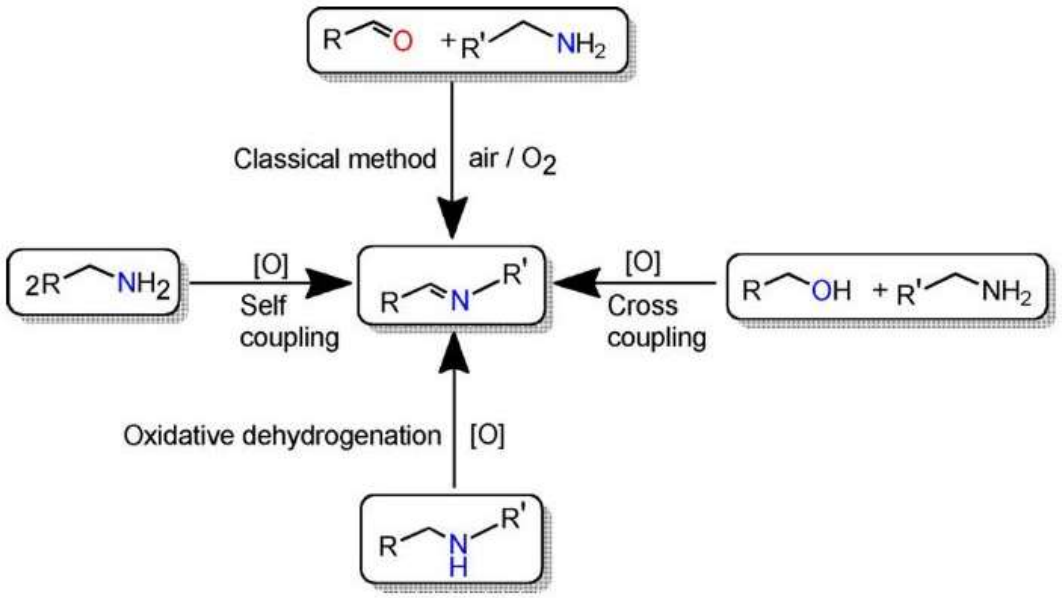

Figure 5:26: Reaction diagram of imine formation

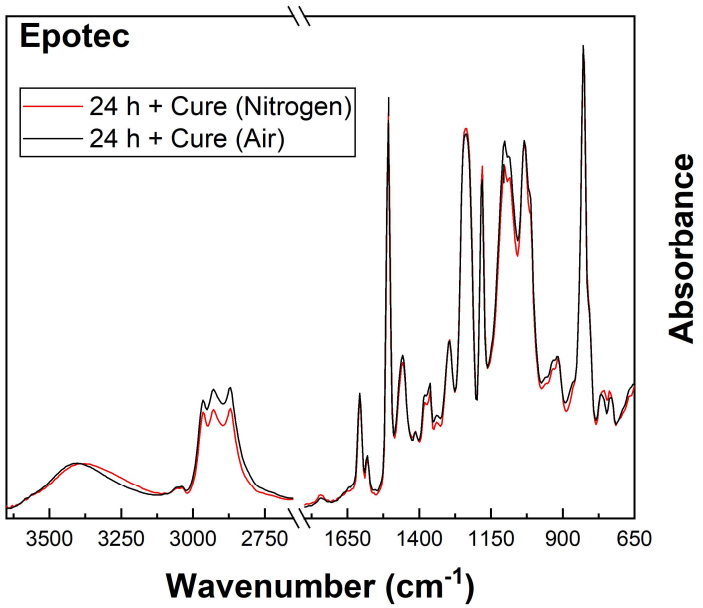

Figure 5:27: FTIR spectra of Epotec microbond samples with a 24 h pre-curing stage under air and inert nitrogen atmospheres

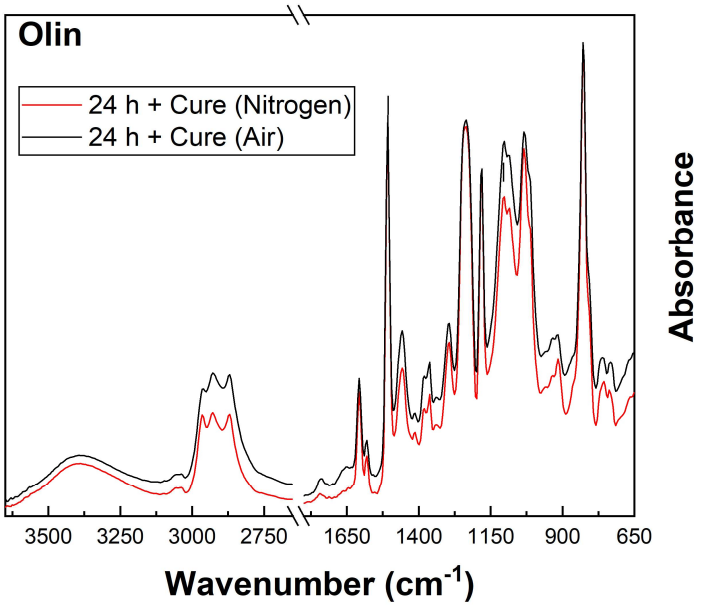

Figure 5:28: FTIR spectra of Olin microbond samples with a 24 h pre-curing stage under air and inert nitrogen atmospheres

Droplet spectra generally reflected the IFSS data presented in Chapter 4, in that there was little significant difference between samples where the 24 h standing time was conducted under inert or standard laboratory atmosphere. In the Epotec spectra, characteristic peaks associated with the epoxy/amine curing reaction were similar in both cases, indicating that samples had cured to a similar extent. A small peak at 1735 cm^{-1} attributable to a carbonyl group was visible as has been reported by Zinck *et al.* [83]. Peak intensity of carbonyl groups was not affected by the pre-curing atmosphere and did not appear to contribute to droplet cure state in any significant way. Furthermore, the development of an additional band at 1661 cm^{-1} indicative of formation of an imine group was not observed. In the Olin spectra, carbonyl peak intensity was slightly increased when the standing time was performed under air. Additionally, a shoulder peak in the region of 1658 cm^{-1} that may be indicative of the imine peak reported by Zinck *et al.* was observed when droplets were pre-cured under standard air atmosphere. The appearance of peaks attributable to carbonyl or imine groups, however, did not appear to have an influence on droplet cure state. In fact, reduced 915 cm^{-1} peak intensity in the spectra showing both carbonyl and imine groups indicated that degree of conversion was higher than the droplets pre-cured under inert atmosphere. Both microbond and FTIR results would appear to refute the hypothesis that imine formation is the cause of discrepancies between micro- and macroscale samples in these diamine-cured epoxy systems.

5.4.6 Relationship Between Droplet Cure State and IFSS

Microdroplet cure state variability within a typical "successful" microbond data set and development of a direct relationship between IFSS and cure state measurements was investigated. 332-TETA microbond samples were applied to 50 µm steel wire and interfacial adhesion was characterised using the microbond test. The cure state of individual post-test microbond samples was then assessed using FTIR and matched to the corresponding IFSS values. The use of steel wire microbond samples ensured that "sub-droplets" were not created during the initial application of the droplet to the fibre. Accordingly, increased droplet size and absence of sub-droplets meant that spectra were collected only from the post-test microdroplet. Comparable experiments using glass fibre samples resulted in spectra being generated from neighbouring droplet clusters and were limited by the size of the FTIR diamond interface. Degree of cure (α) of microbond samples and corresponding IFSS and embedded length is shown in *Figure 5:29*.

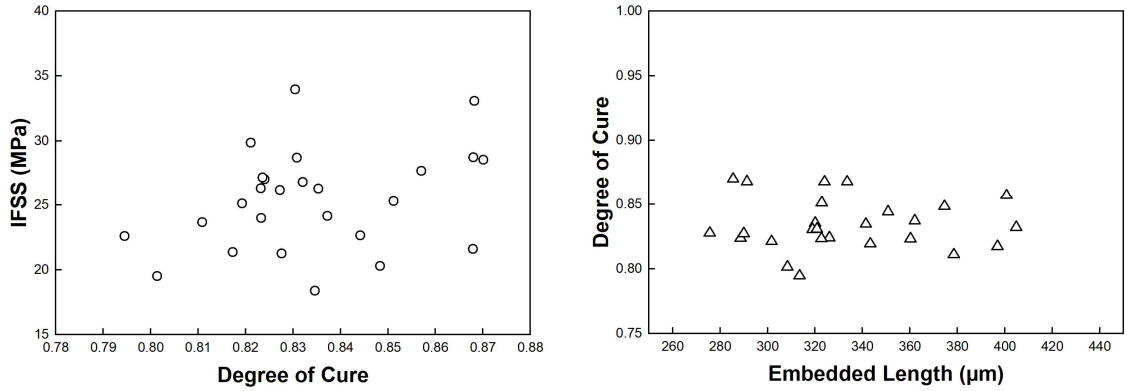

Figure 5:29: Variation in microbond sample cure state

FTIR spectra appeared to indicate that the degree of cure within a 30 specimen set of well-cured microbond samples may vary between microbond samples. Despite all samples being prepared and cured to an identical procedure, degree of cure of individual microbond samples varied between 0.77 and 0.87 with an average of 0.83. No linear relationship between droplet embedded length and degree of cure was observed, indicating that cure state in microbond samples was not particularly sensitive to droplet size up to embedded lengths of around 400 µm. An FTIR microscopy method may be more suitable for direct comparison of individual IFSS measurements and further development of a one-to-one relationship between micromechanical and spectroscopic data without the need for modification to sample preparation procedure.

5.5 CONCLUSIONS

The work described in Chapter 5 was undertaken to address a fundamental need identified in some of the earliest literature regarding the compatibility of the microbond test with thermosetting epoxy matrices. Namely, the need for a method to directly characterise the cure state of microbond droplet samples. More specifically, a method to investigate why the degree to which two commercial epoxy resin systems formed cured axisymmetric droplets suitable for microbond testing was dependent on the inclusion of a room temperature pre-curing stage, while a reference DGEBA/TETA system was seemingly unaffected.

Off-stoichiometric matrix compositions were used as an initial model of the varying extents of curing agent evaporation that might exist in microbond droplets. Glass transition temperature and degree of cure were highest at the stoichiometric ratio and reduced as curing agent was removed. Additionally, it was shown that a loss of 40% of the initial curing agent content was sufficient to reduce matrix T_g from around 80–90°C to approximately room temperature in the Epotec and Olin resin systems. In the 332-TETA reference system, a loss of 40% of the initial curing agent reduced T_g from a stoichiometric value of 124°C to around 68°C, and a reduction of more than 60% of the initial curing agent was necessary to induce a sub-ambient T_g.

Glass fibres were substituted by steel wire of 50 μm diameter in the preparation of microbond samples to improve signal clarity due to the combination of controllable and consistent increased microdroplet size and a favourable reflectance effect. The method allowed the cure state of individual microbond samples to be accurately measured using a conventional benchtop FTIR instrument. Degree of cure measured directly from microbond samples was compared to off-stoichiometric spectral and thermal analysis data to infer curing agent loss and droplet T_g.

FTIR spectra of Epotec and Olin microbond samples cured immediately at elevated temperature showed unreacted epoxy groups, reduced hydroxyl group and secondary amine accumulation, and a weaker etherification peak, commensurate with spectra indicating a non-stoichiometric epoxy-amine network. Quantitative analysis of unreacted epoxy groups and determination of cure state indicated that droplet samples cured immediately had degrees of conversion in the region of 0.55, indicating a loss of up to 60% of the initial curing agent and a sub-ambient glass transition temperature. Conversely, samples that were allowed to pre-cure at room temperature for a minimum of 2 h before curing showed increased degree of cure (0.87–0.93) and droplet T_g some 80°C greater than that of immediately cured samples. Good correlation was shown between micromechanical and spectroscopic methods, in that an

increase in IFSS was commensurate with spectra indicating droplets were closer to the stoichiometric ratio and had higher degrees of cure. A clear relationship between apparent interfacial adhesion and droplet cure state was thus demonstrated.

In the commercial resin systems, microbond T_g appeared to reach a value comparable to that of the bulk matrix sample following a 2 to 12 h standing time after which microbond and bulk T_g values remained generally comparable. Conversely, despite consistently high IFSS values and invariant cure state with respect to standing time, droplet T_g of the TETA-cured reference system was consistently some 30–40°C lower than that of bulk matrix. Furthermore, the introduction of a pre-curing time did not achieve parity between droplet and bulk cured matrix properties. The result implies that this behaviour is not limited to curing agents identified as volatile (such as IPD or m-PDA). Instead, it may be proposed that all microdroplet samples may be affected by this issue to some degree, the extent of which is determined by the curing agent. By extension, many of the matrix and curing agent combinations in the previous microbond literature that do not appear to show excessively poor droplet curing may still have unrecognised sub-optimal material properties. In such cases, the validity of the test results may be questioned and values of interfacial shear strength may not be truly representative.

Curing agent evaporation was also successfully mitigated to reproducibly prepare samples suitable for microbond testing with high degrees of cure by adding excess curing agent to the matrix mixture to counterbalance the loss. Conversely, T_g reduced linearly in bulk matrix specimens as excess curing agent was added. Of the two solutions presented, a pre-curing time is generally more advisable to attain parity between microscale and macroscale matrix properties as excess curing agent will produce materials with undefined system chemistry.

Interfacial testing methods are often employed to measure the influence of factors such as fibre surface treatment, application and screening of sizings, and degradation thereof. Changes in IFSS as the result of such alterations may be less significant than the influence of the cure state of the matrix microdroplet. Accordingly, the route taken in creating microbond samples, and the potential effect of discrepancies in microscale curing and resulting disparity between droplet and bulk matrix material properties must be carefully considered.

CHAPTER 6: SUMMARY AND RECOMMENDATIONS FOR FUTURE WORK

6.1 SUMMARY OF CONCLUSIONS

Round-Robin Study of Glass Fibre Sizing and IFSS

In Chapter 2, a round-robin study of the adhesion enhancing capabilities of a wide range of silane coupling agents and full sizing packages was investigated. The application of a series silane coupling agents (APS/GPTMS/MPTMS) increased glass fibre/epoxy apparent IFSS by approximately 17–20% compared to unsized fibres. Little significant difference between the various silane coatings indicated that despite some measure of universal increase to adhesion properties, specific chemical interactions between the glass fibre and epoxy matrix were not changed much by the silane used. Investigation of the adhesion enhancing properties of silane coupling agents was extended to a range of epoxysilane chemistries using an in-house immersion coating process. The highest value of adhesion was achieved with a GPMES coupling agent. While it is not immediately clear why adhesion was increased by GPMES compared to the other epoxysilanes, the adhesion enhancing capabilities of this coupling agent may have been responsible for comparable IFSS values attained in a series of epoxy-compatible full sizing formulations (SE1500, SE2020, W2020). Furthermore, the use of a matrix-incompatible full sizing resulted in adhesion properties lower than that of the unsized fibres despite the presence of an undisclosed coupling agent. An apparent adhesion-inhibiting effect of the thermoplastic film former appeared to counteract any improvement due to the silane.

Acetone extraction of fully sized fibres showed that IFSS was improved compared to the as-received fibres in all cases. High apparent IFSS following acetone extraction may be attributable to the bound portion of the sizing remaining on the fibre surface. This bound portion may consist primarily of a silane coupling agent, but the possibility of interaction with residual epoxy film former bound to the silane cannot be discounted. Increased IFSS compared to the as-received fibres may be related to removal of residual surface impurities or improved coupling agent homogeneity by removal of excessively bound silane aggregates. Alternatively, this behaviour may be related to the removal of sizing additives and processing agents whose contribution to the properties of the composite are not well defined.

Finally, glass fibres were treated with an unreacted DGEBA epoxy/acetone solution serving as both a model film former only sizing and a post-sizing treatment. Interfacial adhesion values approximating and even exceeding those attainable with a number of silane coupling agents and full sizing packages were achieved by coating unsized fibres with

epoxy/acetone solution concentrations of 2 to 10 wt.%. Lower concentration solutions produced adhesion values generally comparable to that of the unsized fibres. IFSS was improved following epoxy/acetone treatment and the order of maximum IFSS achieved was reflected by the initial IFSS of the fibres before treatment (unsized < silane only < full sizing). Coating SE2020 fibres with a 10 wt.% solution, in fact, produced the highest IFSS values measured over the course of the round-robin investigation. Total sizing content was lower for silane coated and fully sized fibres treated with the same solution concentration due to pre-existing sizing components preventing penetration of the fibre bundles by the epoxy as effectively as unsized bundles However, an apparent minimum LOI threshold necessary to confer enhanced adhesion properties appeared to have been reached. Increased IFSS as a result of the epoxy sizing application may have been attributable to interdiffusion of the epoxy sizing with the epoxy matrix material and enhanced cross-linking at the interface between unreacted DGEBA in the sizing and amine curing agent.

Thermal Degradation of Glass Fibre Sizing

In Chapter 3 the thermal degradation of a number of experimental and commercial glass fibre sizings was investigated using thermal analysis, spectroscopic, and micromechanical testing methods. TGA of three fully sized epoxy-compatible glass fibres indicated the majority of the mass loss occurred at 200–400°C and was attributable to the decomposition of the polymeric film former component of the sizing. TGA data was used to quantify the depletion of the sizing layer thickness as treatment temperature was increased. An initial 70–80 nm sizing layer was reduced by approximately 50% following 300°C heat treatment and removed almost entirely following treatment at 500°C.

FTIR spectra of thermally degraded fully sized glass fibres indicated that an O-H group potentially attributable to surface hydroxyl groups or a lubricant was completely removed between 250–300°C. Furthermore, the intensity of spectral bands attributed to an epoxy resin film former (1608/1508 cm^{-1}) decreased with increasing treatment temperature and were removed completely at 300–350°C. Reduction of peak intensities showed excellent correlation with TGA data that indicated that sizing mass loss in in the 200–400°C range was attributable to degradation of an epoxy film former. Reduction of epoxy species in the 25–200°C region observed in the spectral data was likely due to higher sensitivity of the method compared to TGA of sized fibre bundles. Spectra of fibres treated at 350–500°C were comparable to that of silane sized fibres indicating that residue of degraded silane coupling agent may have remained present on the glass fibre surface. Increased peak intensity of a carbonyl group

(C=O) band at 1731 cm^{-1} following higher treatment temperatures may have been due to oxidation of the epoxy film former component in the sizing.

Interfacial adhesion measurements showed that IFSS had an inverse relationship with fibre treatment temperature and was concurrent with decomposition of the glass fibre sizing measured by TGA. Reduced IFSS appeared to onset at 300–350°C and at treatment temperatures of 400°C and above interfacial adhesion was comparable to that of unsized fibres, suggesting that the majority of the sizing components which influence IFSS had been removed. While the film former component of the sizing accounted for the majority of the measured mass loss in the sizing, comparison of micromechanical and spectroscopic results indicated that reduced IFSS did not onset until the point at which the epoxy film former had been completely removed (300–350°C). This result could suggest that complete removal of the film former is detrimental to the chemical bonding potential of the sizing, though the fact that no significant loss of IFSS is observed when the amount of film former present has been severely reduced in the 250–300°C temperature range may suggest that degradation of the silane coupling agent was primarily responsible. Spectra of fibres treated at 500°C indicated that some residues of degraded silane coupling agent material were present at the glass fibre surface, though the silane coupling agent may have been degraded to the extent that the adhesion-enhancing capabilities were lost. Interfacial adhesion may also have been inhibited at higher treatment temperatures by the accumulation of weakly bound oxidised film former/sizing material on the glass fibre surface, corresponding to the carbonyl group growth observed in the spectra of heat treated samples.

Microscale Curing Performance of Epoxy Resins in the Microbond Test

In Chapter 4, the microscale curing performance of a number of amine-cured epoxy resins and the influence of processing parameters was investigated. Microbond testing results showed that the degree to which two commercial amine-cured epoxy systems resins formed cured droplets suitable for microbond testing was dependent on a modification to the recommended macroscale schedule. Microbond samples showed exceedingly low IFSS values when exposed to immediate heating, failed to cure, and deformed plastically under loading. Poor microdroplet curing and low apparent droplet T_g was attributable to a stoichiometric imbalance caused by evaporation of the curing agent. Off-stoichiometric droplet behaviour was further evidenced by a number of modifications to the curing schedule and sample preparation methodology. The inclusion of a room temperature pre-curing stage for a minimum of 2 h had a profound effect on apparent IFSS, after which further standing times showed no significant

improvement. This behaviour may make microbond tests: I) poor in informing macroscale decisions regarding composite processing parameters, or II) impossible to perform due to droplet deformation such that certain matrix and sizing combinations cannot be evaluated at the single fibre level without significant changes to the recommended cure cycle for macroscopic specimens.

The standing time necessary to produce cured droplets was significantly lower than the gel time. While evaporation of volatile curing agents appeared to occur in the early stages of curing, the pre-curing time necessary to prevent evaporation may be related to the time taken for each curing agent molecule to form a single intermolecular hydrogen bond during the pre-gelation stage. Microbond samples cured with TETA initially appeared unaffected by microscale curing issues and cured successfully without the need for curing schedule modifications. Glass transition temperatures of cured bulk matrix samples of all three resin systems were independent of curing cycle modification and the inclusion of a pre-curing stage.

DSC of poorly cured microbond samples using a cluster of similarly-sized droplets applied on lengths of steel wire showed that a minimum four droplets (total weight less than 1 mg) were necessary to generate sufficient signal to discriminate a clear step transition. A microdroplet T_g of approximately 40°C was measured, which was less than half that of the bulk matrix samples cured according to the same temperature schedule was measured. Furthermore, in-situ observation of curing using hot-stage microscopy indicated that the pre-curing stage significantly reduced volumetric shrinkage during the heating stage. Accordingly, the route taken in creating microbond samples and the potential effect of discrepancies in microscale curing behaviour must be carefully considered. The literature review presented and experimental work presented in Chapter 4 casts reasonable doubt on the results of the abundance of literature published on the utilisation of the microbond test in works where no apparent problem was detected or discussed.

Characterisation of Microbond Sample Cure State and Droplet T_g

The work described in Chapter 5 was undertaken to address a fundamental need identified in some of the earliest literature regarding the compatibility of the microbond test with thermosetting epoxy matrices. Namely, the need for a method to directly characterise the cure state of microbond droplet samples. More specifically, a method to investigate why the degree to which two commercial epoxy resin systems formed cured droplets suitable for microbond testing was dependent on the inclusion of a room temperature pre-curing stage, while a reference DGEBA/TETA system was seemingly unaffected.

Off-stoichiometric matrix compositions were used as an initial model of the varying extents of curing agent evaporation that might exist in microbond droplets. A relationship between DSC measured glass transition temperature and degree of cure (α) determined by FTIR was established for each matrix. Glass fibres were substituted by 50 μm diameter steel wire in the preparation of microbond samples to improve signal clarity due to the combination of controllable and consistent increased microdroplet size and a favourable reflectance effect. Droplet degree of cure was determined by FTIR and droplet glass transition temperature was estimated by comparison to off-stoichiometric data.

FTIR spectra of Epotec and Olin microbond samples cured immediately at elevated temperature showed unreacted epoxy groups, reduced hydroxyl and secondary amine group accumulation, and a weaker etherification peak, commensurate with spectra indicating a non-stoichiometric epoxy-amine network. Quantitative analysis of unreacted epoxy groups and determination of cure state indicated that droplet samples cured immediately had degrees of conversion in the region of 0.55, indicating a loss of up to 60% of the initial curing agent and a sub-ambient glass transition temperature. Conversely, samples that were allowed to react at room temperature for a minimum of 2 h before curing showed increased degree of cure (0.87–0.93) and droplet T_g some 80°C greater than that of immediately cured samples. Good correlation was shown between micromechanical and spectroscopic methods, in that an increase in IFSS was commensurate with spectra indicating droplets were closer to the stoichiometric ratio and had higher degrees of cure. A clear relationship between apparent interfacial adhesion and droplet cure state was thus demonstrated.

Conversely, despite consistently high IFSS values and invariant cure state with respect to standing time, droplet T_g of the TETA-cured reference system was consistently some 20–40°C lower than that of the bulk matrix. Furthermore, the introduction of a pre-curing time did not achieve parity between droplet and bulk cured matrix properties. The result implies that poor droplet curing behaviour is not limited to volatile curing agents. By extension, many of the matrix and curing agent combinations in the previous microbond literature that do not appear to show excessively poor droplet curing may still have unrecognised sub-optimal material properties. In such cases, the validity of the test results may be questioned and values of interfacial shear strength may not be truly representative.

6.2 RECOMMENDATIONS FOR FUTURE WORK

It was shown in Chapter 2 that a GPMES coupling promoted excellent adhesion-enhancing properties in a round-robin investigation of a wide range of glass fibre sizings. It was also shown that IFSS comparable to and even exceeding that of silane coupling agents and full matrix-compatible sizing packages could be achieved by the application of an unreacted epoxy/acetone solution of sufficient solution concentration.

Further interesting areas for future research are primarily concerned with the scalability of these findings to practical composite properties. It is recommended that glass fibre treatment with 2 wt.% unreacted DGEBA epoxy/acetone solution be expanded to treatment of larger quantities of fibres and scaled up laminate production. If the adhesion enhancing capabilities of these treatments are to be considered of genuine practical relevance, it must be verified that increased adhesion is reflected in practical composite properties and is not solely related to some parameter of the microbond testing method. If successful, this could be expanded to production of an experimental sizing produced on a bushing.

Consideration should also be given to the fact that IFSS of glass fibres that were already sized with silane or a full sizing was improved considerably following an epoxy/acetone "post-sizing" procedure, and that such treatments produced the highest IFSS values achieved over the course of the investigation. Further parameters that may be investigated in working towards optimised adhesion with epoxy sizings may involve variations on the degree of DGEBA cross-linking and an extended range of matrix materials. Increased understanding of the apparent sawtooth behaviour observed in the load versus displacement plots of epoxy sized microbond samples would also be desirable.

While increased understanding of the relationship between glass fibre sizing and interfacial adhesion is a laudable goal, lack of transparency regarding the exact composition of the majority of glass fibre sizing formulations and the reputation of sizing as something of a "black box" technology limits fundamental understanding in the field. A co-operative effort between both the scientific community and the glass fibre industry is required if the fundamental adhesion properties of fibre sizings are to be better understood and the full potential of the next generation of composite materials realised. Significant development in this area is typically handicapped by commercial considerations. Further areas of research may involve investigation of relatively new fibre and matrix material combinations (such as Elium) whose interfacial properties are not well reported.

In Chapter 3 it was shown that loss of interfacial adhesion onset at the point at which the film former had been completely removed and at temperatures where the silane coupling agent

began to degrade. While it was shown that the reduced IFSS correlated well to degradation of the fibre sizing at comparable temperatures the thermogravimetric analysis method used was not ideal. This work could be expanded on by a quasi-isothermal thermogravimetric study of fibre sizing mass loss that is more representative of the thermal history of the furnace treatments. This is most likely achievable with either a TGA instrument that allows for the total fibre (and sizing) mass to be increased. Alternatively, a modification to the sample preparation procedure by hermetically sealing small bundles of sized fibres in a pin-holed DSC pan may enhance thermogravimetric resolution of sizing volatiles.

In Chapter 4, an apparent disparity in curing performance between microscale droplet samples and cured matrix properties was identified when samples were subjected to the same temperature schedule. That a varied range of amine chemistries showed some form of susceptibility to this behaviour is good indication that renewed investigation and serious discussion of this phenomena in the literature is overdue. It is worth reasserting that as the combined citations of the seminal publications on the development of the microbond technique approaches one thousand, only an extremely small number of authors have recognised the potential influence of sub-optimal droplet properties and even then, detailed investigations are rarely reported. Despite microscale curing performance being identified as an area for improvement in some of the earliest critical reviews of the microbond test, little significant effort to address the issue directly has been undertaken. It is advised that investigation of microbond curing behaviour be extended to a wider range of fibre and matrix combinations and independent methods of characterising droplet cure state and material properties be pursued.

The FTIR method proposed in Chapter 5 allows assessment of droplet cure state using a conventional benchtop FTIR instrument by a simple modification to the microbond sample preparation procedure. The small specimen sizes involved, however, requires the use of an adjustable probe and can be considered a destructive testing method. A pyrolysis gas chromatography technique may be able to more effectively determine amine loss during cure than certain spectroscopic methods and microcalorimetry may be efficient. However, a non-destructive method of droplet cure state assessment is highly desirable. FTIR microscopy would appear to be an excellent proposal for a non-destructive method of characterisation of microbond sample cure states. Such a method would allow for accurate measurements over multiple points on the droplet and eliminates the need for modification to the sample preparation procedure. Determination of a direct relationship between the degree of cure and

apparent IFSS within the same microbond data set would be a worthwhile development of the work presented in this thesis.

In any case, a concerted effort towards characterisation of the cure state of matrix droplets by all practitioners of the microbond testing method is greatly encouraged. Any investigation of the adhesion properties of sizing composition and thermoset processing parameters should necessitate comparable data between droplet and bulk cured matrix properties to ensure that the microbond test can be considered reliable in making informed decisions on a comparable macroscale matrix chemistry. If the microbond test is to continue to enjoy widespread utilisation across a range of fibre and matrix combinations, renewed discussion and investigation of droplet cure state and efforts to address some of the earliest issues identified in the method would be beneficial to all practitioners of micromechanical testing and the wider interface community. If the microbond test is to be presented as an efficient and robust methodology for effectively characterising the fibre/matrix interface it is essential for this phenomena to be understood in greater detail.

REFERENCES

[1] Thomason JL. Glass Fibre Sizings: A Review of the Scientific Literature. Blurb Inc.; 2012.

[2] Peters L. Influence of Glass Fibre Sizing and Storage Conditions on Composite Properties. Solid Mechanics and Its Applications 2018;245:19–31.

[3] Drown EK, Al Moussawi H, Drzal LT. Glass fiber “sizings” and their role in fibre-matrix adhesion. Journal of Adhesion Science and Technology 1991;5:865–81.

[4] Thomason J. A review of the analysis and characterisation of polymeric glass fibre sizings. Polymer Testing 2020;85:1–13.

[5] Drzal LT, Rich MJ, Koenig MF, Lloyd PF. Adhesion of Graphite Fibers to Epoxy Matrices: II. The Effect of Fiber Finish. The Journal of Adhesion 1983;16:133–52.

[6] Hughes JDH. The CarbonvFibre/epoxy interface-A Review. Composites Science and Technology 1991;41:13–45.

[7] Thomason JL. Investigation of Composite Interphase Using Dynamic Mechanical Analysis: Artifacts and Reality. Polymer Composites 1990;11:105–13.

[8] Drzal LT. The Effect of Polymeric Matrix Mechanical Properties on the Fiber-Matrix Interfacial Shear Strength. Materials Science and Engineering 1990;A126:289–93.

[9] Yuan JJ, Kennedy JM, Edier DD. Modelling the Dynamic Response of the Fiber/Matrix Interphase in Continuous Materials. Fiber, Matrix, and Interface Properties, ASTM STP 1290; 1996, p. 67–83.

[10] Montgomery CB. Multiscale Characterization of Carbon Fiber-Reinforced Epoxy Composites. PhD Thesis, University of Illinois, 2018.

[11] Thomason JL. The interface region in glass fibre-reinforced epoxy resin composites: 3. Characterization of fibre surface coatings and the interphase. Composites 1995;26:487–98.

[12] Jean-Baptiste D. Interface in composite materials. Pure and Applied Chemistry 1981;53:2223–32.

[13] Hull D, Clyne T. An Introduction to Composite Materials. Cambridge: Cambridge University Press; 1996.

[14] Wallenberger FT, Watson JC, Li H, Industries PPG. Glass Fibers. ASM Handbook 2001;21:27–34.

[15] Hollaway LC. A review of the present and future utilisation of FRP composites in the civil infrastructure with reference to their important in-service properties. Construction and Building Materials 2010;24:2419–45.

[16] Rafiee R. On the mechanical performance of glass-fibre-reinforced thermosetting-resin pipes: A review. Composite Structures 2016;143:151–64.

[17] Thomason JL, Adzima LJ. Sizing up the interphase: An insider's guide to the science of sizing. Composites Part A: Applied Science and Manufacturing 2001;32:313–21.

[18] Plueddeman EP. Silane Coupling Agents. 1982.

[19] Thomason JL. Interfaces and interfacial effects in glass reinforced thermoplastics. Proceedings of the 28th Risø International Conference on Materials Science, Roskilde: 2007.

[20] Koenig JL, Emadipour H. Mechanical characterization of the interfacial strength of glass-reinforced composites. Polymer Composites 1985;6:142–50.

[21] Zhuang RC, Burghardt T, Plonka R, Liu JW, Mäder E. Affecting glass fibre surfaces and composite properties by two stage sizing application. Express Polymer Letters 2010;4:798–808.

[22] Herrera-Franco PJ, Drzal LT. Comparison of methods for the measurement of fibre/matrix adhesion in composites. Composites 1992;23:2–26.

[23] Pitkethly MJ. The Use of Interfacial Test Methods in Composite Materials Development. Fiber, Matrix, and Interface Properties, ASTM STP 1290; 1996, p. 34–46.

[24] Dey M, Deitzel JM, Gillespie JW, Schweiger S. Influence of sizing formulations on glass/epoxy interphase properties. Composites Part A: Applied Science and Manufacturing 2014;63:59–67.

[25] Drzal LT, Madhukar M. Fibre-matrix adhesion and its relationship to composite mechanical properties. Journal of Materials Science 1993;28:569–610.

[26] Kelly A, Tyson WR. Tensile properties of fibre-reinforced metals: Copper/tungsten and copper/molybdenum. Journal of the Mechanics and Physics of Solids

1965;13:329–50.

[27] Zhandarov S, Mäder E. Analysis of a pull-out test with real specimen geometry. Part I: Matrix droplet in the shape of a spherical segment. Journal of Adhesion Science and Technology 2013;27:430–65.

[28] Piggott MR, Xiong Y. Direct Observation of Debonding in Fiber Pull-Out Specimens. Fiber, Matrix, and Interface Properties, ASTM STP 1290; 1996, p. 84–91.

[29] Miller B, Muri P, Rebenfeld L. A Microbond Method for Determination of the Shear Strength of a Fiber/ Resin Interface. Composites Science and Technology 1987;28:17–32.

[30] Herrera-Franco PJ, Rao V, Drzal LT, Chiang MYM. Bond strength measurement in composites-Analysis of experimental techniques. Composites Engineering 1992;2:31–45.

[31] Day RJ, Cauich Rodrigez J V. Investigation of the micromechanics of the microbond test. Composites Science and Technology 1998;58:907–14.

[32] Penn LS, Lee SM. Interpretation of Experimental Results in the Single Pull-out Filament Test. Journal of Composites Technology & Research 1989;11:23–30.

[33] Zhi C, Long H, Miao M. Influence of microbond test parameters on interfacial shear strength of fiber reinforced polymer-matrix composites. Composites Part A: Applied Science and Manufacturing 2017;100:55–63.

[34] Yang L, Thomason JL. Development and application of micromechanical techniques for characterising interfacial shear strength in fibre-thermoplastic composites. Polymer Testing 2012;31:895–903.

[35] Wagner HD, Gallis HE, Wiesel E. Study of the interface in Kevlar 49-epoxy composites by means of microbond and fragmentation tests: effects of materials and testing variables. Journal of Materials Science 1993;28:2238–44.

[36] Minty RF, Yang L, Thomason JL. The influence of hardener-to-epoxy ratio on the interfacial strength in glass fibre reinforced epoxy composites. Composites Part A: Applied Science and Manufacturing 2018;112:64–70.

[37] Downes KA, Thomason JL. A method to measure the influence of humidity and temperature on the interfacial adhesion in polyamide composites. Composite Interfaces 2015;22:757–66.

[38] McDonough WG, Antonucci JM, Dunkers JP. Interfacial shear strengths of dental resin-glass fibers by the microbond test. Dental Materials 2001;17:492–8.

[39] Kang SK, Lee DB, Choi NS. Fiber/epoxy interfacial shear strength measured by the microdroplet test. Composites Science and Technology 2009;69:245–51.

[40] Sheu GS, Shyu SS. Surface properties and interfacial adhesion studies of aramid fibres modified by gas plasmas. Composites Science and Technology 1994;52:489–97.

[41] Ozzello AD, Grummon DS, Drzal LT, Kalantar J, Loh I-H, Moody RA. Interfacial Shear Strength of Ion Beam Modified UHMW-PE Fibers in Epoxy Matrix Composites. Materials Resarch Society Symposium: Interfaces Between Polymers, Metals, and Ceramics Proceedings, vol. 153, 1989, p. 217–22.

[42] Craven JP, Cripps R, Viney C. Evaluating the silk/epoxy interface by means of the Microbond Test. Composites Part A: Applied Science and Manufacturing 2000;31:653–60.

[43] Liu FP, Wolcott MP, Gardner DJ, Rials TG. Characterization of the interface between cellulosic fibers and a thennoplastic matrix. Journal of Composite Interfaces 1994;432:419–32.

[44] Liu Z, Yuan X, Beck AJ, Jones FR. Analysis of a modified microbond test for the measurement of interfacial shear strength of an aqueous-based adhesive and a polyamide fibre. Composites Science and Technology 2011;71:1529–34.

[45] Koyanagi J, Yoneyama S, Nemoto A, Melo JDD. Time and temperature dependence of carbon/epoxy interface strength. Composites Science and Technology 2010;70:1395–400.

[46] Chizyuka C, Munakaampe GM. Effects of Hydrothermal Ageing on the Microbond Interfacial Shear Strength of NaOH Treated Sisal Fibre Reinforced Polyester Composites . 2017.

[47] Yang L, Thomason JL. Interface strength in glass fibre-polypropylene measured using the fibre pull-out and microbond methods. Composites Part A: Applied Science and Manufacturing 2010;41:1077–83.

[48] Dirand X, Hilaire B, Soulier JP, Nardin M. Interfacial shear strength in glass-fiber/vinylester-resin composites. Composites Science and Technology 1996;56:533–9.

[49] Hunston D, McDonough W. Test Protocol for Single-Fiber Fragmentation Test. International Round Robin, 2000.

[50] Feih S, Wonsyld K, Minzari D, Westermann P, Lilholt H. Testing procedure for the single fiber fragmentation test 2004.

[51] Mahato B, Babarinde VO, Abaimov SG, Lomov S V., Akhatov I. Interface strength of glass fibers in polypropylene: Dependence on the cooling rate and the degree of crystallinity. Polymer Composites 2020;41:1310–22.

[52] Awal A, Cescutti G, Ghosh SB, Müssig J. Interfacial studies of natural fibre/polypropylene composites using single fibre fragmentation test (SFFT). Composites Part A: Applied Science and Manufacturing 2011;42:50–6.

[53] Tripathi D, Jones FR. Single fibre fragmentation test for assessing adhesion in fibre reinforced composites. Journal of Materials Science 1998;33:1–16.

[54] Favre JP, Jacques D. Stress transfer by shear in carbon fibre model composites - Part 1 Results of single-fibre fragmentation tests with thermosetting resins. Journal of Materials Science 1990;25:1373–80.

[55] Dai SR, Piggott MR. The strengths of carbon and kevlar fibres as a function of their lengths. Composites Science and Technology 1993;49:81–7.

[56] Nairn JA, Liu YC, Galiotis C. Analysis of Stress Transfer from the Matrix to the Fiber Through an Imperfect Interface: Application to Raman Data and the Single-Fiber Fragmentation Test. Fiber, Matrix, and Interface Properties, ASTM STP 1290; 1996, p. 47–66.

[57] Galiotis C. Interfacial studies on model composites by laser Raman spectroscopy. Composites Science and Technology 1991;42:125–50.

[58] Piggott MR. Failure processes in the fibre-polymer interphase. Composites Science and Technology 1991;42:57–76.

[59] Figueroa JC, Carney TE, Schadler LS, Laird C. Micromechanics of single filament composites. Composites Science and Technology 1991;42:77–101.

[60] Feillard P, Désarmot G, Favre JP. Theoretical aspects of the fragmentation test. Composites Science and Technology 1994;50:265–79.

[61] Mandell JF, Chen JH, Mcgarry FJ. A microdebonding test for in situ assessment of

fibre / matrix bond strength in composite materials. International Journal of Adhesion and Adjesives 1980:40–4.

[62] Chen EJH, Young JC. The microdebonding testing system: A method of quantifying adhesion in real composites. Composites Science and Technology 1991;42:189–206.

[63] Desaeger M, Verpoest I. On the use of the micro-indentation test technique to measure the interfacial shear strength of fibre-reinforced polymer composites. Composites Science and Technology 1993;48:215–26.

[64] Medina M C, Molina-Aldareguía JM, González C, Melendrez MF, Flores P, LLorca J. Comparison of push-in and push-out tests for measuring interfacial shear strength in nano-reinforced composite materials. Journal of Composite Materials 2016;50:1651–9.

[65] Godara A, Gorbatikh L, Kalinka G, Warrier A, Rochez O, Mezzo L, et al. Interfacial shear strength of a glass fiber/epoxy bonding in composites modified with carbon nanotubes. Composites Science and Technology 2010;70:1346–52.

[66] Mandell J, Grande D, Tsiang T-H, McGarry F. Modified Microdebonding Test for Direct In Situ Fiber/Matrix Bond Strength Determination in Fiber Composites. Composite Materials: Testing and Design (Seventh Conference) 1986:87-87–22.

[67] Larson BK, Drzal L. Glass fibre sizing/matrix interphase formation in liquid composite moulding : effects on fibre / matrix adhesion and mechanical properties 1994;25:711–21.

[68] Jacques D, Favre JP. Determination of the Interfacial Shear Strength by Fibre Fragmentation in Resin Systems with Small Rupture Strain. Proceedings of the 6th International Conference on Composite Materials, 1987, p. 471–80.

[69] Cranmer DC, Deshmukh U V., Coyle TW. Comparison of methods for determining fiber/matrix interface frictional stresses in ceramic matrix composites. ASTM Special Technical Publication 1990;STP:124–35.

[70] Pitkethly MJ, Favre JP, Gaur U, Jakubowski J, Mudrich SF, Caldwell DL, et al. A round-robin programme on interfacial test methods. Composites Science and Technology 1993;48:205–14.

[71] Gaur U, Miller B. Microbond method for determination of the shear strength of a fiber/resin interface: Evaluation of experimental parameters. Composites Science and

Technology 1989;34:35–51.

[72] Straub A, Slivka M, Schwartz P. A study of the effects of time and temperature on the fiber/matrix interface strength using the microbond test. Composites Science and Technology 1997;57:991–4.

[73] Adusumalli RB, Weber HK, Roeder T, Sixta H, Gindl W. Evaluation of experimental parameters in the microbond test with regard to lyocell fibers. Journal of Reinforced Plastics and Composites 2010;29:2356–67.

[74] Haaksma RA, Cehelnik MJ. A Critical Evaluation of the Use of the Microbond Method for Determination of Composite Interfacial Properties. Materials Research Society Symposium Proceedings 1990;170:71–6.

[75] Li Q, Nian G, Tao W, Qu S. Size Effect on Microbond Testing Interfacial Shear Strength of Fiber-Reinforced Composites. Journal of Applied Mechanics 2019;86.

[76] Gao X, Jensen RE, Li W, Deitzel J, McKnight SH, Gillespie JW. Effect of Fiber Surface Texture Created from Silane Blends on the Strength and Energy Absorption of the Glass Fiber/Epoxy Interphase. Journal of Composite Materials 2008;42:513–34.

[77] Pandey G, Kareliya CH, Singh RP. A study of the effect of experimental test parameters on data scatter in microbond testing. Journal of Composite Materials 2012;46:275–84.

[78] Laurikainen P, Kakkonen M, von Essen M, Tanhuanpää O, Kallio P, Sarlin E. Identification and compensation of error sources in the microbond test utilising a reliable high-throughput device. Composites Part A: Applied Science and Manufacturing 2020;137.

[79] Morlin B, Czigany T. Cylinder test: Development of a new microbond method. Polymer Testing 2012;31:164–70.

[80] Chou CT, Gaur U, Miller B. The effect of microvise gap width on microbond pull-out test results. Composites Science and Technology 1994;51:111–6.

[81] Heilhecker H, Cross W, Pentland R, Griswold. C, Kellar JJ, L. Kj. The Vice Angle in the Microbond Test. Journal of Materials Science Letters 2000;19:2145–7.

[82] Järvelä P, Laitinen KW, Purola J, Törmälä P. The three-fibre method for measuring glass fibre to resin bond strength. International Journal of Adhesion and Adhesives 1983;3:141–7.

[83] Zinck P, Wagner HD, Salmon L, Gerard JF. Are microcomposites realistic models of the fibre/matrix interface? II. Physico-chemical approach. Polymer 2001;42:6641–50.

[84] Liu B, Liu Z, Wang X, Zhang G, Long S, Yang J. Interfacial shear strength of carbon fiber reinforced polyphenylene sulfide measured by the microbond test. Polymer Testing 2013;32:724–30.

[85] Tamrakar S, Haque BZ, Gillespie JW. High rate test method for fiber-matrix interface characterization. Polymer Testing 2016;52:174–83.

[86] Miller B, Gaur U, Hirt DE. Measurement and mechanical aspects of the microbond pull-out technique for obtaining fiber/resin interfacial shear strength. Composites Science and Technology 1991;42:207–19.

[87] Schultheisz CR, Schutte CL, McDonough WG, Macturk KS, McAuliffe M, Kondagunta S, et al. Effect of Temperature and Fiber Coating on the Strength of E-Glass Fibers and the E-Glass/Epoxy Interface for Single-Fiber Fragmentation Samples Immersed in Water. Fiber, Matrix, and Interface Properties, ASTM STP 1290; 1996, p. 103–31.

[88] Wada A, Fukuda H. Microbond Test for the Fiber/Matrix Interfacial Shearing Strength. Proceedings of the 12th International Conference on Composite Materials (ICCM-12), 1999.

[89] Padmanabhan K. A novel microbond bundle pullout technique to evaluate the interfacial properties of fibre-reinforced plastic composites. Bulletin of Materials Science 2017;40:737–44.

[90] Charlier Q, Lortie F, Gérard JF. Interfacial adhesion in glass-fiber thermoplastic composites processed from acrylic reactive systems, a multi-scale experimental analysis. International Journal of Adhesion and Adhesives 2020;98.

[91] Laurikainen P. Characterization of the Aging of Glass-Fibre Reinforced Polymers. Master's Thesis, Tampere University of Technology, 2017.

[92] Burn DT, Harper LT, Johnson M, Warrior NA, Yang L, Thomason J. The influence of coupling agent, fibre sizing and matrix degradation on the interfacial shear strength between carbon fibre and polypropylene. Proceedings of the 16th European Conference on Composite Materials (ECCM 2014), 2014.

[93] Tanoglu M, Ziaee S, Mc Knight SH, Palmese GR, Gillespie JW. Investigation of

properties of fiber/matrix interphase formed due to the glass fiber sizings. Journal of Materials Science 2001;36:3041–53.

[94] Tanoglu M, McKnight SH, Palmese GR, Gillespie JW. Effects of glass-fiber sizings on the strength and energy absorption of the fiber/matrix interphase under high loading rates. Composites Science and Technology 2001;61:205–20.

[95] Feresenbet E, Raghavan D, Holmes GA. The influence of silane coupling agent composition on the surface characterization of fiber and on fiber-matrix interfacial shear strength. Journal of Adhesion 2003;79:643–65.

[96] Karger-Kocsis J, Mahmood H, Pegoretti A. Recent advances in fiber/matrix interphase engineering for polymer composites. Progress in Materials Science 2015;73:1–43.

[97] Mäder E. Study of fibre surface treatments for control of interphase properties in composites. Composites Science and Technology 1997;57:1077–88.

[98] Berg J, Jones FR. The role of sizing resins, coupling agents and their blends on the formation of the interphase in glass fibre composites. Composites Part A: Applied Science and Manufacturing 1998;29:1261–72.

[99] Zhao FM, Takeda N. Effect of interfacial adhesion and statistical fiber strength on tensile strength of unidirectional glass fiber/epoxy composites. Part I: experiment results. Composites Part A: Applied Science and Manufacturing 2000;31:1203–14.

[100] Pisanova E, Máder E. Acid-base interactions and covalent bonding at a fiber-matrix interface: Contribution to the work of adhesion and measured adhesion strength. Journal of Adhesion Science and Technology 2000;14:415–36.

[101] Drzal LT, Sugiura N, Hook D. The role of chemical bonding and surface topography in adhesion between carbon fibers and epoxy matrices. Composite Interfaces 1996;4:337–54.

[102] Zinck P, Wagner HD, Salmon L, Gerard JF. Are microcomposites realistic models of the fibre/matrix interface? I. Micromechanical modelling. Polymer 2001;42:5401–13.

[103] Zinck P, Pay MF, Rezakhanlou R, Gerard JF. Mechanical characterisation of glass fibres as an indirect analysis of the effect of surface treatment. Journal of Materials Science 1999;34:2121–33.

[104] Plonka R, Mäder E, Gao SL, Bellmann C, Dutschk V, Zhandarov S. Adhesion of epoxy/glass fibre composites influenced by aging effects on sizings. Composites Part

A: Applied Science and Manufacturing 2004;35:1207–16.

[105] Zinck P, Mäder E, Gerard JF. Role of silane coupling agent and polymeric film former for tailoring glass fiber sizings from tensile strength measurements. Journal of Materials Science 2001;36:5245–52.

[106] Mäder E, Gao S lin, Plonka R. Static and dynamic properties of single and multi-fiber/epoxy composites modified by sizings. Composites Science and Technology 2007;67:1105–15.

[107] Jensen RE, McKnight SH. Inorganic-organic fiber sizings for enhanced energy absorption in glass fiber-reinforced composites intended for structural applications. Composites Science and Technology 2006;66:509–21.

[108] Gao X, Jensen RE, McKnight SH, Gillespie JW. Effect of colloidal silica on the strength and energy absorption of glass fiber/epoxy interphases. Composites Part A: Applied Science and Manufacturing 2011;42:1738–47.

[109] Gao X, Gillespie JW, Jensen RE, Li W, Haque BZ, McKnight SH. Effect of fiber surface texture on the mechanical properties of glass fiber reinforced epoxy composite. Composites Part A: Applied Science and Manufacturing 2015;74:10–7.

[110] Thomason JL. Glass Fibre Sizing: A Review of Size Formulation Patents. Blurb Inc.; 2015.

[111] Petersen H. Investigation of sizing - from glass fibre surface to composite interface. PhD Thesis, Technical University of Denmark, 2017.

[112] Peters PWM, Springer GS. Effects of Cure and Sizing on Fiber-Matrix Bond Strength. Journal of Composite Materials 1987;21:157–71.

[113] Xu L, Drzal LT. Improvement of adhesion between vinylester resin and carbon fibers. Proceedings of the 13th International Conference on Composite Materials (ICCM-13), 2001.

[114] Vautard F, Drzal LT. Carbon fiber-vinyl ester interfacial adhesion improvement by the use of an epoxy coating. Proceedings of the 17th International Conference on Composite Materials (ICCM-17), 2009.

[115] Vautard F, Xu L, Drzal LT. Carbon fiber-vinyl ester interfacial adhesion improvement by the use of an epoxy coating. Major Accomplishments in Composite Materials and Sandwich Structures: An Anthology of ONR Sponsored Research, Springer; 2009, p.

27–50.

[116] Zhang J. Different surface treatments of carbon fibers and their influence on the interfacial properties of carbon fiber. PhD Thesis, École Centrale des Arts et Manufactures, 2012.

[117] Zhang Q, Liu L, Jiang D, Yan X, Huang Y, Guo Z. Home-made epoxy emulsion sizing agent for treating carbon fibers: Thermal stability and mechanical properties. Journal of Composite Materials 2015;49:2877–86.

[118] Zhang RL, Huang YD, Liu L, Tang YR, Su D, Xu LW. Effect of the molecular weight of sizing agent on the surface of carbon fibres and interface of its composites. Applied Surface Science 2011;257:1840–4.

[119] He H, Li K, Gao F. Improvement of the bonding between carbon fibers and an epoxy matrix using a simple sizing process with a novolac resin. Construction and Building Materials 2016;116:87–92.

[120] Liao YT, Tung IC. Properties of carbon fibre-polymer interfaces. Journal of Materials Science Letters 1991;10:272–5.

[121] Sáez-Rodriguez E. Regeneration the strength of thermally recycled glass fibres using chemical treatments. PhD Thesis, University of Strathclyde, 2016.

[122] Naviroj S, Culler SR, Koenig JL, Ishida H. Structure and Adsorpiton of Characteristics pf Silane Coupling Agents on Silica and E-Glass Fiber; Dependence on pH. Journal of Colloid and Interface Science 1984;97.

[123] Petersen HN, Kusano Y, Brøndsted P, Almdal K. The influence of removing sizing on strength and stiffness of conventional and high modulus E-glass fibres. IOP Conference Series: Materials Science and Engineering 2016;139.

[124] Thomason JL. A note on the investigation of the composite interphase by means of thermal analysis. Composites Science and Technology 1992;44:87–90.

[125] Vazquez A, Ambrustolo M, Moschiar SM, Reboredo MM, Gerard JF. Interphase Modification in Unidirectional Glass-Fiber Epoxy Composites. Composite Science and Technology 1998;58:549–58.

[126] Thomason JL, Yang L, Minty RF. Are silanes the primary driver of interface strength in glass fibre composites? (exploring the relationship of the chemical and physical parameters which control composite interfacial strength). Proceedings of the 18th

European Conference on Composite Materials (ECCM18), 2018.

[127] Dwight DW, Fowkes FM, Cole DA, Kulp MJ, Sabat PJ, Salvati L, et al. Acid-base interfaces in fiber-reinforced polymer composites. Journal of Adhesion Science and Technology 1990;4:619–32.

[128] Gorowara RL, Kosik WE, McKnight SH, McCullough RL. Molecular characterization of glass fiber surface coatings for thermosetting polymer matrix/glass fiber composites. Composites Part A: Applied Science and Manufacturing 2001;32:323–9.

[129] Lenhart JL, Dunkers JP, Van Zanten JH, Parnas RS. Characterization of sizing layers and buried polymer/sizing/substrate interfacial regions using a localized fluorescent probe. Journal of Colloid and Interface Science 2003;257:398–407.

[130] Zhang R, Huang Y, Liu L, Tang Y, Su D, Xu L. Influence of sizing emulsifier content on the properties of carbon fibers and its composites. Materials and Design 2012;33:367–71.

[131] Liu Z, Hao B, Zhang Y. Control interfacial properties and tensile strength of glass fibre/PP composites by grafting poly(ethylene glycol) chains on glass fibre surface. RSC Advances 2015;5:40668–77.

[132] Zeng X, Yu S, Lai M, Sun R, Wong CP. Tuning the mechanical properties of glass fiber-reinforced bismaleimide-triazine resin composites by constructing a flexible bridge at the interface. Science and Technology of Advanced Materials 2013;14.

[133] Mäder E, Jacobasch HJ, Grundke K, Gietzelt T. Influence of an optimized interphase on the properties of polypropylene/glass fibre composites. Composites Part A: Applied Science and Manufacturing 1996;27:907–12.

[134] Thomason JL, Schoolenberg GE. An investigation of glass fibre/polypropylene interface strength and its effect on composite properties. Composites 1994;25:197–203.

[135] Shi J, Bao L, Kobayashi R, Kato J, Kemmochi K. Reusing recycled fibers in high-value fiber-reinforced polymer composites: Improving bending strength by surface cleaning. Composites Science and Technology 2012;72:1298–303.

[136] Marston C, Gabbitas B, Adams J. The effect of fibre sizing on fibres and bundle strength in hybrid glass carbon fibre composites. Journal of Materials Science 1997;32:1415–23.

[137] Tsai KH, Kim KS. The micromechanics of fiber pull-out. Journal of the Mechanics and Physics of Solids 1996;44:1147–59.

[138] Matrenichev V, Belone MCL, Palola S, Laurikainen P, Sarlin E. Resizing approach to increase the viability of recycled fibre reinforced composites. Materials 2020;13.

[139] Diddens C. Detailed finite element method modeling of evaporating multi-component droplets. Journal of Computational Physics 2017;340:670–87.

[140] Diddens C, Kuerten JGM, van der Geld CWM, Wijshoff HMA. Modeling the evaporation of sessile multi-component droplets. Journal of Colloid and Interface Science 2017;487:426–36.

[141] Thomason JL, Yang L, Bryce D, Minty R. An exploration of the relationship of chemical and physical parameters in the micromechanical characterisation of the apparent interfacial strength in glass fibre epoxy systems. IOP Conference Series: Materials Science and Engineering 2016;139.

[142] Minty R. The Influence of Matrix Stoichiometry on Interfacial Adhesion in Composites for Wind Turbine Applications. PhD Thesis, University of Strathclyde, 2018.

[143] Feih S, Boiocchi E, Mathys G, Mathys Z, Gibson AG, Mouritz AP. Mechanical properties of thermally-treated and recycled glass fibres. Composites Part B: Engineering 2011;42:350–8.

[144] Yang L, Thomason JL. Effect of silane coupling agent on mechanical performance of glass fibre. Journal of Materials Science 2013;48:1947–54.

[145] Thomason JL, Yang L, Meier R. The properties of glass fibres after conditioning at composite recycling temperatures. Composites Part A: Applied Science and Manufacturing 2014;61:201–8.

[146] Thomason J, Jenkins P, Yang L. Glass Fibre Strength-A Review with Relation to Composite Recycling. Fibers 2016;4.

[147] Nagel U, Yang L, Kao CC, Thomason JL. Effects of Thermal Recycling Temperatures on the Reinforcement Potential of Glass Fibers. Polymer Composites 2018;39:1032–40.

[148] Gao P, Su KB, Ward Y, Weng LT. Effects of chemical composition and thermal stability of finishes on the compatibility between glass fiber and high melting temperature thermoplastics. Polymer Composites 2000;21:312–21.

[149] Rudzinski S, Häussler L, Harnisch CH, Mäder E, Heinrich G. Glass fibre reinforced polyamide composites: Thermal behaviour of sizings. Composites Part A: Applied Science and Manufacturing 2011;42:157–64.

[150] Pham QT, Chern CS. Thermal stability of organofunctional polysiloxanes. Thermochimica Acta 2013;565:114–23.

[151] Petersen HN, Kusano Y, Brøndsted P, Almdal K. Analysis of Glass Fibre Sizing. Surface Engineering or Materials and Manufacturing Processes 2014.

[152] Sándor M, Nistor CL, Szalontai G, Stoica R, Nicolae CA, Alexandrescu E, et al. Aminopropyl-silica hybrid particles as supports for humic acids immobilization. Materials 2016;9:1–16.

[153] Belone MCL. Thermogravimetric Analysis of Resized Glass and Carbon Fibres. Master's Thesis, Tampere University, 2019.

[154] Petersen HN, Kusano Y, Brøndsted P, Almdal K. Preliminary Characterization of Glass Fiber Sizing. Proceedings of the 34th Risø International Symposium on Materials Science: Processing of Fibre Composites-Challenges for Maximum Materials Performance 2013:333–40.

[155] Bashir ST. A chemical approach to regenerating the performance of thermally damaged glass fibres. PhD Thesis, University of Strathclyde, 2019.

[156] Sherif G, Chukov D, Tcherdyntsev V, Torokhov V. Effect of formation route on the mechanical properties of the polyethersulfone composites reinforced with glass fibers. Polymers 2019;11:15–7.

[157] Thomason JL. The interface region in glass fibre-reinforced epoxy resin composites: 1. Sample preparation, void content and interfacial strength. Composites 1995;26:467–75.

[158] Kennerley JR, Fenwick NJ, Pickering SJ, Rudd CD. The properties of glass fibers recycled from the thermal processing of scrap thermoset composites. Journal of Vinyl and Additive Technology 1997;3:58–63.

[159] Åkesson D, Foltynowicz Z, Christéen J, Skrifvars M. Microwave pyrolysis as a method of recycling glass fibre from used blades of wind turbines. Journal of Reinforced Plastics and Composites 2012;31:1136–42.

[160] Pender KR. Recycling , regenerating and reusing reinforcement glass fibres. PhD

Thesis, University of Strathclyde, 2018.

[161] Yang L, Sáez ER, Nagel U, Thomason JL. Can thermally degraded glass fibre be regenerated for closed-loop recycling of thermosetting composites? Composites Part A: Applied Science and Manufacturing 2015;72:167–74.

[162] Thomason JL, Nagel U, Yang L, Sáez E. Regenerating the strength of thermally recycled glass fibres using hot sodium hydroxide. Composites Part A: Applied Science and Manufacturing 2016;87:220–7.

[163] Bikiaris D, Matzinos P, Prinos J, Flaris V, Larena A, Panayiotou C. Use of silanes and copolymers as adhesion promoters in glass fiber/polyethylene composites. Journal of Applied Polymer Science 2001;80:2877–88.

[164] Roux C, Denault J, Champagne MF. Parameters regulating interfacial and mechanical properties of short glass fiber reinforced polypropylene. Journal of Applied Polymer Science 2000;78:2047–60.

[165] Fu SY, Lauke B, Zhang YH, Mai YW. On the post-mortem fracture surface morphology of short fiber reinforced thermoplastics. Composites Part A: Applied Science and Manufacturing 2005;36:987–94.

[166] Mizuguchi J, Tsukada Y, Takahashi H. Recovery and Characterization of Reinforcing Fibers from Fiber Reinforced Plastics by Thermal Activation of Oxide Semiconductors. Materials Transactions 2013;54:384–91.

[167] Bryce D, Thomason JL, Yang L. An Investigation of Fibre Sizing on the Interfacial Strength of Glass-Fibre Epoxy Composites. Proceedings of the 18th European Conference on Composite Materials (ECCM18), 2018.

[168] Thomason JL. Glass Fibre Sizing: A Review. Composites Part A: Applied Science and Manufacturing 2019;127.

[169] Salmon L, Thominette F, Pays MF, Verdu J. Hydrolytic degradation of model networks simulating the interfacial layers in silane-coupled epoxy/glass composites. Composites Science and Technology 1997;57:1119–27.

[170] Li Z, Liu J, Yuan Y, Li E, Wang F. Effects of surface fluoride-functionalizing of glass fiber on the properties of PTFE/glass fiber microwave composites. RSC Advances 2017;7:22810–7.

[171] Guo Z, Pereira T, Choi O, Wang Y, Hahn HT. Surface functionalized alumina

nanoparticle filled polymeric nanocomposites with enhanced mechanical properties. Journal of Materials Chemistry 2006;16:2800–8.

[172] Ishida H, Koenig JL. Fourier transform infrared spectroscopic study of the structure of silane coupling agent on E-glass fiber. Journal of Colloid And Interface Science 1978;64:565–76.

[173] González MG, Cabanelas JC, Baselga J. Applications of FTIR on Epoxy Resins – Identification , Monitoring the Curing Process , Phase Separation and Water Uptake. Infrared Spectroscopy - Materials Science, Engineering and Technology, 2012, p. 261–84.

[174] Nikolic G, Zlatkovic S, Cakic M, Cakic S, Lacnjevac C, Rajic Z. Fast fourier transform IR characterization of epoxy GY systems crosslinked with aliphatic and cycloaliphatic EH polyamine adducts. Sensors 2010;10:684–96.

[175] Zhuang RC, Burghardt T, Mäder E. Study on interfacial adhesion strength of single glass fibre/polypropylene model composites by altering the nature of the surface of sized glass fibres. Composites Science and Technology 2010;70:1523–9.

[176] Yao L, Li M, Wu Q, Dai Z, Gu Y, Li Y, et al. Comparison of sizing effect of T700 grade carbon fiber on interfacial properties of fiber/BMI and fiber/epoxy. Applied Surface Science 2012;263:326–33.

[177] Mailhot B, Morlat-Thérias S, Ouahioune M, Gardette JL. Study of the degradation of an epoxy/amine resin, 1 photo- and thermo-chemical mechanisms. Macromolecular Chemistry and Physics 2005;206:575–84.

[178] Jenkins PG. Understanding physical changes and strength loss of E-glass fibres following exposure to elevated temperatures. Materials Science and Technology 2017;33:255–64.

[179] Delor-Jestin F, Drouin D, Cheval PY, Lacoste J. Thermal and photochemical ageing of epoxy resin-Influence of curing agents. Polymer Degradation and Stability 2006;91:1247–55.

[180] Doblies A, Boll B, Fiedler B. Prediction of thermal exposure and mechanical behavior of epoxy resin using artificial neural networks and Fourier transform infrared spectroscopy. Polymers 2019;11.

[181] Thomason JL, Dwight DW. XPS analysis of the coverage and composition of coatings

on glass fibres. Journal of Adhesion Science and Technology 2000;14:745–64.

[182] Thomason JL, Nagel U, Yang L, Bryce D. A study of the thermal degradation of glass fibre sizings at composite processing temperatures. Composites Part A: Applied Science and Manufacturing 2019;121:56–63.

[183] Rao V, Herrera-Franco P, Ozzello AD, Drzal LT. A Direct Comparison of the Fragmentation Test and the Microbond Pull-out Test for Determining the Interfacial Shear Strength. The Journal of Adhesion 1991;34:65–77.

[184] Rao V, Drzal LT. Loss of Curing Agent During Thin Film (Droplet) Curing of Thermoset Material. The Journal of Adhesion 1991;22:245–9.

[185] Biro DA, Pleizier G, Deslandes Y. Application of the Microbond Technique . IV . Improved Fiber-Matrix Adhesion by RF Plasma Treatment of Organic Fibers. Journal of Applied Polymer Science 1993;47:883–94.

[186] Bartolomeo P, Chailan JF, Vernet JL. Micromechanical and Microscopic Effects of Preprocessing on Interfacial Shear Stress of Glass Fiber-Cynate Ester Resins Composite. Proceedings of the 12 International Conference on Composite Materials International Conference on Composite Materials, Paris: 1999.

[187] Zinck P, Gérard JF. Thermo-hydrolytic resistance of polyepoxide-glass fibres interfaces by the microbond test. Composites Science and Technology 2008;68:2028–33.

[188] Charlier Q, Lortie F, Gerard P, Gerard JF. Interfacial adhesion between glass fibers and acrylic-based matrices as studied by micromechanical testing. Proceedings of the 20th International Conferences on Composite Materials (ICCM-20), 2015.

[189] Ash JT, Cross WM, Kellar JJ. Estimation of the true interfacial shear strength for composite materials with the microbond test. Proceedings of the ASME 2013 International Mechanical Engineering Congress and Exposition, 2013.

[190] Laurikainen P, Jokinen J, Lindgren M, Kallio P, Kanerva M, Oreski G, et al. High throughput mechanical micro-scale characterization of composites and the utilization of the results in finite element analysis. Proceedings of the 18th European Conference on Composite Materials (ECCM18) 2018.

[191] Mak M, Lowe A, Jar B, Stachurski Z, Fitzgerald J. Improvements to the microdroplet single fibre composite test. Journal of Materials Science Letters 1998;17:645–7.

[192] Patel A, Kravchenko O, Manas-Zloczower I. Effect of curing rate on the microstructure and macroscopic properties of epoxy fiberglass composites. Polymers 2018;10.

[193] Biro DA, McLean P, Deslandes Y. Application of the Microbond Technique: Characterization of Carbon Fiber-Epoxy Interfaces. Polymer Engineering and Science 1991;37:1250–6.

[194] Prime B, Gotro J. Thermoset Characterization. InnoCentrix; 2003.

[195] Minty RF, Thomason JL, Yang L, Stanley W, Roy A. Development and application of novel technique for characterising the cure shrinkage of epoxy resins. Polymer Testing 2019;73:316–26.

[196] Calventus Y, Montserrat S, Hutchinson JM. Enthalpy relaxation of non-stoichiometric epoxy-amine resins. Polymer 2001;42:7081–93.

[197] Palmese GR, McCullough RL. Effect of epoxy-amine stoichiometry on cured resin material properties. Journal of Applied Polymer Science 1992;46:1863–73.

[198] Vanlandingham MR, Eduljee RF, Gillespie JW. Relationships between Stoichiometry, Microstructure, and Properties for Amine-Cured Epoxies. Journal of Applied Polymer Science 2001;71:699–712.

[199] Vincent L, Mija A, Sbirrazzuoli N. Liquid crystalline and isotropic epoxy thermosets: Mechanism and kinetics of non-isothermal degradation. Polymer Degradation and Stability 2007;92:2051–7.

[200] Lee TM, Ma CCM, Hsu CW, Wu HL. Syntheses of Epoxy-Bridged Polyorganosiloxanes and the Effects of Terminated Alkoxysilanes on Cured Thermal Properties. Journal of Applied Polymer Science 2006;99:3491–9.

[201] Mijović J. Processing-morphology-property relationships in epoxy resins containing an organometallic cobalt complex. Journal of Applied Polymer Science 1990;40:1337–56.

[202] De Nograro FF, Guerrero P, Corcuera MA, Mondragon I. Effects of Chemical Strucutre of Hardener on Curing Evolution and on the Dynamtic Mechanical Behaviour of Epoxy Resins. Journal of Applied Polymer Science 1995;56:177–92.

[203] Dannenberg H, Harp WR. Determination of Cure and Analysis of Cured Epoxy Resins. Analytical Chemistry 1956;28:86–90.

[204] Strong AB. Fundamentals of Composites Manufacturing: Materials, Methods, and Applications. 1992.

[205] Cholake ST, Mada MR, Raman RKS, Bai Y, Zhao XL, Rizkalla S, et al. Quantitative Analysis of Curing Mechanisms of Epoxy Resin by Mid- and Near- Fourier Transform Infra Red Spectroscopy. Defence Science Journal 2014;64:314–21.

[206] Achilias DS, Karabela MM, Varkopoulou EA, Sideridou ID. Cure kinetics study of two epoxy systems with Fourier Tranform Infrared Spectroscopy (FTIR) and Differential Scanning Calorimetry (DSC). Journal of Macromolecular Science, Part A: Pure and Applied Chemistry 2012;49:630–8.

[207] Sahagun CM, Morgan SE. Thermal control of nanostructure and molecular network development in epoxy-amine thermosets. ACS Applied Materials and Interfaces 2012;4:564–72.

[208] Rogers MG. The structure of epoxy resins using NMR and GPC techniques. Journal of Applied Polymer Science 1972;16:1953–8.

[209] Garcia FG, Soares BG. Determination of the epoxide equivalent weight of epoxy resins based on diglycidyl ether of bisphenol A (DGEBA) by proton nuclear magnetic resonance. Polymer Testing 2003;22:51–6.

[210] Sandreczki TC, Brown IM. Electron Paramagnetic Resonance Studies of Amine-Cured Epoxy Resins: Dependence of Nitroxide Spin-Probe Mobility on Cross-Link Density, Free Volume, and Temperature. Macromolecules 1984;17:1789–94.

[211] Smith RE, Larsen FN, Long CL. Epoxy resin cure. II. FTIR analysis. Journal of Applied Polymer Science 1984;29:3713–26.

[212] Puglia D, Valentini L, Armentano I, Kenny JM. Effects of single-walled carbon nanotube incorporation on the cure reaction of epoxy resin and its detection by Raman spectroscopy. Diamond and Related Materials 2003;12:827–32.

[213] Hardis R, Jessop JLP, Peters FE, Kessler MR. Cure kinetics characterization and monitoring of an epoxy resin using DSC, Raman spectroscopy, and DEA. Composites Part A: Applied Science and Manufacturing 2013;49:100–8.

[214] Lange J, Altmann N, Kelly CT, Halley PJ. Understanding vitrification during cure of epoxy resins using dynamic scanning calorimetry and rheological techniques. Polymer 2000;41:5949–55.

[215] de la Vega A, Kovacs JZ, Bauhofer W, Schulte K. Combined Raman and dielectric spectroscopy on the curing behaviour and stress build up of carbon nanotube-epoxy composites. Composites Science and Technology 2009;69:1540–6.

[216] Lionetto F, Maffezzoli A. Monitoring the cure state of thermosetting resins by ultrasound. Materials 2013;6:3783–804.

[217] Douša P, Koňák C, Fidler V, Dušek K. Cure monitoring of epoxy resins by fluorescence quenching. Polymer Bulletin 1989;22:585–92.

[218] Cañavate J, Colom X, Pagès P, Carrasco F. Study of the curing process of an epoxy resin by FTIR spectroscopy. Polymer-Plastics Technology and Engineering 2000;39:937–43.

[219] Fraga F, Eva C V, Rodriquez-Nunez E, Martinez-Ageitos JM. Curing kinetics of the epoxy system diglycidyl ether of bisphenol A/isophoronediamine by Fourier transform infrared spectroscopy. Polymers for Advanced Technologies 2008;19:1623–8.

[220] Fraga F, Burgo S, Rodrguez Nez E. Curing kinetic of the epoxy system BADGE n = 0/1,2 DCH by Fourier Transform Infrared Spectroscopy (FTIR). Journal of Applied Polymer Science 2001;82:3366–72.

[221] Fouchal F, Knight JAG, Dickens PM. Monitoring the polymerization of a diglycidyl ether bisphenol-A/2,2′- dimethl-4,4′-methylenebis (cyclohexylamine) matrix with a Fourier transform infrared optical fibre sensor. Proceedings of the Institution of Mechanical Engineers, Part L: Journal of Materials: Design and Applications 2004;218:331–42.

[222] Fouchal F, Knight JAG, Dickens P, Garrington N. On-line Monitoring of Epoxy Resin Cure using Infrared Spectroscopy. Proceedings of the 2001 International Solid Freeform Fabrication Symposium, 2001, p. 441–51.

[223] Karayannidou EG, Achilias DS, Sideridou ID. Cure kinetics of epoxy-amine resins used in the restoration of works of art from glass or ceramic. European Polymer Journal 2006;42:3311–23.

[224] Fu Y, Sun D, Liu X, An X, Zhang X. The curing kinetic analysis of epoxy based on FT-IR. Proceedings of the 3rd International Conference on Material, Mechanical and Manufacturing Engineering (IC3ME 2015), 2015, p. 286–90.

[225] Li YF, Xiao MZ, Wu Z, Peng K, Han CM, Xiang W, et al. Effects of epoxy/hardener

stoichiometry on structures and properties of a diethanolamine-cured epoxy encapsulant. IOP Conference Series: Materials Science and Engineering 2016;137.

[226] Mijović J, Andjelić S. Monitoring of reactive processing by remote mid infra-red spectroscopy. Polymer 1996;37:1295–303.

[227] Escola MA, Moina CA, Gómez ACN, Ybarra GO. The determination of the degree of cure in epoxy paints by infrared spectroscopy. Polymer Testing 2005;24:572–5.

[228] Fondeur F, Koenig JL. Microsopic FT-IR Studies of Epoxy Adhesive Films on Chemically Treated Aluminum. Applied Spectroscopy 1993;47:1–6.

[229] Swinehart DF. The Beer-Lambert Law. Journal of Chemical Education 1962;39:333–5.

[230] Zlatkovic S, Raskovic LJ, Nikolic GS, Stamenkovic J. Investigation of emulsified hydrous epoxy systems. Facta Univsersitatis, Series;:Working and Living Environemental Protection 2005;2:401–7.

[231] Omrani A, Simon LC, Rostami AA, Ghaemy M. Cure Kinetics FTIR Study of Epoxy/Nickel-Imidazole System. International Journal of Chemical Kinetics 2008;43:154–60.

[232] Saeedi IA, Andritsch T, Vaughan AS. On the dielectric behavior of amine and anhydride cured epoxy resins modified using multi-terminal epoxy functional network modifier. Polymers 2019;11.

[233] Meyer F, Sanz G, Eceiza A, Mondragon I, Mijović J. The effect of stoichiometry and thermal history during cure on structure and properties of epoxy networks. Polymer 1995;36:1407–14.

[234] Carothers WH. Polymers and polyfunctionality. Transactions of the Faraday Society 1936;32:39–49.

[235] Poisson N, Lachenal G, Sautereau H. Near- and mid-infrared spectroscopy studies of an epoxy reactive system. Vibrational Spectroscopy 1996;12:237–47.

[236] Antoon MK, Starkey KM, Koenig JL. Application of Fourier Transform Infrared Spectroscopy to Quality Control of the Epoxy Matrix. In: Tsai SW, editor. Composite Materials: Testing and Design (Fifth Conference), American Society for Testing and Materials; 1979, p. 541–52.

[237] Ray R, Hazari AS, Lahiri GK, Maiti D. Ruthenium-Catalyzed Aerobic Oxidation of Amines. Chemistry - An Asian Journal 2018;13:2138–48.

[238] Xu L. Interfacial Engineering of the Interphase Between Carbon Fibers and Vinyl Ester Resin. PhD Thesis, Michigan State University, 2003.

APPENDICES

APPENDIX A: CALCULATION OF EPOXY/AMINE STOICHIOMETRIC RATIO

Epoxy equivalent weight was calculated using *Eq. A-1*

$$EEW = \frac{Molecular\ weight\ of\ epoxy\ resin}{Number\ of\ epoxy\ groups} \quad \text{(Eq. A-1)}$$

Amine equivalent weight was by calculated using *Eq. A-2*.

$$AEW = \frac{Molecular\ weight\ of\ amine}{Number\ of\ amine\ \text{reactive}\ hydrogen\ atoms} \quad \text{(Eq. A-2)}$$

The amine/epoxy stoichiometric ratio was calculated using *Eq. A-3*.

$$Stoichiometric\ ratio = \frac{AEW}{EEW} * 100 \quad \text{(Eq. A-3)}$$

Epoxy and amine molecular weights, reactive amine hydrogens (functionality), EEW, AEW, and stoichiometric ratios for the epoxy resin matrices used in the investigation are summarised in *Table A-1*.

Epoxy	$M_{W,epoxy}$ (g/mol)	Curing Agent	$M_{W,amine}$ (g/mol)	Functionality	EEW (g/mol)	AEW (g/mol)	Stoichiometric Ratio (phr)
332	340.4	TETA	146.2	6	170.2	24.4	14.3
332	340.4	IPD	170.3	4	170.2	42.6	25.0
332	340.4	PPD	230.0	4	170.2	57.5	33.8
332	340.4	DAP	74.1	4	170.2	18.5	10.9
332	340.4	DETA	103.2	5	170.2	20.6	12.1
332	340.4	TEPA	189.3	7	170.2	27	15.9

Table A-1: Summary of epoxy/amine stoichiometry

APPENDIX B: CALCULATION OF SIZING LAYER THICKNESS

Epoxy Film Former Sizing Layer Thickness

The thickness of the glass fibre sizing layer, was calculated using TGA data [238]. A typical TGA thermogram is shown in *Figure B:1*. It was assumed that both the glass fibre and sizing layer behaved like perfect cylinders and that the sizing layer was uniformly distributed. Unsized glass fibres were Advantex glass of density 2.62 g/cm^3. Sizing density of 1.16 g/cm^{3}was equal to the density of the DER 332 epoxy resin used as the solvent component of the sizing was fully evaporated during the drying stage. Glass fibre and epoxy resin densities were determined from respective technical data sheets.

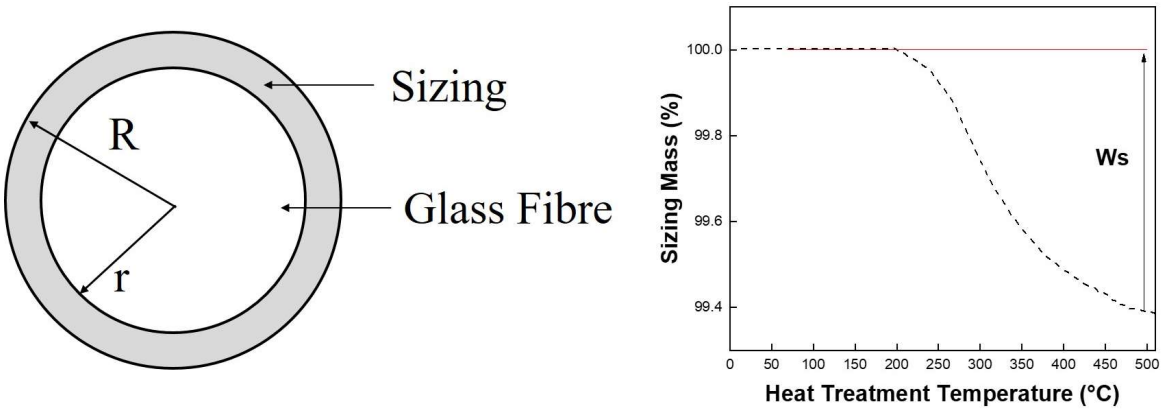

Figure B:1: Glass fibre sizing layer model

The mass of the sizing determined by TGA is given by *Eq. B-1*.

$$W_s = \frac{\pi(R^2 - r^2)\rho_{sizing}}{\pi[(R^2 - r^2)\rho_{sizing} + r^2\rho_{fibre}]} \qquad \text{(Eq. B-1)}$$

The total thickness of the sized glass fibre is given by *Eq. B-2*

$$R = \sqrt{\frac{W_s}{1 - W_s}\frac{\rho_{fibre}}{\rho_{sizing}}r^2 + r^2} \qquad \text{(Eq. B-2)}$$

The sizing layer thickness is given by *Eq. B-3*

$$t = R - r = \sqrt{\frac{W_s}{1 - W_s}\frac{\rho_{fibre}}{\rho_{sizing}}r^2 + r^2} - r \qquad \text{(Eq. B-3)}$$

Where: W_s is the mass fraction of the sizing, R is sized fibre radius (nm), r is unsized fibre radius (nm), ρ_{fibre} is the density of the fibre (g/cm^3), ρ_{sizing} is the density of the sizing (g/cm^3) and t is the thickness of the sizing layer (nm).

Sizing Layer Depletion

Values of ρ_{fibre} were 2.62 g/cm^3 for Advantex glass fibres (SE1500, SE2020) and 2.58 g/cm^3 for HiPer-tex glass fibres (W2020) and were determined from technical data sheets. The value of ρ_{sizing} was assumed to be 1 g/cm^3 for full sizing formulations. Initial sizing layer thickness was determined using the total mass of degraded sizing. Layer thicknesses at a given temperature were calculated using the mass fraction of the sizing measured at the same temperature. Remaining sizing layer thickness at a given temperature (t_R) was calculated by subtracting the layer thickness at that temperature (t_{temp}) from the initial layer thickness and is given by *Eq. B-4*.

$$t_R = t - t_{temp.} \qquad \text{(Eq. B-4)}$$

Where: t_R is the thickness of the sizing layer remaining (nm), t is the total sizing layer thickness (nm), and t_{temp} is the reduction in the sizing layer thickness at a given temperature (nm).

Sizing layer degradation with increasing heat treatment temperature for SE1500, SE2020, and W2020 glass fibres is shown in *Figure B:2*.

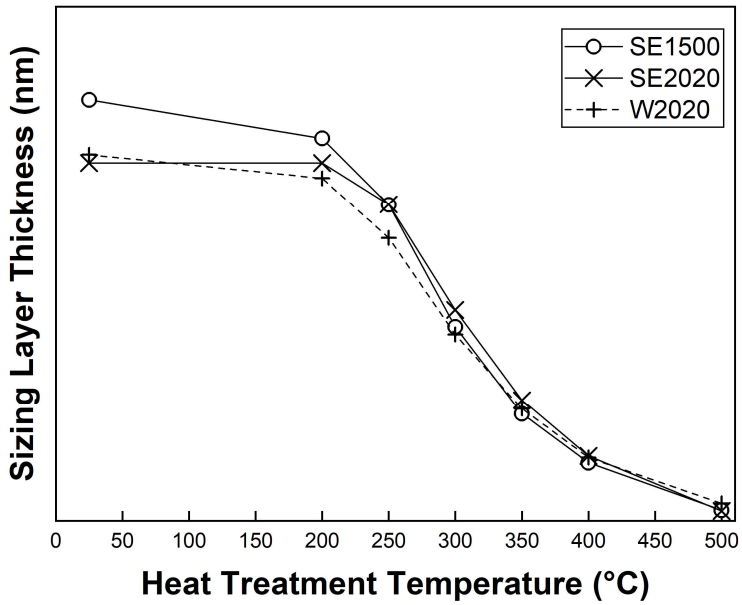

Figure B:2: Sizing layer thickness versus treatment temperature

APPENDIX C: SUMMARY OF MICROBOND CURING ISSUES/SOLUTIONS

Material [Ref.]	Conclusion	Solution
Various thermoset adhesives [82]	Evaporation of components involved in polymerisation. Degree of cure in microdroplets not measurable.	-
Epoxy/m-PDA [74]	Same cure cycle as bulk resulted in poor droplet curing. Evaporation of curing agent verified with FTIR microscopy.	Procedure to create cured droplets needed.
Epoxy/m-PDA [41]	Evaporation of curing agent.	Room temperature pre-cure (18 h).
Epoxy/m-PDA [183]	Evaporation of curing agent. Immediate curing resulted in low T_g droplets. No improvement from excess curing agent or amine-rich atmosphere.	Room temperature pre-cure (24 h) allows gelation and prevents loss of curing agent.
Epoxy/m-PDA [120]	Failed to cure at the stoichiometric ratio due to adsorption of m-PDA onto the fibre surface.	Samples prepared with excess curing agent.
Epoxy/m-PDA [22]	Properties of microbond samples lower than fragmentation due to loss of curing agent caused by surface-to-volume ratio.	-
Epoxy/Jeffamine D230 [91]	Phase separation during sample preparation. Possible interaction with atmospheric moisture.	Allow resin to gelate (2 h) before application to fibre.
Epoxy/Tonox [185]	Possible evaporation of curing agent affecting stoichiometry.	Curing under nitrogen and amine-rich environment had no effect.
Epoxy/MDEA [83]	Pre-cure had little effect. Imine group formation reduces number of amine functions available to react.	Amine-cured samples should be cured under inert atmosphere.
Epoxy/MTHPA [83]	Pre-cure had a detrimental effect. Surface moisture possibly contributes to hydrolysis of anhydride.	For anhydride-cured samples, standing time should not be implemented.
Epoxy (unspecified) [90]	Dimensional effect on auto-acceleration. Droplets didn't cure fully under supplier-recommended conditions	High post-cure temperature to ensure matrix droplets are fully cured.
PMMA [90]	Evaporation of acrylic monomers during microbond samples preparation. Dimensional effect on auto-acceleration	Addition of paraffin wax to acrylic resin. High temperature post-cure.
Polyester/MEKP [189]	40–50% evaporation of styrene out of microdroplets responsible for data scatter and stiffness variability	-
Vinyl ester [48]	Vaporisation of styrene	-
Vinyl ester [91]	Vaporisation of styrene	Cure in styrene-rich atmosphere.

APPENDIX D: MATLAB SCRIPT FOR AUTOMATED MICROGRAPH PROCESSING

```
clear all
close all

%% Before running image analysis script

% Set initial inputs
% Check data set for out-of-focus images

%% Initial inputs

% Set results export filename
filename = '.xlsx';
sheetnumber = 1;

% Set temperature schedule (start:rate(°C/min):end)
T2565 = 25:2:65;
T65(1,1:210) = 65;
T6575 = 65:2:75;
T75(1,1:420) = 75;
Temperature = [T2565 T65 T6575 T75];

% Set fibre diameter threshold (µm)
MaxDiameter = 15.8;
ActualFibreD = 15;
MinDiameter = 14.5;

% Set droplet diameter threshold (µm)
MinDroplet = 19;

% Set micrograph collection time (minutes)
tstep = 1;

% Set pixels/µm scale
p2um = 9.5805;

% Define thresholds for channel 1
%Red
channel1Min = 155;
channel1Max = 255;

% Define thresholds for channel 2
%Green
channel2Min = 0;
channel2Max = 250;

% Define thresholds for channel 3
%Blue
channel3Min = 0;
channel3Max = 255;
```

```
%% Select folder for image processing

%Folder must contain image files only
selpath = uigetdir(path);
listing = dir(selpath);

%Remove non image files from folder
listing(1:2, :) = [];

% Count number of images to process
NumImages = length(listing);

%% Loop setup

i = 1;
for i = 1:NumImages

%% Loading each image sequentially

% Loads number i image
name = extractfield(listing(i,1),'name');
folder = extractfield(listing(i,1),'folder');
pathname = string(strcat(folder, '\', name)); %loads number i image
I = imread(pathname);
% I = imread('Test Image.JPG');

%% Determine image size

[h,w,~] = size(I);

%% Threshold operation for Boolean image

% Create Boolean image based on selected thresholds
BW = (I(:,:,1) >= channel1Min ) & (I(:,:,1) <= channel1Max) & ...
(I(:,:,2) >= channel2Min ) & (I(:,:,2) <= channel2Max) & ...
(I(:,:,3) >= channel3Min ) & (I(:,:,3) <= channel3Max);

% Fill in voids in image
WB = imcomplement(BW);
se = strel('disk',300);
closeWB = imclose(WB,se);
%closeWW = imclose(gpuArray(WW),se);

% Retain fibre/droplet region
ROIcloseWB = bwpropfilt(closeWB, 'Area', 1);

%% Measurement of droplet dimensions

% create matrices for the upper/lower limits of the fibre/droplet
[row,col] = find(ROIcloseWB==1);
ROIy = zeros(h,w);
for step = 1:(size(row))
ROIy(row(step),col(step)) = row(step);
end
clear row col step
```

```
Maxpos = max(ROIy);
ROIymin = ROIy;
ROIymin(ROIymin==0) = h;
Minpos = min(ROIymin);

%Find diameter along fibre length
D = (Maxpos - Minpos) ./ p2um;
x = [0:(w-1)] ./ p2um;

%Find fibre diameter
Dfibre = min(D, [], 'all');

%Isolate droplet
Ddrop = D;
Ddropmask = Ddrop>MinDroplet;
Ddrop = Ddrop .* Ddropmask;

% Adjust key processing parameter to suitable value
usercheck = 0;
if i == 1
while usercheck == 0
close all
figure
line(x,D)
hold on
line(x,Ddrop)

MinDroplet = input('Input corrected minimum droplet diameter
parameter');

Ddrop = D;
Ddropmask = Ddrop>MinDroplet;
Ddrop = Ddrop .* Ddropmask;

close all
figure
line(x,D)
hold on
line(x,Ddrop)

usercheck = input('is this acceptable. 1 for yes and 0 for no.');
end
end

% Removing large droplets at edges of the image
Ddropcheck = Ddrop;
dropletcheck = 0;
while dropletcheck == 0
grad = gradient(Ddropcheck);
[~,maxdx] = max(Ddropcheck);
[~,maxx] = find(grad>0.8);
[~,minx] = find(grad<-0.8);
[~,xminpos] = min(abs(maxdx-maxx));
[~,xmaxpos] = min(abs(maxdx-minx));
xmin = maxx(xminpos);
xmax = minx(xmaxpos);
Dtarget = Ddropcheck(1, xmin:xmax);
X = [0:(w-1)] ./ p2um;
```

```
[~,W] = size(Dtarget);

if min(Ddropcheck(1,maxdx:end))==0 && min(Ddropcheck(1,1:maxdx))==0
dropletcheck = 1;
end

if min(Ddropcheck(1,1:maxdx))~=0
foundzeros = find(Ddropcheck == 0);
Ddropcheck(1,1:(maxdx+1)) = 0;
nextzero = min(foundzeros);
Ddropcheck(1,maxdx:nextzero) = 0;
end

if min(Ddropcheck(1,maxdx:end))~=0
foundzeros = find(Ddropcheck == 0);
Ddropcheck(1,(maxdx-1):end) = 0;
nextzero = max(foundzeros);
Ddropcheck(1,nextzero:maxdx) = 0;
end
end

% Remove poor end values
DTarget = Dtarget(:,2:W-2);
XTarget = [0:(W-4)] ./ p2um;

% Calculate volume
MaxD(i) = max(DTarget);
MaxL(i) = W/p2um;
FibreD(i) = Dfibre;
Volume(i) = (4/3) * pi * (MaxD(i)/2)^2 * (MaxL(i)/2);
Volumenofibre(i) = Volume(i) - ((pi * (Dfibre/2)^2) * MaxL(i));
Time(i) = (i-1) * tstep;

%% Check fibre diameter against known diameter and thresholds
if MaxDiameter > Dfibre < MinDiameter
FibreCheck(i) = 0;
else
FibreCheck(i) = 1;
end
end

%% Results processing

% Data output
ResultsTable = table(MaxD.', MaxL.', Volume.', Volumenofibre.',
Time.', FibreCheck.',FibreD.');
writetable(ResultsTable,filename,'Sheet',sheetnumber,'Range','A1')

%Plot figure
figure
subplot(4,1,1)
line(Time,MaxD)
subplot(4,1,2)
line(Time,MaxL)
subplot(4,1,3)
line(Time,Volumenofibre)
subplot(4,1,4)
line(Time,FibreD)
```